Inhibition of PI3K/MAPK Signaling with Simultaneous DNA Damage in Cancer Cells by Lipidic Nanoparticles

A Thesis

submitted to partial fulfilment of the degree of

Doctor of Philosophy

By

Sandeep Kumar Palvai
ID: 20123206

Research Supervisor
Dr. Sudipta Basu

INDIAN INSTITUTE OF SCIENCE EDUCATION AND RESEARCH

PUNE

2018

Dedicated to

My Parents and Teachers

CERTIFICATE

This is to certify that the work incorporated in this entitled **"Inhibition of PI3K/MAPK Signaling with Simultaneous DNA Damage in Cancer Cells by Lipidic Nanoparticles"** submitted by Sandeep Kumar Palvai carried out by candidate at Indian Institute of Science Education and Research (IISER), Pune, under my supervision. The work presented here or any part of it has not been included in any other thesis submitted previously for the award of any degree or diploma from any other university or institution.

Date: 13/10/2017

Dr. Sudipta Basu
(Research Supervisor)
Ramalingaswami Fellow
IISER, Pune - 411008
India.

Declaration

I hereby declare that the thesis entitled **"Inhibition of PI3K/MAPK Signaling with Simultaneous DNA Damage in Cancer Cells by Lipidic Nanoparticles"** submitted for Doctor of Philosophy in chemistry at Indian Institute of Science Education and Research (IISER), Pune, has not been submitted by me to any other university or institution. This work presented here was carried out at the Indian Institute of Science Education and Research, Pune, India under the supervision of Dr. Sudipta Basu.

Date: 13/10/2017

Sandeep Kumar Palvai
ID-20123206
(Senior Research Fellow)
Department of Chemistry
IISER, Pune- 411008
India.

ACKNOWLEDGEMENTS

I would like to thank all the people who helped and supported me in completing this doctoral dissertation without whom this would not have been possible. Foremost, I wish to thank my supervisor **Dr. Sudipta Basu**, for accepting me into his group. During my tenure, he gave me intellectual freedom in my work, invaluable suggestions, constant encouragement, and support in all my endeavours, supported my attendance at various conferences, thus contributed to a rewarding graduate school experience. A person with a kind and positive disposition, Sir has always made himself available to clarify my doubts despite his busy schedules and I consider it as a great opportunity to do my doctoral programme under his guidance. I would like to thank **Dr. H. N. Gopi** and **Dr.BLV Prasad** for being my research advisory committee (RAC) members and providing me valuable comments during RAC meetings, which enabled me to notice the shortcomings of work and make necessary improvements. I thank **Prof. K.N. Ganesh**, Director, IISER-Pune, for the academic support and the facilities provided to carry out the research work at the Institute.

I am extremely thankful to my collaborator **Dr, Rajdeep Chowdhury (BITS, Pilani)** for his support in performing biological experiments in chapter 2. I also thank **Dr. Mayurikha Lahiri, Dr. KundanSen Gupta and Dr. Nagraj Balasubramniya** and their lab members from IISER Pune, Biology Dept. for constructive discussions and extending research facilities in their laboratory. I thank **Prof. M. Jayakannan**, **Dr. Harinath Chakrapani, and Dr. SG Srivatsan** for their extensive freedom given me to access various instruments facilities.

I would like to thank all the faculty members in the department of chemistry IISER Pune, for interactive scientific discussions and teaching me various chemistry courses.

Special thanks to my present and former lab mates for their support and cooperation which made my life memorable at IISER, Pune especially, Kamil, Sohan, Abhik, Aditi, Chandra, Nikunj, Shalini, Sumer, Suhas, Meenu, and Aman.

I take this occasion to say my earnest thanks to Piyush More for providing me experimental hands-on-training on different aspects of cell culture methods and MTT assays. I also thank Poulomi (NCL Pune) and Ramesh (NCCS Pune) for their commendable help in performing several biological experiments.

I would like to thank all instruments technicians and purchase department people of IISER Pune for their support: Pooja, Deepali (NMR), Swati (MALDI), Meghna (AFM), Anil, Yatish (FE-SEM) Vijay (CLSM), Rupali (FACS), Nitin (NMR), Mahesh Jadhav, and Shabnam.

I am indebted to many other friends for providing an inspiring and fun filled environment around me, especially Kiran, Ganesh, Gopal, Rajesh, Bapu, Rajendra, Shivakoti, Harikrishna, Nasimha, Venki, Kishor, Rajkumar, Mahesh, Shiva, Subbu, Dinesh, Jagan, Reman, Naresh, and all other friends. I also thank all the staff members in administration, finance, accounts, especially, Mr. Mayuresh, and Mr. Tushar for their immediate help whenever I needed them. I also thank the entire housekeeping and cleaning depot for keeping campus clean and clear.

I would like to acknowledge with tremendous and deep thanks to my parents especially my father for his whole hearted support and encouragement.

Financial support from UGC and IISER Pune is greatly acknowledged.

Sandeep

TABLE OF CONTENTS

Chapter 1: PI3K and MAPK Signaling in Cancer and Targeting by Nanoplatform ***1-26***

1.1 History of cancer 2

1.2 Hallmarks of Cancer 3

1.3 Cell signalings pathways 4-10

1.3.1 Phosphatidylinositol-3-kinase (PI3K) signaling 5

1.3.2 Mitogen-activated protein kinase (MAPK) signaling 7

1.4 Challenges in targeting PI3K and MAPK signaling in cancer 8-10

1.5 Cancer nanomedicine 11-17

1.5.1 Advantages of nanoparticles-mediated co-delivery of drugs 11-13

1.5.2 Essential characteristics of the nanoparticles 13-17

1.6 Nanoparticle-mediated PI3K and MAPK signaling in cancer 17

1.7 Aim of thesis 18

1.8 References 19-26

Chapter 2: Vitamin D3 nanoparticle-mediated targeting of PI3K pathway in synergy with DNA damaging drugs in cancer cell ***27-57***

2.1 Introduction 28

2.2 Results and Discussion 29

2.2.1 Rationale for choosing the drug combinations 29

2.2.2 Rationale for choosing the Vitamin D3 as vector 30

2.2.3 Synthesis and characterization of vitamin D3 nanoparticles with dual drugs 30-36

2.2.4 Release of dual drugs from vitamin D3 nanoparticles 36

2.2.5 Stability of the vitamin D3 nanoparticles 37-39

2.2.6 *In vitro* cytotoxicity assay 39-46

2.2.7 Mechanism of action 46

2.2.8 Internalization of vitD3–PI103–proflavine-NP 48

2.3 Conclusions 49

2.4 Experimental methods 50-55
2.4.1 Materials 50
2.4.2 Synthesis of dual drug loaded vitamin D3 nanoparticles 51
2.4.3 Quantification of drug loading in the nanoparticles 51
2.4.4 Determination of the hydrodynamic diameter of dual drug loaded nanoparticles by dynamic light scattering (DLS) 52
2.4.5 Field-emission scanning electron microscopy (FESEM) of Nanoparticles 52
2.4.6 Atomic force microscopy (AFM) of nanoparticles 52
2.4.7 Transmission electron microscopy (TEM) of nanoparticles 52
2.4.8 Determination of dual drug release from the nanoparticles 53
2.4.9 Cell culture 53
2.4.10 MTT cytotoxicity assay 53
2.4.11 Creation of resistant cell lines 54
2.4.12 WST-1 cytotoxicity assay 54
2.4.13 Trypan blue cell viability assay 54
2.4.14 Western blot analysis for PARP 54
2.4.15 Caspase-3 protease assay 55
2.4.16 Fluorescent imaging of nanoparticle internalization 55
2.5 References 55-57

Chapter 3: Chimeric nanoparticle mediated targeting of PI3K signaling in combination with DNA damage. ***58-92***

3.1 Introduction 59
3.2 Results and Discussion
3.2.1 Development of cholesterol−drug conjugates 60
3.2.2 Development of ChNPs 60-63
3.2.3 Stability of the ChNPs 63-65
3.2.4 Release of Triple drugs from ChNPs 65
3.2.5 *In Vitro* cytotoxicity assay of ChNPs in cancer cells 66-71
3.2.6 Apoptosis induced by ChNPs 71
3.2.7 Cellular Internalization of ChNPs 72-77
3.2.8 Mechanism of action of ChNPs 77
3.3 Conclusion 78

3.4 Experimental Methods 79-83
3.4.1 Synthesis of conjugate (2) 79
3.4.2 Synthesis of cholesterol-PI103 conjugate (3) 79
3.4.3 Synthesis of cholesterol-doxorubicin conjugate (4) 80
3.4.4 Synthesis of aquated cisplatin (5) 81
3.4.5 Synthesis of cholesterol-cisplatin conjugate (6) 81
3.4.6 Synthesis of chimeric nanoparticles (ChNPs) 81
3.4.7 Determination of size, shape, and morphology of ChNPs 82
3.4.8 Stability of ChNPs 82
3.4.9 Quantification of drug loading in ChNPs 82
3.4.10 Release of triple drugs from ChNPs 82
3.4.11 Cell viability assay 82
3.4.12 FACS analysis for apoptosis detection 83
3.4.13 Cellular internalization by CLSM 83
3.4.14 General procedure for Western blot analysis 83
3.5 References 91-92

Chapter 4a: Self-assembled oleic acid nanoparticle mediated inhibition of mitogen activated protein kinase signaling in combination with DNA damage in cancer cells ***93-129***
4a.1. Introduction 94
4a.2 Results and Discussion 94
4a.2.1 Synthesis of oleic acid-drug conjugates 95
4a.2.2 Engineering self-assembled oleic acid nanoparticles (OA-NPs) 96-100
4a.2.3 Stability of OA-NPs 100-102
4a.2.4 Dual drug release 102-104
4a.2.5 *In vitro* cytotoxicity assay 104-106
4a.2.6 Induction of apoptosis 106
4a.2.7 Cellular internalization 107-113
4a.2.8 Mechanism of action 113
4a.3 Conclusions 114

4a.4 Experimental Section 114-119
4a.4.1 Materials 114
4a.4.2 Synthesis of oleic acid-AZD6244 conjugate (2) 115
4a.4.3 Synthesis of oleic acid-cisplatin conjugate (4) 115
4a.4.4 Synthesis of oleic acid-ethylenediamine conjugate (5) 116
4a.4.5 Synthesis of oleic acid-FITC conjugate (6) 116
4a.4.6 Synthesis of self-assembled oleic acid nanoparticles (OA-NPs) 117
4a.4.7 Determination of critical aggregation concentration (CAC) 117
4a.4.8 Determination of size, shape and morphology 117
4a.4.9 Stability 118
4a.4.10 Quantification of drug loading 118
4a.4.11 Determination of drug release 118
4a.4.12 Cell viability 118
4a.4.13 Cellular internalization 118
4a.4.14 Cellular internalization mechanism 119
4a.4.15 Apoptosis detection 119
4a.4.16: Detection of apoptosis by fluorescence activated cell sorting (FACS) 119
4a.4.17 Western blot analysis 117
4a.5. References 127-129

Chapter 4b: Targeting MAPK signaling Pathway in Colorectal Cancer Cells by Hyaluronic acid Cotaed Oleic acid Nanoparticles 130-153

4b.1. Introduction 131
4b.2 Results and discussion 132-148
4b.2.1 Engineering hyaluronic acid coated oleic acid nanoparticle 132-134
4b.2.2 Hyaluronic acid coating 134
4b.2.3 Drug release 135-137
4b.2.4 Stability 137
4b.2.5 Cellular internalization 138
4b.2.5.1 CD44 expression 138
4b.2.5.2 Cellular uptake by confocal microscopy 139
4b.2.5.3 Hyaluronic acid mediated cellular uptake by CLSM 140
4b.2.5.4 Hyaluronic acid mediated cellular uptake by FACS 141

4b.2.6 Mechanism of internalization
4b.2.6.1 Cellular uptake pathways by CLSM 141
4b.2.6.2 Cellular uptake pathways by FACS 142-143
4b.2.7 Inhibition of MAPK signaling with DNA damage
4b.2.7.1 Inhibition of MAPK signaling 144
4b.2.7.2 DNA damage 145
4b.2.8 Apoptosis and cell death 145
4b.2.9 Cell viability 146-148
4b.3 Conclusions 148
4b.4 Experimental section 148-151
4b.4.1 Materials 148
4b.4.2 Synthesis of oleic acid-drug conjugat 149
4b.4.3 Synthesis of hyaluronic acid cloaked oleic acid nanoparticles (HA-OA-NPs) 149
4b.4.4 Size, surface charge, shape and morphology determination of HA-OA-NPs 149
4b.4.5 Quantification of dual drug loading in HA-OA-NPs 149
4b.4.6 Determination of dual drug release from HA-OA-NPs 149
4b.4.7 Stability of HA-OA-NPs 150
4b.4.8 Determination of CD44 expression on cancer cells by flow cytometry 150
4b.4.9 Cellular internalization study by confocal microscopy 150
4b.4.10 Cellular internalization study by flow cytometry 151
4b.4.11 Western blot analysis 151
4b.4.12 Detection of apoptosis by flow cytometry 151
4b.4.13 *In vitro* cytotoxicity assay 151
4b.5 References 152-153

Chapter 5: Hyaluronic acid coated Chimeric Nanoparticle: Targeting MAPK-PI3K signalinghub in colon cancer cells 154-198

5.1 Introduction 155
5.2 Results and discussion 156-172
5.2.1 Engineering hyaluronic acid coated chimeric nanoparticle (HA-ChNPs) 156
5.2.1.1 Choosing drug combinations and vector 156

5.2.1.2 Synthesizing hyaluronic acid coated chimeric nanoparticles (HA-ChNPs)
156-160
5.2.2 Cellular uptake of HA-ChNPs 160-163
5.2.3 Mechanism of cellular internalization 163-167
5.2.4 Inhibition of PI3K and MAPK signalling 167-168
5.2.5 Cell cycle arrest and apoptosis 168
5.2.6 Cell viability assay 170-172
5.3 Conclusion 172
5.4 Materials and Methods 172
5.4.1 Material 172
5.4.2 Synthesis of Cholesterol-drug-Conjugates
5.4.2.1 Synthesis of Cholesterol-AZD6244 Conjugate (2) 172
5.4.2.2 Synthesis of Cholesterol-PI103-Conjugate (3) 173
and cholesterol-cisplatin conjugate (4) 173
5.4.2.3 Synthesis of Cholesterol-Ethylenediamine Conjugate (5) 173
5.4.2.4 Synthesis of Cholesterol-FITC Conjugate (6) 174
5.4.3 Synthesis of Hyaluronic acid coated Chimeric Nanoparticles (HA-ChNPs) 174
5.4.4 Size, surface charge, shape and morphology determination of HA-ChNPs 175
5.4.5 Quantification of triple drug loading in HA-ChNPs 175
5.4.6 Determination of triple drug release from HA-ChNPs 175
5.4.7 Cellular internalization study by confocal microscopy 175
5.4.8 Cellular internalization study by flow cytometry 176
5.4.9 Western blot analysis 176
5.4.10 Detection of apoptosis by flow cytometry 176
5.4.11 Cell Cycle Analysis 176
5.4.12 *In vitro* cytotoxicity assay 176
5.5 References 181-182
Synopsis 183-185

List of Publications

1. **S. Palvai,** L. Anandi, M. Bessy, S. Roy, M. Lahiri, S. Basu. Drug-Triggered Self-Assembly of Linear Polymer into Nanoparticle for Simultaneous Delivery of Hydrophobic and Hydrophilic Drugs in Breast Cancer. *ACS Omega,* **2017**, ***2,*** 8730–8740**.**

2. **S. Palvai,** M. M. Kuman, S. Basu. Hyaluronic Acid Layered Chimeric Nanoparticles: Targeting MAPK-PI3K Signaling Hub in Colon Cancer Cells. *ACS Omega* **2017**, *2*, 7868-7880.

3. **S. Palvai,** M. M. Kuman, and S. Basu. Hyaluronic Acid Cloaked Oleic acid Nanoparticle Inhibits MAPK Signaling with Sub-cellular DNA Damage in Colon Cancer. *J. Mater. Chem. B*, **2017**, *5*, 3658-3666.

4. **S. Palvai**, P. More, N. Mapara, J. Nagraj, R. Chowdhury and S. Basu. Self-Assembled Oleic Acid Nanoparticle Mediated Inhibition of Mitogen-Activated Protein Kinase Signaling in Combination with DNA Damage in Cancer Cells. *ChemNanoMat*. **2016**, *2*, 201-211.

5. **S. Palvai** and S. Basu. Biocompatible Vitamin D3 Nanoparticles in Drug Delivery. DOI number: 10.5599/obp.8.16 **(Book Chapter)**

6. **S. Palvai**, P. More, N. Mapara, and S.Basu. Chimeric Nanoparticle: a Platform for Simultaneous Targeting of Phosphatidylinositol-3-kinase Signaling and Damaging DNA in Cancer Cells. *ACS Appl. Mater. Interfaces* **2015**, *7*, 18327–18335.

7. **S. Palvai**, J. Nagraj, N. Mapara, R. Chowdhury and S. Basu. Dual drug Loaded Vitamin D3 Nanoparticle to Target Drug Resistance in Cancer. *RSC Advances* **2014**, 4, 57271-57281.

8. R. K. Koninti, **S. Palvai**, S. Satpathi, S. Basu, and P. Hazra. Loading of an Anti-cancer Drug into Mesoporous Silica Nano-channels and its Subsequent Release to DNA. *Nanoscale* **2016**, *8,* 18436-18445.

9. S. Ellipilli, **S. Palvai** and K.N. Ganesh. Fluorinated Peptide Nucleic Acids with Fluoroacetyl Side Chain Bearing 5-(F/CF3)-Uracil: Synthesis and Cell Uptake Studies. *J. Org. Chem.* **2016**, *81*, 6364-6373.

10. S. Patil, M. M. Kuman, **S. Palvai** and S. Basu. Impairing the Powerhouse in Colon Cancer Cells by Hydrazide-hydrazone Based Small Molecule. ***(****ACS Omega, Accepted****).***

Thesis Abstract

In recent years, phosphatidylinositol 3-kinase (PI3K) and mitogen activated protein kinase (MAPK) signaling pathways have received enormous attention as a target for cancer therapeutics since they are deregulated in many human cancers. Numerous small molecules were designed to inhibit the key players of these pathways. However, small molecule therapy is limited owing to emergence of drug resistance (extrinsic or intrinsic) and lack of specificity to tumor tissue which leads to off-target toxicity. To overcome these, in my thesis I have focused on inhibiting signaling pathways with simultaneous downstream DNA damage in cancer cells by merging the expertise of chemical biology and nanotechnology. In the following chapters, I have engineered nontoxic, biodegradable lipidic nanoparticles comprising signaling inhibitors and DNA-damaging agents together, which we expect to be accumulated in tumor tissue via enhanced permeability and retention (EPR) effect and receptor mediated endocytosis, internalize into the cancer cells and release their payloads to inhibit these signaling pathways simultaneously by inducing DNA damage.

Chapter 1 summarizes the role of PI3K and MAPK in tumor genesis in different cancers and emergence of signaling pathways as potential target in cancer therapy. We highlighted the efforts made to inhibit these signaling pathways by small molecule kinase inhibitors, their limitations, necessity and advantage of combination therapy of signaling inhibitors and DNA damaging agents and challenges in using these combination therapies in the clinics. We also highlighted the role of nanotechnology and current efforts made to achieve the successful inhibition of PI3K and MAPK signalings in various cancer cells by nanotechnology platforms. Finally, this chapter describes importance of inhibition of PI3K and MAPK signaling in combination with DNA damaging agents by nanotechnology platforms and the aim of thesis.

Chapter 2 describes the synthesis of nontoxic vitamin D3 nanoparticles comprising PI3K inhibitor (PI103) in combination with DNA damaging drugs (cisplatin/ doxorubicin/proflavine). We characterized these nanoparticles by by light scattering and electron microscopy techniques which proved particles are in spherical shape with sub 200 nm size. A slow and sustained release of drugs from NPs was observed over a period of time rather burst release at tumor physiological pH = 5.4. These nanoparticles showed improved efficacy in synergistic manner in human hepatocellular carcinoma cells (Hep3B), as well as cisplatin

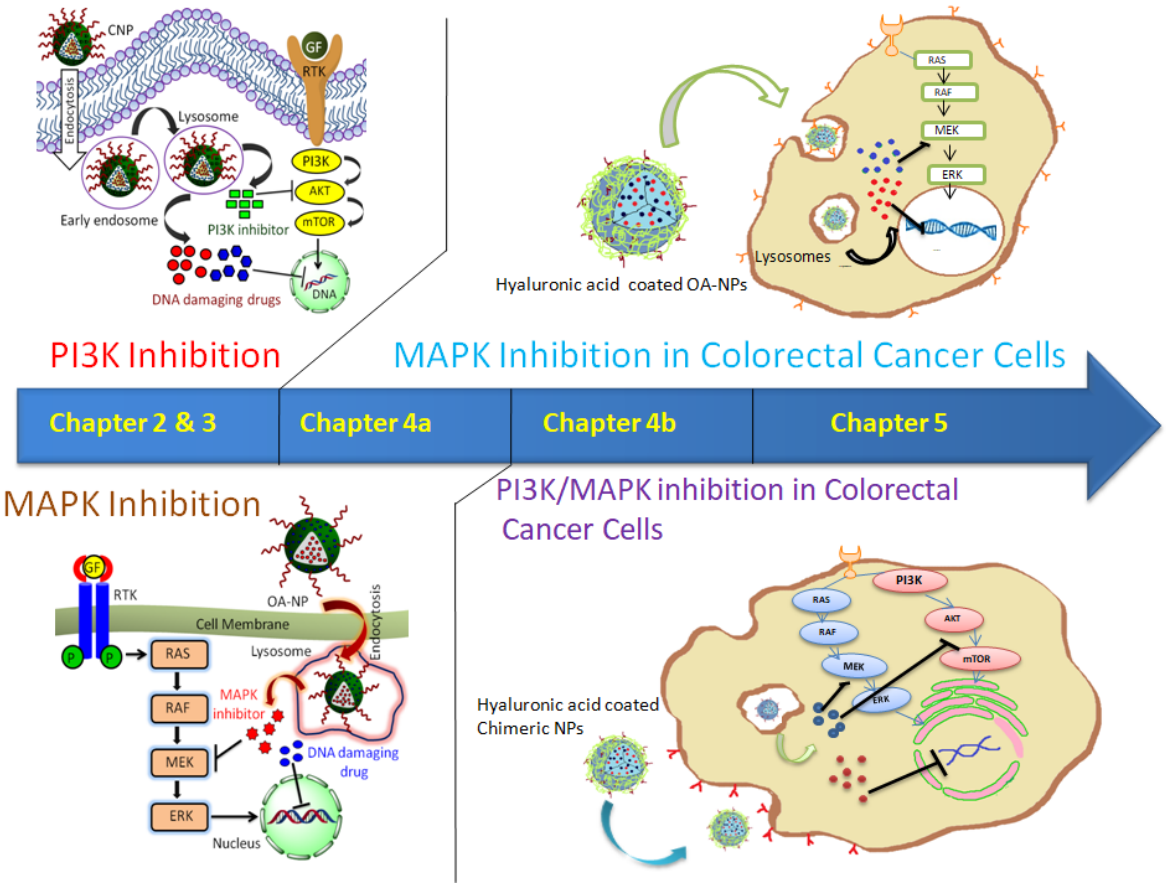

Fig. 1 Schematic diagram of inhibiting signaling pathways in cancer cells by multi drug loaded nanoparticle.

resistant-Hep3B (Hep3B-R) cells compared to monotherapy by inducing apoptosis through a DNA damaging mechanism. Finally, vitD3–PI103–proflavine-NP internalized into Hep3B-R cells considerably faster compared to Hep3B cells, as visualized by fluorescent microscopy.

Chapter 3 reports triple drug (PI103, cisplatin, and doxorubicin) loaded cholesterol based chimeric nanoparticle (ChNPs) to inhibit PI3K signaling with simultaneous DNA damage (Fig. 1) in various cancer cells including drug resistant cells and to achieve improved therapeutic efficacy. All three drugs were chemically conjugated to biocompatible cholesterol and formulated into chimeric nanoparticles (ChNPs). A ratiometric drug loading of all three drug conjugates in ChNPs was obtained. Confocal laser scanning microscopy (CLSM) imaging revealed that these ChNPs were internalized into sub-cellular lysosomes through endocytosis in a time dependent mode over 6 h and retained inside for 48 h in HeLa, MDA-MB-231, and MCF7 cells. ChNPs inhibited PI3K pathway by downregulating pAKT and

damaging DNA in HeLa cells also induced apoptosis. Interestingly, ChNPs induced improved cytotoxicity in all these cancer cells compared to free drug combination and this effect was even more severe in drug resistance cells.

Chapter 4 was subdivided in to two chapters.

Chapter 4a deals with successful targeting MAPK signaling with simultaneous DNA damage in cancer cells. We engineered novel nontoxic oleic acid nanoparticles (OA-NPs) comprising MEK inhibitor (AZD6244) and DNA damaging agent (cisplatin) to target MAPK signaling in cancer cells. Drug molecules were chemically conjugated to oleic acid and were co-self-assembled into 120 nm sized particles. OA-NPs showed controlled release of drugs at tumor pH mimic (pH = 5.5). These OA-NPs internalized into HeLa cells by macropinocytosis pathway and inhibited MAPK signaling, induced DNA damage in cervical cancer cells. Moreover, NPs showed enhanced cytotoxicity in several cancer cells including drug resistant ones.

Chapter 4b further focuses on targeting MAPK signaling selectively in colorectal cancer cells where MAPK signaling pathway is highly up regulated. To this end we have decorated OA-NPs surface with hyaluronic acid polysaccharide to target CD44 receptors over-expressed on the colorectal cancer cell surface (Fig. 1). Interestingly, HA coated OA-NPs were internalized into CD44 receptor over-expressed colon cancer cells (HCT116) *via* CD44 receptor-mediated and clathrin-mediated endocytosis. Theses NPs inhibited phosphorylation of extracellular signal-regulated kinases (ERK1 and ERK2) and damaged sub-cellular DNA to induce remarkable colon cancer cell (HCT-116 and DLD-1) death in contrast to free drug cocktail at 24 h post incubation.

Chapter 5 deals with simultaneous targeting of both PI3K and MAPK signaling together in colon cancer cells (Fig. 1). Crosstalk between PI3K and MAPK pathway often would lead to failure of monotherapy where a single pathway is targeted. To address this, we have engineered hyaluronic acid coated chimeric nanoparticles (HA-ChNPs) which contain PI3K and MAPK signaling inhibitors (PI103 and AZD6244) and a DNA damaging agent (cisplatin). All three drugs were chemically conjugated to cholesterol and co-self-assembled into chimeric nanoparticles which were further coated with hyaluronic acid. These HA-ChNPs internalized into cells by receptor-mediated endocytosis and caused cell death at much lower IC_{50} values compared to free drug mixture. HA-ChNPs induced apoptosis and

demonstrated cell cycle arrest at G1 phase by successfully inhibiting both PI3K and MAPK pathway in colon cancer cells.

Chapter 1

PI3K and MAPK Signaling in Cancer and Targeting by Nanoplatform

1.1 History of Cancer

Cancer is a major health problem and the second most common cause of death worldwide after cardiovascular disease.[1] According to the International Agency for Research on Cancer (IARC), in 2012 there were 8.2 million cancer deaths and 14.1 million new cancer cases worldwide. It was estimated that, by 2030, the global burden could grow to 21.7 million new cancer cases and 13 million cancer deaths.[2]

Cancer is defined as an abnormality in cell division leading to uncontrolled growth to develop a tumor (Fig. 1).[3] Cancer can develop in any of the body's tissues, there are more than 200 different types of cancer, and can be grouped based on the type of the cell they start growing in.[4,5] Almost all the cancers have similar basic characteristics with tissue specific unique features.[6] All types of cancer cells continuously grow divide and re-divide by avoiding cell death and form new abnormal cells. An invasive tumor (malignant) in later stages translocate to other parts of the body through the blood circulation and begin to grow at new tissue (metastasis).[7]

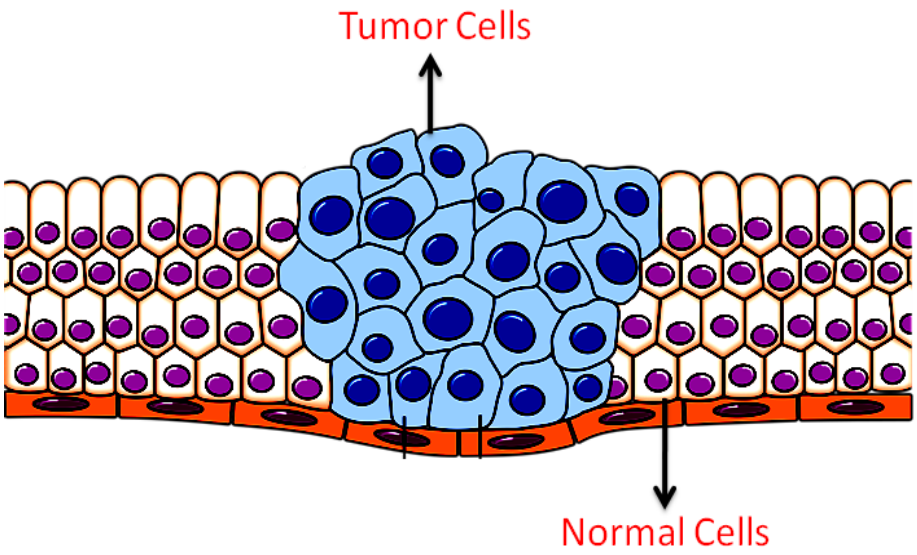

Fig. 1 Schematic diagram of cancer and normal cells.

Initiation and progression of the cancer is caused by both several external factors (radiation, chemicals, tobacco, and infectious organism) and internal factors within the cell (mutations that occur from metaboloism, harmones, inherited mutations etc.) However, in most of the cancers it takes months and years to accumulate these mutations in the DNA and to become

detectable. The phenomenal research in the last 50 years cancer biology has provided us the insights into how cancer cells develop.

1.2 Hallmarks of Cancer

Generally, most tumors arise as a consequence of genetic or epigenetic alterations in the cells.[8-10] Mutations to DNA in the cells and therefore, changes to the genes involved in cell

Fig. 2 Hallmarks of cancer.

maintenance such as proto oncogenes, tumor suppressor genes, suicide genes, and DNA-repair genes push that particular cell to undergo uncontrolled growth.[11, 12] Most of the time DNA damage in healthy cells can be repaired. Unfortunately, in cancer cells, gene mutations make the cell incapable of correcting DNA damage and unable to commit suicide (programmed cell death) leading to uncontrollable cell growth.[13] With these abnormalities, tumor cells develop several distinct features across time such as sustaining proliferative signaling, evading growth suppressors, resisting cell death, enabling replicative immortality, inducing angiogenesis, and activating invasion and metastasis which are defined as

"*Hallmarks of Cancer*" by D. Hanahan and R. Weinberg (Fig. 2).[14] All the "*Hallmarks of Cancer*" are tightly regulated by signaling pathways that control cell growth and division, cell death, cell fate, and cell motility. Mutations in the proto oncogenes are common in all kind of cancers which lead to the over-activation of the proteins involved in the growth promoting signaling pathways.[15-20] Thus, the cell proliferation occurs at much faster than it would in the un-mutated cell.

1.3 Cell signaling pathways

Cellular signaling pathways are complex networks which are highly interconnected with each other (Fig. 3).[21] There are large number of intracellular signaling pathways receive information from different growth factors at the cell surface through the receptor proteins which are embedded in the plasma membrane and integrate these information to regulate diverse biological processes including protein synthesis, cell growth, differentiation, cell architecture and polarity, motility, and programmed cell death (apoptosis).[22, 23]

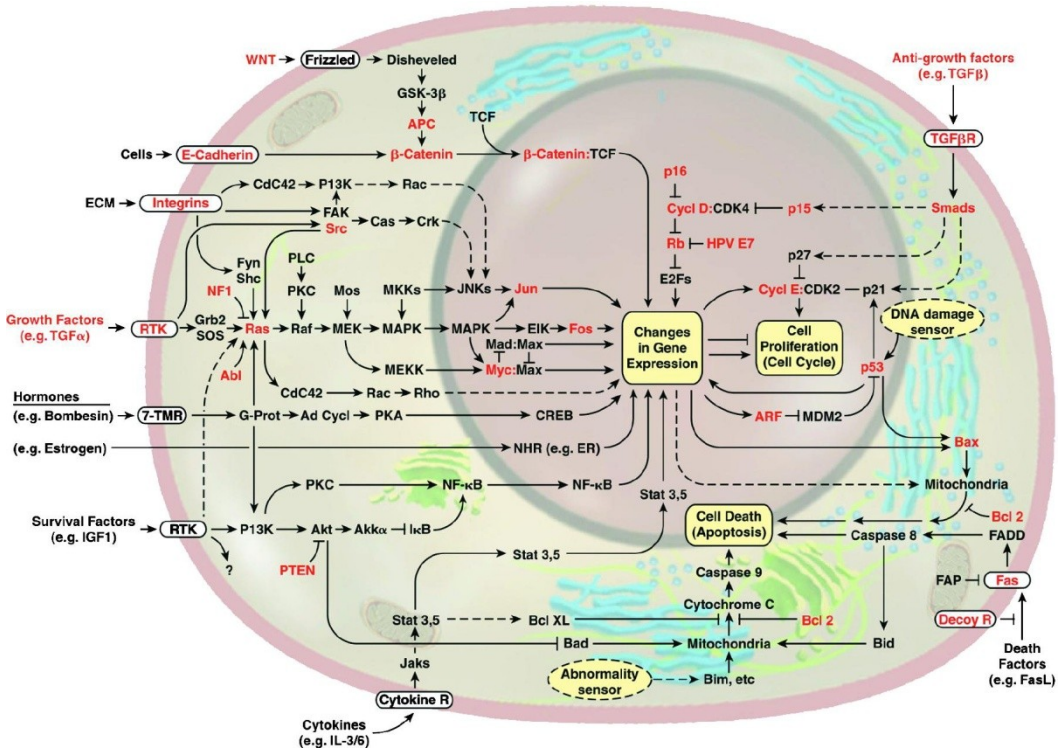

Fig. 3 The cell signaling network (*Cell*, 2000, **100,** 57-70. *Reprinted with the permission from Cell Press. Copyright © 2000*).

Typically, such signaling is triggered with a growth factor (a protein that stimulates division) binding with the cell surface receptors leading to a conformational change in the trans-membrane domain. Subsequently, a stimulatory signal was conveyed to the proteins in the cytoplasm. Further, these proteins transmit stimulatory signals to the nucleus through a series of interaction with other proteins in the cell. Finally, this division-promoting message in the cell's nucleus activates a set of genes that promote different cellular functions like division, growth, proliferation, differentiation and so on. Mutations in the proto oncogenes, which code the proteins involved in these signaling pathways cause overproduction of growth factors. These factors stimulate the growth of neighboring cells as well as, the cells that just produced through autocrine and paracrine signaling. Some other oncogenes produce aberrant receptor proteins that continuously release stimulatory signals into the cytoplasm even in the absence of growth factors in the environment. Moreover, several other oncogenes disturb components of the signal cascade in such a way that the nucleus in the cell continuously receives stimulatory messages, even when growth factor receptors are not involved in triggering them. Phosphatidylinositol-3-kinase (PI3K) and mitogen-acivated protein kinase (MAPK) signaling pathways are major survival and growth signaling cascades of a cell.[24-28] PI3K-AKT-mTOR and RAS-RAF-MEK-ERK pathways are the most studied and commonly deregulated pathways in many cancers such as lung, breast, colorectal, pancreatic cancers and melanoma.[28-31]

1.3.1 Phosphatidylinositol-3-kinase (PI3K) signaling: Phosphatidylinositol-3-kinase (PI3K) is a family of lipid kinases, a major signaling cascade downstream of growth factor receptor tyrosine kinases (RTKs). Upon activation by growth factor stimulation through RTKs on the cell surface, PI3K catalyzes the phosphatidylinositol-3,4,5-triphosphate (PtdIns (3,4,5) or PIP3) production from phosphatidylinositol-4,5-triphosphate (PtdIns (4,5) or PIP2).There are four well-described isoforms of Class I PI3K (a, b, d and g encoded by PIK3CA, PIK3CB, PIK3CD and PIK3CG respectively) which catalyze the phosphorylation on 30 position of the inositol ring of phosphoinositides, and most importantly, the conversion of PIP2 to the second messenger PIP3. This in turn, activates a number of different proteins mainly the serine/threonine kinase Akt (also known as protein kinase B) in the cell. The activated Akt, further, modulates downstream signaling including stimulation of mammalian target of rapamycin (mTOR). The net effect of PI3K-Akt signaling is inhibition of apoptosis, growth, motility, and stimulation of cell proliferation (Fig. 4).[25, 32] Phosphatase and tensin

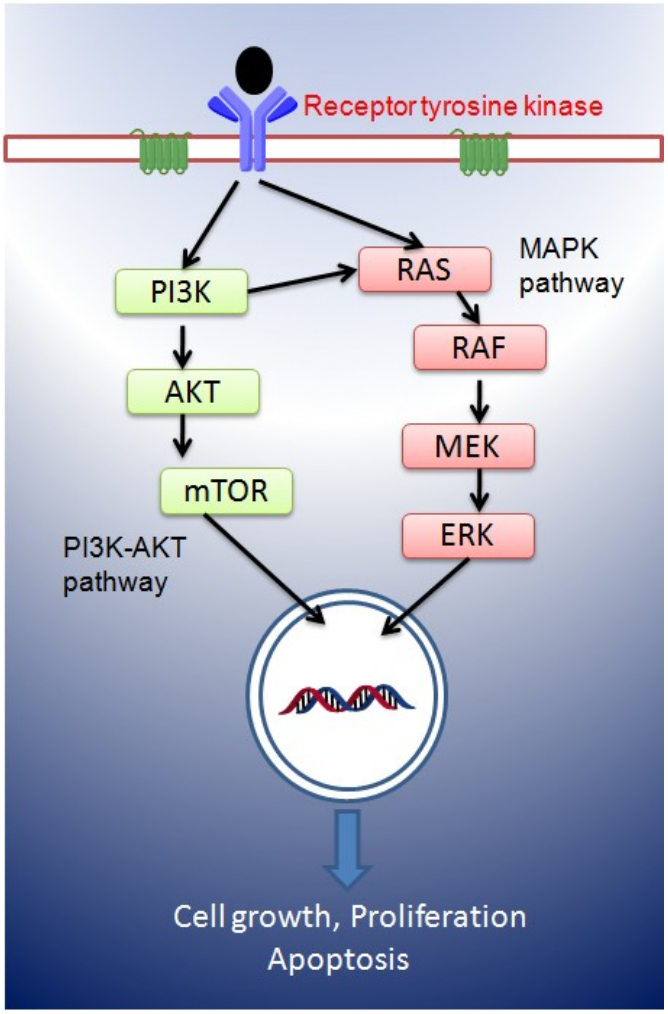

Fig. 4 Schematic diagram of PI3K-akt-mTOR and Ras-Raf-Mek-Erk (MAPK) pathways.

homolog (PTEN), major tumor suppressor, is a negative regulator of the PI3K pathway, which dephosphorylates PIP3 to PIP2.

It is invariably found that PI3K-Akt pathway is "switched on" in cancers since it is central to many aspects of cell growth and survival. PI3K signaling and its components are the most perturbed pathway in human cancers (Table 1).[31, 33, 34] The alterations include mutations in the *PIK3CA* gene, encoding the p110 catalytic subunit of PI3K, is commonly found in more than 50 % of bowel cancers and 26 % of all breast cancers. Loss of expression of *PTEN* is found in more than 50 % of all cancers, including melanoma, glioma, and prostate cancer. *AKT* amplification, overexpression, and mutation, are commonly found in breast, head and neck, pancreatic, gastric, ovarian, and colorectal cancers.[35-40]

1.3.2 Mitogen-activated protein kinase (MAPK) signaling: The mitogen-activated protein kinase (MAPK) pathway is another crucial signaling cascade consisting of RAS, RAF, mitogen-activated and extracellular-signal regulated kinase kinase (MEK), and extracellular signal-regulated kinase (ERK). The MAPK signaling cascade is activated by several growth factors and hormones through their cognate tyrosine kinase receptors (RTKs).[41] Ligand binding to RTKs results in activation of RAS, leading to phosphorylation of RAF followed by downstream activation of MEK and ERK. Finally, these signaling cascades mediate important cellular functions mainly cell survival, protein synthesis, mitosis, and differentiation (Fig. 4).[42-44] Moreover, the RAS-RAF-MEK-ERK pathway is also able to stimulate angiogenesis through changes in the gene expression that

Gene	Alteration	Tumor type	Frequency (%)
PIK3CA	Mutation	Breast	25%
		Endometrial	26%
		Urinary tract	21%
		Colon	12%
		Ovarian	10%
	Amplification	Head and neck	42%
		Squamous cell lung	66%
		Gastric	36%
		Colon	37.9%
		Breast	9%
PIK3R1	Mutation	Glioma	4 %
		Colon	3 %
AKT1	Mutation	Colon	1 %
		Breast	4 %
		Ovarian	1 %
		Lung	0 %
	Amplification	Gastric	20%
		Breast	1%
AKT2	Mutation	Colon	1%
		Breast	0 %
	Amplification	Pancreas	20%
		Ovarian	14.1%
		Breast	3%
AKT3	Mutation	Melanoma	1.5%
	Amplification	Breast	9.9%
PTEN	Monoallelic mutation	Glioma	75%
		Colon	20%
		Breast	40 – 50%
		Lung	37%
		Prostate	42%
	Biallelic mutation	Endometrial	50%
		Glioblastoma	30%
		Prostate	10%
		Breast	5%

Table 1. Genetic alterations of the PI3K pathway (*Expert Opini. Ther. Targets*, 2012, **16**, S17-S27. *Reprinted with the permission from Taylor & Francis, copyright © 2018*).

Tumour type	Pathway mutations[43]
Breast	–
Colon	KRAS (45%), BRAF (12%)
Pancreatic	KRAS (90%)
Ovarian	BRAF (30%)
Prostate	–
Melanoma	NRAS (15%), BRAF (66%)
Non-small-cell lung	KRAS (35%)
Glioma	–
Papillary thyroid	HRAS,KRAS and NRAS (60%); BRAF (35–70%)
ALL, AML	NRAS (30%)

Table 2. Human tumors exhibiting activated RAS–MAPK signaling. (*Nat. Rev. Cancer,* 2004, **4**, 937-947. *Reprinted with the permission from Springer Nature, Copyright © 2004*)

is involved in the formation of the new blood vessels. MAPK pathway is deregulated in many cancers. RAS is the most mutated oncogene in many human cancers, K-Ras mutations are found in 72–90 % of pancreatic cancers, 45 % of colon cancers and 15-50 % of lung cancers.[45]

1.4 Challenges in targeting PI3K and MAPK signaling in cancer

The fact that PI3K and MAPK signaling pathways are upregulated in many cancers and promote cell proliferation, survival and metastasis in cancer made it is apparent that components of these pathways have become major targets for innovative anticancer drug development.[33, 46-50] Researchers have developed several effective inhibitors specific for the key components of PI3K and MAPK pathways. PI3K inhibitors include NVP-BEZ235, PI103 (dual AKT/mTOR inhibitor), LY29004, Wortmannin, PX-866 (PI3K, other related kinases), A-443654, GSK690693 (AKT inhibitor) and rapamycin (mTOR inhibitor).[51-57] MAPK pathway inhibitors include AZD6244, PD0325901, XL518 and ARRY-142886 (MEK inhibitor), PLX-4720, PLX 4032 and SB-590885 (mutant B-Raf specific inhibitor).[58-62] Most of these inhibitors are currently being used for therapy while others are under evaluation in clinical trials. Despite tremendous progress, clinical translation of small molecule signaling inhibitors still seems to be challenging. One major reason is that many tumors escape single kinase inhibition by developing several extrinsic or intrinsic drug resistance mechanisms after drug treatment.[63, 64] The intrinsic drug resistance mechanism emerges from the already

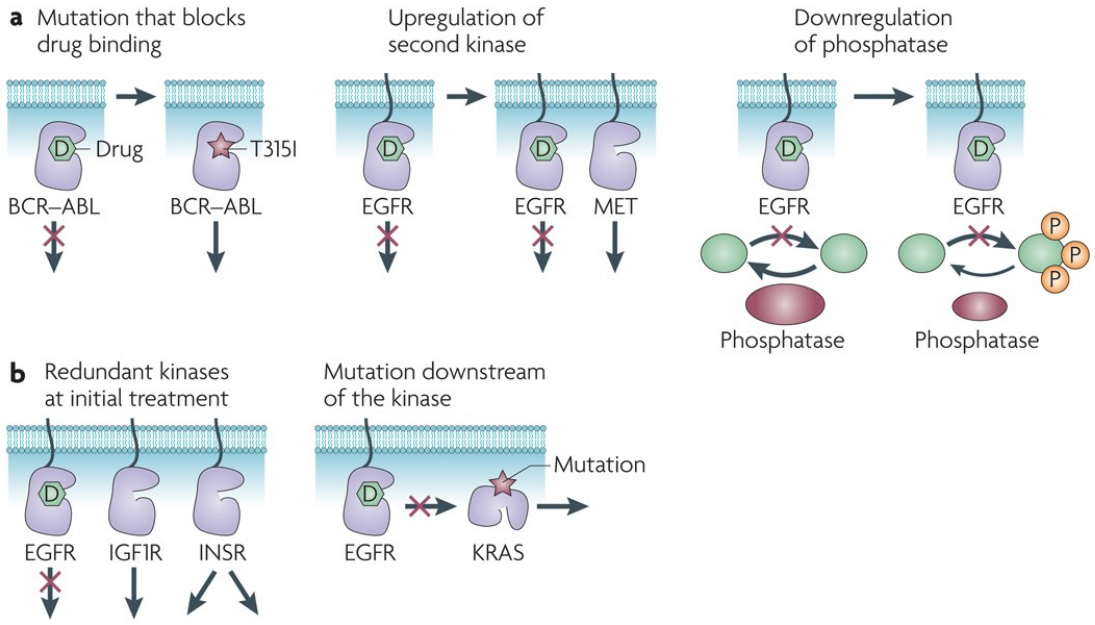

Fig. 5 Mechanism of acquired (a) and intrinsic resistance (b). *(Nat. Rev. Cancer*, 2010, **10**, 130-137. *Reprinted with the permission from Springer Nature, Copyright © 2010)*

existing multiple signaling pathways that bypass the drug target and extrinsic resistance mechanism include down-regulation of phosphatases (tumor suppressors) and activation of surrogate kinases that can be substituted for the drug target during treatment (Fig. 5).[65-69] Furthermore, the therapeutic window of these PI3K and MAPK inhibitors is narrow because healthy cells also require PI3K/MAPK signaling for survival and proliferation resulting in severe adverse effects including cardio-toxicity, developmental dis-regulation and metabolic disorders linked to carbohydrate intake.[70]

To overcome these resistance mechanisms, it is highly required to target cancerous cells at multiple levels to achieve enhanced therapeutic results. One of the promising approaches is using a combination regimen of signaling (PI3K/MAPK) inhibitors and DNA-damaging agents.[71-74] For example, in PTEN deficient cells high PI3K survival signaling in the cells protects them from accumulated DNA damage, which renders tumor cells sensitive to the combination of PI3K inhibitors and DNA-damaging agents in preclinical studies.[75] Schult et al. identified that the dual phosphatidylinositol 3-kinase (PI3K) and mammalian target of rapamycin (mTOR) inhibitor NVP-BEZ235 have exerted improved antitumor activity *in vitro* when it was combined with cytotoxic drugs such as cytarabine, doxorubicin or dexamethasone compared to single-drug treatment.[76] On the other hand, Huynh et. al.

reported that MEK inhibition by AZD6244 in combination with DNA damaging agent (doxorubicin) resulted in improved tumor volume reduction than free AZD6244 treatment alone.[77] Yang et al. also validated that combination of sorafenib (multikinase inhibitor, Raf inhibitor) with DNA damaging agent (cisplatin) resulted in synergistic inhibition of tumor cell proliferation.[78]

Despite several advantages of combination chemotherapy, conventional "cocktail" administration of drugs still face several hurdles and require significant improvements to be successful in clinical trials. While *in vitro* cellular studies have generated promising results for combinatorial regimens, their clinical successes are often limited with little improvement in efficacy and augmented toxic side effects to the patients.[79] Another major limiting factor of clinical success of combination chemotherapy is inherent diverse pharmacokinetics among different drug molecules. Upon systemic administration, due to distinctive physiological fate of drug molecules they undergo non-uniform bio-distribution leading to divergences in tissue distribution of each drug, which hampers the benefit of combination therapy. Thus controlling the therapeutic cocktails that reach the diseased tissues and cells in appropriate concentrations became a major clinical challenge. Furthermore, due to lack of tissue specificity conventional mixture of cancer therapeutic molecules distributing non-specifically in the human body, thus affect both cancerous and non-cancerous healthy cells. This non-specific bio-distribution results in excessive toxicity to healthy cells, tissues, and organs finally ends up with several adverse side effects including neurotoxicity, nephrotoxicity, cardiotoxicity, developmental disorders, hair loss, organ dysfunction, and weakness, leading to a poor quality of life for the cancer patients. For example, the majority of MEK inhibitors effectiveness was limited in clinical trials due to their side effects including cardiotoxicity, skin rash and visual disturbances. Common side effects of AZD6244 (MEK inhibitor) include diarrhea, vomiting, nausea, and swelling of the body.[80] DNA-damaging agents, such as cisplatin, carboplatin, and doxorubicin usage is significantly limited by nephrotoxicity, myelosuppression and cardiotoxicity respectively. Furthermore, conventional chemotherapy also suffers from inadequate accessibility of drug molecules to tumor tissue, rapid abolition, and poor solubility. To overcome these problems associated with conventional chemotherapy and to obtain full potential of combination therapy, researchers have used nanotechnology-based platforms for the co-delivery of drugs with similar/ different physiochemical properties to the diseased sites.[81]

1.5 Cancer nanomedicine

1.5.1 Nanotechnology platforms in cancer therapy: Nanotechnology deals with 1 to 1000 nm sized materials (Fig. 6) and the term "Nanotechnology" was first used by Taniguchi in 1974.[82] The advent of nanotechnology has offered unprecedented applications in various fields including nanotechnology-based medicine (nanomedicine).

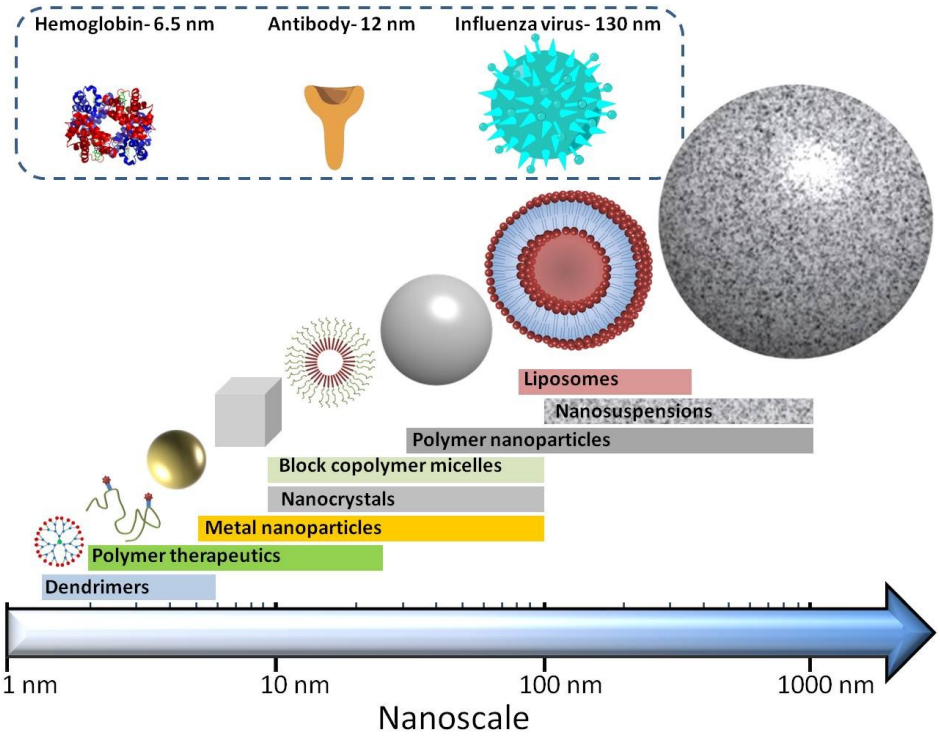

Fig. 6 This illustrative figure shows the different structures of nanomedicines and their approximate sizes. *(Adapted from http://www.britishsocietynanomedicine.org/what-is-nanomedicine.html)*

Nanomedicines are extensively used to improve the therapy and quality of lives of patients suffering from several diseases including different types of cancer, nephrological disorders, fungal infections, multiple sclerosis, chronic pain, and emphysema. Nanomedicines play a crucial role especially in drug delivery by packing drugs (small molecules, antibodies, proteins and siRNAs) into nanometer size platforms, ensuring therapeutic amount of the drug accumulation to the areas that require treatment in the body. Nanoscale particles have offered more favorable pharmacokinetic and pharmacodynamic profiles as compared to conventional

drugs. Several nanomedicines were already approved by U.S. Food and Drug Administration (FDA) to treat several types of cancers and are available in the market. Doxil, the first approved nanomedicine by the FDA is being used to treat ovarian cancer

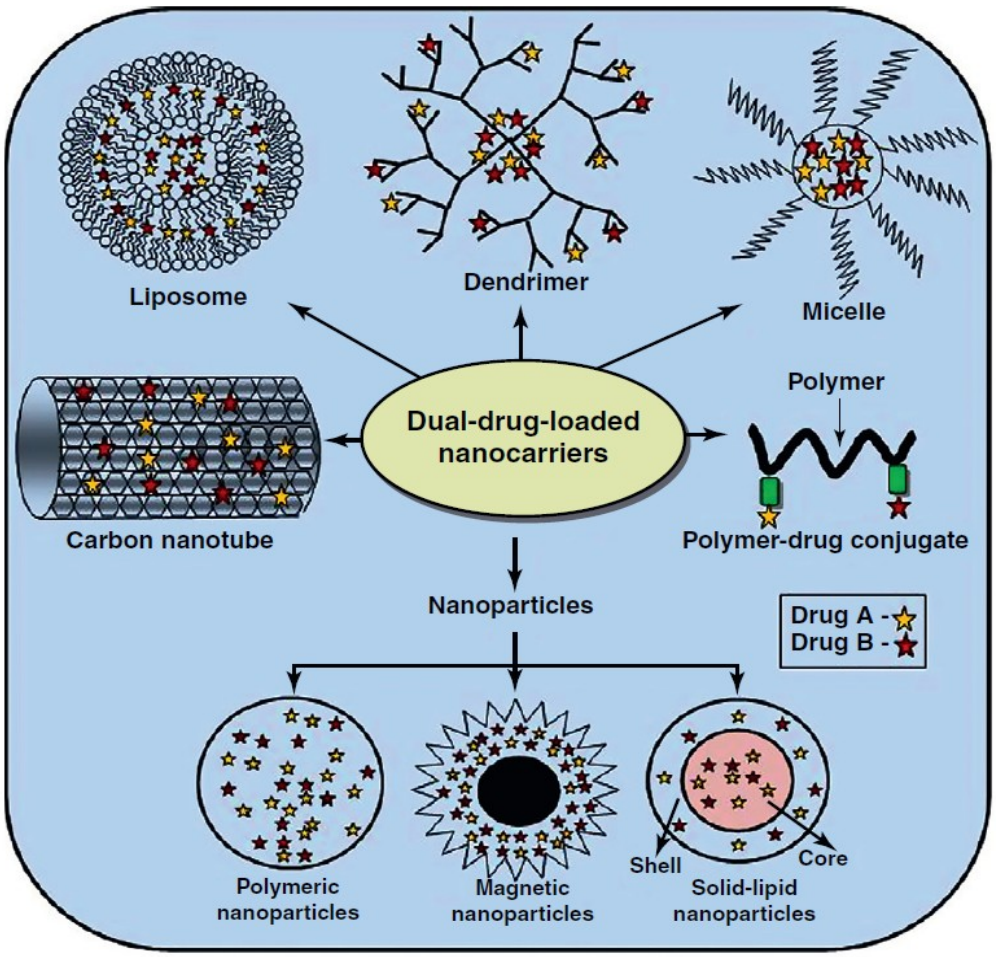

Fig. 7 Diagrammatic representation of different types of nanocarriers for combination drug delivery (*Drug Discov. Today*, 2012, **17**, 1044-1052. *Reprinted with the permission from Elsevier Ltd, Copyright © 2012*).

and multiple myeloma.[83] Later several other nanomedicines have been approved by FDA such as Abraxane (albumin-bound paclitaxel nanoparticle) and Onivyde (liposome-encapsulated irinotecan) to treat breast and metastatic pancreatic cancer respectively. Several other nano-formulations are currently in different stages of clinical trials.[83]

Recently, nanocarriers are attaining increasing attention for their tremendous ability of co-encapsulating multiple therapeutic agents into a single carrier for synchronized delivery into diseased tissues.[84-86] Various nano-platforms such as liposomes, dendrimers, polymeric micelles, mesoporous silica particles, carbon materials (carbon dots, graphene oxide, nanodiamond and carbon nanotubes) and solid lipid nanoparticles have been developed to carry broad classes of therapeutics having diverse pharmacokinetics.[87-92]

1.5.2 Advantages of nanoparticle-mediated co-delivery of drugs

1. Vehicle uniformity: Conventional cocktail chemotherapy fails to achieve optimum concentrations in tumor tissues due to the inherently different pharmacokinetic among different drugs, nanotechnology-based combination chemotherapy can achieve uniformity *in vivo* pharmacokinetics of different chemotherapeutics by co-encapsulating multiple drugs inside a single carrier.[93, 94]

2. Passive and active targeting: Nanodelivery systems mitigate cytotoxicity to normal tissues while enhancing synergistic cytotoxicity by accumulating and delivering their payloads specifically at tumor tissue by passive or active targeting methods. Passive targeting exploits the characteristic leaky vasculature of tumors to allow nanocarriers to extravasate (escape) into the tumor tissues and allows them to release drugs whereas, free drugs may diffuse non-specifically throughout the body. This mechanism is collectively known as enhanced permeability and retention effect (EPR effect), which was proposed by Maeda and colleagues.[95] Several experiments carried out by using liposomes of different mean size indicated that the threshold nanoparticle size for extravasation into tumors is ~400 nm, while other studies have proved that particles with diameters <200 nm are more efficient to get accumulated in tumor tissue by exploiting EPR effect.[96] Another way of targeting tumor tissues selectively is by using active targeting strategy, where nanoparticle surface is modified with targeting agents such as ligands, which bind to a particular overexpressed receptor on the cell surface. Several targeting ligands such as antibodies, antibody fragments, peptides, aptamers, whole proteins (e.g., transferrin) natural polymers and different small molecules (e.g., folic acid, biotin) have been used to target nanoparticles actively. [97]

3. Protection from biological barriers: Conventional chemotherapeutic agents often get cleared from blood circulation by macrophages thus their short circulation time is insufficient to reach and kill the cancer cells. Nanoplatforms protect drugs from premature degradation before reaching intended sites, increase blood circulation time, and bioavailability of the drug

molecules. Poor solubility of the drug molecules is another problem of conventional chemotherapy which makes them unable to cross the biological membrane. Most of the anticancer drugs are hydrophobic and exhibit poor solubility, which results in reduced bioavailability. Nanoparticles can efficiently increase the solubility of the drugs. Several lipidic and polymeric nanoformulations improved the solubility of hydrophobic drugs by encapsulating them inside the particle. [98-102]

A multidrug resistance protein, p-glycoprotien (Pgp) is another major barrier for the drug molecules. Pgp is overexpressed on the cancer cell surface and prevents drug accumulation inside the cell by acting as an efflux pump thus develops drug resistance. Several studies proved that nanoplatforms can overcome Pgp mediated drug resistance by directly introducing the drug molecules inside the cells without triggering Pgp pump. One strategy is to incorporate both chemotherapeutic agent and Pgp inhibitor such as verapamil in a single nanocarrier to overcome P-glycoprotein mediated drug resistance.[103-107]

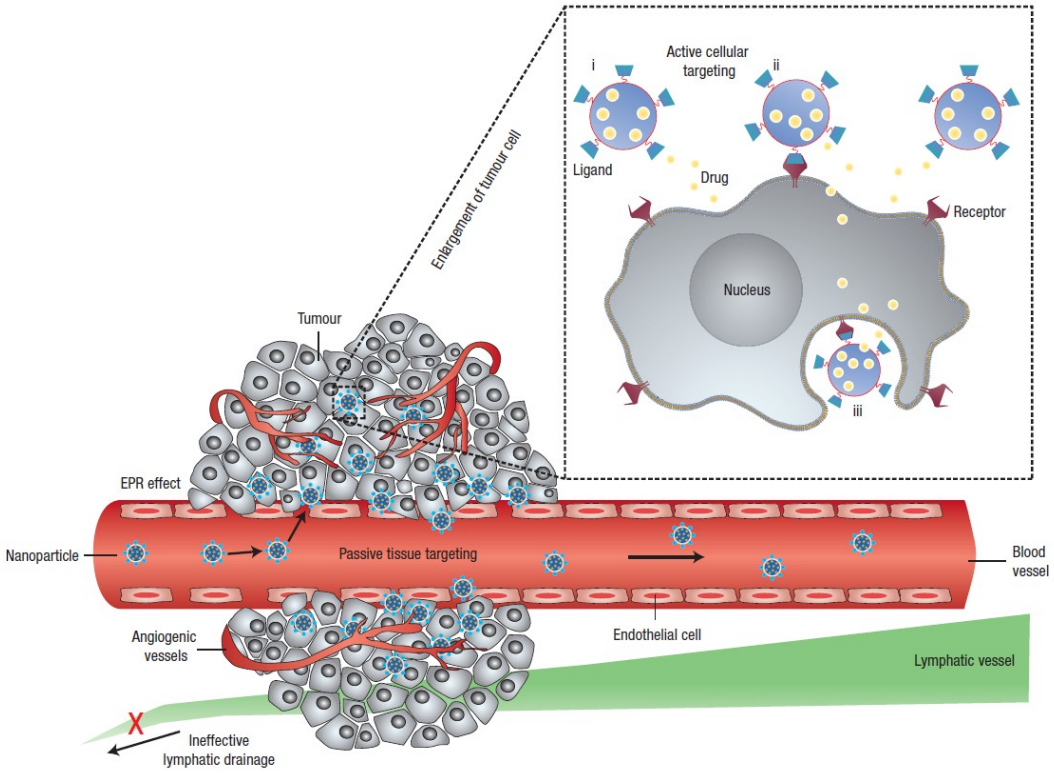

Fig. 8 Schematic diagram of enhanced permeation and retention effect (EPR), passive and active targeting of nanoparticles in tumor tissue. (*Nat. Nanotechnol*, 2007, **2**, 751–760. *Reprinted with the permission from Springer Nature, Copyright © 2007*).

4. Controlled loading and release: Although combination therapy is efficacious not all the ratios of drugs result in synergistic effects. It is evident that only certain ratios of combined agents can give synergistic effects, while other ratios of the same drugs are only additive or even antagonistic.[108,81] Hence, it is highly desired to expose the cells *in vivo* in an optimum ratio to achieve synergistic results. Nanoparticles can ensure the ratiometric loading of drug combinations and deploy at the diseased site.[81, 88, 109] Controlled release of the drug molecules in the tumor cells is also very important as it can normalize the pharmacokinetics, biodistribution, and stability of chemically different drugs that independently have dissimilar pharmacological behaviors. Nanoformulations especially long-circulating formulations can release drugs at controlled ratios continuously. NPs also provide the feasibility of independent tuning of release rates of each drug which is simply not possible with rapidly clearing free drugs. Co-release of drugs in the same tissue or cell can be achieved by making the nanoparticle stimuli (pH, light, temperature, electric or magnetic field) responsive to increase efficacy and to reduce off-target exposure.[110, 111]

1.5.3 Essential characteristics of the nanoparticles: The physicochemical properties of the nanoparticles, such as size, shape, surface properties, drug loading, and release, are important factors to be considered while engineering a nanoparticle delivery system as they determine the fate of the particle in the systemic circulation and the efficacy of the treatment.

1. Size and shape of the Nanoparticles are crucial parameters to be considered in designing NPs as it can influence their bio-distribution, and mechanism of cellular internalization. NPs with diameters smaller than 6 nm are rapidly eliminated from the body upon administration because they can be excreted by the kidneys. Whereas a nanomaterial having the diameter greater than 6 nm cannot be eliminated by the kidneys.[112] NPs with diameters larger than 200 nm are accumulated in the spleen and liver. In order to make long-circulating nanoparticles that can accumulate inside tumor tissues through the fenestrations between the endothelial cells of blood vessels, a size between 30 nm and 200 nm is required.[113] Shape of the nanoparticles also plays crucial role in circulation time and internalization into the tissue. Several reports revealed that NPs with spherical geometries are less likely to marinate to vessel walls and have few binding points with endothelial cells. Nonspherical discoidal geometries, are more likely to have tumbled and oscillatory effects in the vasculature, also

have more tendency of nanoparticle–cell wall contact and exhibit potential extravasation through fenestrations in vasculature.[114]

2. Surface properties play a significant role in influencing the nanoparticles properties such as pharmacokinetics, biodistribution, and biocompatibility. The major limitation of nanoplatform application is the inability to reach diseased sites by avoiding accumulation in the healthy tissues. A mononuclear phagocytic system (MPS), consisting of phagocytic cells and macrophages in the liver and spleen sequesters the nanoparticles immediately after injection by a procedure called opsonisation.[115] A positively charged NPs when administered into the bloodstream they quickly absorbed by serum proteins, allowing them to be recognized and eliminated by MPS also NPs with hydrophobic surface is cleared from the bloodstream very quickly. To avoid rapid blood clearance of the NPs various stratagies were used. Grafting of PEG to the surface of NPs provides a hydrating layer that hinders protein corona formation. In another strategy, NPs surface is decorated with CD47 peptides after which macrophages identify the NPs as 'self', whereby phagocytosis is avoided.[116] Finally, creating biomimetic surface on the NPs by coating them with cell membranes extracted from autologous red blood cells (RBC) and leukocytes has been the attractive strategy to substantially prolong *in vivo* circulation of the NPs.[117, 118]

3. Drug loading and their efficient release from NPs are other important factors to take into the account in engineering NPs. Higher drug loading is needed as it can reduce the possible toxicity from the carrier while lowering the amount of drug carrier used. The controlled long-term release of drugs from NPs is preferred at tumor tissue over a rapid initial release (burst release) as it reduces both the number and frequency of administrations necessary to maintain a therapeutic level.[119, 120]

4. Biocompatibility of nanocarrier is the most important parameter, to ensure safe and effective use of nanomaterials for medical applications. It is compulsory to study the interaction between a material and the biological system. In general, a material is considered biocompatible when it interacts with the body without inducing intolerable toxic, immunogenic, carcinogenic and thrombogenic responses.[121] Furthermore, clearance of NPs after its introduction into the body and completion of their intended functions is often a desirable goal. The biodegradable nanoparticles, i.e. those which can be digested internally

and cleared from the body afterward, are ideal for medical applications over non-biodegradable particles (e.g. metal colloids, ceramics) which cannot be digested and cleared from the body and created undesired carrier toxicity.[122, 123]

1.6 Nanoparticle-mediated inhibition of PI3K and MAPK signaling in cancer

Nanoparticle-mediated targeting of PI3K and MAPK signaling specifically in cancer tissues is currently in its infancy. A handful of attempts were made to engineer signaling inhibitors loaded polymeric and lipidic nanoparticles to improve the clinical outcomes of the small molecule signaling inhibitors. Harfouche et al. synthesized biodegradable PLGA nanoparticle comprising a potent PI3 kinase inhibitor, LY294002, to target PI3K signaling in melanoma. These NPs showed inhibition of downstream Akt phosphorylation, leading to inhibition of proliferation of B16/F10 melanoma cells and induced apoptosis *in vitro*.[124] In another study Kulkarni et al. engineered 108 nm supramolecular nanoparticle (SNP) by loading PI103 and PI828 (PI3K inhibitors) (Fig.9). PI103 and PI828 were conjugated to cholesterol by an ester and carbamate linkages. These cholesterol drug conjugates were formulated into nano-assemblies by mixing them with phosphatidylcholine (PC) and distearoylphosphatidylethanolamine polyethyleneglycol (DSPE-PEG). SNP released encapsulated drug molecules in a controlled manner in the cell lysate which attributed to the cleavage of ester and carbamate linkers in acidic and enzymatic (carboxylesterases) conditions respectively. Further, SNPs exhibited inhibition of phosphorylation of Akt, mTOR *in vivo* and increased antitumor efficacy as compared with PI103 and PI828.[125] Recently, Mizrachi et.al developed p-selectin-targeted delivery systems for BYL719 (a PI3Ka inhibitor, currently in clinical development for solid tumors) to target highly up-regulated PI3 kinase pathway in head and neck squamous cell carcinomas. The engineered p-selectin-targeted nanoparticles by encapsulating BYL719 was achieved by specific accumulation of BYL719 in the tumor milieu which resulted in tumor growth inhibition at a lower concentration of BYL719 than a free drug with oral administration.[126] Basu et al. developed PD98059 encapsulated PLGA nanoparticle for selective inhibition of MAPK signaling in cancer cells. PD98059 was chemically conjugated to PLGA via amide linkage and self-assembled drug loaded NPs entered cancer cells by endocytosis and showed sustained release of the active drug. The NPs

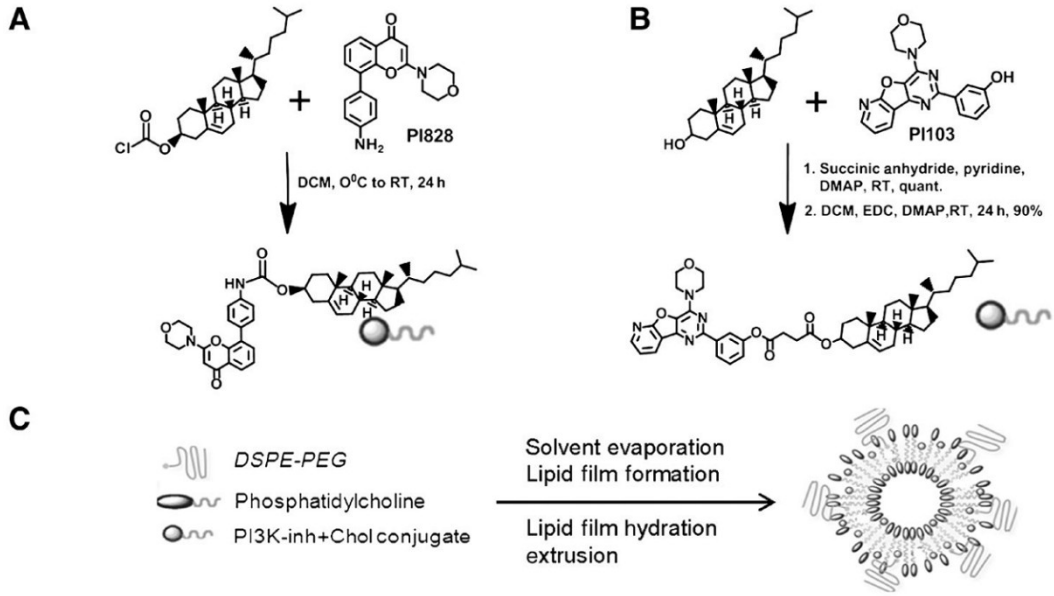

Fig. 9 Synthesis and characterization of SNP. Synthetic scheme of conjugation of PI828 (A) and PI103 (B) to cholesterol *via* carbamate and ester linkages, respectively. (C) schematic representation of self-assembly of SNPs. (*Cancer Res.,* 2013, **73,** 6987-6997. *Reprinted with the permission from American Association for Cancer Research, Copyright © 2013*).

Inhibited phosphorylation of downstream extracellular signal-regulated kinase, subsequently inhibited the proliferation of melanoma and lung carcinoma cells also induced apoptosis *in vitro*. Moreover, the MAPK inhibition with NPs treatment followed by cisplatin significantly inhibited tumor growth in melanoma-bearing mice as compared to either drug alone.[127] Hee Kang et al. synthesized cationic liposomes by encapsulating PD0325901 (MEK inhibitor) in lipid layer and Mcl1-specific siRNA (siMcl1) was complexed to cationic liposomes for their co-delivery to cancer cells, which resulted in improved tumor cell killing and inhibited tumor growth in mice.[128]

1.7 Aim of thesis

Although nanotechnology has made an enormous improvement in tumor-specific delivery of drug molecules, interestingly inhibition of PI3K and MAPK signaling with simultaneous DNA damage in cancer cells by using nanotechnology platform was not much explored as a

next-generation therapeutic strategy. The development of nontoxic nanoparticles to attain ratio-metric transport of kinase inhibitors and DNA-damaging drugs in combination would be promising to achieve augmented efficacy by targeting multiple pathways in cancer cells.
This thesis work is focused on the inhibition of PI3K and MAPK signaling pathways with simultaneous DNA damage in cancer cells by engineering biodegradable and nontoxic lipidic nanoparticles by active and passive targeting modalities. In this thesis, we aimed at evaluating synergism between PI3K inhibitors and different DNA damaging agents when packed in a single nanoparticle. Efforts were also put to inhibit PI3K and MAPK signaling with simultaneous DNA damage selectively in colorectal cancer cells where these pathways are highly upregulated by active targeted hyaluronic acid coated nanoparticles.

The thesis work is further divided into four chapters and the scientific outcome has been reported in detail.

1.8 References

1. A. Sudhakar, *J. Cancer Sci. Ther.*, 2009, **1**, 1-4.
2. American Cancer Society. https://www.cancer.org/research/cancer-facts-statistics/global.html
3. Cancer Facts & Figures 2017, American Cancer Society. https://www.cancer.org/research/cancer-facts-statistics/all-cancer-facts-figures/cancer-facts-figures-2017.html
4. H. Lodish, A. Berk, SL. Zipursky , et al. Molecular Cell Biology. 4th edition. New York: W. H. Freeman; 2000. Section 24.1, Tumor Cells and the Onset of Cancer. Available from: https://www.ncbi.nlm.nih.gov/books/NBK21590/
5. Let's beat cancer sooner, Cancer Research UK, http://www.cancerresearchuk.org/about-cancer/what-is-cancer/how-cancer-starts/types-of-cancer
6. National Institutes of Health (US); NIH Curriculum Supplement Series [Internet]. Understanding Cancer. https://www.ncbi.nlm.nih.gov/books/NBK20362/
7. D. X. Nguyen, P. D. Bos and J. Massagué, *Nat. Rev. Cancer*, 2009, **9**, 274-84.
8. B. Sadikovic, K. Al-Romaih, J. Squire and M. Zielenska, *Curr. Genomics*, 2008, **9**, 394-408.

9. E. Baxter, K. Windloch, F. Gannon and J. S. Lee, *Cell Biosci.*, 2014, **4**, 45.
10. R. Jaenisch and A. Bird, *Nature Genet.*, 2003, **33**, 245-254.
11. M. G. Vander Heiden, L. C. Cantley and C. B. Thompson, *Science*, 2009, **324**, 1029-1033.
12. G. Evan and T. Littlewood, *Science*, 1998, **281**, 1317-1322.
13. A. L. Jackson and L. A. Loeb, *Mutat. Res.*, 2001, **477**, 7-21.
14. D. Hanahan and R. A. Weinberg, *Cell*, 2011, **144**, 646-674.
15. S. Courtois-Cox, S. M. G. Williams, E. E. Reczek, B. W. Johnson, L. T. McGillicuddy, C. M. Johannessen, P. E. Hollstein, M. MacCollin and K. Cichowski, *Cancer cell*, 2006, **10**, 459-472.
16. C. A. Pratilas, B. S. Taylor, Q. Ye, A. Viale, C. Sander, D. B. Solit and N. Rosen, *Proc. Natl. Acad. Sci. U.S.A.*, 2009, **106**, 4519-4524.
17. K. M. Haigis, K. R. Kendall, Y. Wang, A. Cheung, M. C. Haigis, J. N. Glickman, M. Niwa-Kawakita, A. Sweet-Cordero, J. Sebolt-Leopold and K. M. Shannon, *Nature Genet.*, 2008, **40**, 600-608.
18. P. Blume-Jensen and T. Hunter, *Nature*, 2001, **411**, 355.
19. Y. Samuels and K. Ericson, *Curr. Opin. Oncol*, 2006, **18**, 77-82.
20. L. Zhao and P. K. Vogt, *Oncogene*, 2008, **27**, 5486.
21. G. S. Martin, *Cancer cell*, 2003, **4**, 167-174.
22. J. Schlessinger, *Cell*, 2000, **103**, 211-225.
23. C. Marshall, *Cell*, 1995, **80**, 179-185.
24. M. C. Mendoza, E. E. Er and J. Blenis, *Trends Biochem. Sci.*, 2011, **36**, 320-328.
25. L. C. Cantley, *Science*, 2002, **296**, 1655-1657.
26. R. Seger and E. G. Krebs, *FASEB J.*, 1995, **9**, 726-735.
27. A. Bonni, A. Brunet, A. E. West, S. R. Datta, M. A. Takasu and M. E. Greenberg, *Science*, 1999, **286**, 1358-1362.
28. P. J. Roberts and C. J. Der, *Oncogene*, 2007, **26**, 3291.
29. R. J. Shaw and L. C. Cantley, *Nature*, 2006, **441**, 424.
30. A. De Luca, M. R. Maiello, A. D'Alessio, M. Pergameno and N. Normanno, *Expert Opin. Ther. Targets*, 2012, **16**, S17-S27.
31. K.-K. Wong, J. A. Engelman and L. C. Cantley, *Curr. Opin. Genet. Dev.*, 2010, **20**, 87-90.
32. J. Liang and J. M. Slingerland, *Cell Cycle*, 2003, **2**, 336-342.

33. K. D. Courtney, R. B. Corcoran and J. A. Engelman, *J. Clin. Oncol.*, 2010, **28**, 1075-1083.
34. T. Yuan and L. Cantley, *Oncogene*, 2008, **27**, 5497-5510.
35. J. A. Engelman, J. Luo and L. C. Cantley, *Nat. Rev. Genet.*, 2006, **7**, 606-619.
36. Z. Jehan, P. Bavi, M. Sultana, J. Abubaker, R. Bu, A. Hussain, G. Alsbeih, N. Al-Sanea, A. Abduljabbar and L. H. Ashari, *J. Pathol.*, 2009, **219**, 337-346.
37. M. Keniry and R. Parsons, *Oncogene*, 2008, **27**, 5477-5485.
38. M. Davies, K. Stemke-Hale, C. Tellez, T. Calderone, W. Deng, V. Prieto, A. Lazar, J. Gershenwald and G. Mills, *Br. J. Cancer*, 2008, **99**, 1265-1268.
39. D. W. Parsons, T.-L. Wang, Y. Samuels, A. Bardelli, J. M. Cummins, L. DeLong, N. Silliman, J. Ptak, S. Szabo and J. K. Willson, *Nature*, 2005, **436**, 792-792.
40. T. Kirkegaard, C. J. Witton, J. Edwards, K. V. Nielsen, L. B. Jensen, F. M. Campbell, T. G. Cooke and J. Bartlett, *Histopathology*, 2010, **56**, 203-211.
41. R. J. Shaw and L. C. Cantley, *Nature*, 2006, **441**, 424-430.
42. C. Peyssonnaux and A. Eychène, *Biol. Cell*, 2001, **93**, 53-62.
43. J. A. McCubrey, L. S. Steelman, W. H. Chappell, S. L. Abrams, E. W. Wong, F. Chang, B. Lehmann, D. M. Terrian, M. Milella and A. Tafuri, *BBA-Mol. Cell Res.*, 2007, **1773**, 1263-1284.
44. R. E. Chen and J. Thorner, *BBA-Mol. Cell Res.*, 2007, **1773**, 1311-1340.
45. A. K. Murugan, J. Dong, J. Xie and M. Xing, *Cell Cycle*, 2009, **8**, 2122-2124.
46. A. S. Dhillon, S. Hagan, O. Rath and W. Kolch, *Oncogene*, 2007, **26**, 3279-3290.
47. J. S. Sebolt-Leopold, *Oncogene*, 2000, **19**, 6594.
48. P. Cohen, *Nat. Rev. Drug Discov.*, 2002, **1**, 309-315.
49. R. C. Stein and M. D. Waterfield, *Mol. Med. Today*, 2000, **6**, 347-358.
50. J. A. Engelman, *Nat. Rev. Cancer*, 2009, **9**, 550-562.
51. S.-M. Maira, F. Stauffer, J. Brueggen, P. Furet, C. Schnell, C. Fritsch, S. Brachmann, P. Chène, A. De Pover and K. Schoemaker, *Mol. Cancer Ther.*, 2008, **7**, 1851-1863.
52. T.-J. Liu, D. Koul, T. LaFortune, N. Tiao, R. J. Shen, S.-M. Maira, C. Garcia-Echevrria and W. A. Yung, *Mol. Cancer Ther.*, 2009, **8**, 2204-2210.
53. N. T. Ihle, R. Williams, S. Chow, W. Chew, M. I. Berggren, G. Paine-Murrieta, D. J. Minion, R. J. Halter, P. Wipf and R. Abraham, *Mol. Cancer Ther.*, 2004, **3**, 763-772.
54. C. J. Vlahos, W. F. Matter, K. Y. Hui and R. F. Brown, *J. Biol. Chem.*, 1994, **269**, 5241-5248.

55. J. Bain, L. Plater, M. Elliott, N. Shpiro, C. J. Hastie, H. Mclauchlan, I. Klevernic, J. S. C. Arthur, D. R. Alessi and P. Cohen, *Biochem. J.*, 2007, **408**, 297-315.
56. Z. N. Demidenko, M. Shtutman and M. V. Blagosklonny, *Cell Cycle*, 2009, **8**, 1896-1900.
57. Z. N. Demidenko and M. V. Blagosklonny, *Aging (Albany NY)*, 2009, **1**, 1008-1016.
58. J. A. McCubrey, M. Milella, A. Tafuri, A. M. Martelli, P. Lunghi, A. Bonati, M. Cervello, J. T. Lee and L. S. Steelman, *Curr. Opin. Investig. Drugs*, 2008, **9**, 614-630.
59. H. Huynh, K. C. Soo, P. K. Chow and E. Tran, *Mol. Cancer Ther.*, 2007, **6**, 138-146.
60. J. A. McCubrey, L. S. Steelman, S. L. Abrams, W. H. Chappell, S. Russo, R. Ove, M. Milella, A. Tafuri, P. Lunghi and A. Bonati, *Expert Opin. Emerg. Drugs.*, 2010, **15**, 203-223.
61. A. Sharma, M. A. Tran, S. Liang, A. K. Sharma, S. Amin, C. D. Smith, C. Dong and G. P. Robertson, *Cancer Res.*, 2006, **66**, 8200-8209.
62. A. K. Takle, M. J. Bamford, S. Davies, R. P. Davis, D. K. Dean, A. Gaiba, E. A. Irving, F. D. King, A. Naylor and C. A. Parr, *Bioorganic Med. Chem. Lett.*, 2008, **18**, 4373-4376.
63. Z. A. Knight, H. Lin and K. M. Shokat, *Nat. Rev. Cancer*, 2010, **10**, 130-137.
64. A. Kulkarni, P. Pandey, P. Rao, A. Mahmoud, A. Goldman, V. Sabbisetti, S. Parcha, S. K. Natarajan, V. Chandrasekar, D. Dinulescu, S. Roy and S. Sengupta, *ACS Nano*, 2016, **10**, 8154-8168.
65. J. M. Stommel, A. C. Kimmelman, H. Ying, R. Nabioullin, A. H. Ponugoti, R. Wiedemeyer, A. H. Stegh, J. E. Bradner, K. L. Ligon, C. Brennan, L. Chin and R. A. DePinho, *Science*, 2007, **318**, 287-290.
66. C. S. Karapetis , S. Khambata-Ford , D. J. Jonker , C. J. O'Callaghan , D. Tu , N. C. Tebbutt , R. J. Simes , H. Chalchal , J. D. Shapiro , S. Robitaille , T. J. Price , L. Shepherd , H.-J. Au , C. Langer , M. J. Moore and J. R. Zalcberg *N. Engl. J. Med.*, 2008, **359**, 1757-1765.
67. W. Pao, T. Y. Wang, G. J. Riely, V. A. Miller, Q. Pan, M. Ladanyi, M. F. Zakowski, R. T. Heelan, M. G. Kris and H. E. Varmus, *PLoS Med.*, 2005, **2**, e17.
68. N. V. Sergina, M. Rausch, D. Wang, J. Blair, B. Hann, K. M. Shokat and M. M. Moasser, *Nature*, 2007, **445**, 437-441.
69. I. K. Mellinghoff, M. Y. Wang, I. Vivanco, D. A. Haas-Kogan, S. Zhu, E. Q. Dia, K. V. Lu, K. Yoshimoto, J. H. Huang and D. J. Chute, *N. Engl. J. Med.*, 2005, **2005**, 2012-2024.

70. P. Castel, E. Toska, Z. S. Zumsteg, F. J. Carmona, M. Elkabets, A. Bosch and M. Scaltriti, *Mol. Cell. Oncol.*, 2014, **1**, e963447.
71. D. Marklein, U. Graab, I. Naumann, T. Yan, R. Ridzewski, F. Nitzki, A. Rosenberger, K. Dittmann, J. Wienands, L. Wojnowski, S. Fulda and H. Hahn, *PLoS ONE*, 2012, **7**, e52898.
72. H. Richly, B. Henning, P. Kupsch, K. Passarge, M. Grubert, R. Hilger, O. Christensen, E. Brendel, B. Schwartz and M. Ludwig, *Ann. Oncol.*, 2006, **17**, 866-873.
73. L. Dal Lago, V. D'Hondt and A. Awada, *Oncologist*, 2008, **13**, 845-858.
74. A. S. Martins, C. Mackintosh, D. H. Martín, M. Campos, T. Hernández, J.-L. Ordóñez and E. de Alava, *Clinic. Cancer Res.*, 2006, **12**, 3532-3540.
75. C. Bassi, J. Ho, T. Srikumar, R. Dowling, C. Gorrini, S. Miller, T. Mak, B. Neel, B. Raught and V. Stambolic, *Science*, 2013, **341**, 395-399.
76. C. Schult, M. Dahlhaus, A. Glass, K. Fischer, S. Lange, M. Freund and C. Junghanss, *Anticancer Res.*, 2012, **32**, 463-474.
77. H. Huynh, P. K. Chow and K.-C. Soo, *Mol. Cancer Ther.*, 2007, **6**, 2468-2476.
78. Q. Yang, S. Zhang, M. Kang, R. Dong and J. Zhao, *Oncol. Rep.*, 2015, **33**, 2537-2544.
79. M. Di Maio, P. Chiodini, V. Georgoulias, D. Hatzidaki, K. Takeda, F. M. Wachters, V. Gebbia, E. F. Smit, A. Morabito and C. Gallo, *J. Clin. Oncol.*, 2009, **27**, 1836-1843.
80. R. Bernabé, A. Patrao, L. Carter, F. Blackhall and E. Dean, *Future Oncol.*, 2016, **12**, 2545-2560.
81. L. D. Mayer, T. O. Harasym, P. G. Tardi, N. L. Harasym, C. R. Shew, S. A. Johnstone, E. C. Ramsay, M. B. Bally and A. S. Janoff, *Mol. Cancer Ther.*, 2006, **5**, 1854-1863.
82. A. Nikalje, *Med. Chem*, 2015, **5**, 081-089.
83. J. Shi, P. W. Kantoff, R. Wooster and O. C. Farokhzad, *Nature Reviews Cancer*, 2017, **17**, 20-37.
84. R. Cheng, F. Meng, C. Deng, H.-A. Klok and Z. Zhong, *Biomaterials*, 2013, **34**, 3647-3657.
85. M. Das and S. K. Sahoo, *PLoS One*, 2012, **7**, e32920.
86. X. Song, Y. Zhao, S. Hou, F. Xu, R. Zhao, J. He, Z. Cai, Y. Li and Q. Chen, *Eur. J. Pharm. Biopharm.*, 2008, **69**, 445-453.

87. L. Liao, J. Liu, E. C. Dreaden, S. W. Morton, K. E. Shopsowitz, P. T. Hammond and J. A. Johnson, *J. Am. Chem. Soc.*, 2014, **136**, 5896-5899.
88. N. Kolishetti, S. Dhar, P. M. Valencia, L. Q. Lin, R. Karnik, S. J. Lippard, R. Langer and O. C. Farokhzad, *Proc. Natl. Acad. Sci. U.S.A.*, 2010, **107**, 17939-17944.
89. L. Zhang, J. Xia, Q. Zhao, L. Liu and Z. Zhang, *Small*, 2010, **6**, 537-544.
90. T. Jiang, R. Mo, A. Bellotti, J. Zhou and Z. Gu, *Adv. Funct. Mater.*, 2014, **24**, 2295-2304.
91. Y. Wang, S. Gao, W.-H. Ye, H. S. Yoon and Y.-Y. Yang, *Nat. Mater.*, 2006, **5**, 791-796.
92. P. Parhi, C. Mohanty and S. K. Sahoo, *Drug Discov. Today*, 2012, **17**, 1044-1052.
93. Q. Hu, W. Sun, C. Wang and Z. Gu, *Adv. Drug Deliv. Rev.*, 2016, **98**, 19-34.
94. P. G. Tardi, N. Dos Santos, T. O. Harasym, S. A. Johnstone, N. Zisman, A. W. Tsang, D. G. Bermudes and L. D. Mayer, *Mol. Cancer Ther.*, 2009, **8**, 2266-2275.
95. H. Maeda, J. Wu, T. Sawa, Y. Matsumura and K. Hori, *J. Control. Release*, 2000, **65**, 271-284.
96. R. A. Petros and J. M. DeSimone, *Nat. Rev. Drug Discov.*, 2010, **9**, 615-627.
97. R. Bazak, M. Houri, S. El Achy, S. Kamel and T. Refaat, *J Cancer Res. Clin. Oncol.*, 2015, **141**, 769-784.
98. D. P. Ferris, J. Lu, C. Gothard, R. Yanes, C. R. Thomas, J. C. Olsen, J. F. Stoddart, F. Tamanoi and J. I. Zink, *Small*, 2011, **7**, 1816-1826.
99. C. K. Kim, P. Ghosh, C. Pagliuca, Z.-J. Zhu, S. Menichetti and V. M. Rotello, *J. Am. Chem. Soc.*, 2009, **131**, 1360-1361.
100. W. J. Gradishar, *Expert opin. pharmacother.*, 2006, **7**, 1041-1053.
101. C. Oerlemans, W. Bult, M. Bos, G. Storm, J. F. W. Nijsen and W. E. Hennink, *Pharm. Res.*, 2010, **27**, 2569-2589.
102 J. Rios-Doria, A. Carie, T. Costich, B. Burke, H. Skaff, R. Panicucci and K. Sill, *J. Drug Deliv.*, 2012, **2012**.
103. M. Chidambaram, R. Manavalan and K. Kathiresan, *J. Pharm. Pharm. Sci.*, 2011, **14**, 67-77.
104. S. S. Suri, H. Fenniri and B. Singh, *J. Occup. Med. Toxicol.*, 2007, **2**, 16.
105. I. Brigger, C. Dubernet and P. Couvreur, *Adv. Drug Deliv. Rev.*, 2002, **54**, 631-651.
106. C. E. Soma, C. Dubernet, D. Bentolila, S. Benita and P. Couvreur, *Biomaterials*, 2000, **21**, 1-7.
107. M. L. Amin, *Drug Target Insights*, 2013, **7**, 27-34.

108. T.O. Harasym, P.G. Tardi, S.A. Johnstone, M.B. Bally, A.S. Janoff, and L.D. Mayer Fixed drug ratio liposome formulations of combination cancer therapeutics, in Liposome Technology, 3rd edition, volume III (Gregoriadis, G., ed.), pp 25-48, Informa Healthcare (2007).

109. L. Miao, S. Guo, J. Zhang, W. Y. Kim and L. Huang, *Adv. Funct. Mater.,* 2014, **24,** 6601-6611.

110. R. K. Pathak and S. Dhar, *J. Am. Chem. Soc.,* 2015, **137,** 8324-8327.

111. L. Liao, J. Liu, E. C. Dreaden, S. W. Morton, K. E. Shopsowitz, P. T. Hammond and J. A. Johnson, *J. Am. Chem. Soc.,* 2014, **136,** 5896-5899.

112. H. S. Choi, W. Liu, P. Misra, E. Tanaka, J. P. Zimmer, B. I. Ipe, M. G. Bawendi and J. V. Frangioni, *Nat. Biotechnol.,* 2007, **25,** 1165-1170.

113. A. Albanese, P. S. Tang and W. C. Chan, *Annu. Rev. Biomed. Engi,* 2012, **14,** 1-16.

114. F. Gentile, C. Chiappini, D. Fine, R. C. Bhavane, M. S. Peluccio, M. M.-C. Cheng, X. Liu, M. Ferrari and P. Decuzzi, *J. Biomech.,* 2008, **41,** 2312-2318.

115. S. M. Moghimi and H. M. Patel, *Adv. Drug Deliv. Rev,* 1998, **32,** 45-60.

116. P. L. Rodriguez, T. Harada, D. A. Christian, D. A. Pantano, R. K. Tsai and D. E. Discher, *Science,* 2013, **339,** 971-975.

117. A. Parodi, N. Quattrocchi, A. L. van de Ven, C. Chiappini, M. Evangelopoulos, J. O. Martinez, B. S. Brown, S. Z. Khaled, I. K. Yazdi, M. V. Enzo, L. Isenhart, M. Ferrari and E. Tasciotti, *Nat. Nanotechnol.,* 2013, **8**, 61-68.

118. C.-M. J. Hu, L. Zhang, S. Aryal, C. Cheung, R. H. Fang and L. Zhang, *Proc. Natl. Acad. Sci. U.S.A.,* 2011, 10**8,** 10980-10985.

119. L. Hu, H. Zhang and W. Song, In*ternational J. Pharm. Sci. Res.,* 2012, **3**, 2888.

120. S. Gelperina, K. Kisich, M. D. Iseman and L. Heifets, *Am. J. Respir. Crit. Care Med.,* 2005, **172,** 1487-1490.

121. X. Li, L. Wang, Y. Fan, Q. Feng and F.-z. Cui, *J. Nanomater.,* 2012, 20**12,** 19-26.

122. M. A. Dobrovolskaia, P. Aggarwal, J. B. Hall and S. E. McNeil, *Mol. Pharm.,* 2008, **5**, 487-495.

123. D. E. Owens and N. A. Peppas, In*ternational J. Pharm.,* 2006, **307,** 93-102.

124. R. Harfouche, S. Basu, S. Soni, D. M. Hentschel, R. A. Mashelkar and S. Sengupta, *Angiogenesis,* 2009, **12,** 325-38.

125. A. A. Kulkarni, B. Roy, P. S. Rao, G. A. Wyant, A. Mahmoud, M. Ramachandran, P. Sengupta, A. Goldman, V. R. Kotamraju and S. Basu, *Cancer Res.,* 2013, **73,** 6987-6997.

126. A. Mizrachi, Y. Shamay, J. Shah, S. Brook, J. Soong, V. K. Rajasekhar, J. L. Humm, J. H. Healey, S. N. Powell and J. Baselga, *Nat. Commun.,* 2017, **8**, 14292.

127. S. Basu, R. Harfouche, S. Soni, G. Chimote, R. A. Mashelkar and S. Sengupta, *Proc. Natl. Acad. Sci. U.S.A.,* 2009, **106,** 7957-7961.

128. S. H. Kang, H.-J. Cho, G. Shim, S. Lee, S.-H. Kim, H.-G. Choi, C.-W. Kim and Y.-K. Oh, *Pharm. Res.,* 2011, **28,** 3069-3078.

Chapter 2

Vitamin D3 Nanoparticle-Mediated Targeting of PI3K Pathway in Synergy with DNA Damaging Drugs in Cancer Cells

2.1 Introduction

Hyperactivation of the phosphoinositide-3-kinase (PI3K) signaling cascade is one of the most frequently altered pathways in cancer.[1] Activation of PI3K signaling can happen in the cell either by over expression of upstream RTKs or deactivation of tumor suppressor phosphatase PTEN. Direct pharmacological inhibition of the PI3K signaling with small molecules has emerged as an attractive anti-cancer clinical strategy.[2] However, PI3K inhibition by using small molecule inhibitors fails to elicit dramatic or durable responses because of emerging several intrinsic or extrinsic drug resistances.

On the other hand, several reports showed that DNA damage response and PI3K signaling networks are interconnect at multiple nodes.[3] Moreover, numerous preclinical[4-6] and clinical[7] studies proved that DNA damage can activate PI3K/AKT pathway in several cancers, which further results in the promotion of chemo-resistance[8-10]. Therefore, targeting the PI3K-AKT signaling axis in combination with DNA damaging therapies has been a potential strategy in PI3K-driven tumors to induce synergistic cancer cell killing. However, simultaneous inhibition of PI3K signaling and inducing DNA damage in the tumor cells by drug cocktail administration is troublesome as their nonspecific diffusion leads to escalated toxicity. Moreover, the drugs face the challenge of overcoming the biological barriers to reach the tumor targets in appropriate concentrations and combinations that offer the effective therapeutic efficacy.

In order to overcome the challenges associated with the conventional cocktail administration of multiple drugs we adopted nanotechnology to deploy the dual drugs (PI3K inhibitors + DNA damaging agents) at tumor tissue while minimizing the off-target toxicity. However, the prudent choice of nanovectors based on their biocompatibility and biodegradability is currently one of the major challenges in nanomedicine.[11-16] Inspired by the need for developing novel nontoxic and biodegradable nanovectors to inhibit PI3K pathway along with inducing DNA damage, the aim of the study was to develop a nontoxic vitamin D3 nanoparticle as a versatile platform to load and deliver combination of PI3Kinhibitors and DNA damaging agents to cancer cells to overcome drug resistance. In this current study, we have engineered vitamin D3 nanoparticles that can simultaneously contain phosphatidylinositol-3-kinase (PI3K) inhibitor (PI103) and DNA damaging drugs (cisplatin or doxorubicin or proflavine) in combination. These sub 200 nm vitamin D3 particles allowed the high loading of the dual drugs and released them in increased quantity at pH = 5.5

(mimics the lysosomal compartment inside tumor cells) compared to that at pH = 7.4 (mimics the blood circulation) in a slow and sustained manner over 72 h. VitD3–PI103–CDDP-NP (PI103 and cisplatin loaded nanoparticle) and vitD3–PI103–Dox-NP (PI103 and Doxorubicin loaded nanoparticle) showed synergistic cytotoxic effects by inducing apoptosis through DNA damage mechanism in hepatocellular carcinoma cells (Hep3B) and cisplatin resistant hepatocellular carcinoma cells (Hep3B-R). Finally, vitD3–PI103–proflavine-NP (PI103 and proflavine loaded nanoparticle) was rapidly internalized inside the cells to induce cell death in cisplatin resistant Hep3B cells. These dual drug containing vitaminD3 nanoparticles showed their potential to simultaneously deploy PI3K inhibitor and DNA damaging drugs inside the tumor to overcome drug resistance.

2.2 Results and Discussion

2.2.1Rationale for choosing the drug combinations:

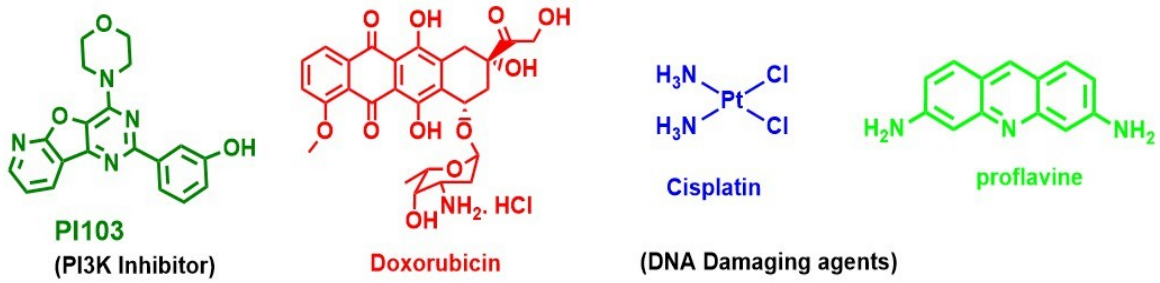

Fig. 1 Chemical structures of PI103 (PI3K inhibitor), doxorubicin, cisplatin, and proflavine (DNA damaging agents)

We have selected PI103, a dual Akt–mTOR inhibitor currently used in clinical study[17, 18] PI3K signaling and its downstream mammalian target of rapamycin (mTOR) are highly aberrant in different human malignancies.[19, 20] However, inhibiting mTOR with rapamycin and its analogues triggers the feedback mechanism to hyperactivate upstream Akt signaling through an IGF-1R dependent pathway.[21] Therefore, dual Akt-mTOR inhibitor would be more efficient to inhibit PI3K-Akt-mTOR cascade. Moreover, PI103 showed enhanced apoptosis in combination with another clinically approved DNA damaging drug doxorubicin in glioblastoma.[22] However, PI103 has low hydrophilicity and rapid *in vivo* metabolism.[23] Furthermore, doxorubicin shows dose dependent cardiotoxicity among the patients.[24, 25] We have selected a DNA damaging drug cisplatin (CDDP), which is widely used in clinics for

the treatment of different types of cancers.[26-28] However, cisplatin treatment leads to severe dose dependent nephro toxicity to the patients[29, 30] Moreover, very often cisplatin treatments result in the development of chemo resistance leading to the therapeutic failure due to various molecular mechanisms.[31, 32] Recently, it was shown that DNA damage induced by cisplatin upregulates PI3K signaling for survival of cancer cells.[33] As a result, a rational combination of cisplatin with a class I PI3K inhibitor PI103 showed synergistic enhancement in inducing apoptosis in liposarcoma.[34] Finally, we have selected a DNA minor groove binder fluorescent anticancer acridine derivative proflavine[35, 36] in combination with PI103 to assess their potential in cancer cell killing. However, there are no reports of combination therapy using proflavine and PI103 in cancer to date.

2.2.2 Rationale for choosing vitamin D3 as vector: For successful translation into the clinics, the nanovector synthesis should be easy with high yield and purity in few steps, capable of incorporating different drugs, releasing the active drugs in a controlled fashion and finally digested and degraded into non-toxic entities to minimize adverse toxicity. To address these, we anticipated that naturally occurring molecules would be the appropriate choice for developing novel drug delivery vehicles. Vitamin D3 (cholecalciferol) is an essential lipid soluble vitamin, which is biodegradable and non-toxic molecule. Vitamin D3 is biosynthesized in the human body from its precursor 7-dehydrocholesterol by using sunlight and metabolized in the liver and kidney. Vitamin D3 is also taken as an important ingredients in our daily diet.[37] Furthermore, vitamin D3 is structurally similar with cholesterol (an important component of cellular membranes). Vitamin D3 was completely unexplored for drug delivery purposes, for the first time Patil et.al. explored vitamin D3 as a vector in nanoparticle synthesis and to deliver different clinically used cytotoxic drugs (paclitaxel and doxorubicin) to kill cervical cancer cells.[38] Inspired by its biocompatibility and biodegradability we have chosen vitamin D3 as a vector to synthesis the nanoparticles comprising PI3K inhibitor and DNA damaging drugs simultaneously.

2.2.3 Synthesis and characterization of vitamin D3nanoparticles with dual drugs: We have chemically conjugated PI103 with vitamin D3 (1, Fig. 2a) using ester linkage through a biocompatible succinic acid linker to obtain vitamin D3–succinic acid–PI103 conjugate (2) by a previously described method.[38] We engineered vitamin D3 nanoparticles with dual drugs using a lipid-film hydration-extrusion method[39] using L-α-phosphatidylcholine (PC),

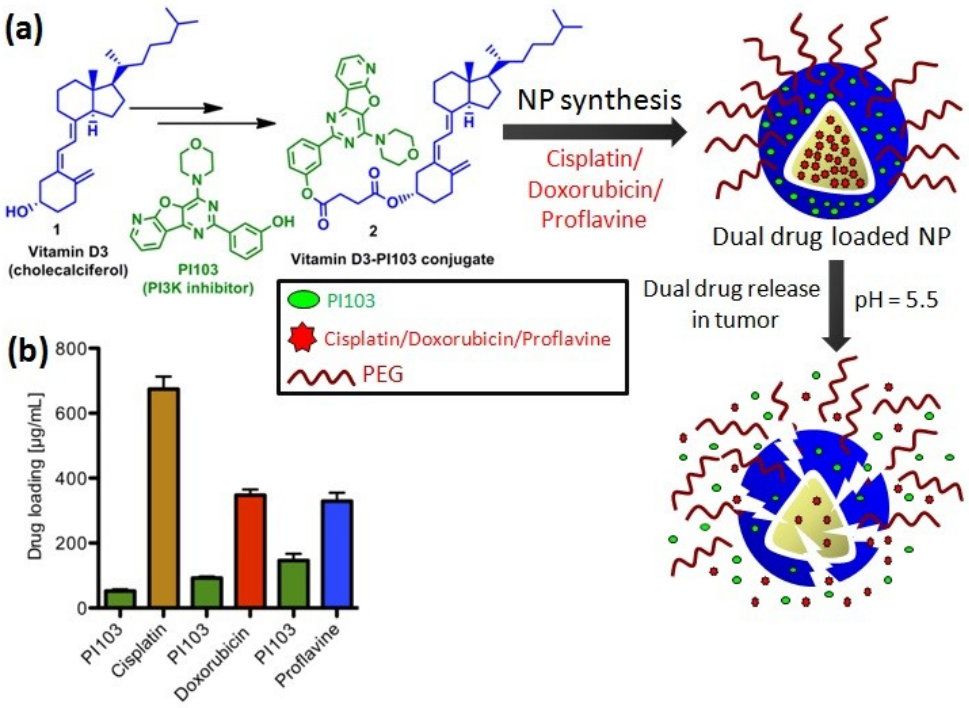

Fig. 2 Synthesis of dual drug loaded vitamin D3 nanoparticle. (a) Synthetic scheme of vitamin D3–PI103-conjugate and dual drug loaded nanoparticle. (b) Loading of different drugs in dual drug loaded nanoparticles determined by UV-Vis spectroscopy.

1,2-distearoyl-*sn*-glycero-3-phosphoethanolamine-N-[amino (polyethyleneglycol)2000] (DSPE-PEG), vitamin D3–succinic acid–PI103 conjugate (2) and drugs (cisplatin or doxorubicin or proflavine) in 2 : 0.2 : 1 : 0.4 weight ratio. PC was very carefully selected because of its biocompatibility. DSPE-PEG was chosen to cover the surface of the nanoparticles with poly ethylene glycol (PEG) to reduce opsonisation, clearance by the reticulo endothelial system (RES) and to ensure a long half-life in the blood circulation.[40] The loading of different drugs in the nanoparticles were quantified using UV-Vis spectroscopy by concentration versus absorbance graph at different characteristics wave length, λ_{max} = 340 nm, 444 nm, 490 nm and 706 nm for PI103, proflavine, doxorubicin and cisplatin, respectively (Fig. 3). The mean drug loading in vitD3–PI103–CDDP-NP was found to be = 23.8 ± 2.4 µg of PI103 and 306.4 ± 17.6 µg of cisplatin (cisplatin encapsulation efficiency = 67.4 %) per mg of formulation (Fig. 2b). Moreover, mean drug loading in vitD3–PI103–Dox-NP was 42.0 ± 2.2 µg for PI103 and 158.0 ± 7.9 µg for doxorubicin (doxorubicin encapsulation efficiency = 34.7 %) per mg of the final formulation.

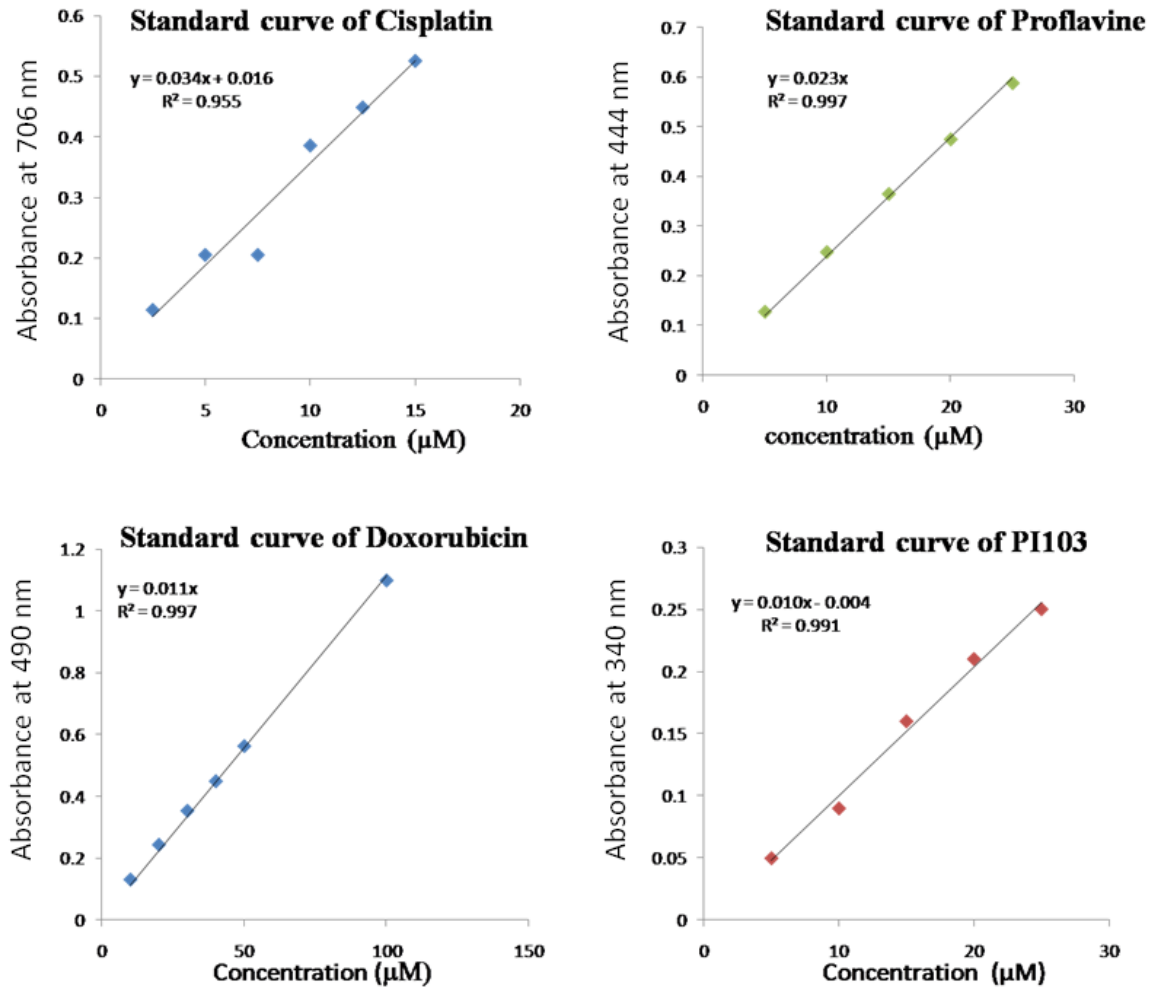

Fig. 3 Concentration *vs* absorbance calibration graph for cisplatin, proflavine, doxorubicin and PI103 at their characteristic λ_{max} = 706 nm, 444 nm, 490 nm and 340 nm respectively determined by UV-VIS spectroscopy.

Finally, mean drug loadings for PI103 and proflavine in vitD3–PI103–proflavine-NP were found to be equal to 66.4 ± 9.4 µg and 149.5 ± 11.9 µg respectively, (proflavine encapsulation efficiency = 32.9 %) per mg of the final formulation (mean ± SEM, n = 3).

We also quantified the loading efficiency and encapsulation efficiency using reverse phase high performance liquid chromatography (RP-HPLC) through concentration *vs.* peak area graphs (Fig. 4a and b). The loading of doxorubicin and proflavine were found to be 120.9 ± 6.2 µg (encapsulation efficiency = 26.6 %) and 93.2 ± 4.3 µg (encapsulation efficiency = 20.4 %) per mg of final formulation, respectively (Fig. 4c).

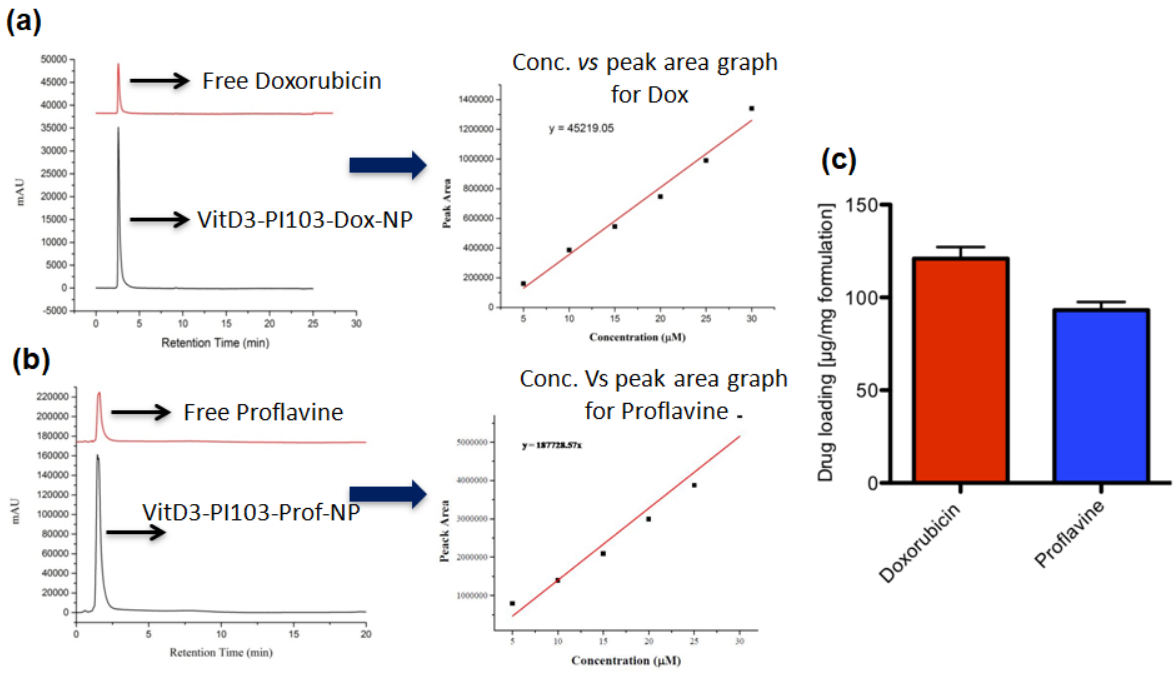

Fig. 4 (a-b) RP-HPLC traces and concentration *vs.* peak area graph for free doxorubicin, vitD3-PI103-Dox-NP and free proflavine, vitD3-PI103-Proflavine-NP respectively. (c) Loading graph of doxorubicin and proflavine in vitD3-PI103-Dox-NP and vitD3-PI103-Proflavine-NP respectively.

The hydrodynamic diameter and the polydispersity index (PDI) of the dual drug loaded nanoparticles were determined by dynamic light scattering (DLS). The hydrodynamic diameter were found to be equal to 193 ± 0.4 nm (PDI = 0.3 ± 0.006), 168 ± 0.2 nm (PDI = 0.09 ± 0.02) and 175 ± 0.6 nm (PDI = 0.1 ± 0.006) for vitD3–PI103–CDDP-NP, vitD3–PI103–proflavine-NP and vitD3–PI103–Dox-NP, respectively (Fig. 5a–c). We also visualized the size, shape, and morphology of these dual drug loaded nanoparticles by field-emission scanning electron microscopy (FE-SEM, Fig. 5d–f), atomic force microscopy (AFM, Fig. 5g–i) and transmission emission microscopy (TEM, Fig. 6). From DLS, FESEM, AFM and TEM data, it was evident that the dual drug loaded vitamin D3 nanoparticles are monodispersed and spherical in shape having less than 200 nm sizes, which was ideal for tumor internalization through passive targeting. We further confirmed the presence of cisplatin invitD3–PI103–CDDP-NP by energy-dispersive X-ray spectroscopy (EDX) measurement (Fig. 7a). We also confirmed the presence of doxorubicin and proflavine in vitD3–PI103–

Dox-NPand vitD3–PI103–proflavine-NP by fluorescence spectroscopy compared to free doxorubicin and proflavine, respectively (Fig. 7b).

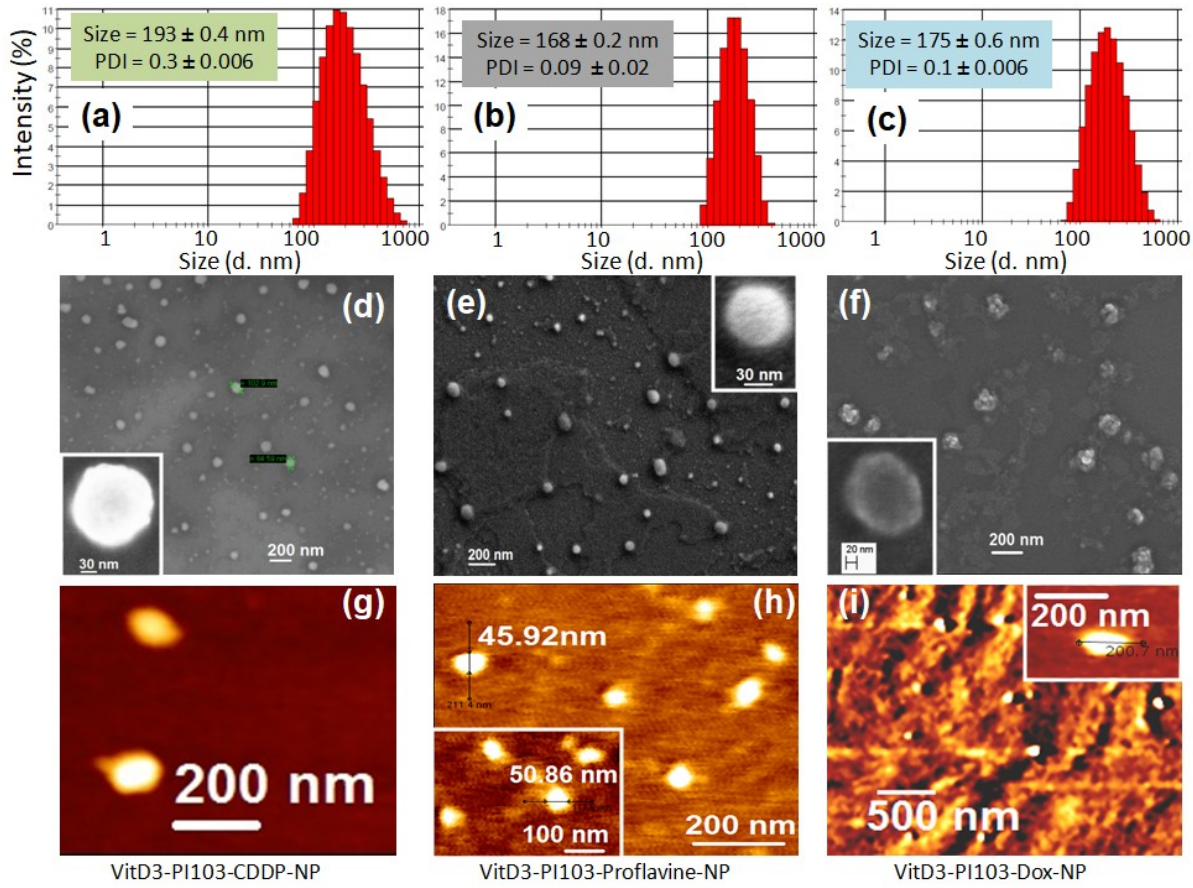

Fig. 5 Determination of size, shape and morphology of different dual drug loaded vitamin D3 nanoparticles. (a–c) DLS of vitD3–PI013–CDDP-NP, vitD3–PI103–proflavine-NP and vitD3–PI103–Dox-NP, respectively. (d–f) FESEM images of vitD3–PI013–CDDP-NP, vitD3–PI103–proflavine-NP and vitD3–PI103–Dox-NP, respectively. (g–i) AFM images of vitD3–PI013–CDDP-NP, vitD3–PI103–proflavine-NP and vitD3–PI103–Dox-NP, respectively.

Previous study showed that hydrophilic drug encapsulation leads to considerably higher drug loading in vitamin D3 nanoparticles compared to the encapsulation of hydrophobic drugs.[38] From this data, we anticipated that the vitamin D3 nanoparticle might have a very thin hydrophobic lipid layer with a hydrophilic core leading to a higher hydrophilic drug loading in the core and a lower hydrophobic drug loading in the lipid layer. In this study, we further

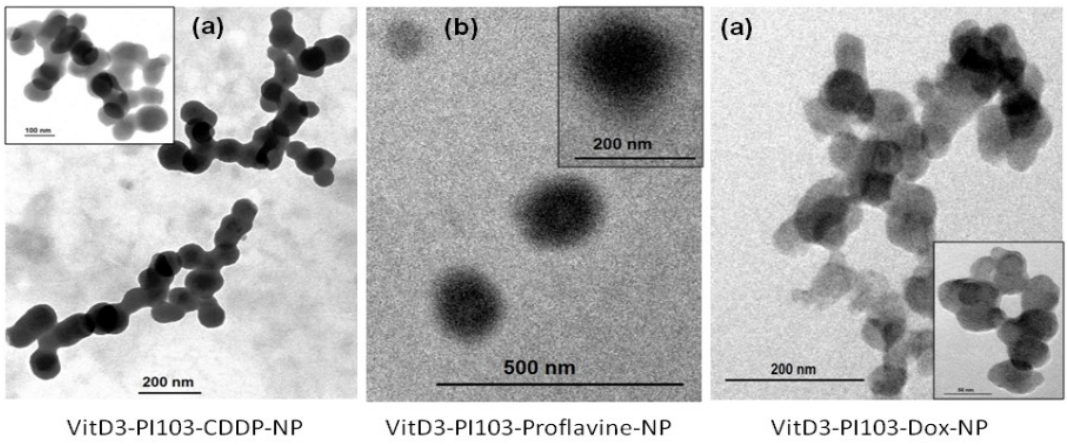

Fig. 6 (a-c) TEM images of VitD3-PI103-CDDP-NP, VitD3-PI103-Proflavine-NP and VitD3-PI103-Dox-NP respectively.

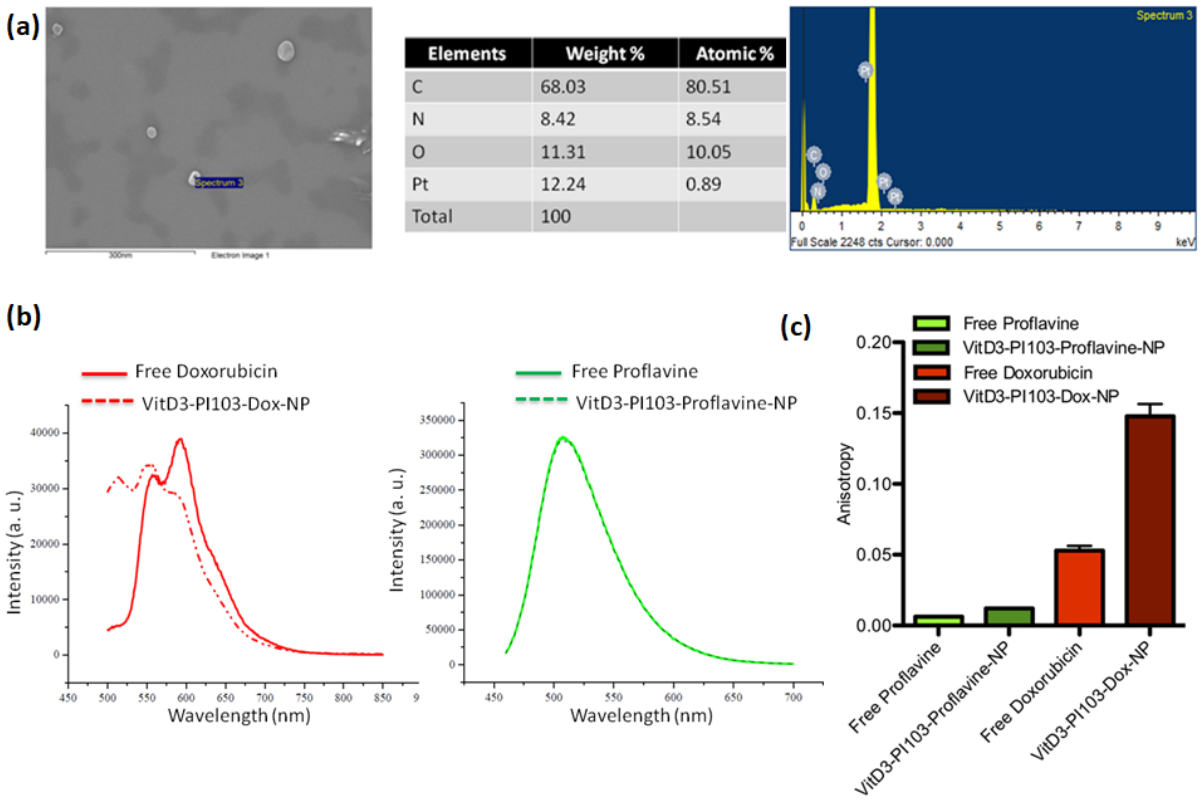

Fig. 7 (a) Characterization of Pt in VitD3-PI103-CDDP-NP by energy-dispersive X-ray spectroscopy (EDX) (b) Fluorescence emission spectra of VitD3-PI103-Dox-NP and free Doxorubicin, VitD3-PI103-Proflavine-NP and free proflavine (c) Change in steady state fluorescence anisotropy in free Proflavine and free Doxorubicin with VitD3-PI103-Proflavine-NP and VitD3-PI103-Dox-NP

wanted to understand the localization of the encapsulated drugs inside the vitamin D3 nanoparticles. We performed a steady-state fluorescence anisotropy study that provides insight into the surrounding environment of proflavine and doxorubicin inside the nanoparticles. A high anisotropy value implies that the drug molecules experience a restricted environment. The mean fluorescence anisotropy of vitD3–PI103–proflavine-NP was found to be equal to 0.012 ± 0.0003, compared to the anisotropy of free proflavine, which is equal to 0.006 ± 0.0003 (Fig. 7c). However, vitD3–PI103–Dox-NP showed a mean anisotropy value of 0.148 ± 0.009, compared to the mean anisotropy of 0.053 ± 0.003 shown by free doxorubicin in water. These changes in steady-state fluorescent anisotropy values indicate that proflavine accumulated into the hydrophilic core of the nanoparticle leading to marginal change in anisotropy value, whereas doxorubicin enters into the more hydrophobic lipid layer leading to the significant 2.8 fold increase in anisotropy value.[41]

2.2.4 Release of dual drugs from vitamin D3 nanoparticles: We evaluated the release profiles of different drugs from the dual drug loaded vitamin D3 nanoparticles because the nanoparticles should release the dual drugs in a slow and sustained manner over a long period of time to be successful in the clinics. The nanoparticles were designed to be administered through intravenous injection into the blood stream to accumulate into tumor tissue through the EPR effect. Once inside the tumor tissues, the nanoparticles should be internalized into the cells through the lysosomal compartments. We incubated different drug loaded nanoparticles in pH = 5.5 solution at 37 °C in 1000 Dalton MWCO dialysis membrane. We selected the solution of pH = 5.5 because it mimicked the acidic lysosomal compartments inside the cells.[42, 43] We quantified the amount of released drugs in predetermined time points outside the dialysis bags using concentration versus absorbance graphs (Fig. 3) by UV-Vis spectroscopy at different characteristics λ_{max} values for different drugs. The vitD3–PI103–CDDP-NP showed a slow and sustained release profile for 72 h, having released 79.22 ± 2.6 % of cisplatin at 23 h and 78.83 ± 8.4 % of PI103 in 47 h (Fig. 8a). However, vitD3–PI103–proflavine-NP released 86.15 ± 4.0 % of proflavine at 48 h and 72.87 ± 2.1 % of PI103 at 96 h (Fig. 8b). Finally, vitD3–PI103–Dox-NP demonstrated 47.05 ± 3.4 % release of doxorubicin at 72 h and 91.55 ± 2.8 % of PI103 release at 11 h (mean ± SEM, n = 3) (Fig. 8c). To mimic the blood stream, we also incubated the dual drug loaded nanoparticles in physiological pH of 7.4 at 37 °C and quantified the dual drug release. The vitD3–PI103–

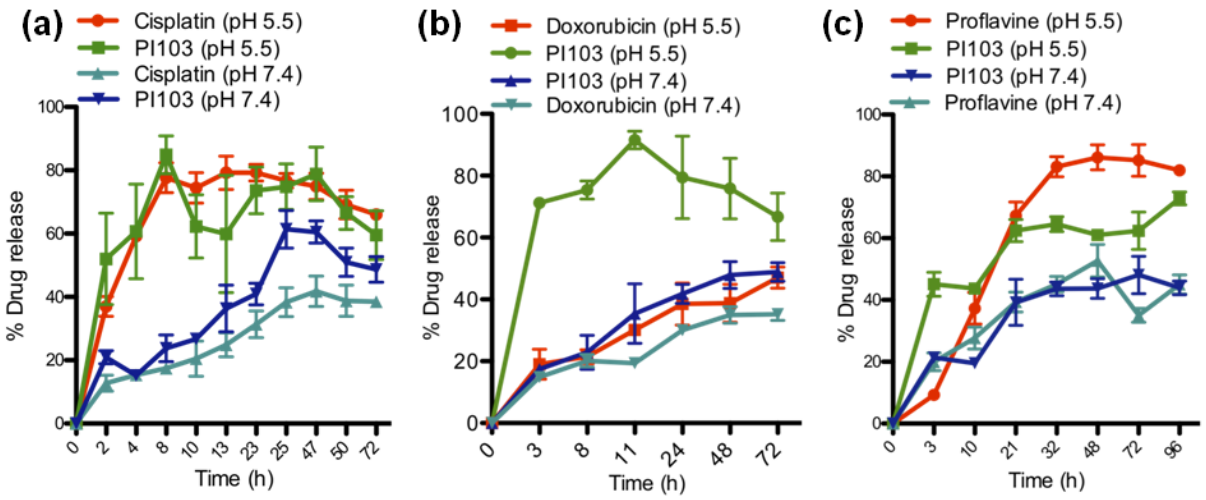

Fig. 8 Release profile of different dual drugs from nanoparticles at pH = 5.5 and 7.4. (a) Release of cisplatin and PI103 from vitD3–PI103–CDDP-NP over 72 h. (b) Release of PI103 and doxorubicin from vitD3–PI103–Dox-NP over 72 h (c) Release of proflavine and PI103 from vitD3–PI103–proflavine-NP over 96 h.

CDDP NP released 41.8 ± 4.8 % of cisplatin at 47 h and 61.4 ± 5.9 % of PI103 at 25 h (Fig. 8a). However, vitD3–PI103–Dox-NP showed 48.8 ± 3 % PI103 and 35.2 ± 1.9 % doxorubicin release over 72 h (Fig. 8b). Finally, vitD3–PI103–proflavine-NP released 45.0 ± 3.1 % of proflavine at 96 h and 48.1 ± 6 % of PI103 at 72 h (Fig. 8c). We rationalized that the phenolic ester linkage in vitD3–PI103 conjugate (2) is more labile at pH = 5.5 compared to pH = 7.4, which triggered the enhanced release of PI103 at the acidic pH. From these release kinetics experiments it was clear that higher amount of dual drugs were released from the nanoparticles in acidic pH compared to physiological pH in a slow and sustained manner over 72–96 h which would be advantageous for *in vivo* intravenous drug administration. This slow and sustained release of dual drugs in lysosomal compartment (pH = 5.5) could also lead to prolonged cytotoxicity effects of these nanoparticles in cancer cells and delay the mechanism to evolve drug resistance.

2.2.5 Stability of the vitamin D3 nanoparticles: To be successful in the clinics, the dual drug loaded nanoparticles should be stable inside the blood circulatory system at 37 °C to reach the tumor by EPR effect. We evaluated the stability of the different dual drug loaded vitamin D3 nanoparticles by measuring their change in hydrodynamic diameter and PDI values over 15 days by incubating them at 37 °C. The size of the vitD3–PI103–CDDP-NP

changed from 173 ± 0.5 nm to 166 ± 1.5 nm with change in PDI from 0.105 ± 0.01 to 0.156 ± 0.01 over 15 days (Fig. 9a and b). However, vitD3–PI103–Dox-NPs showed a change in size from 172 ± 1.1 nm to 163 ± 0.5 nm with change in PDI from 0.1 ± 0.01 to 0.18 ± 0.01 over 15 days. vitD3–PI103–proflavine-NP demonstrated a higher change in size from 170 ± 2.2 nm to 230 ± 7.1 with a significant change in PDI from 0.05 ± 0.01 to 0.38 ± 0.05 over 15 days. From this stability data, it is clear that vitD3–PI103–CDDP-NP and vitD3–PI103–Dox-NP are stable over 15 days at 37 °C. However, vitD3–PI103–proflavine-NP showed aggregation over 15 days. Furthermore, we wanted to evaluate the stability of the dual drug loaded nanoparticles in the blood stream after intravenous injection.

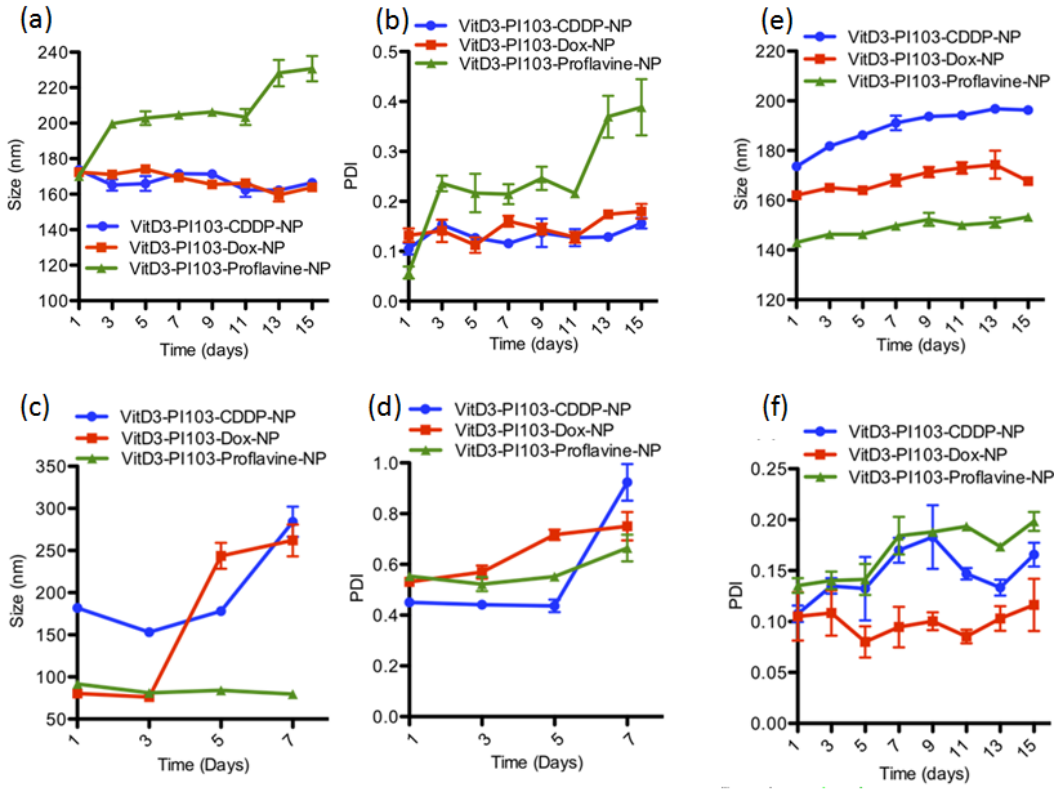

Fig. 9 Stability of different dual drug loaded vitamin D3 nanoparticles at 37 °C over 15 days. (a) Change in hydrodynamic diameter of different vitamin D3 nanoparticles. (b) Change in PDI values of different vitamin D3 nanoparticles. (c-d) Stability of different dual drug loaded vitamin D3 nanoparticles in serum at 37 °C for 7 days determined by DLS. Stability of different dual drug loaded vitamin D3 nanoparticles at 4 °C for 15 days. (**e**) Change in hydrodynamic diameter and (**f**) PDI values determined by DLS.

We incubated different dual drug loaded vitamin D3 nanoparticles in serum at 37 °C for 7 days and evaluated the hydrodynamic diameter and PDI values by DLS every alternate day. VitD3–PI103–CDDP-NP showed an increase in size from 181 ± 2 nm to 284 ± 17.9 nm (change in PDI = 0.45 to 0.92) over 7 days (Fig. 9c and d). Moreover, vitD3–PI103–Dox-NP showed an increase in size from 80 ± 1.3 nm to 262 ± 18 nm (change in PDI = 0.5 to 0.75) over 7 days. Finally, vitD3–PI103–proflavine-NP demonstrated negligible change in size from 91 ± 0.7 nm to 79 ± 1.8 nm (change in PDI =0.5 to 0.6) over 7 days. From this stability study it was clear that vitD3–PI103–CDDP-NP and vitD3–PI103–Dox-NP were stable in serum for 5 days and vitD3–PI103–proflavine-NP was stable for 7 days, which was sufficient to allow the entry into the tumor by the EPR effect. To apply these dual drug loaded vitamin D3 nanoparticles in clinics, the nanoparticles should also be stable for a longer time at lower temperature storage conditions. We also evaluated the stability of these nanoparticles at 4 °C. The size of thevitD3–PI103–CDDP-NP slightly increased from 173 ± 0.3 nm to 196.26 ± 0.7 nm with an increase in PDI value from 0.1 ± 0.008 to 0.1 ± 0.01 over 15 days (Fig. 9e and f). However, vitD3–PI103–Dox-NP showed negligible increase in size from 162 ± 1.7 nm (PDI = 0.1 ± 0.02) to 167 ± 0.6 nm (PDI = 0.116 ± 0.026) over 15 days. Finally, the size of the vitD3–PI103–proflavine-NP also increased from 143 ± 1.1 nm to 153 ± 0.8 nm with an increment in PDI value from 0.13 ± 0.007 to 0.19 ± 0.009 over 15 days. From the stability data at 4 °C, it was evident that all different dual drug loaded nanoparticles showed a steady increment in size and PDI values over 15 days, however, having sub 200 nm hydrodynamic diameter, which is ideal for extravasation into the tumor through the EPR effect. All the data were determined as mean ± SEM, n = 3.

2.2.6 *In vitro* cytotoxicity assay: *(All the in vitro assays discussed in this chapter were performed in collaboration with Dr.Rajdeep Chowdhury Lab, BITS-Pilani)*

We evaluated the *in vitro* cytotoxicity assay of our dual drug loaded vitamin D3 nanoparticles in human hepatocellular carcinoma -Hep3B cells. The cytotoxicity was quantified by MTT assay after 24 h post-incubation with the dual drug containing nanoparticles and free drugs as control. The vitD3–PI103–CDDP-NP showed considerably lower IC_{50} = 28.05 μM (cell viability = 13.1 % at 80 μM cisplatin concentration) or more cytotoxicity compared to IC_{50} = 49.08 μM (cell viability = 34.7 % at 80 μM) for free cisplatin (Fig. 10a). Similarly, vitD3–PI103–Dox-NP demonstrated IC_{50} = 6.9 μM (cell viability = 3.8 % at 80 μM doxorubicin

concentration) compared to free doxorubicin showing IC_{50} = 18.4 µM (cell viability = 15.5 % at 80 µM) (Fig. 10b).

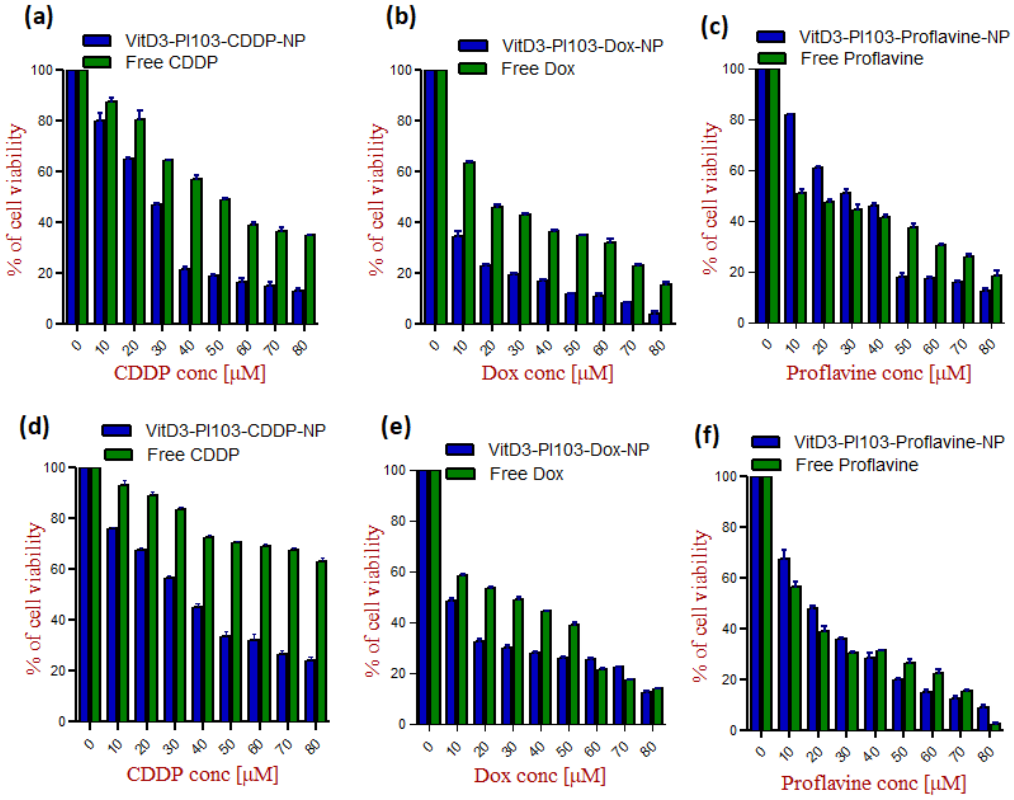

Fig. 10 (a–c) *In vitro* cell viability assay of vitD3–PI103–CDDP-NP, vitD3–PI103–Dox-NP and vitD3–PI103–proflavine-NP, respectively, in Hep3B cells at 24 h post-incubation by MTT assay. (d–f) *In vitro* cell viability assay of vitD3–PI103–CDDP-NP, vitD3–PI103–Dox-NP and vitD3–PI103–proflavine-NP, respectively, in Hep3B-R cells at 24 h post-incubation by MTT assay.

Finally, in contrast, vitD3–PI103–proflavine-NPs showed higher IC_{50}= 30.5 µM (cell viability = 12.6 % at 80 µM proflavine concentration) compared to IC_{50}= 10.1 µM (cell viability = 18.5 % at 80 µM) for free proflavine (Fig. 10c). To fully understand the effect of dual drug loaded nanoparticles, we also evaluated the cytotoxicity effect of the mono drug loaded vitD3-NPs as controls in Hep3B cells at 24 h post-incubation.VitD3–Dox-NP showed IC_{50}= 87.7 µM with 42.1 % cell viability at 100 µM concentration (Fig. 11a). Moreover, vitD3–CDDP-NP demonstrated IC_{50}= 93.7 µM with 44.5 % cell viability at 100 µM (Fig. 11b). Finally, vitD3–proflavine-NP showed improved IC_{50} = 47.5 µM having 12.6 % cell viability at 80 µM (Fig. 11c). Interestingly, vitD3–PI103-NP showed almost negligible cytotoxicity in Hep3B cells with IC_{50} = 156.2 µM (Fig. 11d). Evidently, empty vitD3-NP showed almost negligible cytotoxicity (cell viability = 76.8 %) even at 100 µM concentration

(Fig. 11e). From this cell viability assay it was clear that different dual drug loaded vitamin D3 nanoparticles induced dose dependent cytotoxicity better than the single drug treatment in Hep3B cells. Proflavine was, however, an exception.

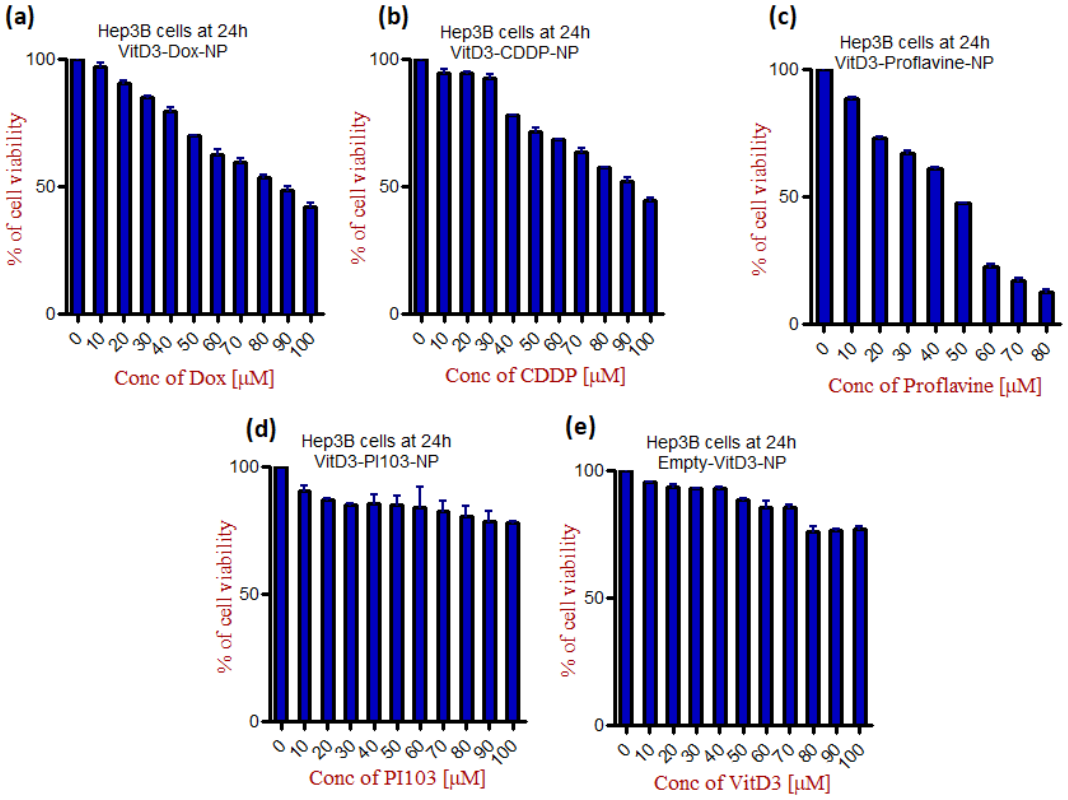

Fig. 11 (a-e) MTT assay of vitD3-Dox-NP, vitD3-CDDP-NP, vitD3-Proflavine-NP, vitD3-PI103-NP and empty vitD3-NP in Hep3B cells at 24 h post-incubation respectively.

To evaluate the potential of the dual drug loaded nanoparticles to overcome the drug resistance, cisplatin resistant Hep3B-R cells were developed from Hep3B cells. Cisplatin resistance was induced in Hep3B cells by exposing them with a very high dose (1 μM) of cisplatin, recovering the small population of live cells and repeating the cisplatin treatment in several cycles till the cells become comparatively cisplatin resistant (Fig. 12a, b). We further evaluated the effect of dual drug loaded vitamin D3 nanoparticles in Hep3B-R cells by MTT assay. Interestingly, vitD3–PI103–CDDP-NP showed considerably lower IC_{50} = 36.3 μM with 24.0 % viable cells (at 80 μM concentration of cisplatin) compared to IC_{50} = 70 μM with 63.1 % viable cells (at 80 μM) for free cisplatin treatment in resistant cells (Fig. 10d).

Similarly, vitD3–PI103–Dox-NP also showed considerably lower IC_{50} = 9.76 µM having 12.8 % of viable cells (at 80 µM concentration of doxorubicin) compared to IC_{50} = 29.51 µM with 13.9 % of viable cells for free doxorubicin (at 80 µM) (Fig. 10e). Finally, vitD3–PI103–

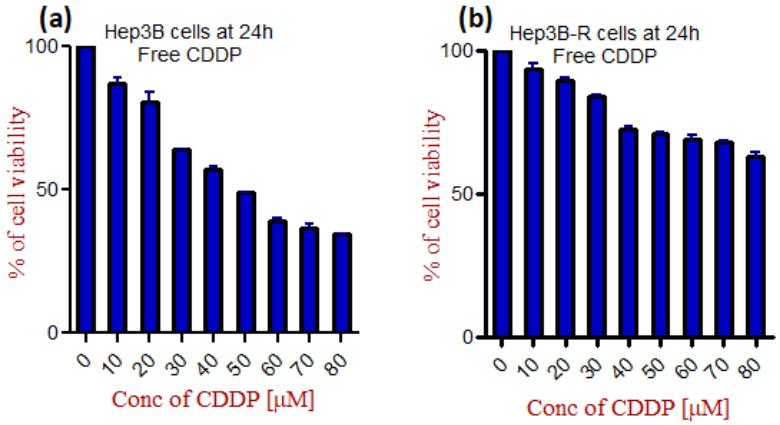

Fig. 12 MTT assay of free CDDP in Hep3B and Hep3B-R cells in different concentration at 24 h post-incubation.

proflavine-NP showed IC_{50} = 19.14 µM having 8.7 % viable cells (at 80 µM proflavine concentration) compared to IC_{50} = 11.27 µM for free proflavine having 2.5 % viable cells (at 80 µM) (Fig. 10f). We also evaluated the effect of monodrug loaded vitD3-NPs in Hep3B-R cells at 24 h post-incubation. VitD3–Dox-NP induced 42.6 % cell viability at 100 µM with IC_{50} = 86.4 µM (Fig. 13a). Moreover, vitD3–CDDP-NP showed 40.3 % cell viability at 100 µM with IC_{50} = 79.5 µM (Fig. 13b). Finally, vitD3–proflavine-NP demonstrated 9.7 % cell viability at 80 µM having IC_{50} = 27.4 µM (Fig. 13c). Interestingly, vitD3–PI103-NP showed almost negligible cytotoxicity in Hep3BR cell with IC_{50}= 93.9 µM (Fig. 13d). Empty vitD3-NP showed negligible cytotoxicity in Hep3B-R cells with 80.3 % cell viability even at 100 µM concentration (Fig. 13e). From these MTT assays, it was evident that the dual drug loaded vitamin D3 nanoparticles induced considerably higher cytotoxicity in human hepatocellular carcinoma cells Hep3B and cisplatin resistant Hep3B-R cells compared to the monotherapy.

To understand the cytotoxicity of the dual drug loaded nanoparticles in Hep3B and Hep3B-R cells, we used the Chou-Talalay method[44] to determine whether the drug combination effect was synergistic, additive or antagonistic. In Hep3B cells, vitD3–PI103–CDDP-NP and

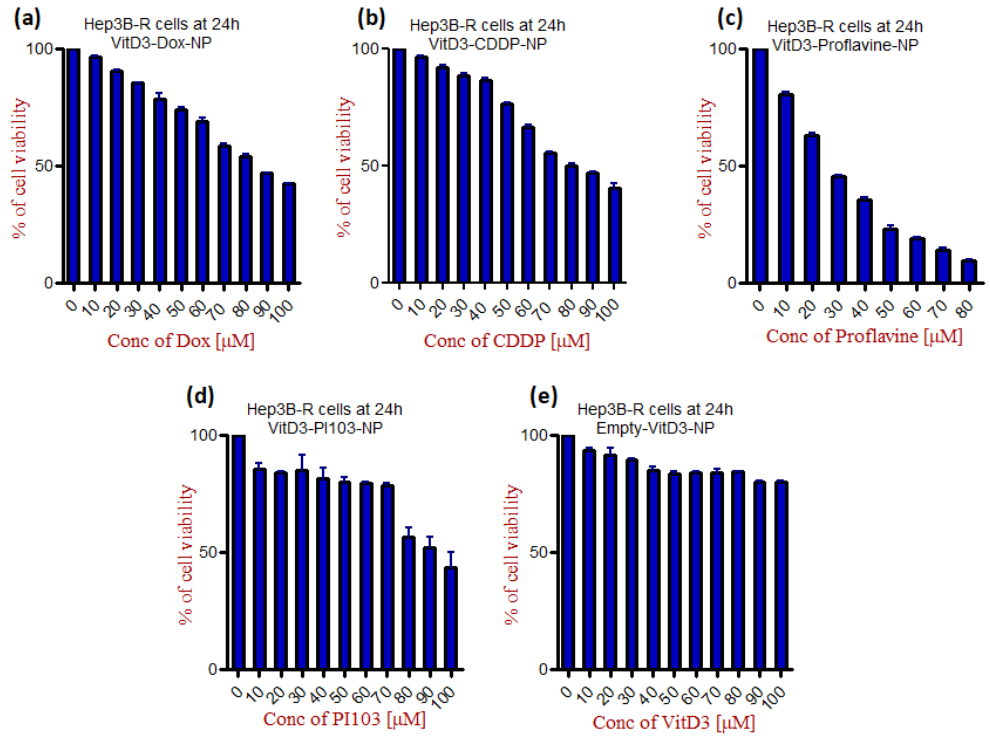

Fig. 13 (a-e) MTT assay of vitD3-Dox-NP, vitD3-CDDP-NP, vitD3-Proflavine-NP, vitD3-PI103-NP and empty vitD3-NP in Hep3B-R cells at 24 h post-incubation respectively.

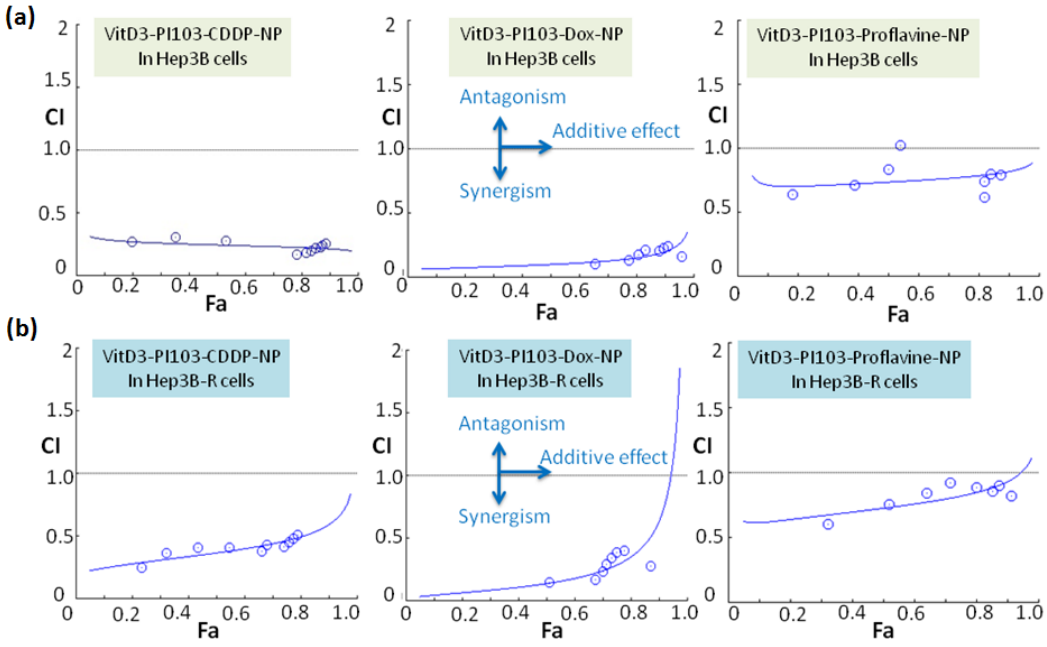

Fig. 14 Chou-Talaly analysis of vitD3-PI103-CDDP-NP, vitD3-PI103-Dox-NP and vitD3-PI103-Proflavine-NP in Hep3B cells (a) and HEP3B-R cells (b) to determine synergistic, additive and antagonistic effects.

vitD3–PI103–Dox-NP showed combination index (CI) values that varied from 0.17 to 0.31 which clearly indicated the strong synergistic effect. However, vitD3–PI103–proflavine-NP showed CI value variation from 0.62 to 1.02, which showed slight synergy to nearly additive effect (Fig. 14a). Similarly, in Hep3B-R cells, vitD3–PI103–CDDP-NP and vitD3–PI103–Dox-NP showed strong synergy (CI = 0.15 to 5.0), in contrast to vitD3–PI103–proflavine-NP, which showed weak synergy to nearly additive effect (CI = 0.60 to 0.92) (Fig. 14b). From this Chou-Talalay analysis, it was clear that the combination of PI103 with CDDP or doxorubicin showed strong synergistic effect both in Hep3B and Hep3B-R cells. However, the combination of PI103 with proflavine showed weak synergy to almost additive effect in both the hepatocellular carcinoma cell lines.

Moreover, we also evaluated the cytotoxicity of vitD3–PI103–CDDP-NP by colorimetric assay (**WST-1** based) based on the enzymatic cleavage of the tetrazolium salt WST-1 to formazan by cellular mitochondrial dehydrogenase present in viable cells.[45] VitD3–PI103–CDDP-NP showed IC_{50} = 32.2 µM with 13.1 % cell viability at 100 µM concentration, whereas vitD3–CDDP-NP and free CDDP showed IC_{50} = 104.1 µM (with 52 % cell viability at100 µM) and IC_{50} = 50 µM (with 16.8 % cell viability at 100 µM), respectively (Fig. 15a) Empty vitD3-NP showed almost negligible cytotoxicity in Hep3B cells with 76.4 % cell viability at100 µM. Similarly, we also evaluated the cytotoxicity of vitD3–PI103–CDDP-NP by WST-1 assay in Hep3B-R cells at 24 h post-incubation. In Hep3B-R cells vitD3–PI103–CDDP-NP demonstrated 24.4 % cell viability at 100 µM concentration with IC_{50} = 44.8 µM (Fig. 15b). Moreover, vitD3–CDDP-NP and free CDDP showed considerably less cytotoxicity having 37.6 % (IC_{50} = 82.2 µM) and 31.1 % (IC_{50} = 72.8 µM) cell viability, respectively, at 100 µM (Fig. 17b). Empty vitD3-NP showed marginal cytotoxicity with 77.8 % cell viability at 100 µM. These WST-1 assays supported the data of vitD3–PI103–CDDP-NP observed by MTT assay. We further evaluated the cytotoxicity effect of vitD3–PI103–CDDP-NP using trypan blue assay to determine the number of viable cells after the treatments. In Hep3B cells, vitD3–PI103–CDDP-NP significantly reduced the number of viable cells to 1.1 ± 10^4 compared to the number of viable cells in no treatment control = 4.5 ± 10^4, vitD3-NP = 3.7 ± 10^4, vitD3–CDDP-NP = 1.4 ± 10^4 and free CDDP = 1.2 ± 10^4 (Fig. 16a). Similarly, in Hep3B-R cells, vitD3–PI103–CDDP-NP reduced the number of viable cells to 0.9 ± 10^4 compared to the number of viable cells in the control = 3.8 ± 104, vitD3-NP = 3.1 ± 10^4, vitD3–CDDP-NP = 1.3 ± 10^4 and free CDDP = 2.8 ± 10^4 (Fig. 16b). This trypan blue assay also validated the cytotoxicity effect of vitD3–PI103–CDDP-NP in Hep3B and

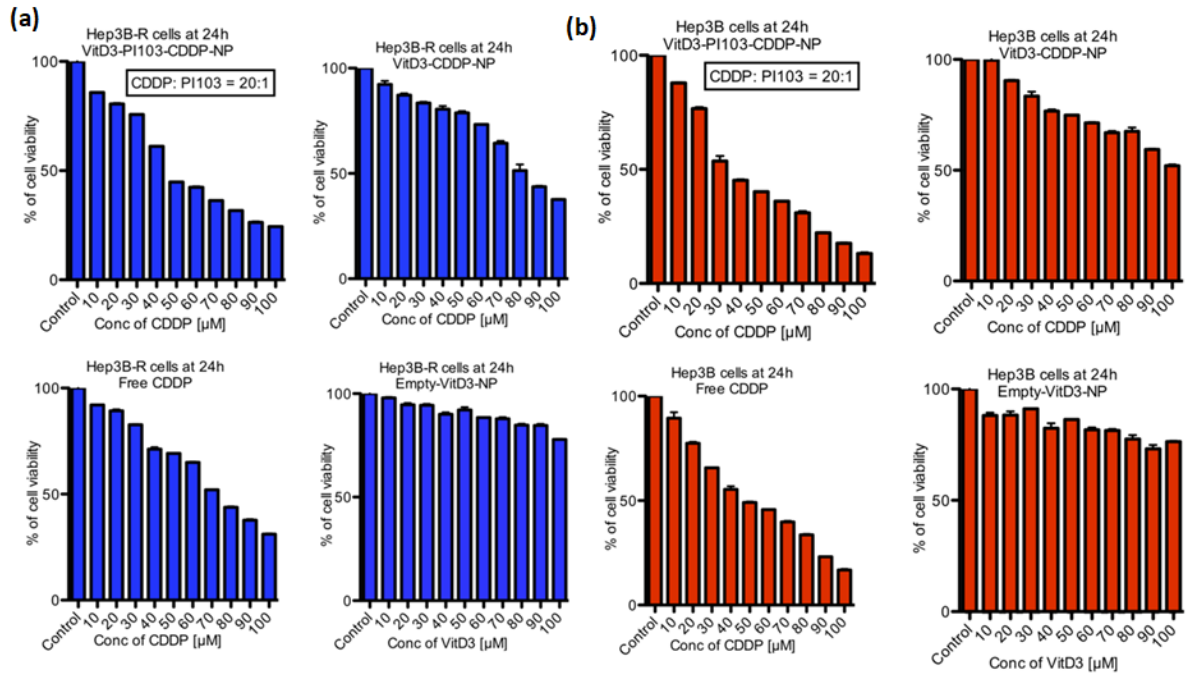

Fig. 15 WST-1 assay of vitD3-PI103-CDDP-NP, vitD3-CDDP-NP, free CDDP and empty-vitD3-NP in Hep3B cells (a) and HEP3B-R cells (b) at 24 h post-incubation.

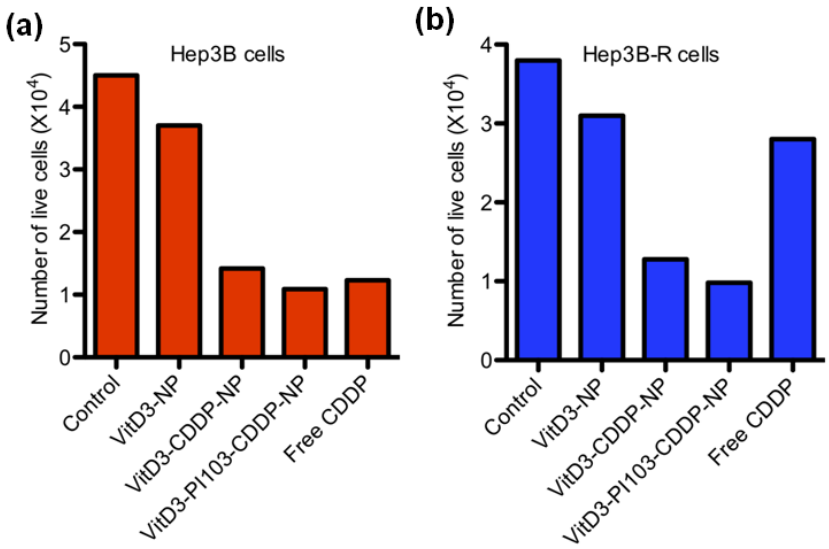

Fig. 16 (a-b) Trypan blue assay of vitD3-PI103-CDDP-NP with proper controls in Hep3B and Hep3B-R cells at 24h post-incubation respectively.

Hep3B-R cells. We also evaluated the potential of vitD3–PI103–CDDP-NP in a 5-fluorouracil (5-FU) resistant Hep3B cells because 5-FU has been widely used to treat the different types of cancers. However, overcoming 5-FU resistance remained one of the major obstacles in clinics.[46] We treated 5-FU resistant Hep3B cells (Hep3B–5FU-R) with vitD3–PI103–CDDP-NP in a dose dependent manner and evaluated the cell viability at 24 h post incubation. Interestingly, vitD3–PI103–CDDP-NP showed considerably less IC_{50} = 37.9 µM (Fig. 17a) compared to IC_{50} = 70 µM for free 5-FU (data not shown). This cell viability assay demonstrated that our dual drug loaded vitamin D3 nanoparticles can also be successfully used to overcome 5-FU resistance in cancer chemotherapy. These results can have a significant impact in the treatment of drug resistance in cancer.

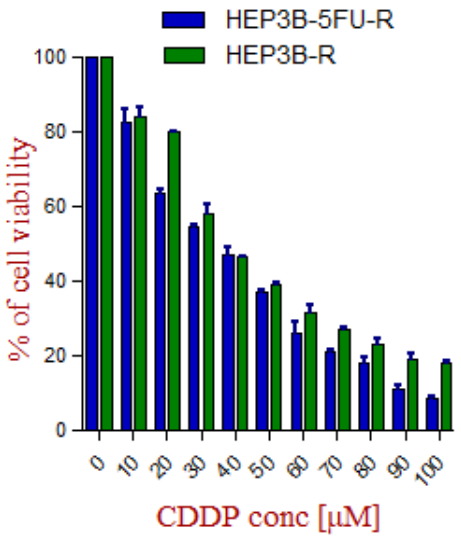

Fig. 17 (a) Cell viability assay of vitD3-PI103-CDDP-NP in 5-FU resistant Hep3B-5FU-R cells and cisplatin resistant Hep3B-R cells after 24h post incubation**.**

2.2.7 Mechanism of action: To gain the insight into the cellular response evoked by vitD3–PI103–CDDP-NP and vitD3–PI103–Dox-NP, we monitored and quantified the poly (ADP-ribose) polymerase (PARP) as a marker for the DNA damage repair mechanism[47] by western blot analysis in Hep3B cells after 24 h post-incubation. On treatment with vitD3–PI103–CDDP-NP and vitD3–PI103–Dox-NP, the cleaved PARP expression (carboxy-terminal catalytic domain having a molecular weight of 89 kDa) was significantly increased compared to that without treatment and 5-fluorouracil (5-FU, a positive control) treatment (Fig. 18), which was evident from the SDS-PAGE image by immuno-blotting and quantification. However, vitD3–PI103–CDDP-NP andvitD3–PI103–Dox-NP showed increased cleaved

PARP expression similar to the treatments with free CDDP and free doxorubicin, respectively. This western blot analysis clearly showed that the dual drug loaded vitD3-NPs induced cytotoxicity by DNA damage. Furthermore, we evaluated the mechanism of the action of the dual drug loaded NPs in inducing apoptosis. A colorimetric protease assay was performed to quantify the amount of caspase-3 as a marker of apoptosis[48] after 24 h of post-incubation with vitD3–PI103–CDDP-NP and vitD3–PI103–Dox-NP. VitD3–PI103–CDDP-NP showed 1.6 fold and 1.3 fold increase of caspase-3activity in Hep3B and Hep3B-R cells, respectively, with respect to un-treated controls (Fig. 19a) In contrast vitD3–PI103–Dox-NP showed 0.9 fold and 1.1 fold

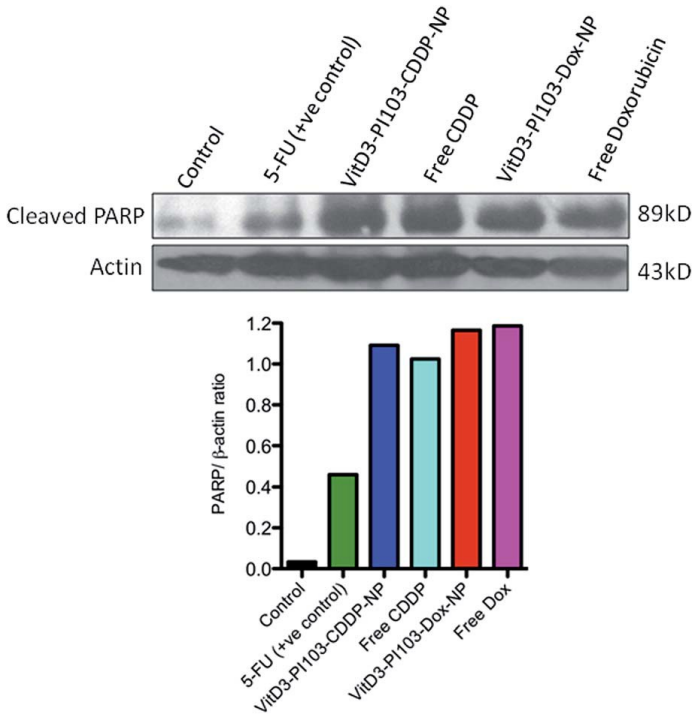

Fig. 18 Western blot analysis of vitD3–PI103–CDDP-NP and vitD3–PI103–Dox-NP treatments in Hep3B cells to show cleaved PARP expression with b-actin as control.

increase in caspase-3 expression in Hep3B and Hep3B-R cells, respectively (Fig. 19b). This caspase-3 assay clearly demonstrated that vitD3–PI103–CDDP-NP and vitD3–PI103–Dox-NP showed cytotoxic effects by inducing apoptosis in both Hep3B and Hep3B-R cells

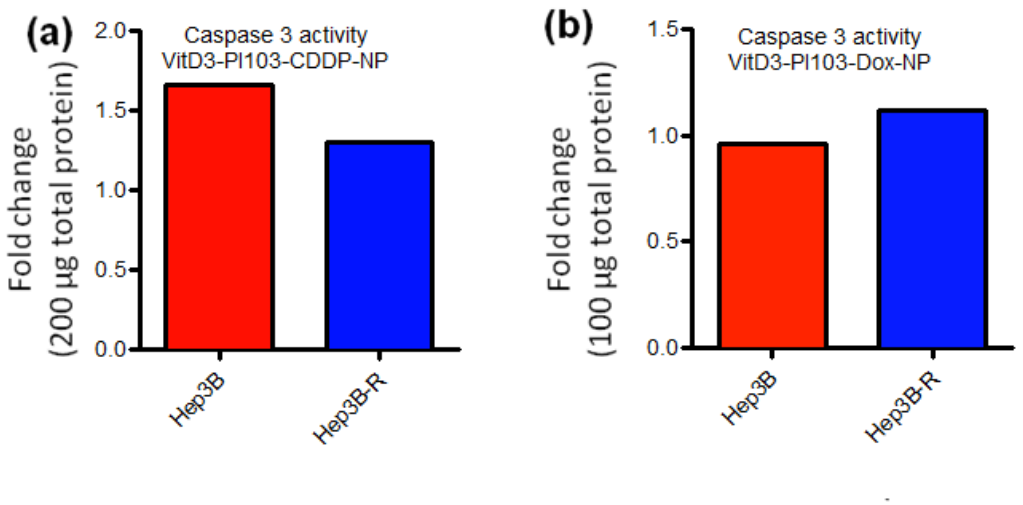

Fig. 19 (a, b) Caspase-3 activity of vitD3-PI103-CDDP-NP and vitD3-PI103-Dox-NP in Hep3B and Hep3B-R cells with respect to un-treated control with 200 µg and 100 µg of total protein content respectively.

2.2.8 Internalization of vitD3–PI103–proflavine-NP:

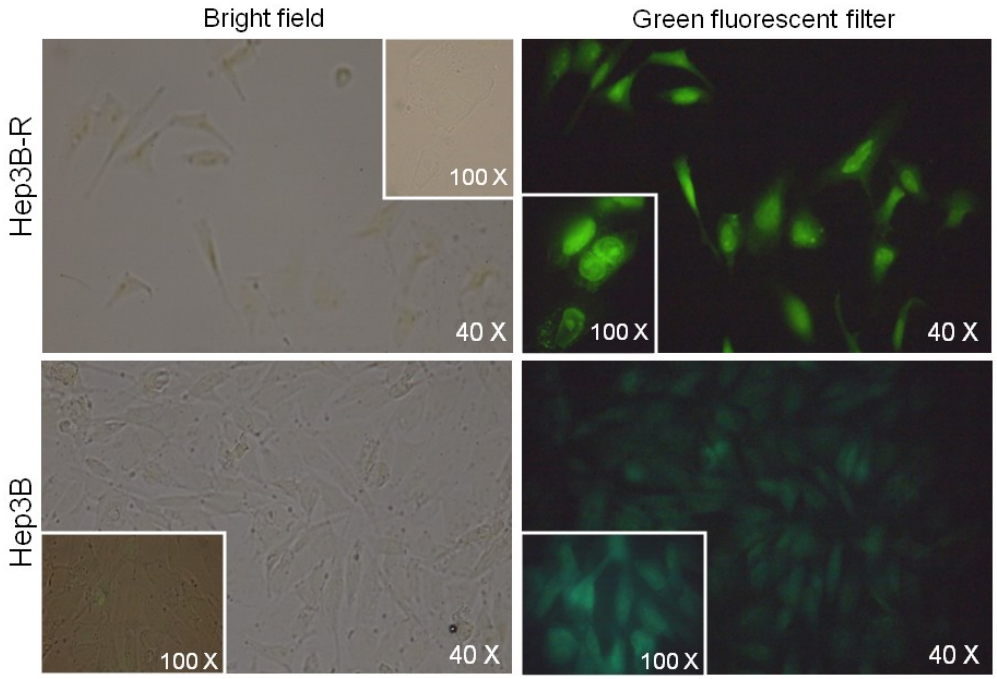

Fig. 20 Internalization of vitD3–PI103–proflavine-NP in Hep3B-R (upper panel) and Hep3B (lower panel) cells visualized by epifluorescent microscopy at 3 minutes of post-incubation.

To visualize the internalization of the dual drug loaded vitaminD3-NPs, we treated both Hep3B and Hep3B-R cells with green fluorescent vitD3–PI103–proflavine-NP and imaged the cells using fluorescence microscopy. The vitD3–PI103–proflavine-NPs were found to be rapidly internalized into the cisplatin resistant Hep3B-R cells within 3 minutes of post-incubation (Fig. 20, upper panel). However, vitD3–PI103–proflavine-NPs were considerably less internalized into the Hep3B cells within 3 minutes of post-incubation (Fig. 20, lower panel). From these epifluorescence images, it was evident that cisplatin resistant Hep3B cells rapidly internalized the vitD3–PI103–proflavine-NPs compared to the non-cisplatin resistant Hep3B cells. We anticipate that all the dual drug loaded vitamin D3-NPs were rapidly internalized into Hep3B-R cells compared to Hep3B cells leading to improved efficacy in the cisplatin resistant hepatocellular carcinoma cells compared to non-resistant cells. Interestingly, the electrical property of a cancerous cell is considerably different to that of a normal cell. Therefore, the cancer cells are found to exhibit lower electrical membrane potentials, lower electrical impedance and a complete alteration of the membrane lipid profile than their normal counterparts.[49] The altered lipid profile in cancer cells leads to improved permeability. We speculate that a similar altered lipid profile is also exhibited in drug resistant cancer cells compared to the non-resistant counterpart. However, the mechanism of improved internalization in resistant cells needs further investigation.

2.3 Conclusions

In this study, we have developed PI3K Inhibitor (PI103) loaded in combination with different DNA damaging drugs (doxorubicin, cisplatin and proflavine) NPs having a size range below 200 nm, which would be ideal for tumor insertion by the EPR effect. These nanoparticles showed high drug loading and increased dual drug release over 72 h at pH = 5.5 (mimics lysosomal compartments inside the cells) compared to pH = 7.4 (mimics blood stream). Moreover, these nanoparticles showed excellent stability over 2 weeks at 37 °C (body temperature), as well as at 4 °C (storage temperature). The nanoparticles showed improved efficacy in human hepatocellular carcinoma cells (Hep3B), as well as cisplatin resistant-Hep3B (Hep3B-R) cells compared to monotherapy by inducing apoptosis through a DNA damaging mechanism. Moreover, vitD3–PI103–CDDP-NP and vitD3–PI103–DOX-NP have exerted synergistic cell killing of both HEP-3B and Hep3B-R cells and vitD3–PI103–CDDP-NPshowed highly improved cytotoxicity in 5-FU resistant Hep3B–5FU-R cells compared to

free 5-FU.Finally, these nanoparticles internalized into the cisplatin resistant Hep3B-R cells very quickly compared to the non-resistant Hep3B cells. In future, *in vivo* efficacy of these dual drug containing nanoparticles needs to be evaluated in a cisplatin resistant xenograft model to apply these strategies in the clinics, as well as to overcome the drug resistant mechanism by the rational combination of drugs.

2.4 Experimental methods

2.4.1 Materials: All the reactions were performed under inert conditions unless otherwise indicated. All the commercially obtained compounds were used without further purification. Ethyl acetate, petroleum ether, dry dichloromethane (DCM), methanol, dimethyl sulfoxide (DMSO), cholecalciferol, succinic anhydride, sodium sulphate, pyridine, N-(3-dimethylaminopropyl)-N-ethylcarbodiimidehydrochloride (EDC), L-a-phosphatidylcholine (PC), sephadex G-25, uranyl acetate dehydrate, cisplatin, proflavine hydrochloride, copper grid for TEM, mica sheet for AFM, silicon wafer for FE-SEM and 3-(4,5-dimethylthiazol-2-yl)-2,5-diphenyltetrazolium bromide (MTT) were purchased from Sigma-Aldrich. PI103 and doxorubicin were purchased from SelleckChemicals. 1,2-Distearoyl-sn-glycero-3-phosphoethanolamine-N-[amino(polyethylene glycol) 2000] (DSPE-PEG) and the mini handheld Extruder kit (including 0.2 μM Whatman Nucleopore Track-Etch Membrane, Whatman filter supports and 1.0 mL Hamiltonian syringes) were purchased from Avanti Polar Lipids Inc. Analytical thin-layer chromatography (TLC)was performed using precoated silica gel aluminum sheets60 F254 purchased from EMD Laboratories. Minimal essential medium (MEM), fetal bovine serum (FBS), phosphate buffer saline (PBS), penicillin and streptomycin were purchased from Invitrogen. Hep3B cells were obtained from National Centre for Cell Science (NCCS), Pune. Spots on the TLC plates were visualized using alkanine permanganate or phosphomolybdicacidhydrate in methanol. The release kinetic data, drug loading, nanoparticle size and cell viability assay were plotted using GraphPad Prism software. Each sample was done in triplicate. Epifluorescence images were captured using an Olympus-BX-41microscope. WST-1 reagent (cat # 11644807001) was obtained from Roche. Chou-Talalay analysis was done using CompuSyn software from *http://www.combosyn.com/feature.html*. Trypan blue dye was obtained from Bio-Rad. RIPA buffer, Tween-20 and protease cocktail inhibitors were purchased from Sigma-Aldrich. PARP antibody was purchased from Cell Signaling Technology. b-actin antibody and

peroxidase conjugated antirabbit and antimouse IgG were obtained from Santa Cruz Biotechnology. CPP32 colorimetric protease assay kit was obtained from Invitrogen.

2.4.2 Synthesis of dual drug loaded vitamin D3 nanoparticles: 5.0 mg of L-a-phosphatidylcholine (PC), 2.5 mg of vitamin D3–PI103 conjugate (2) and 0.5 mg of 1,2-distearoyl-snglycero-3-phosphoethanolamine-N-[amino(polyethylene glycol)2000] (DSPE-PEG) were dissolved in 5.0 mL DCM. The solvent was evaporated using a rotary evaporator, and a thin and uniform lipid film was thus obtained. 1 mg of drug (cisplatin, doxorubicin or proflavine) dissolved in 1.0 mL of H_2O was added into the lipid layer and it was hydrated for 2 h at 60 °C. To remove residual non encapsulated drugs, the nanoparticles solution was passed though a Sephadex G-25 column and extruded through 200 nm Whatman polycarbonate membrane at 60 °C to obtain sub 200 nm particles. The dual drug loaded nanoparticles were stored at 4 °C for further use.

2.4.3 Quantification of drug loading in the nanoparticles: A calibration curve was plotted in the concentration range of 2.5 – 15 µM (for cisplatin), 10 – 100 µM (for doxorubicin), and 5 – 25 µM for both PI103 and proflavine individually, by diluting the 1 µM standard stock solution of drugs in DMSO. The absorbance was measured at 706 nm for cisplatin, 490 nm for doxorubicin, 444 nm for proflavine and 340 nm for PI103 against the corresponding solvent blank. The linearity was plotted for absorbance (A) against concentration (C). To determine the drug loading in nanoparticles, they were dissolved in spectroscopic grade DMSO in 2.5 %, 5 % and 7.5 % dilution. Absorbance was measured at characteristic wavelength against the corresponding solvent blank in 200 mL quartz cuvette and from the calibration curve, drug loading was measured. The quantification of cisplatin was done using a solution of o-phenylenediamine in DMF heated at 100 °C for 4 h, till the solution turned deep green in color. For the calibration curve, 1 µM stock was prepared by dissolving cisplatin into 1.2 µg mL^{-1} solution of o-phenylenediamine. The range of further dilutions from 2.5 µM to 15 µM was obtained by diluting stock solution with DMF. The absorbance was measured at 706 nm (which is characteristic λ_{max} for cisplatin against DMF as blank). The linear relationship was obtained by plotting the absorbance values (A) against corresponding concentrations (C). To estimate drug loading, 5 mL, 10 mL, and 15 mL of nanoparticle solutions were dissolved in 200 mL o-phenylenediamine solution (1.2 µg mL^{-1} of DMF). The mixture was then heated at 100 °C for 4 h until a greenish yellow color appeared. Absorbance was measured at characteristic wavelength against the corresponding solvent blank in 200 mL quartz cuvette and from the calibration curve, drug loading was

measured in triplicate. Stock solutions were prepared in different concentrations (5, 10, 15, 20, 25, and 30 µM concentrations of doxorubicin and proflavine in 1 : 1 water acetonitrile mixture) and filtered through 0.22 µM filters and injected (25 mL) into an Agilent high performance liquid chromatography (HPLC) attached with a diode-array detector (λmax = 496 nm and 260 nm for doxorubicin and proflavine, respectively) and a Zorbax SB C-18 reversed phase column (250 µM ± 4.6 µM, 5 µM).

A mobile phase of water: acetonitrile was used with a run time of 40 min; multistep gradient technology with a flow rate of µg mL^{-1} starting with 80 % : 20 % / 0–5 min, 40 % : 60 % / 5–30 min, 80 % : 20 % / 30–35 min, and 80 % : 20 % / 35–40 min. Peak areas and retention times were recorded and a calibration graph was obtained by plotting peak area versus the concentration of doxorubicin and proflavine. Drug loading was determined in triplicate by dissolving nanoparticles in 1 : 1 ratio of water and acetonitrile in 2.5 %, 5 % and 7.5 % dilutions, which were then filtered through 0.22 µm filters before injection. The peak area was measured and from the calibration curve, drug loading was measured.

2.4.4 Determination of the hydrodynamic diameter of dual drug loaded nanoparticles by dynamic light scattering (DLS): The mean hydrodynamic diameter of the dual drug loaded nanoparticles was measured by dynamic light scattering (DLS) method using Zetasizer Nano2590 (Malvern, UK). 50 mL of nanoparticle solution was diluted to 1 mL using DI water and 3 sets of 10 measurements each were performed at 90 degree scattering angle to get the average particle size.

2.4.5 Field-emission scanning electron microscopy (FESEM) of nanoparticles: 5 µL of nanoparticles in water was placed on a silicon chip without any dopant, and it was allowed to dry at room temperature under vacuum desiccators for 4hours. The silicon chip was then gold-coated (10–15 nm thickness) using Quorum, Q150T-E5. The FESEM measurements were done using a Carl Zeiss, Ultra plus, scanning electron microscope at an operating voltage of 4.0 kV.

2.4.6 Atomic force microscopy (AFM) of nanoparticles: 10 µL of nanoparticles in water was placed on a mica sheet and dried under vacuum desiccators for 4 h. The shape and size of the nanoparticles were determined using Nano Wizard Atomic Force Microscopy (AFM).

2.4.7 Transmission electron microscopy (TEM) of nanoparticles: 15 µL of nanoparticles in water was placed on a TEM copper grid. After 30 min, this sample drop was wicked off by

using filter paper, and then 15 µL of freshly prepared 0.25 % uranyl acetate (2.5 mg uranyl acetate in 1 mL dd water) solution was placed on the TEM copper grid. After 1 min, uranyl acetate solution was wicked off and the sample was washed three times with 15 µL dd water each time. The sample was dried overnight on a clean dust-free surface under a funnel. The nanoparticles were imaged using Tecnai G2 20-Twin LR-TEM instruments.

2.4.8 Determination of dual drug release from the nanoparticles: Concentrated 200 mL drug loaded nanoparticles we resuspended in 200 mL solution of pH 5.5 or in PBS buffer (pH = 7.4) and sealed in a dialysis membrane (MWCO = 2000 Dalton). The dialysis bags were then suspended in 10 mL pH 5.5 solution or in PBS buffer (pH = 7.4) at room temperature with gentle shaking. 400 mL of the solution was withdrawn from the incubation medium and was collected at predetermined time intervals. The released dual drugs were quantified by a UV-vis spectrophotometer.

2.4.9 Cell culture: Human hepatocellular carcinoma cell line, Hep3B (obtained from NCCS Pune), were cultured at 37 °C, 5 % CO_2, in minimal essential medium (MEM) supplemented with 10 % fetal bovine serum (FBS), 100 units per mL penicillin, and 100 µg mL^{-1} sreptomycin. The cells were typically grown to 60–70 % confluency, rinsed in phosphate-buffered saline (PBS) and placed into fresh medium prior to treatments.

2.4.10 MTT cytotoxicity assay: For determining the *in vitro* cytotoxicity, the cells were seeded at a density of 4000 cells per well in a 96 well plate and incubated overnight under optimum culture conditions. The drug stocks were prepared in DMSO. The cells were treated with various drugs or nanoparticles at different concentrations for 24 hours. A DMSO (0.2 %) control was also performed. Following the treatment, 20 µL of MTT dissolved in 1x PBS was added to each well at a final concentration of 1 µg mL^{-1} and incubated for 4 h. Formazan crystals that were formed due to the presence of live cells were solubilized in DMSO. Readings were obtained at 495 nm with a differential filter of 630 nm using a microplate reader. The experiment was performed in triplicate, and a paired t-test was used to determine the statistical significance (at 5 % level of significance).

2.4.11 Creation of resistant cell lines: The sensitivity of Hep3B cells to cisplatin was initially evaluated. IC50 was determined by MTT assay. To create drug-resistant cell lines, Hep3B cells were given an insult of a very high concentration of cisplatin (1 µM). The high dose drug treatment was repeated on cells that revived after each insult, and this cycle was continued for several times. Cells surviving the repeated cycles of drug treatment were found

to be comparatively resistant to cisplatin (Hep3B-R) than parental untreated cells (Hep3B). Resistance to cisplatin was checked by MTT assay. The cells were subsequently maintained at IC_{50}.

2.4.12 WST-1 cytotoxicity assay: Hep3B and Hep3B-R cells growing in log phase were briefly seeded at a density of 4000 cells per well in a 96 well plate and incubated for 24 hours with 5 % CO_2 at 37 °C. The cells were treated with vitD3–PI103–CDDP-NP, vitD3–CDDP-NP, free CDDP and empty-vitD3-NP at various concentrations for 24 hours. Following the drug treatment, WST1 reagent was added (10 µL in 100 µL media) in all the wells and incubated for 4 hours. Then, absorbance was measured at 450 nm using a microplate reader. The percentage of viable cells was calculated using the following formula: Viability (%) = (mean absorbance value of drug treated cells)/(mean absorbance value of control) ± 100.

2.4.13 Trypan blue cell viability assay: Hep3B and Hep3B-Rcells growing in log phase were briefly seeded at a density of 4 ± 104 in a 6 well plate and incubated for 24 hours with 5 % CO2 at 37 °C. The cells were treated with vitD3–PI103–CDDP-NP, vitD3–PI103-NP, vitD3–CDDP-NP, empty vitD3-NP and free CDDP at various concentrations with untreated cells as control for 24 hours. Post treatment, the cells were washed with 1X PBS and trypsinised. The cells were spin down and resuspended in fresh media, 20 mL of which was mixed with 2 mL of trypan blue dye and placed in a dual chamber cell counter slide. The viability was checked using an automated cell counter (BioRad, USA).

2.4.14 Western blot analysis for PARP: Cells were seeded at a density of 1 X 10^6 in a 60 mm dish and maintained at 5 % CO_2 at 37 °C in an incubator. After the treatment for 24 hours, the cells were harvested by scraping in RIPA buffer supplemented with protease cocktail inhibitor. Briefly, 40 µg of protein was loaded per sample by standard SDS-PAGE on 10 % gel and electrophoretically transferred onto a PVDF membrane. After blocking in 5 % non fat dry milk in 1X TBS and 0.01 % Tween-20, proteins were imune-detected using antibodies against PARP (dilution 1 : 1000, Cell Signaling Technology). The equal loading of protein was verified using b-actin (1 : 2000, SantaCruz Biotechnology) antibodies. Peroxidase conjugated antirabbit and antimouse IgG (1 : 10 000 and 1 : 20 000, Santa CruzBiotechnology) were used as secondary antibodies followed by the detection of specific signals using ECL western blotting substrate. The densitometric quantification of PARP normalized to b-actin band intensities was done with ImageJ1.47 (National Institute of Health, Bethesda, MD, USA).

2.4.15 Caspase-3 protease assay: Caspase-3 activity was determined using CPP32 colorimetric protease assay. The cells were seeded at a density of 1 x10^6 in a 60 mm dish and maintained at 5 % CO_2 at 37 °C in an incubator. After treatment for 24 hours, the cells were harvested by cell lysis buffer and either 100 µg or 200 µg of protein lysate were loaded in a 96 well plate. Caspase-3 activity was determined by adding DEVD-pNA substrate and incubating for 2 hours in the dark at 37 °C. The samples were read at 405 nm using an enzyme-linked imunosorbent assay (ELISA) microplate reader.

2.4.16 Fluorescent imaging of nanoparticle internalization: Hep3B or Hep3B-R cells were seeded on sterile cover slips kept in 6 cm dishes at a density of 6000 cells per well. After overnight incubation in a normal cell culture conditions mentioned above, the media was removed and the cells were washed three times with 1x PBS and treated with vitD3–PI103–proflavine-NP at a concentration of 30 µM (in MEM media) for 3minutes. The cover slips were washed thrice in 1x PBS and mounted on a slide and observed under fluorescence microscope using an FITC filter (emission wavelength 513–556 nm).

2.5 References

1. A. Arcaro and A. S. Guerreiro, *Curr. Genomics*, 2007, **8**, 271-306.
2. P. Liu, H. Cheng, T. M. Roberts and J. J. Zhao, *Nat. reviews. Drug Discov.*, 2009, **8**, 627-644.
3. S. Matsuoka, B. A. Ballif, A. Smogorzewska, E. R. McDonald, K. E. Hurov, J. Luo, C. E. Bakalarski, Z. Zhao, N. Solimini and Y. Lerenthal, *Science*, 2007, **316**, 1160-1166.
4. J. Brognard, A. S. Clark, Y. Ni and P. A. Dennis, *Cancer Res.*, 2001, **61**, 3986-3997.
5. T. M. Grana, E. V. Rusyn, H. Zhou, C. I. Sartor and A. D. Cox, *Cancer Res.*, 2002, **62**, 4142-4150.
6. D. Hambardzumyan, O. J. Becher, M. K. Rosenblum, P. P. Pandolfi, K. Manova-Todorova and E. C. Holland, *Genes Dev.*, 2008, **22**, 436-448.
7. A. K. Gupta, W. G. McKenna, C. N. Weber, M. D. Feldman, J. D. Goldsmith, R. Mick, M. Machtay, D. I. Rosenthal, V. J. Bakanauskas and G. J. Cerniglia, *Clinic. Cancer Res.*, 2002, **8**, 885-892.

8. B. Mukherjee, H. Choy, C. Nirodi and S. Burma, *Semin. Radiat. Oncol*. 2010, **20**, 250-257.
9. K. A. West, S. S. Castillo and P. A. Dennis, *Drug Resist. Update.*, 2002, **5**, 234-248.
10. A. C. Begg, F. A. Stewart and C. Vens, *Nat. Rev. Cancer*, 2011, **11**, 239-253.
11. D. S. Kohane and R. Langer, *Chem. Sci.*, 2010, **1**, 441-446.
12. E. R. Nelson, S. E. Wardell, J. S. Jasper, S. Park, S. Suchindran, M. K. Howe, N. J. Carver, R. V. Pillai, P. M. Sullivan and V. Sondhi, *Science*, 2013, **342**, 1094-1098.
13. Q. Wu, T. Ishikawa, R. Sirianni, H. Tang, J. G. McDonald, I. S. Yuhanna, B. Thompson, L. Girard, C. Mineo and R. A. Brekken, *Cell Rep.*, 2013, **5**, 637-645.
14. H. Zhang, G. Grüner and Y. Zhao, *J. Mater. Chem. B*, 2013, **1**, 2542-2567.
15. K. Yang, L. Feng, X. Shi and Z. Liu, *Chem. Soc. Rev.*, 2013, **42**, 530-547.
16. T. Liu, L. Li, X. Teng, X. Huang, H. Liu, D. Chen, J. Ren, J. He and F. Tang, *Biomaterials*, 2011, **32**, 1657-1668.
17. Q.-W. Fan, Z. A. Knight, D. D. Goldenberg, W. Yu, K. E. Mostov, D. Stokoe, K. M. Shokat and W. A. Weiss, *Cancer cell*, 2006, **9**, 341-349.
18. P. Workman, P. A. Clarke, F. I. Raynaud and R. L. van Montfort, *Cancer Res.*, 2010, **70**, 2146-2157.
19. J. A. Engelman, *Nat. Rev. Cancer*, 2009, **9**, 550-562.
20. D. M. Sabatini, *Nat. Rev. Cancer*, 2006, **6**, 729-734.
21. X. Wan, B. Harkavy, N. Shen, P. Grohar and L. Helman, *Oncogene*, 2007, **26**, 1932-1940.
22. M.-A. Westhoff, J. Kandenwein, S. Karl, S. Vellanki, V. Braun, A. Eramo, G. Antoniadis, K.-M. Debatin and S. Fulda, *Oncogene*, 2009, **28**, 3586-3596.
23. F. I. Raynaud, S. Eccles, P. A. Clarke, A. Hayes, B. Nutley, S. Alix, A. Henley, F. Di-Stefano, Z. Ahmad and S. Guillard, *Cancer Res.*, 2007, **67**, 5840-5850.
24. M. S. Ewer and S. M. Ewer, *Nat. Rev. Cardiol.*, 2010, **7,** 564-575.
25. G. Minotti, P. Menna, E. Salvatorelli, G. Cairo and L. Gianni, *Pharm. Rev.*, 2004, **56**, 185-229.
26. A. Rossi, M. Di Maio, P. Chiodini, R. M. Rudd, H. Okamoto, D. V. Skarlos, M. Früh, W. Qian, T. Tamura and E. Samantas, *J. Clinic. Oncol.*, 2012, **30**, 1692-1698.
27. A. Lorch, A. Kleinhans, A. Kramar, C. K. Kollmannsberger, J. T. Hartmann, C. Bokemeyer, O. Rick and J. Beyer, *J. Clinic. Oncol.*, 2012, **30**, 800-805.
28. L. Staudacher, P. Cottu, V. Dieras, A. Vincent-Salomon, M. Guilhaume, L. Escalup, T. Dorval, P. Beuzeboc, L. Mignot and J. Pierga, *Ann. Oncol.*, 2010, **22**, 848-856.

29. P. D. Sánchez-González, F. J. López-Hernández, J. M. López-Novoa and A. I. Morales, *Critic. Rev. Toxicol.*, 2011, **41**, 803-821.
30. X. Yao, K. Panichpisal, N. Kurtzman and K. Nugent, *Am. J. Med. Sci.*, 2007, **334**, 115-124.
31. Z. H. Siddik, *Oncogene*, 2003, **22**, 7265-7279.
32. L. Galluzzi, L. Senovilla, I. Vitale, J. Michels, I. Martins, O. Kepp, M. Castedo and G. Kroemer, *Oncogene*, 2012, **31**, 1869-1883.
33. L. L. Belyanskaya, S. Hopkins-Donaldson, S. Kurtz, A. P. Simões-Wüst, S. Yousefi, H. U. Simon, R. Stahel and U. Zangemeister-Wittke, *Int. J. Cancer*, 2005, **117**, 755-763.
34. S. Guo, H. Lopez-Marquez, K. C. Fan, E. Choy, G. Cote, D. Harmon, G. P. Nielsen, C. Yang, C. Zhang and H. Mankin, *PloS One*, 2014, **9**, e93996.
35. W. D. Sasikala and A. Mukherjee, *J. Phys. Chem. B*, 2012, **116**, 12208-12212.
36. W. A. Denny, *Curr. Med. Chem.*, 2002, **9**, 1655-1665.
37. Y. Matsumura and H. Maeda, *Cancer Res.*, 1986, **46**, 6387-6392.
38. S. Patil, S. Gawali, S. Patil and S. Basu, *J. Mater. Chem. B*, 2013, **1**, 5742-5750.
39. P. Sengupta, S. Basu, S. Soni, A. Pandey, B. Roy, M. S. Oh, K. T. Chin, A. S. Paraskar, S. Sarangi and Y. Connor, *Proc. Natl. Acad. Sci. U.S.A.*, 2012, **109**, 11294-11299.
40. J. M. Harris and R. B. Chess, *Nat. Rev. Drug Discov.*, 2003, **2**, 214-221.
41. T. G. Burke and T. R. Tritton, *Biochemistry*, 1985, **24**, 1768-1776.
42. Y. Urano, D. Asanuma, Y. Hama, Y. Koyama, T. Barrett, M. Kamiya, T. Nagano, T. Watanabe, A. Hasegawa and P. L. Choyke, *Nat. Med.*, 2009, **15**, 104-109.
43. J. Gilleron, W. Querbes, A. Zeigerer, A. Borodovsky, G. Marsico, U. Schubert, K. Manygoats, S. Seifert, C. Andree and M. Stöter, *Nat. Biotechnol.*, 2013, **31**, 638-646.
44. T.-C. Chou, *Cancer Res.*, 2010, **70**, 440-446.
45. A. Guertler, A. Kraemer, U. Roessler, S. Hornhardt, U. Kulka, S. Moertl, A. Friedl, T. Illig, E. Wichmann and M. Gomolka, *Radiot. Prot. Dosim.*, 2010, **143**, 487-490.
46. D. B. Longley, D. P. Harkin and P. G. Johnston, *Nat. Rev. Cancer*, 2003, **3**, 330-338.
47. P. Bouwman and J. Jonkers, *Nat. Rev. Cancer*, 2012, **12**, 587-598.
48. A. G. Porter and R. U. Jänicke, *Cell Death Differ.*, 1999, **6**, 99-104.
49. C. D. Cone, *N. Y. Acad. Sci.*, 1974, **238**, 420-435.

Chapter 3

Chimeric Nanoparticle Mediated Targeting of PI3K Signaling in Combination with DNA Damage.

3.1 Introduction

Recognizing the fact that the PI3K-Akt-mTOR signaling pathway is a key regulator of tumor cell survival, proliferation, protein translation, metabolism, angiogenesis and metastasis-associated phenotypes, the PI3K pathway has been considered as one of the most studied targets in cancers.[1-9] The growing evidence have proven that the limited clinical activity with PI3K inhibitors as single-agent treatment is due to activation of parallel and compensatory signaling networks.[10] Therefore, inhibition of such compensatory signaling networks is being investigated in clinical studies to overcome resistance to PI3K inhibition. Survival of cancer cells under stressful conditions by up-regulating PI3K signaling prompted the need for a combination strategy with DNA damaging drugs to enhance therapeutic efficacy in cancer treatment.[4] Several studies showed the synergistic effects of combining PI3K inhibitors with cytotoxic drugs in treating different types of cancers.[11-13] Although, these combination strategies indicated improved therapeutic outcomes, as discussed in previous chapters the drug cocktails can diffuse unsystematically throughout the entire body to escalate severe toxic side effects and poor accumulation into tumor tissue for optimal effects. To address these challenges nanotechnology based platform has been explored in this scenario. A recent report revealed that sequential administration of PI3K inhibitors (PI103 and PI828) followed by cisplatin nanoparticles enhanced the antitumor efficacy in breast cancer.[14] Moreover, in chapter 2 we have observed that nanoparticle mediated PI3K signaling inhibition with DNA damaging agents (cisplatin and doxorubicin) exhibited strong synergism in drug (cisplatin) resistant Hep3B cells and normal Hep3B cells. However, there is no precedence of triple-drug combination therapy with PI103, doxorubicin, and cisplatin in a single nanoparticle package to deliver these combinations of drugs in cancer.[15] Inspired by the improved efficacy of PI3K inhibitors along with doxorubicin and cisplatin, we hypothesized that biocompatible, biodegradable, and versatile chimeric nanoparticles would accumulate inside the cancerous tissue by enhanced vascular permeabilization and internalize into the cancer cells by endocytosis for synchronized targeting of phosphatidylinositol-3-kinase signaling and inducing DNA damage for augmented therapeutic outcomes (Fig. 1c). To this end, we engineered cholesterol based chimeric nanoparticles (ChNPs) that can concurrently deploy PI103, doxorubicin, and cisplatin (Fig. 1b). These ChNPs permitted high triple drug loadings in a controlled ratiometric mode and demonstrated enhanced release in an acidic environment (mimics lysosomes in cancer cells) in a controlled and continuous manner over 120 h related to physiological pH =7.4. These ChNPs exhibited improved cytotoxicity in different cancer

cell lines compared to free drug combination at 24 h and 48 h time points through induction of apoptosis. Moreover, these ChNPs were internalized into the sub cellular lysosomes in a time dependent manner over 6 h and remained inside the cells for 48 h. These ChNPs induced cytotoxicity through apoptosis by damaging DNA, up-regulating the DNA damage repair mechanism, and inhibiting PI3K signaling in HeLa cervical cancer cells. These ChNPs showed their potential for simultaneous controlled loading and deployment of PI103 in rational amalgamation with doxorubicin and cisplatin inside the tumor cells for next-generation targeted cancer therapeutics.

3.2 Results and discussion

3.2.1 Development of cholesterol−drug conjugates: We have chosen nontoxic and biodegradable cholesterol for developing the ChNPs due to its ubiquitous nature as a cellular membrane component. Cholesterol is a neutral lipid, present almost in all types of mammalian cells, plays a major role in the maintenance of the integrity of biologic membranes such as cell membrane. Cholesterol is available in the body either from dietary sources or from *de novo* biosynthesis. The free hydroxyl group in cholesterol (1) was first converted into carboxylic acid by reacting with succinic anhydride, pyridine, and DMAP to achieve conjugate 2 in 77% yield (Fig. 1a). We have chosen succinic acid as it is one of the major components in the tri-carboxylic acid cycle (TCA) in mitochondria in our body.[16] We further reacted conjugate 2 with PI103[17] using EDC and DMAP as coupling reagents to afford a cholesterol-PI103 conjugate (3) in 72 % yield. We also conjugated doxorubicin with conjugate 2 by amide linkage using HBTU/DIPEA to attain a cholesterol-doxorubicin conjugate (4) in 70 % yield. Finally, cisplatin (CDDP) was converted to aquated *cis*-$Pt[(NH_3)_2(OH_2)_2]^{2+}$(5),[18] which was further attached with conjugate 2 by a Pt−carboxylato bond[19] to synthesize a cholesterol−cisplatin conjugate (6) in 90 % yield. The conjugates (2, 3, 4, and 6) were characterized by ^{1}H, ^{13}CNMR, and high resolution mass spectroscopy (HR-MS). Furthermore, conjugate 6 was characterized by ^{195}Pt NMR spectroscopy having peak at −1304 ppm.[20]

3.2.2 Development of ChNPs: We developed the ChNPs from cholesterol−drug conjugates (3, 4, and 6), PC, and a DSPE-PEG_{2000} mixture in different ratios (Fig. 1b).[21] We surface coated the ChNPs with DSPE-PEG_{2000} to provide a "stealth-like" property for evading the immune system and improving long blood circulation half-life.[22] The drug loading in ChNPs was quantified by UV−Vis spectroscopy based on characteristic λ_{max}= 340 nm (PI103), 480

nm (doxorubicin), and 706 nm (cisplatin) from a standard absorbance versus concentration graph (Fig. 3, Chapter 2).

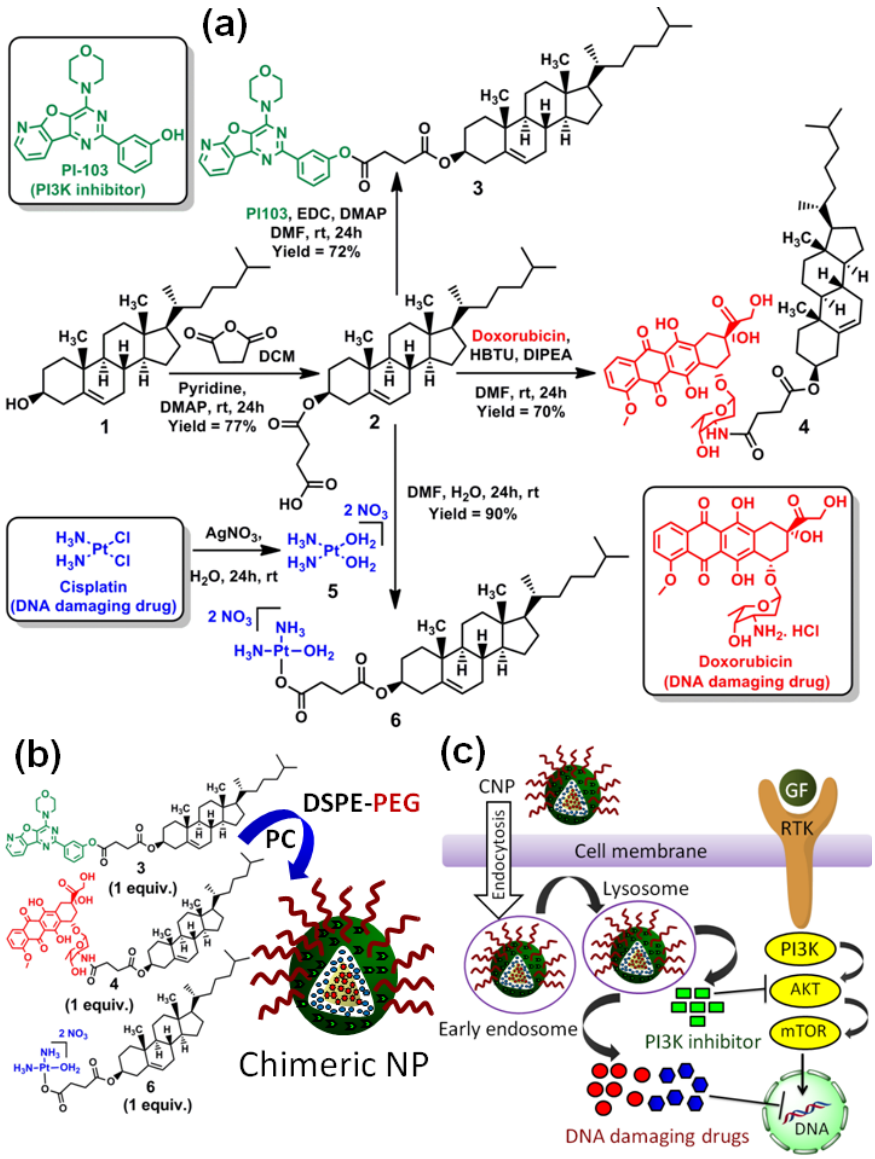

Fig. 1 Schematic diagram of engineering chimeric nanoparticles (ChNPs) and cellular internalization. (a) Synthesis of cholesterol−drug conjugates. (b) Schematic representation of ChNP synthesis. (c) Hypothesized internalization of ChNPs into cancer cells through lysosomes to target PI3K signaling and damage DNA.

It was reported that due to rapid *in vivo* metabolism, it is necessary to achieve a nearly 10-fold increased concentration of PI103 for effective inhibition of PI3K and downstream Akt signaling.[23] Moreover, doxorubicin and cisplatin exert cardio-toxicity and nephrotoxicity to

the patients respectively.[24, 25] Hence, it is highly important to package these drugs in optimal loading in the nanoplatform for effective combination therapy. To obtain the ChNPs with optimized drug loading, the stoichiometric amount of cholesterol-drug conjugates 3, 4 and 6 were varied in different weight ratios. We observed a clear translation of the weight ratios into the final drug loading ratio with high drug loading efficiency in the ChNPs with less than 200 nm size and comparable

Chol-PI103 conjugate (mg)	Chol-Dox conjugate (mg)	Chol-CDDP conjugate (mg)	Loading ratio (PI103:Dox: CDDP)	Size of ChNP (nm)	PDI of ChNP	Drug Loading Efficiency (%)
0.5	0.5	1	0.6: 0.6: 1.0	124.8 ± 11	0.25 ± 0.05	PI103 = 23.6 Dox = 26.6 CDDP = 20.9
1	0.5	0.5	1: 0.4: 0.6	156.0 ± 4	0.15 ± 0.09	PI103 = 20.6 Dox = 21.6 CDDP = 25.8
0.5	1	0.5	0.4: 1: 0.6	128.8 ± 5	0.23 ± 0.04	PI103 = 16.6 Dox = 22.8 CDDP = 23.8
1	1	1	1: 0.8: 0.9	153.7 ± 3	0.06 ± 0.03	PI103 = 20.6 Dox = 20.6 CDDP = 21.8

Table 1. Loading of PI103, doxorubicin and cisplatin in ChNP in a controlled ratio-metric manner for optimum size and drug loading and loading efficiency

polydispersity index (PDI) values, determined by DLS (Table 1). This ratiometric quantification clearly showed that the drug loading ratio could be controlled in the ChNPs based on the need of the patients as well as the tumor types by using different stoichiometric amount of cholesterol-drug conjugates. However, we used PI103: doxorubicin: CDDP = 1:0.8:0.9 loading in ChNPs for further studies having a mean drug loading of 252 μM, 204 μM, and 244 μM for PI103, doxorubicin, and cisplatin, respectively. The mean size of the ChNPs was found to be 153.7 nm in diameter by DLS (Fig. 2a). Size, shape, and morphology of the ChNPs were further visualized by FESEM (Fig. 2b), AFM (Fig. 2c), and TEM (Fig. 2d). DLS and electron microscopy images clearly demonstrated that the ChNPs were spherical in shape, at less than 200 nm in diameter, hence suitable for passive tumor targeting

through the leaky and tortuous vasculature. Furthermore, energy-dispersive X-ray spectroscopy (EDX) measurement was performed to demonstrate the presence of Pt metal from cisplatin in ChNPs (Fig. 3).

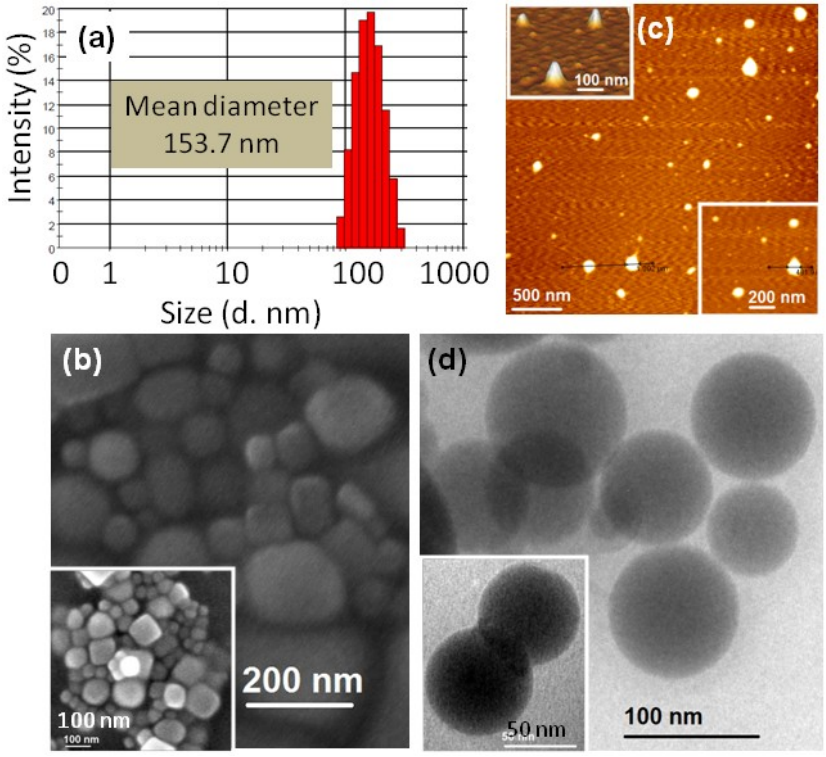

Fig. 2 Characterization of size, shape, and morphology of ChNPs by (a) DLS, (b) FESEM, (c) AFM, and (d) TEM.

3.2.3 Stability of the ChNPs: To translate successfully from bench to bedside, the ChNPs should maintain extensive stability over a long time under storage conditions. We estimated the stability of ChNPs at 4 °C in PBS for 2 weeks by measuring size and PDI using DLS. Size of the ChNPs changed marginally from 159.9 ± 2.9 nm (PDI = 0.105 ± 0.01) to 162.7 ± 1.4 nm (PDI= 0.132 ± 0.004) over 2 weeks (Fig. 4a, b). Further, we measured the stability of the ChNPs at 37 °C in PBS for 2 weeks. The size of the ChNPs increased from 155.0 ± 1.7 nm with PDI = 0.069 ± 0.0 to 159.2 ± 1.3 nm with PDI = 0.81 ± 0.00) over 2 weeks (Fig. 4c, d). For successful *in vivo* drug delivery, ChNPs must show high stability inside the blood flow at body temperature. Therefore, we assessed the stability of ChNPs in cell culture media (DMEM) with 10 % fetal bovine serum (FBS) at 37 °C for 72 h. The size of ChNPs increased from 139.5 ± 0.4 nm to 154.6 ± 6.6 nm (change in PDI = 0.179 ± 0.0

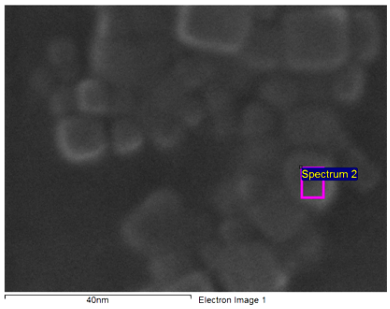

Element	Weight %	Atomic %
C	71.99	85.58
O	15.10	13.48
Pt	12.91	0.94

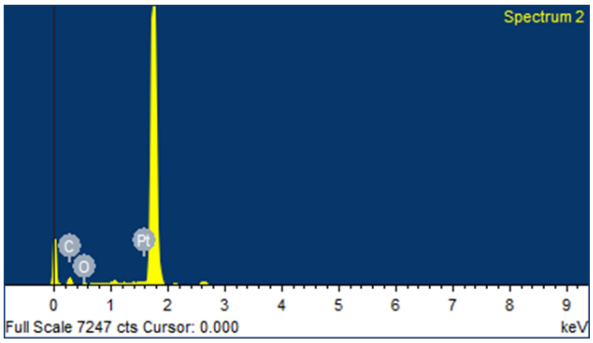

Fig. 3 Determination of Pt metal content in ChNP by energy dispersive X-ray spectroscopy (EDX).

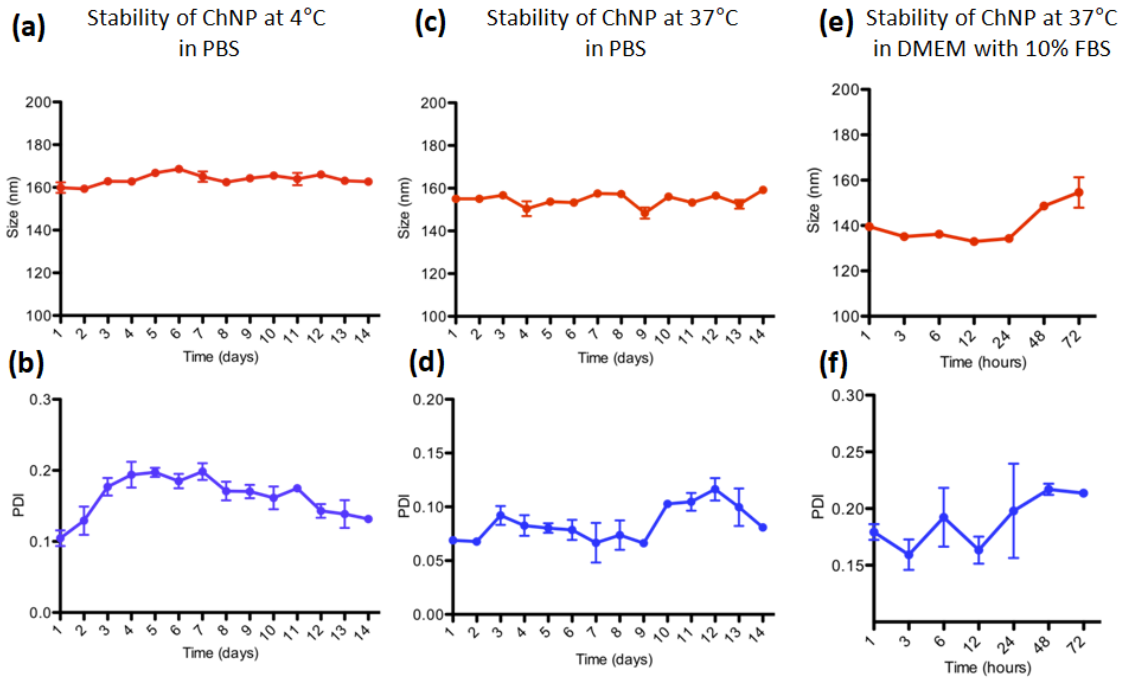

Fig. 4 Stability of ChNP (a-b) at 4 °C in PBS for 14 days, (c-d) at 37 °C in PBS for 14 days and (e-f) at 37 °C in DMEM with 10 % FBS for 72 h determined by DLS.

to 0.214 ± 0.03) (Fig. 4e, f). These stability measurements clearly indicated that ChNPs retained their size under 200 nm without major aggregation at 4 °C and 37 °C in PBS for 2 weeks as well as in the blood flow mimic for 72 h.

3.2.4 Release of triple drugs from ChNPs: After accumulation inside the tumor, the ChNPs must be able to release payloads in a controlled and continuous manner through a prolonged time. Moreover, the sequential administration of drugs in combination strategy plays a crucial role in the therapeutic outcome.[26,27] We anticipated that inhibitingPI3K signaling as a survival pathway followed by DNA damage would lead to better therapeutic efficacy. We quantified the release profile[21] of triple drugs from ChNPs for 120 h at 37 °C in an acidic environment (pH = 5.5), which imitates the lysosomes in the cancer cells.[26] ChNPs released 87.2 ± 5.3 % of PI103 and 42.1 ± 2.6 % of cisplatin at 50 h, whereas 46.4 ±11.8 % of doxorubicin was released at 24 h (Fig. 5a). As a control, we evaluated the amount of triple drugs released from ChNPs by incubating them at physiological pH = 7.4. ChNPs released 49.7 ± 2.5 % of PI103 after 120 h.

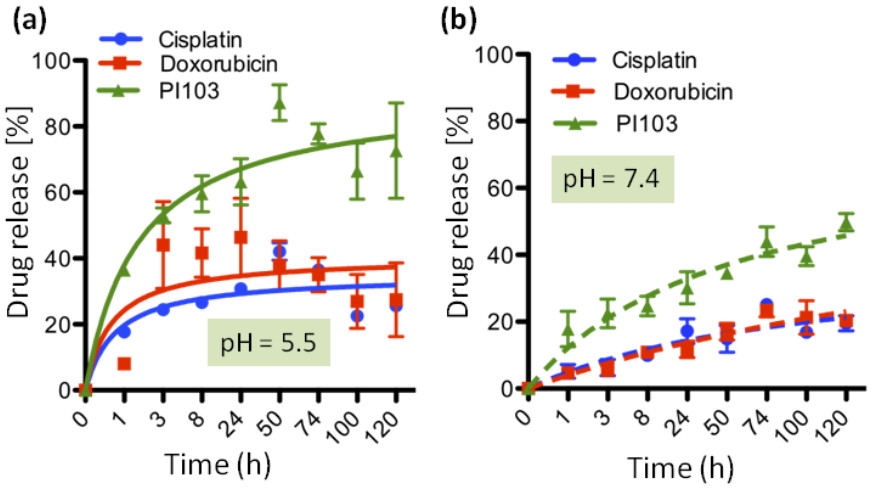

Fig. 5 Release of PI103, doxorubicin, and cisplatin from ChNPs at (a) pH = 5.5, and (b) pH = 7.4 over 120 h.

Whereas, only 23.4 ± 1.9 % of doxorubicin and 25.1 ± 0.8 % cisplatin were released even after 74 h (Fig. 5b). We further evaluated the presence of free PI103, doxorubicin, and cisplatin released from ChNPs at pH = 5.5 after 24 h and 48 h by UV−Vis spectroscopy (Fig. 6). Fig. 6a clearly showed the characteristic peaks at λ_{max} = 480 nm (for free doxorubicin) and 340 nm (for free PI103) in both 24h and 48 h time points (highlighted regions). Fig. 6b also

showed the characteristic peak at λ_{max} = 706 nm for free cisplatin in both 24 h and 48 h (highlighted region).

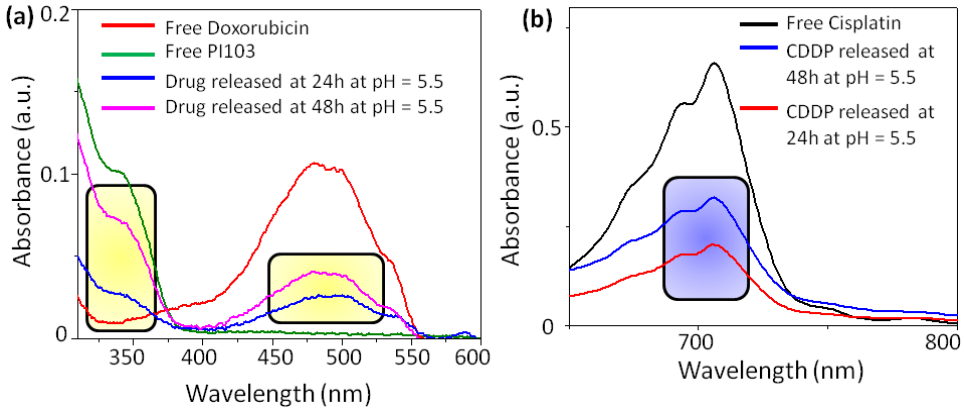

Fig. 6 (a) UV-Vis spectra of released free PI103 and Doxorubicin from ChNP at pH = 5.5 at 24 h and 48 h. (b) UV-Vis spectra of released cisplatin from ChNP at pH = 5.5 at 24 h, and 48 h.

From these UV−Vis data, it was clear that the structures of all the drugs retained after release from ChNPs to show their pharmacological effects. These release data clearly showed that ChNPs exhibited significantly increased improved drug release in a controlled and continuous manner over 120 h in an acidic environment compared to neutral medium. We anticipated that ester, amide, and carboxylato-Pt bonds in the cholesterol-PI103 (3), cholesterol-doxorubicin (4) and cholesterol−cisplatin (6) conjugates respectively, are highly hydrolysable in acidic medium compared to neutral medium, which prompted the superior triple drug release. Furthermore, at pH= 5.5, the aromatic ester bond in conjugate 3 is more hydrolyzable compared to the amide and carboxylato-Pt bond in conjugate 4 and conjugate 6, respectively, leading to the faster and improved release of PI103 compared to doxorubicin and cisplatin. Finally, at pH = 5.5, we observed a decreased accumulative release for all the drugs after 50 h, which we attributed to the possible degradation of all the drugs in acidic condition after prolonged incubation.

3.2.5 *In Vitro* cytotoxicity assay of ChNPs in cancer cells: To assess the effect of the ChNPs in cancer therapy, we determined the *in vitro* efficacy of ChNPs in HeLa cervical cancer cells, HL60 promyelocytic leukemia cells, and MCF7 metastatic breast cancer cells by MTT assay at 24 h and 48 h post incubation. For the MTT assay, we used ChNPs and free drug cocktails having the same PI103/doxorubicin/CDDP = 1:0.8:0.9 ratios. We also estimated the cytotoxicity of dual drug loaded CDDP-Dox-NPs, Dox-PI103-NPs, and

CDDPPI103-NPs as controls. At 24 h, ChNPs showed much less IC_{50} =4.1 µM compared to IC_{50} = 14.4 µM, 6.84 µM, 13.3 µM, and 6.58 µM for the free drug cocktail, CDDP-Dox-NPs, CDDP-PI103-NPs, and Dox-PI103-NPs, respectively, in HeLa cells (Fig. 8a and 9 a–c). Similarly, ChNPs demonstrated IC_{50} = 1.5 µM compared to IC_{50}= 3 µM, 7.35 µM, 1.74 µM, and 0.41 µM for the free drug cocktail, CDDP-Dox-NPs, CDDP-PI103-NPs, and Dox-PI103-NPs, respectively, in HL60 cells at 24 h (Fig. 8b and 10 a–c). Moreover, ChNPs showed IC_{50} = 14.9 µM compared to IC_{50} = 37.5 µM, 5.07 µM, 11.01 µM, and 7.17 µM for the free drug cocktail, CDDP-Dox-NPs, CDDP-PI103-NPs, and Dox-PI103-NPs, respectively, at 24 h in MCF7 cells (Fig. 8c and 11 a–c). At 48 h, ChNPs showed IC_{50} = 0.87 µM which was equal to the IC_{50}

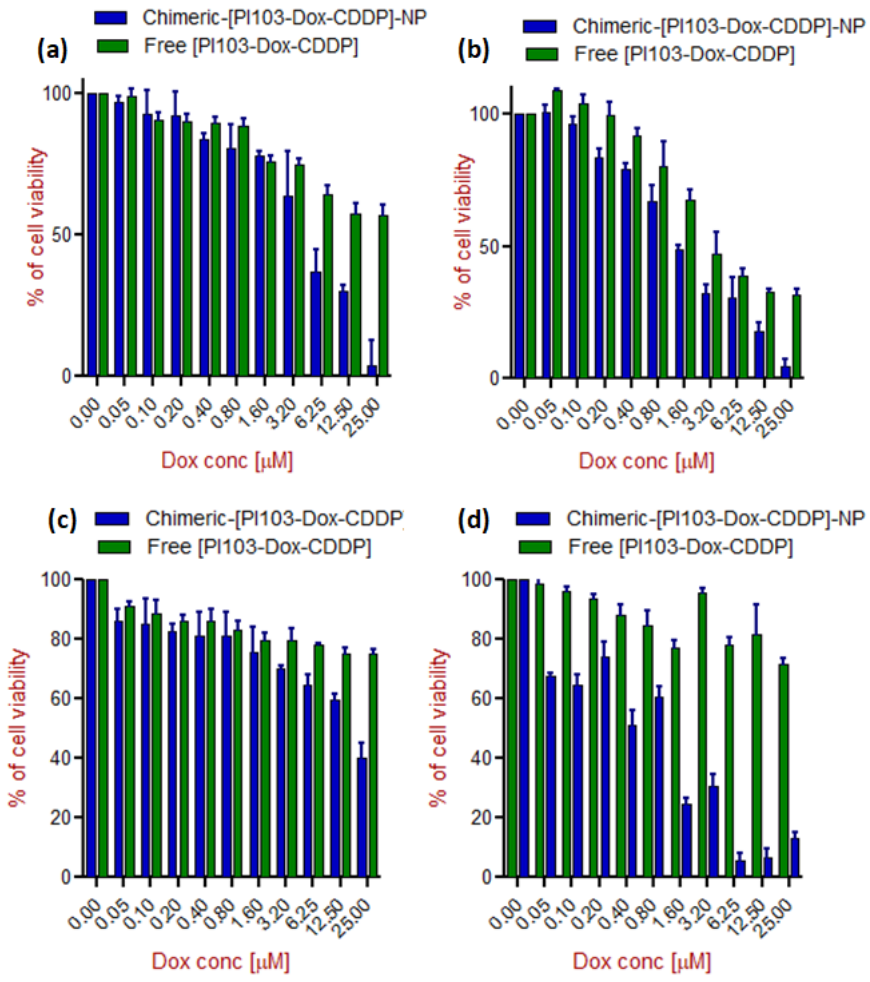

Fig. 7 *In vitro* cytotoxicity assay of ChNPs. (a–d) Cell viability assay of ChNPs in HeLa, HL60, MCF7, and MDA-MB-231 cells for 48 h, respectively.

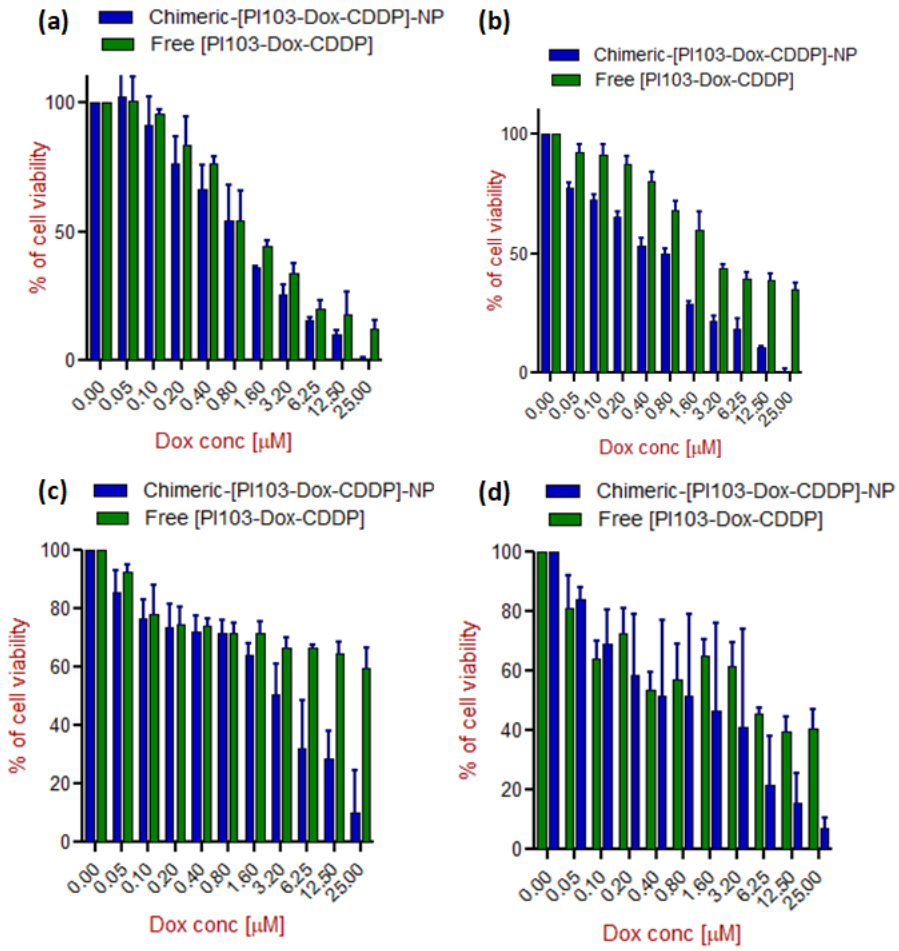

Fig. 8 (a−d) Cell viability assay of ChNPs in HeLa, HL60, MCF7, and MDA-MB-231 cells for 24 h, respectively.

= 0.86 µM for the free drug cocktail for HeLa cells (Fig. 7a). However, at 48 h in HeLa cells, CDDP-Dox-NPs, CDDP-PI103-NPs, and Dox-PI103-NPs showed much higher IC_{50} = 4.89 µM, 3.33 µM, and 4.96 µM, respectively (Fig. 9 d−f). On the other hand, ChNPs showed IC_{50} = 0.8 µM compared to IC_{50} = 1.9 µM, 0.79 µM, 0.07 µM, and 16.2 µM for free drug combination, CDDP-Dox-NPs, CDDP-PI103-NPs, and Dox-PI103-NPs, respectively, in HL60 cells at 48 h (Fig. 7b and Fig. 10 d−f). Furthermore, at 48 h, ChNPs showed IC_{50} = 3.2 µM compared to IC_{50} = 29.9 µM, 3.17 µM, 1.58 µM, and 0.39 µM for the free drug combination, CDDP-Dox-NPs, CDDP-PI103-NPs, and Dox-PI103-NPs, respectively, in MCF7 cells (Fig. 7c and Fig. 11 d−f). We also evaluated the *in vitro* efficacy of ChNPs in the triple negative breast cancer (TNBC) cell line MDA-MB-231 at 24 h and 48 h post-treatment. Interestingly, ChNPs showed extremely enhanced efficacy with IC_{50} = 0.4 µM compared to IC_{50} = 35.8 µM, 23.4 µM, 10.44 µM, and 24.24 µM for the free drug combination, CDDP-

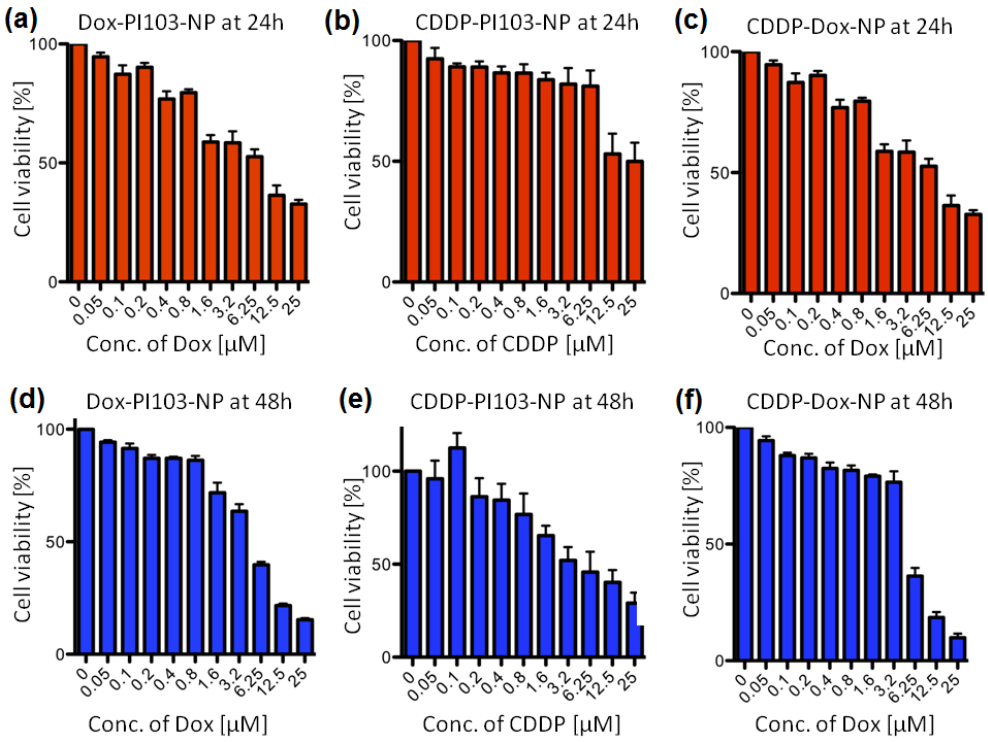

Fig. 9 MTT assay of Dox-PI103-NP, CDDP-PI103-NP and CDDP-Dox-NP at 24 h and 48 h in HeLa cells.

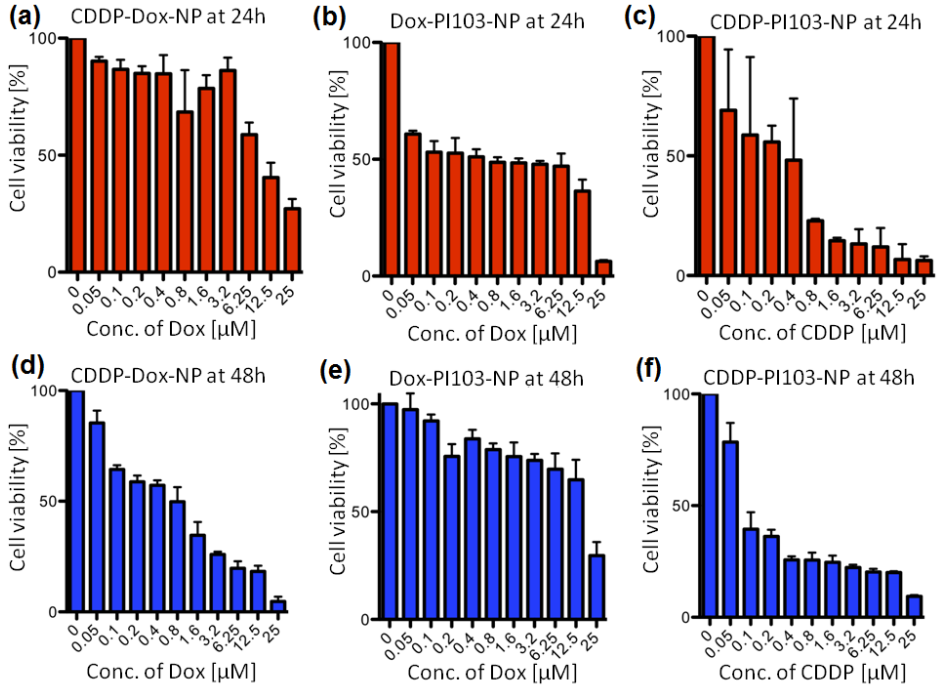

Fig. 10 MTT assay of Dox-PI103-NP, CDDP-PI103-NP and CDDP-Dox-NP at 24 h and 48 h in HL60 cells.

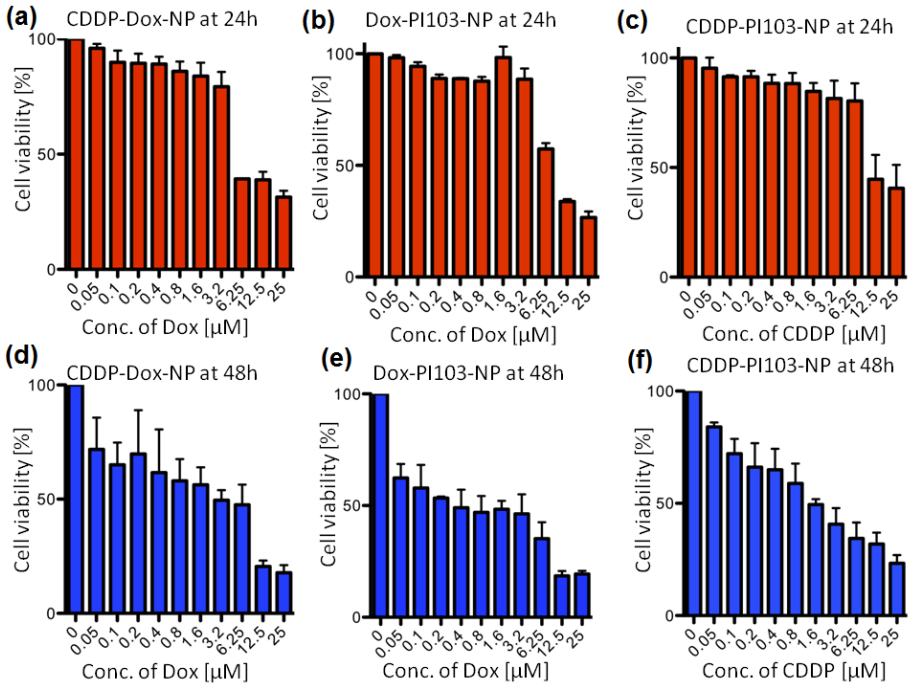

Fig. 11 MTT assay of Dox-PI103-NP, CDDP-PI103-NP and CDDP-Dox-NP at 24 h and 48 h in MCF7 cells.

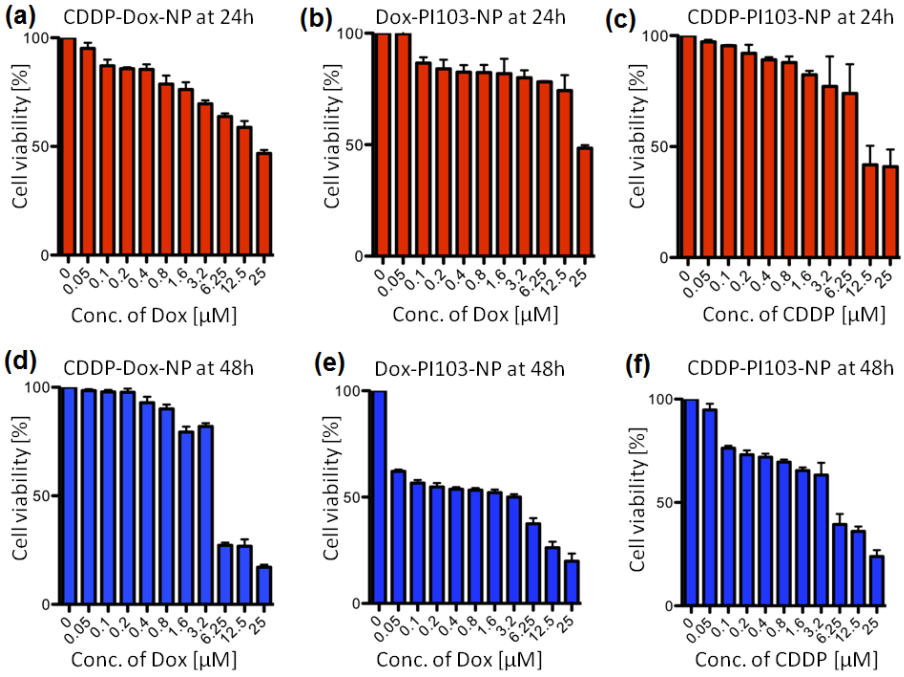

Fig. 12 MTT assay of Dox-PI103-NP, CDDP-PI103-NP and CDDP-Dox-NP at 24 h and 48 h in MDA-MB-231 cells.

Dox-NPs, CDDP-PI103-NPs, and Dox-PI103-NPs, respectively at 24 h (Fig. 8d and 12 a–c). At 48 h post-treatment, ChNPs showed even more improved efficacy with IC_{50} = 0.2 μM compared to IC_{50} = 5.7 μM, 5.24 μM, 4.92 μM, and 3.20 μM for the free drug combinations, CDDP-Dox-NPs, CDDP-PI103-NPs, and Dox-PI103-NPs, respectively (Fig. 7d and Fig. 12 d–f). These cell viability assays demonstrated that ChNPs induced much better efficacy in HeLa and MDA-MB-231 cells with respect to free drug cocktails and dual drug loaded nanoparticles at 24 h and 48h. However, interestingly, in HL60 and MCF7 cells, ChNPs showed much improved efficacy compared to the free drug combination but almost equivalent efficacy compared to dual drug loaded nanoparticles in both 24 h and 48 h.

3.2.6 Apoptosis induced by ChNPs: One of the hallmarks of cancer is its capability to evade apoptosis.[28] Hence, we evaluated the effect of ChNPs in inducing apoptosis in cancer cells. We incubated HeLa cells with ChNPs at IC_{50} values for 24 h, followed by staining the cell surface phosphatidylserine as an early apoptosis marker by green fluorescent Annexin V-FITC dye. We co-stained the cellular DNA of late apoptotic/necrotic cells with red fluorescent propidium iodide (PI). Quantification of early apoptotic, late apoptotic, and necrotic cells was performed using the fluorescence activated cell sorting (FACS) method.

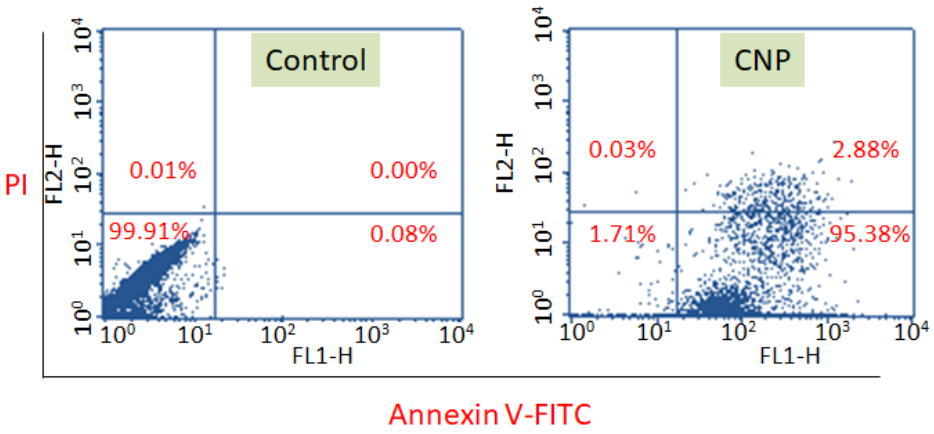

Fig. 13 Fluorescence Assisted Cell Sorting (FACS) analysis of apoptosis caused by ChNPs costained by Annexin V-FITC and PI in HeLa cells for 24 h. The values shown in each quadrant represent the percentage of cells present in healthy (lower left), early apoptotic (lower right), late apoptotic (upper right), and necrotic (upper left) states.

Indeed, ChNPs induced early apoptosis in 95.38 % cells and late apoptosis in 2.88 % cells compared to only 0.08 % and 0 % cells found in the early and late apoptotic stages in the

non-treated control cells (Fig. 13). This FACS analysis clearly demonstrated that ChNPs showed antitumor activity by inducing apoptosis in HeLa cells.

.

3.2.7 Cellular internalization of ChNPs: To envision the temporal cellular internalization mechanism of ChNPs, we incubated HeLa, MDA-MB-231, and MCF7 cells with red fluorescent ChNPs (at 2 µg/mL concentration of doxorubicin) for 1 h, 3 h, and 6 h. The cells were fixed by paraformaldehyde, and acidic lysosomal compartments were stained by green fluorescent LysoTracker Green DND-26 dye. We also stained the nuclei with DAPI (blue) and visualized the cells by using confocal laser scanning microscopy (CLSM).

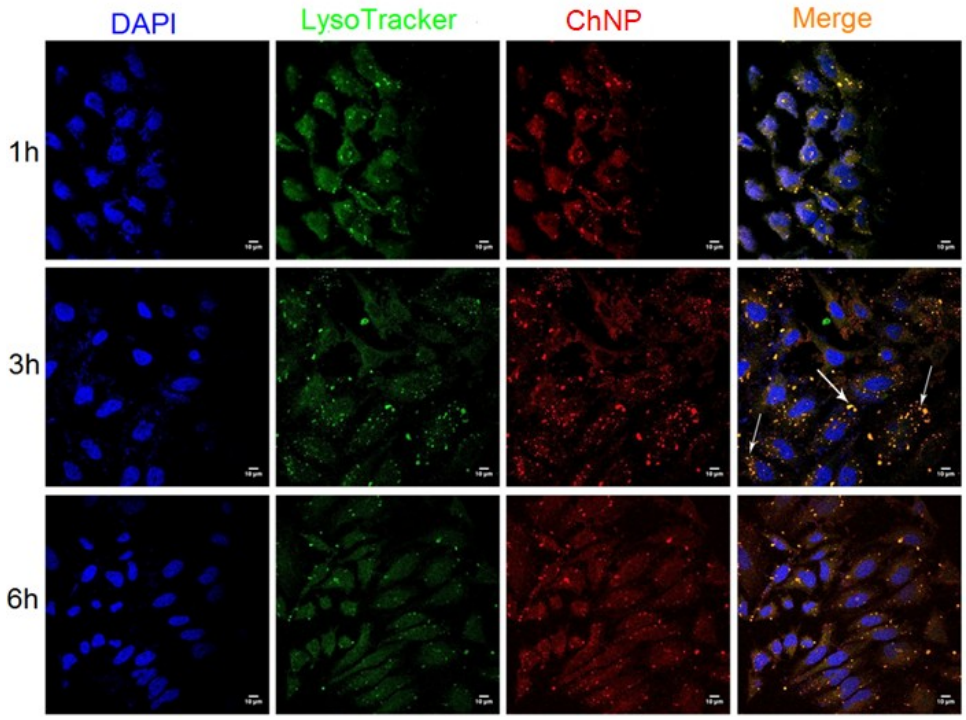

Fig. 14 Internalization of ChNPs in HeLa cells at 1, 3, and 6 h visualized by CLSM. Lysosomes and nuclei were stained by LysoTracker Green DND-26 and DAPI (blue), respectively. The merged images prove the homing (yellow) of ChNPs in lysosomes. Scale = 10 µm.

From Fig. 14, it was clear that the ChNPs entered into HeLa cells temporally over 6 h and localized into the lysosomes, leading to the colocalization of green and red merged into yellow. Quantification of the amount of localization of ChNPs into the lysosomes from

CLSM revealed that the percentage of colocalization was increased from 11.5 % to 19.8 % to 20.7 % from 1 h to 3 h to 6 h, respectively, in HeLa cells (Table 2).

Treatment Time (h)	Image Channels							
	C2 (green), C3 (red)				C1 (blue), C3 (red)			
	Pearson's Correlation Coefficient	Manders Coefficients		Percent volume colocalized	Pearsons' Correlation Coefficient	Manders Coefficients		Percent volume colocalized
		M1 (fraction of C2 over-lapping C3)	M2 (fraction of C3 over-lapping C2)			M1 (fraction of C2 over-lapping C3)	M2 (fraction of C3 over-lapping C2)	
1	0.341	0.342	0.3798	11.46	0.251	0.0914	0.0169	0.13
3	0.557	0.4469	0.5788	19.76	0.123	0.3656	0.0906	2.46
6	0.539	0.4616	0.5943	20.76	0.343	0.5272	0.3461	12.41
24	0.668	0.6496	0.7167	37.97	0.3272	0.8481	0.7884	37.87
48	0.923	0.8145	0.8667	55.02	0.37	0.7561	0.8347	40.22

Table 2. Quantification of colocalization of ChNP into lysosomal compartments and nucleus in 1 h, 3 h, 6 h, 24 h and 48 h time points determined by CLSM in HeLa cells.

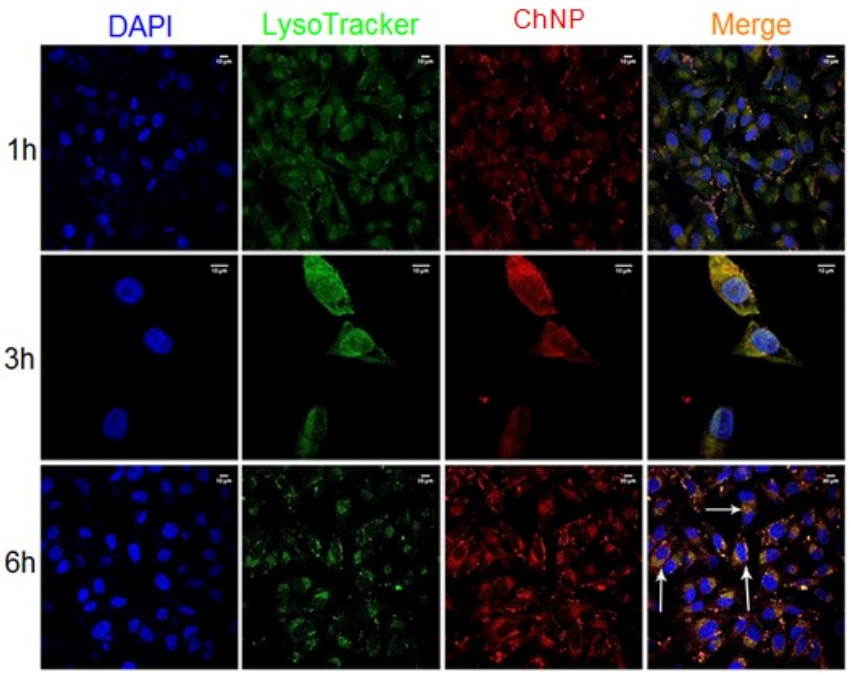

Fig. 15 Internalization of ChNPs in MDA-MB-231 cells at 1, 3, and 6 h visualized by CLSM. Lysosomes and nuclei were stained by LysoTracker Green DND-26 and DAPI (blue), respectively. The merged images illustrate the homing (yellow) of ChNPs in lysosomes. Scale = 10 μm.

Confocal images in Fig. 15 also clearly showed that the ChNPs internalized into the MDA-MB-231 cells very rapidly within 6 h and localized into acidic lysosomal compartments in a

time dependent manner. The CLSM based quantification of the % volume colocalization showed that13.3 %, 22.5 %, and 52.2 % ChNPs were colocalized into lysosomes in 1 h to 3 h to 6 h, respectively (Table 3). Furthermore, CLSM images also revealed that ChNPs internalized and homed in the lysosomal compartments within 6 h in MCF7 cells (Fig. 18).

Treatment Time (h)	Image Channels							
	C2 (green), C3 (red)				C1 (blue), C3 (red)			
	Pearson's Correlation Coefficient	Manders Coefficients		**Percent volume colocalized**	Pearsons' Correlation Coefficient	Manders Coefficients		**Percent volume colocalized**
		M1 (fraction of C2 over-lapping C3)	M2 (fraction of C3 over-lapping C2)			M1 (fraction of C2 over-lapping C3)	M2 (fraction of C3 over-lapping C2)	
1	0.855	0.3862	0.4938	13.28	0.172	0.4926	0.2106	7.28
3	0.589	0.4	0.6096	22.46	0.1834	0.738	0.3563	8.67
6	0.669	0.7521	0.7966	52.2	0.29	0.7556	0.7843	32.3
24	0.761	0.6245	0.8065	37.73	0.248	0.7738	0.9144	43.82
48	0.576	0.5604	0.6667	27.92	0.227	0.8716	1	48.53

Table 3. Quantification of colocalization of ChNP into lysosomal compartments and nucleusin 1h, 3h, 6h, 24h and 48h time points determined by CLSM in MDA-MB-231 cells.

Lipidic nanoparticles have a tendency to be exocytosed from the cells leading to the reduced efficacy in drug delivery.[29] To evaluate the existence of the ChNPs into the cells for an extended period of time, we also evaluated the cellular internalization at 24 h and 48 h time points in HeLa, MDA-MB-231, and MCF7 cells. Confocal microscopy images in Fig. 16, 17, and 18 clearly demonstrated that ChNPs were retained inside the acidic lysosomal compartments for even 24 h and 48 h to show their anticancer activity. Further CLSM based quantification revealed that 37.9 % and 55.0 % colocalization were observed for HeLa cells, compared to 37.7 % and 27.9 % colocalization observed for MDA-MB-231 cells (Tables 2 and 3). We hypothesized that ChNPs will be endocytosed into acidic lysosomal compartments, and in the acidic environment each drug will be released and inhibit their respective targets. From Fig. 16, 17, and 18 it was clear that at 24 h and 48 h, red fluorescent doxorubicin was localized into a blue fluorescent nucleus to afford a merged purple fluorescence signal in

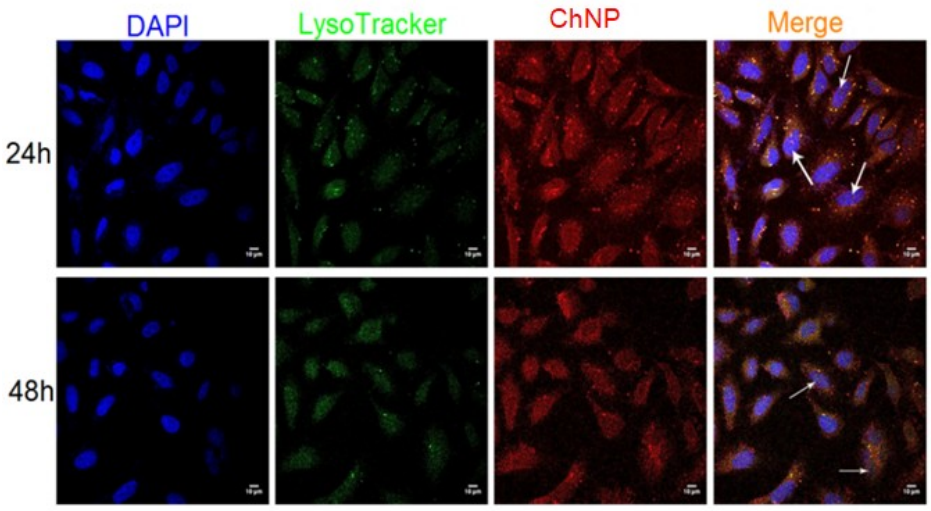

Fig. 16 CLSM images of cellular internalization of ChNPs in HeLa cells at 24h and 48h time points. Acidic lysosomal compartments and nucleus are stained with LysoTracker DND-26 (green) and DAPI (blue) respectively. Yellow portions in merged images show the co-localization of ChNP in lysosomal compartments and a purple portion in merged images show the co-localization of doxorubicin in the nucleus. Scale bar = 10μm.

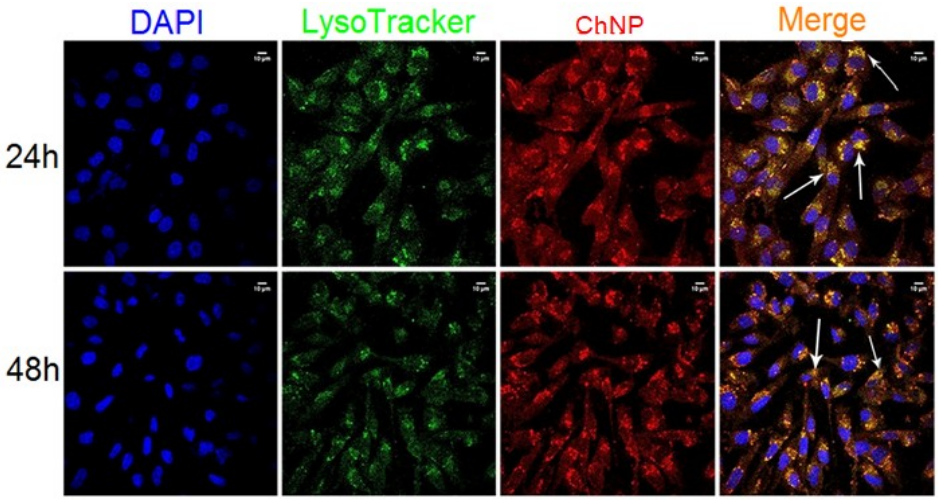

Fig. 17 CLSM images of cellular internalization of ChNPs in MDA-MB-231 cells at 24h and 48h time points. Acidic lysosomal compartments and nucleus are stained with LysoTracker DND-26 (green) and DAPI (blue) respectively. Yellow portions in merged images show the co-localization of ChNP in lysosomal compartments and a purple portion in merged images show the co-localization of doxorubicin in the nucleus. Scale bar = 10μm.

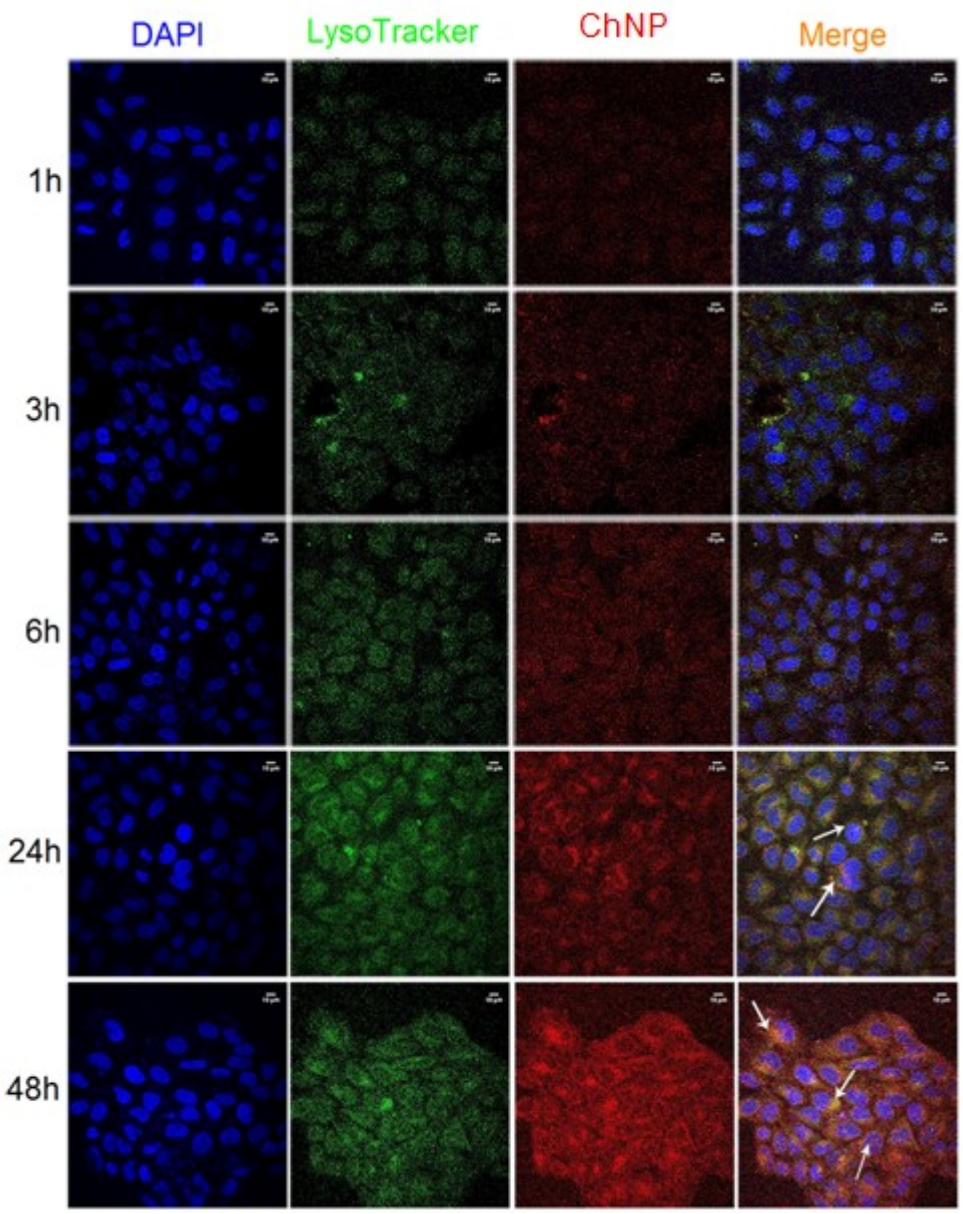

Fig. 18 CLSM images of cellular internalization of ChNPs in MCF7 cells at 1h, 3h, 6h, 24h and 48h time points. Acidic lysosomal compartments and nucleus are stained with LysoTracker DND-26 (green) and DAPI (blue) respectively. Yellow portions in merged images show the co-localization of ChNP in lysosomal compartments. Scale bar = 10μm.

HeLa, MDA-MB-231, and MCF7 cells. We also quantified the colocalization of doxorubicin in the nucleus from CLSM. Tables 2 and 3 showed that the percentage of colocalization of blue and red fluorescence gradually increased from 0.13 % to 40.22 % from 1 h to 48 h in HeLa cells as well as from 7.28 % to 48.5 % from 1 h to 48 h in MDA-MB-231cells. These

CLSM data demonstrated that the ChNPs internalized into HeLa, MDA-MB-231, and MCF7 cells temporally by endocytosis followed by localization into the lysosomes for extended periods of time, leading to further release of triple drugs.

3.2.8 Mechanism of action of ChNPs: Phosphatidylinositol-3-kinase (PI3K) and its primary downstream mediator Akt play important roles in cell survival and proliferation in cancer cells.[30] As a result, PI3K-Akt signaling inhibitor PI103 showed improved efficacy in combination with doxorubicin as a DNA damaging agent.[13] Moreover, PI103 augmented the therapeutic efficacy of cisplatin

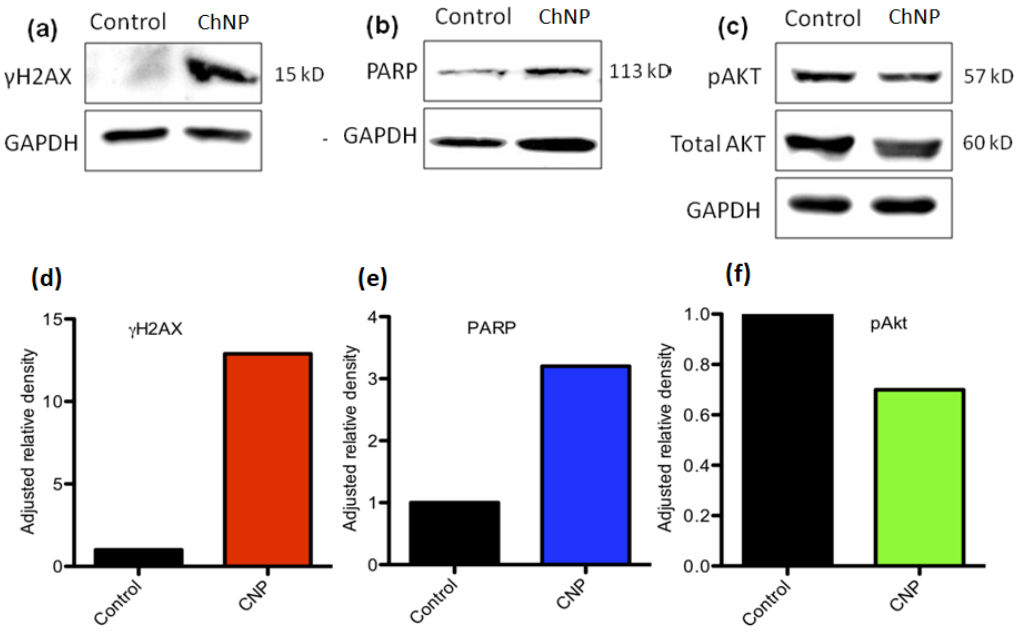

Fig. 19 Expression of (a) γH2AX, (b) PARP, and (c) p-Akt and Quantification of expression of (d) γH2AX (e) PARP and (f) p-Akt in HeLa cells after treatment with ChNP for 24h in HeLa cells, determined from Western blot analysis.

nanoparticles in a breast cancer model.[14] However, there is no precedence of drug combination having PI103, doxorubicin, and cisplatin in a single nanoparticle. Hence, we evaluated the mechanism of action of ChNPs in HeLa after treatment with ChNPs at IC_{50} = 4.1 µM concentration for 24 h and visualized the protein expressions by Western blot. We evaluated the expression of γH2AX to monitor DNA damage.[31] Fig. 19a demonstrated that ChNPs induced significantly increased expression of γH2AX compared to no treatment. Quantification of the relative expression of γH2AX showed a 13-fold increase in ChNP

treated cells compared to no treatment, which clearly indicated that ChNPs showed cytotoxicity by inducing DNA damage (Fig. 19d). After DNA damage, the poly (ADP-ribose) polymerase (PARP) family of proteins get activated to repair the DNA damage. As a result, PARP activation is also a potential biomarker for cellular DNA damage.[32] Evaluation of PARP expression (Fig. 19b) showed that ChNPs activated PARP compared to no treatment control. Furthermore, PARP quantification revealed a 3-fold increase upon incubation with ChNPs relative to no treatment (Fig. 19e). Finally, we evaluated the expression of phospho-Akt, which is a downstream therapeutic target and one of the most important biomarkers in PI3K signaling. From Fig. 19c, it was clear that ChNPs reduced the expression of phosphor-Akt while keeping the total Akt expression unchanged compared to the no treatment control. Quantification from Western blot also showed a 1.4-fold decrease of phosphor-Akt expression upon treatment with ChNPs compared to the control (Fig. 19f). From these Western blot analyses, it was evident that ChNPs demonstrated improved cytotoxicity in HeLa cells by inhibiting PI3K signaling and DNA damage.

3.3 Conclusion

We have engineered cholesterol-based chimeric nanoparticles (ChNPs), which can simultaneously contain PI103, doxorubicin, and cisplatin in a controlled ratiometric manner. The ChNPs released three drugs in a prolonged and continuous manner in enhanced quantity in an acidic medium compared to a neutral medium over 120 h with excellent stability at 4 and 37 °C over 2 weeks as well as in a blood circulation mimic for 72 h. The ChNPs induced improved in vitro cytotoxicity against cervical cancer (HeLa), promyelocytic leukemia cells (HL60), and metastatic breast cancer cells (MCF7) as well as drug resistant triple negative breast cancer cells (MDA-MB-231) compared to the free drug combinations. These ChNPs localized temporally into the acidic lysosomes after endocytosis within 6 h and were retained inside the cells for 48 h in HeLa, MDA-MB-231, and MCF7 cells. Finally, the ChNPs showed their efficacy in HeLa cells by inhibiting PI3K-Akt signaling and inducing DNA damage, leading to the induction of apoptosis.

3.4 Experimental Methods

All the chemicals, reagents, and solvents required for synthesis of cholesterol-drug conjugates and ChNPs were purchased from Sigma-Aldrich. All the anticancer drugs were purchased from Selleck Chemicals. DSPE-PEG2000 and mini extruder were procured from Avanti Polar Lipids Inc. Cell culture media, LysoTracker DND-26, and SlowFade antifade reagents were bought from LifeTechnologies. Antiphospho-Akt (Thr308) rabbit monoclonal antibody was obtained from Merck Millipore.

3.4.1 Synthesis of Conjugate (2): Conjugate 2 was synthesized by following the procedure described in ref 33. Cholesterol (50 mg, 0.129 mmol) was dissolved in pyridine (100 µL) and DCM (5 mL) at room temperature in a round bottom flask. Succinic anhydride (38 mg, 0.387 mmol), and DMAP (15 mg, 0.129 mmol) were added into it and stirred for 24 h at room temperature. After the reaction was completed, solvent was removed by rotary evaporator, and then the crude product was purified by silica gel flash chromatography with dichloromethane/methanol as the mobile phase to afford the desired product as colorless solid. Yield: 48 mg (77 %).

^{1}H NMR: (400 MHz, Chloroform-d) δ = 5.36 (1H, d, J = 4 Hz), 4.68 – 4.58 (1H, m), 2.68 (2H, t, J= 6.9 Hz), 2.60 (2H, t, J = 6.9 Hz), 2.31 (2H, d, J = 7.8 Hz), 2.04 – 1.93 (2H, m), 1.87 (1H, d, J = 2.6 Hz), 1.85– 1.78 (2H, m), 1.66 – 1.41 (8H, m), 1.40 – 1.23 (5H, m,), 1.22 – 1.04 (8H, m), 1.01 (3H, s), 0.91 (3H, d, J =6.5 Hz), 0.87 (3H, d, J = 1.8 Hz), 0.85 (3H, d, J = 1.7 Hz), 0.67 (3H, s), (Fig. 20).

^{13}C NMR: (100 MHz, Chloroform-d) δ = 178.2, 171.7, 139.7, 122.9, 77.5, 77.2, 76.8, 74.7, 56.8, 56.3, 50.1,42.4, 39.9, 39.7, 38.1, 37.1, 36.7, 36.3, 35.9, 32.0, 29.4, 29.1, 28.4, 28.2, 27.8, 24.4, 23.98, 22.9, 22.7, 21.2,19.4, 18.9, 12.0, (Fig. 21).

HR-MS: $[M + Na]^+$ calculated for $C_{31}H_{50}O_4$ = 509.7697; found 509.3504, (Fig. 22).

3.4.2 Synthesis of Cholesterol-PI103 Conjugate (3): Conjugate **3** was synthesized by following the procedure described in ref 31. Cholesterol-succinic acid (2) (5 mg, 0.01mmol), EDC (5.73 mg, 0.03 mmol) and DMAP (2.45 mg, 0.02 mmol) were dissolved in DCM (3 mL) and stirred for 10 min at room temperature. Then PI103 (4.17 mg, 0.012 mmol) was added and stirred for 24 h at room temperature. After 24 h, reaction was quenched by 0.1 N HCl and diluted with DCM (10 mL). The organic layer was washed with water (10 mL X 2)

and brine (5 mL). Then the collected organic solvent was removed by rotary evaporator, and crude product was purified by silica gel flash chromatography with dichloromethane/methanol as the mobile phase to afford pure cholesterol-succinic acid-PI103 conjugate (3). Yield = 6 mg (72 %).

^{1}H NMR: (400 MHz, Chloroform-d) δ = 8.63 – 8.55 (2H, m), 8.39 – 8.31 (1H, m), 8.21 – 8.18 (1H, m), 7.53– 7.42 (2H, m), 7.20 (1H, ddd, *J* = 7.9 Hz, 2.3 Hz, 0.9 Hz), 5.36 (1H, d, *J* = 3.9 Hz), 4.67 (1H, m), 4.26 – 4.16 (4H, m), 3.95 – 3.87 (4H, m), 2.94 (2H, t, *J* = 6.8 Hz), 2.76 (2H, t, *J* = 6.8 Hz), 2.35 (2H, d, *J* = 7.8 Hz), 2.03 – 1.76 (5H, m), 1.63 (4H, s), 1.24 (4H, s), 1.18 – 1.06 (6H, m), 0.99 (4H, s), 0.91 (4H, d, *J* = 6.5 Hz), 0.87 (4H, d, *J* = 1.8 Hz), 0.85 (4H, d, *J* = 1.8 Hz), 0.66 (3H, s), (Fig. 23).

^{13}C NMR: (100 MHz, Chloroform-d) δ = 171.7, 171.2, 162.8, 158.8, 151.0, 149.7, 148.9, 147.3, 140.1,139.7, 133.6, 132.0, 129.4, 125.7, 123.3, 122.9, 121.3, 120.4, 115.5, 77.5, 77.2, 77.2, 76.8, 74.7, 67.1, 56.8,56.2, 50.1, 45.9, 42.4, 39.8, 39.6, 38.2, 37.1, 36.7, 36.3, 35.9, 32.0, 31.9, 29.8, 29.6, 28.4, 28.2, 27.9, 24.4,23.9, 22.9, 22.7, 21.1, 19.4, 18.8, 11.9, (Fig. 24).

HR-MS: $[M + H]^+$ calculated for $C_{50}H_{64}N_4O_6$ = 817.4904; found = 817.4905, (Fig. 25).

3.4.3 Synthesis of cholesterol-doxorubicin conjugate (4): A mixture of compound 2 (5 mg, 0.01 mmol), HBTU (5.68 mg, 0.015 mmol), and DIPEA (2.5 µL, 0.015 mmol) in dry DMF (2 mL) was reacted for 10 min. Doxorubicin·HCl salt (6.9 mg, 0.012 mmol) was added and reacted for 24 h. To quench the reaction, 0.1 N HCl solution was added. The organic layer was washed with water (10 mL X 2). Then the collected organic solvent was dried and product was purified by silica gel column with dichloromethane/methanol as the eluent to afford a pure cholesterol-doxorubicin conjugate (4). Yield =70 %.

^{1}H NMR: (400 MHz, Chloroform-d) δ = 8.05 (1H, d, *J* = 7.7 Hz), 7.79 (1H, t, *J* = 8.1 Hz), 7.40 (1H, d, *J* = 8.2Hz), 5.91 (1H, d, *J* = 8.4 Hz), 5.51 (1H, s), 5.37 – 5.28 (2H, m), 4.76 (2H, d, *J* = 1.8 Hz), 4.64 – 4.52 (1H, m), 4.19 – 4.06 (5H, m), 3.68 (1H, d, *J* = 2.1 Hz), 3.29 (1H, dd, *J* = 18.9 Hz, 1.6 Hz), 3.05 (1H, d, *J* = 18.9 Hz), 2.28 (2H, d, *J* = 7.9 Hz), 1.70 – 1.55 (24H, m), 1.32 – 1.24 (7H, m), 0.99 (3H, s), 0.91 (3H, d, *J* = 6.5 Hz), 0.87 (3H,d, *J* = 1.8 Hz), 0.85 (3H, d, *J* = 1.8 Hz), 0.67 (3H, s), (Fig. 26).

^{13}C NMR: (100 MHz, Chloroform-d) δ = 214.0, 187.3, 186.8, 172.7, 171.2, 161.1, 156.3, 155.8, 139.5,135.9, 135.6, 135.3, 133.7, 122.8, 121.0, 119.9, 118.5, 111.5, 100.8, 77.4, 77.3, 77.1, 76.8, 74.6, 69.7, 68.9,67.2, 65.7, 56.8, 56.7, 56.2, 50.0, 45.5, 42.4, 39.8, 39.6, 38.1,

36.9, 36.6, 36.2, 35.9, 31.9, 31.9, 30.0, 29.7,28.1, 23.9, 22.9, 22.6, 21.1, 19.4, 18.8, 16.9, 11.9, (Fig. 27).

HR-MS: $[M + Na]^+$calculated for $C_{58}H_{77}NO_{14}$ = 1034.5097; found = 1034.5250, (Fig. 28).

3.4.4 Synthesis of aquated cisplatin (5): Synthesis was carried out by following the method described in ref 21. 50 mg of cisplatin was dissolved in 10 mL of water and 56 mg of silver nitrate was added into the solution. Reaction mixture was then stirred at room temperature under dark conditions for 24h. Resultant milky white solution was centrifuged for 15 to 20 minutes to precipitate silver chloride. The supernatant is then filtered through 0.2 µm filter and used for further reaction without any purification.

3.4.5 Synthesis of cholesterol-cisplatin conjugate (6): Conjugate 6 was synthesized using the procedure in ref 21. Cholesterol-succinic acid (**2**) (5 mg, 0.01 mmol) was dissolved in 1 mL DMF and aquated cisplatin (**5**) (600 µL = 3.08 mg, 0.01 mmol) was added into it. The reaction mixture was stirred for 24 hours. After 24 h solvent was evaporated by rotary evaporator and the crude cholesterol-succinic acid-cisplatin conjugate (**6**) was used for chimeric nanoparticle synthesis. Yield = 6.6 mg (90 %).

^{1}H NMR: (400 MHz, DMSO-d6) δ = 5.34 (1H, d, J = 3.5 Hz), 4.78 – 4.31 (5H, m), 2.55 (3H, s), 2.45 (3H, d, J =2.4 Hz), 2.25 (2H, d, J = 7.8 Hz), 1.94 (2H, t, J = 15.5 Hz), 1.86 – 1.71 (3H, m), 1.58 – 1.43 (5H, m), 1.43 –1.28 (5H, m), 1.15 – 1.05 (5H, m), 0.97 (3H, s), 0.89 (3H, d, J = 6.5 Hz), 0.85 (3H, d, J = 2.0 Hz), 0.83 (3H, d, J= 2.0 Hz), 0.65 (3H, s), (Fig. 29).

^{13}C NMR: (100 MHz, DMSO-d6) δ = 177.1, 173.3, 162.3, 139.4, 122.0, 73.3, 56.1, 55.6, 49.4, 41.8, 39.5,37.7, 36.1, 35.7, 34.4, 31.3, 30.7, 28.9, 27.3, 23.2, 22.6, 22.3, 20.5, 19.0, 18.5, 11.6, (Fig. 30).

^{195}Pt NMR: δ = -1304.93, (Fig. 32).

HR-MS: $[M + H]^+$ calculated for $C_{31}H_{57}N_2O_5Pt$ = 715.3878; found = 715.3839, (Fig. 31).

3.4.6 Synthesis of chimeric nanoparticles (ChNPs): ChNPs were synthesized by the method described in ref 20. 6.0 mg of L-α-phosphatidylcholine (PC), 1 mg of each drug conjugates (compound **3**, **4** and **6**) and 0.6 mg of DSPE-PEG were dissolved in 5.0 mL DCM. The solvent was evaporated into a thin and uniform film with the help of a rotary evaporator. After thorough drying with vacuum pump, cholesterol-drugs film was hydrated with 1.0 mL H_2O for 2 h at 60 ˚C. Resultant nanoparticle suspension was passed through Sephadex G-25

column and extruded through 200 nm Whatmann polycarbonate membrane at 60 ˚C to obtain chimeric nano particles (ChNP). The ChNPs were stored at 4 ˚C for further use. The dual drug loaded nanoparticles (CDDP-Dox-NP, Dox-PI103-NP and CDDP-PI103-NP) were synthesized using the same procedure from the corresponding cholesterol-drug conjugates in a 1:1 weight ratio.

3.4.7 Determination of size, shape, and morphology of ChNPs: Size, shape, and morphology of ChNPs were determined by DLS, FESEM, AFM, and TEM. The sample preparation and measurements were done by the methods described in section 2.4.4, 2.4.5, 2.4.6 and 2.4.7 in chapter 2 respectively.

3.4.8 Stability of ChNPs: The stability of the ChNPs was checked at 4 °C and 37 °C by dynamic light scattering method using Zetasizer Nano2590 (Malvern, UK). 50 µL of ChNP solution was diluted to 1 mL using PBS and 3 sets of 10 measurements each were performed at 90 degree scattering angle to get the average particle size and PDI for 14 days. Similarly, 200 µL of ChNP solution was incubated into 800 µL of DMEM containing 10 % FBS for 72 h at 37 °C and particle size and PDI were measured in predetermined time points by DLS to check the stability in blood circulation mimic.

3.4.9 Quantification of drug loading in ChNPs: Loading of each drug in ChNPs was quantified using the UV−Vis spectroscopy method illustrated in section 2.4.3 in chapter 2.

3.4.10 Release of triple drugs from ChNPs: The release of triple drugs in pH = 5.5 and pH = 7.4 were determined using the dialysis method described in section 2.4.8 in chapter 2.

3.4.11 Cell viability assay: 5000 HeLa, MCF-7, HL60 and MDA-MB-231 cells were seeded per well in 96-well microtitre plate and incubated overnight in a 5 % CO_2 incubator at 37 °C. HeLa, MCF7 and HL60 cells were cultures in DMEM media, whereas MDA-MD-231 cells were cultured in RPMI media. Cells were then treated with ChNPs, free drug combinations, CDDP-Dox-NP, Dox-PI103-NP and CDDP-PI103-NP in different concentrations (0.05, 0.1, 0.2, 0.4, 0.8, 1.6, 3.2, 6.4, 12.5, 25 µM) for 24 h and 48 h. 20 µL of MTT reagent (5 mg mL^{-1}) was added to each well and incubated for 4 h at 37 °C. Formazan crystals were then solubilized in 100 µL of the solubilization buffer (10 % SDS in 0.01 M HCl) and incubated overnight. Absorbance was measured spectrophotometrically at 550 nm. The percent cell viability was calculated considering the untreated cells as 100 percent viability and the effectiveness of nanoparticles was compared with the free drug combinations.

3.4.12 FACS analysis for apoptosis detection: For apoptosis detection, 2 X 10^6 HeLa cells were incubated in 6 well plates overnight for attachment and then treated with ChNPs for 24 hours at IC_{50} value. After the treatment, media was removed and cells were trypsinized and washed twice with PBS by means of centrifugation at 750 rpm for 4 min. The cell pellet was then re-suspended in 500 µL of Annexin V binding buffer (FITC Annexin V Apoptosis Detection Kit with PI from BioLegend) followed by addition of 5 µL FITC Annexin V and 10 µL propidium iodide solution and incubated at 25 °C for 15 min. in dark. Cells were then passed through a cell strainer to get uniform cell suspension and analyzed using BD FACS Calibur™ to detect the apoptosis.

3.4.13 Cellular internalization by CLSM: 5 x 10^4 cells (HeLa, MDA-MB-231, and MCF7) were seeded on a coverslip in a 6 well plate and incubated overnight in a 5 % CO_2 incubator at 37 °C for attachment. Cells were then first washed with PBS (pH = 7.4) and then treated with ChNPs considering conjugated doxorubicin as a fluorescent tag (at a concentration equivalent to 2 µg mL^{-1} of doxorubicin) for 1 h, 3 h, and 6 h. Cells were then washed twice with PBS and fixed with 500 µL of paraformaldehyde (3.7 % in PBS, pH = 6.9) by incubating for 10 min at 4 °C. The paraformaldehyde was aspirated and cells were washed trice with PBS. Low pH lysosomes were stained with 1 µM LysoTracker Green DND-26 by incubating the cells at 37 °C for 45 min. The cells were then washed three times to remove the unbound LysoTracker Green DND-26 followed by staining the cells for nuclei with 2 µg mL^{-1} DAPI by incubating at 37 °C for 5 min. Then, cells were washed three times with PBS and mounted on a glass slide using 5 µL *SlowFade*® gold antifade reagents. The slides were subjected to fluorescence imaging using a CLSM (Zeiss LSM 710).

3.4.14 General procedure for Western blot analysis: After 24 h ChNP treatment, HeLa cells were lysed and suspended in sample buffer. Proteins were separated using SDS-polyacrylamide gel electrophoresis (SDS-PAGE) and were transferred to the membrane (electro-blotting). Blotted membrane was then blocked in freshly prepared TBS containing non-fat dry milk (5 %) in case of non-phosphorylated proteins, while in blocking buffer in case of phosphorylated proteins for 1 h with constant agitation at room temperature. Membrane was then rinsed once with TBST and then incubated in the primary antibody solution (H2AX 1:2000 dilution, PARP and AKT 1:1000 dilution and GAPDH 1:5000 dilution) overnight at 4°C with gentle agitation (except 4 hours for GAPDH). Membrane was then washed 3 times (15 min each) with TBST and then incubated in HRP conjugated secondary antibody solution (1:10000 dilutions) for 45 min at room temperature with gentle

agitation. Membrane was again washed thrice with TBST (5 min each) followed by protein detection using Immobilon western chemiluminescent HRP substrate (membrane was incubated in the substrate solution for 1 min). Images were acquired using ImageQuant LAS 4000 (GE Healthcare Lifesciences). After the acquisition, membrane blot was stripped by boiling in distilled water for 5 min and was re-probed for GAPDH protein. Further image processing and intensity calculations were performed using ImageJ software.

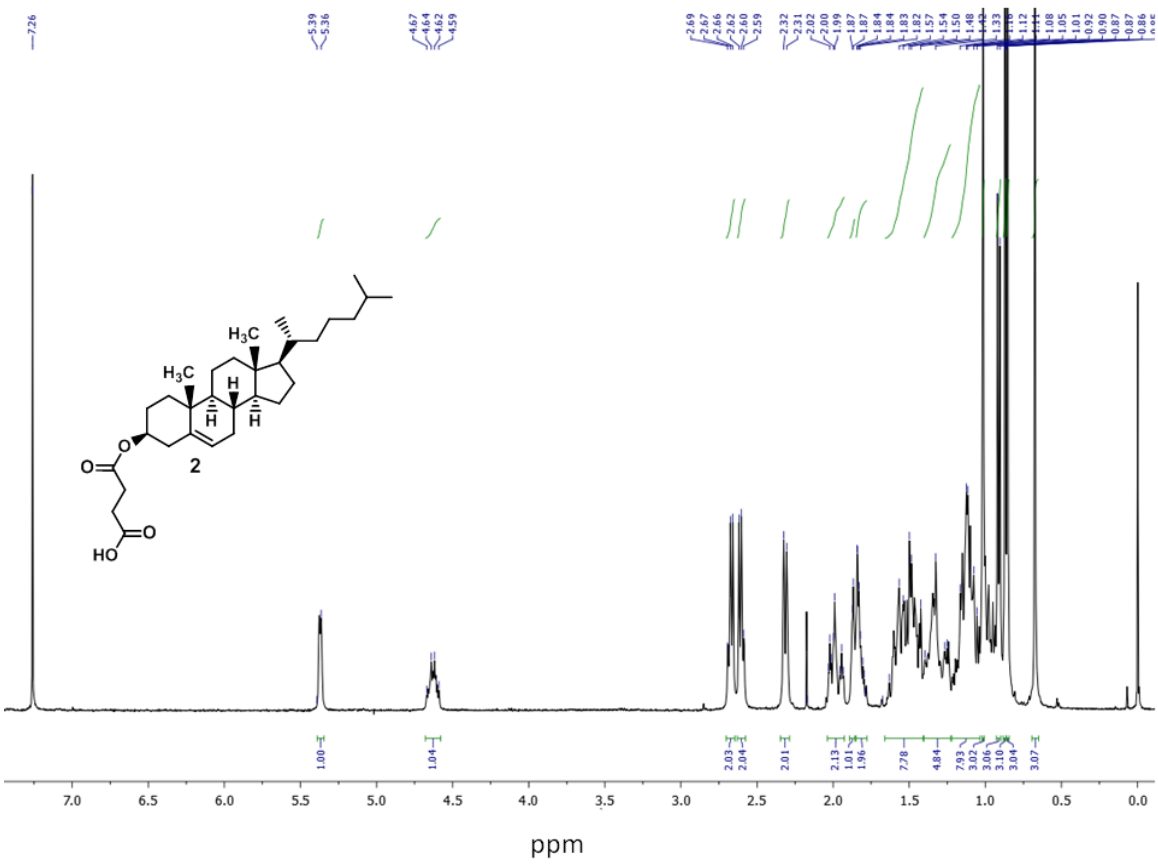

Fig. 20 ^{1}H-NMR spectra of cholesterol-succinic acid conjugate (**2**).

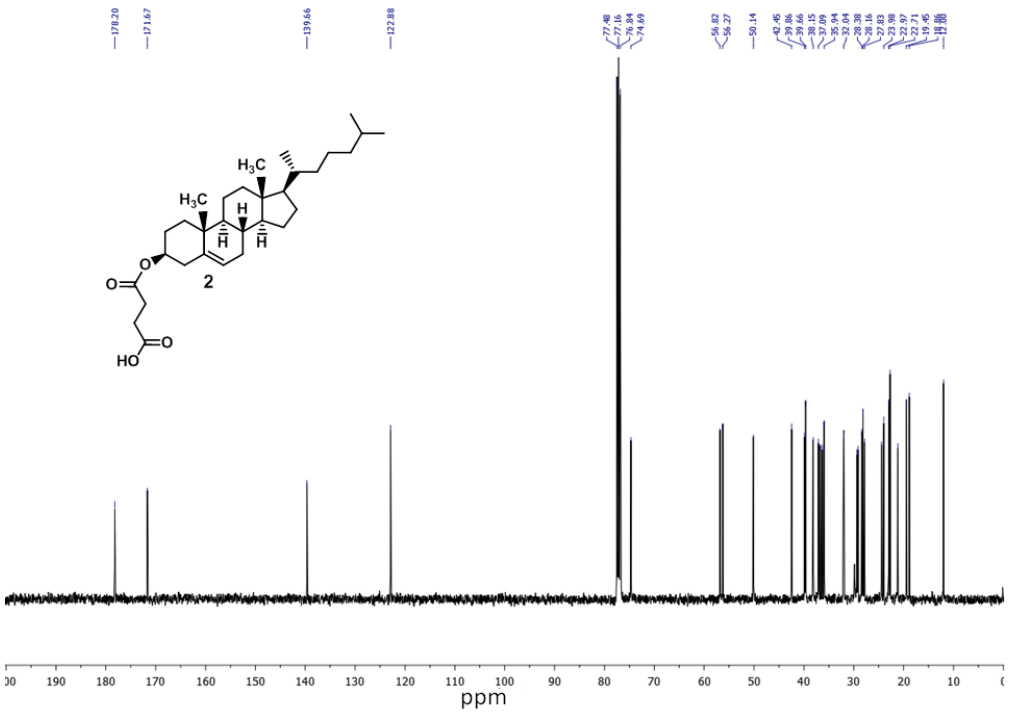

Fig. 21 ^{13}C-NMR spectra of cholesterol-succinic acid conjugate (**2**).

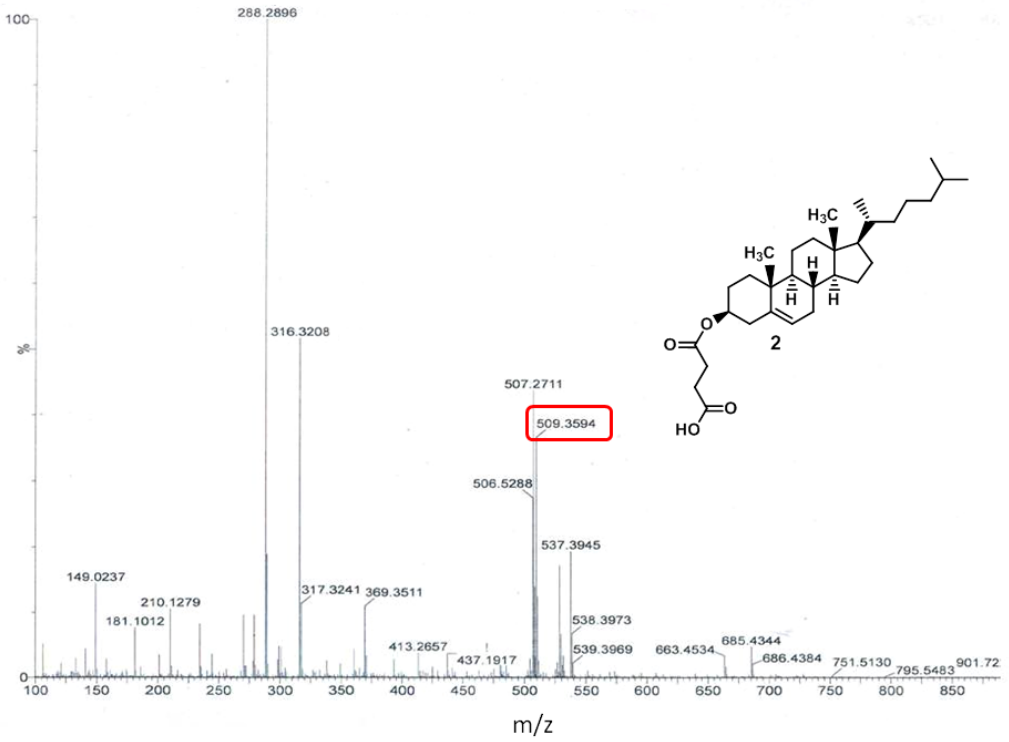

Fig. 22 HR-MS spectra of cholesterol-succinic acid conjugate (**2**).

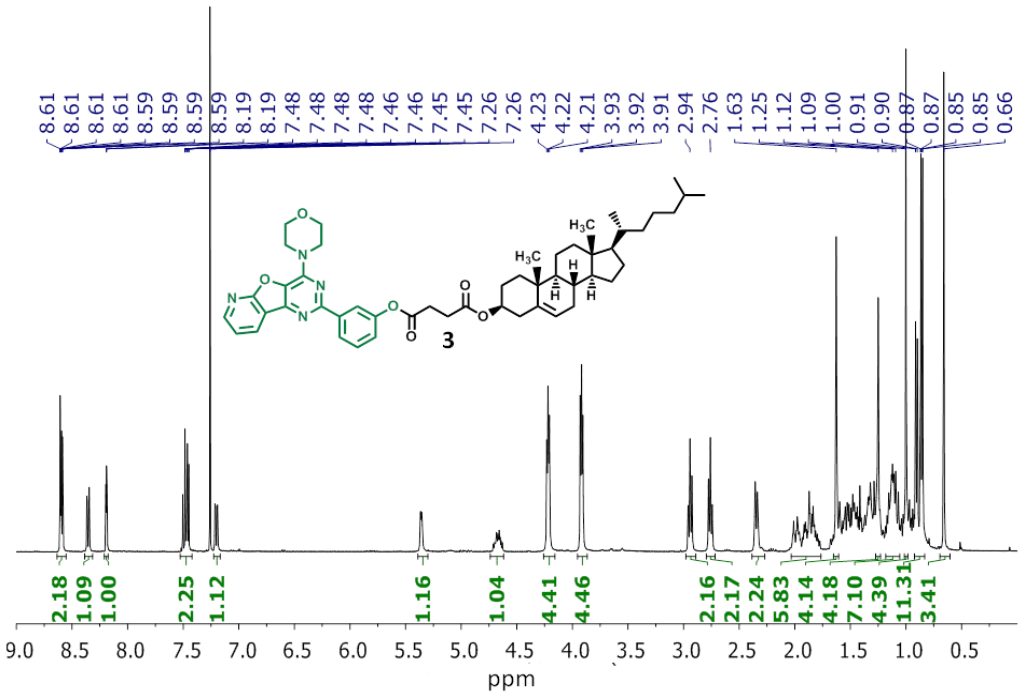

Fig. 23 ^{1}H-NMR spectra of cholesterol-succinic acid-PI103 conjugate (**3**).

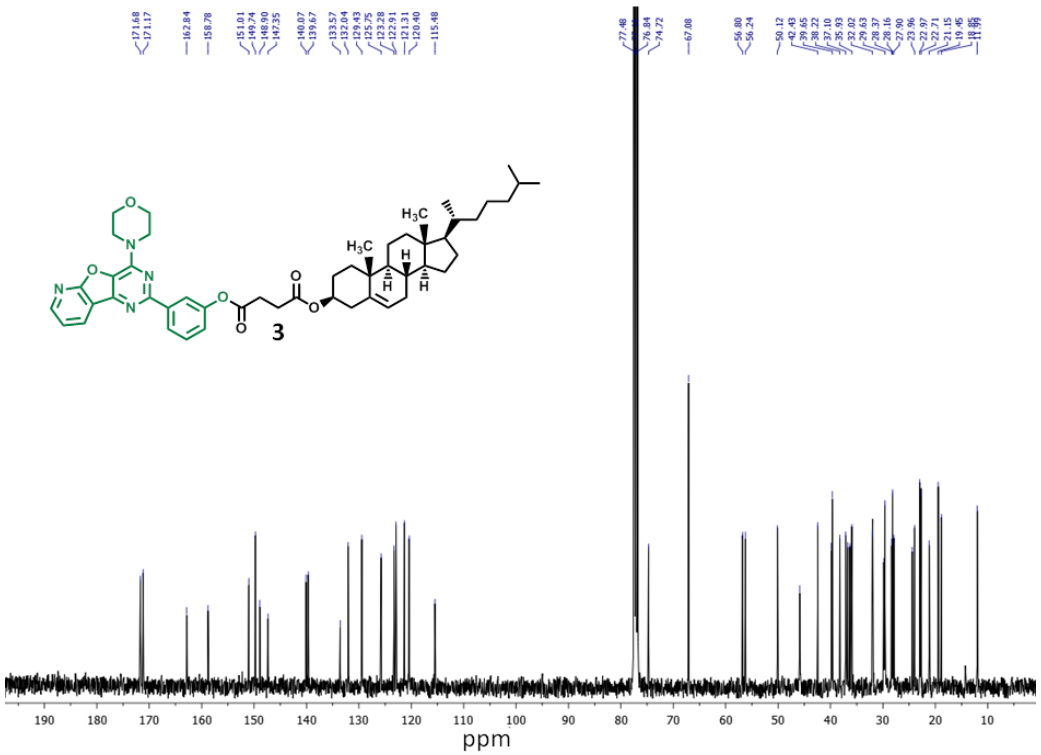

Fig. 24 ^{13}C-NMR spectra of cholesterol-succinic acid-PI103 conjugate (**3**).

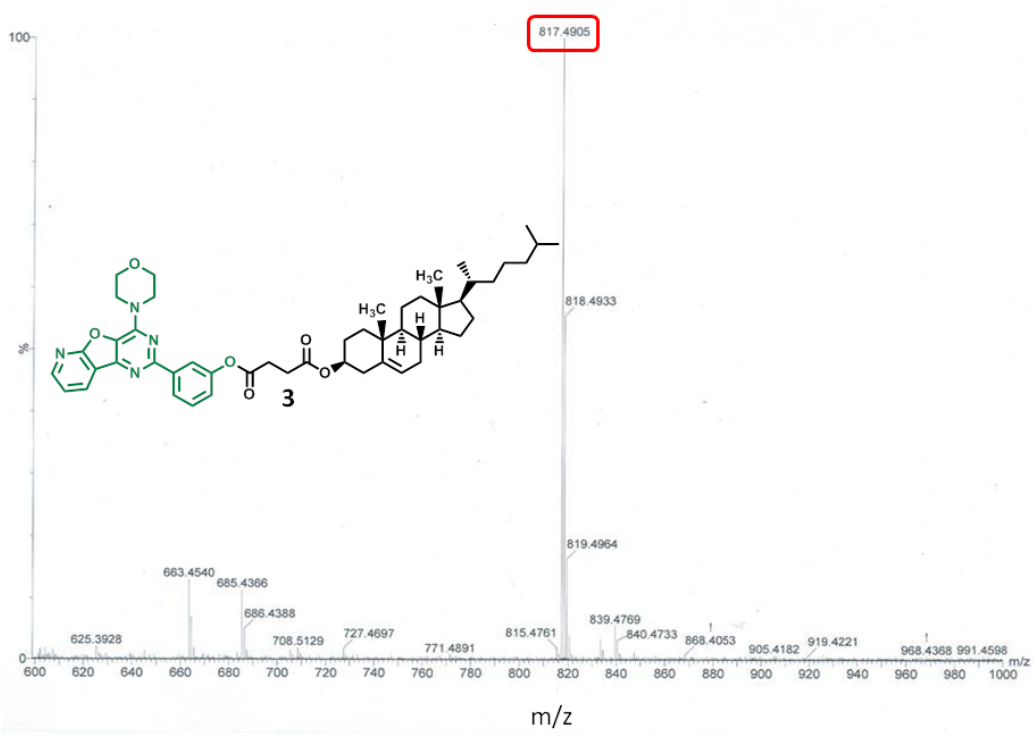

Fig. 25 HR-MS spectra of cholesterol-succinic acid-PI103 conjugate (**3**).

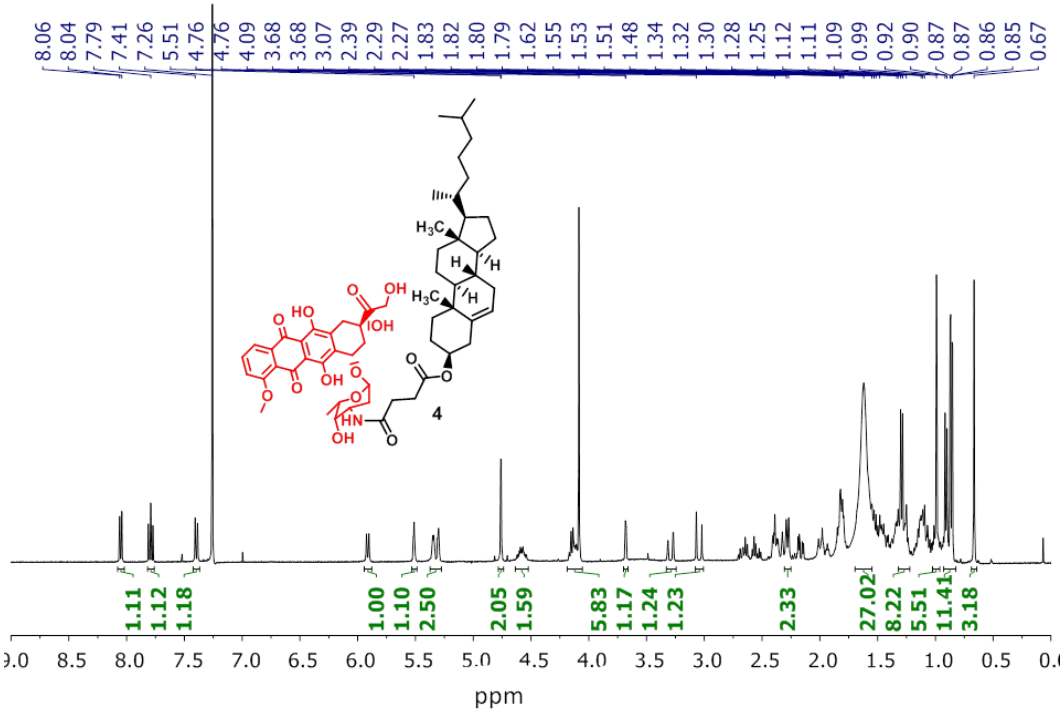

Fig. 26 ^{1}H-NMR spectra of cholesterol-succinic acid-doxorubicin conjugate (**4**).

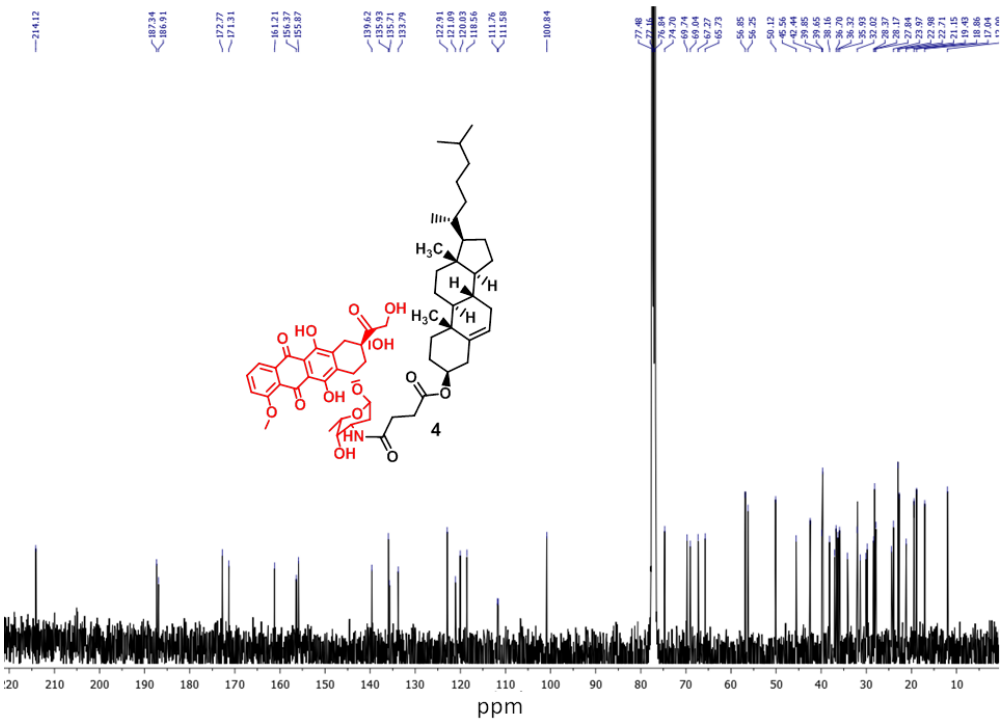

Fig. 27 ^{13}C-NMR spectra of cholesterol-succinic acid-doxorubicin conjugate (**4**).

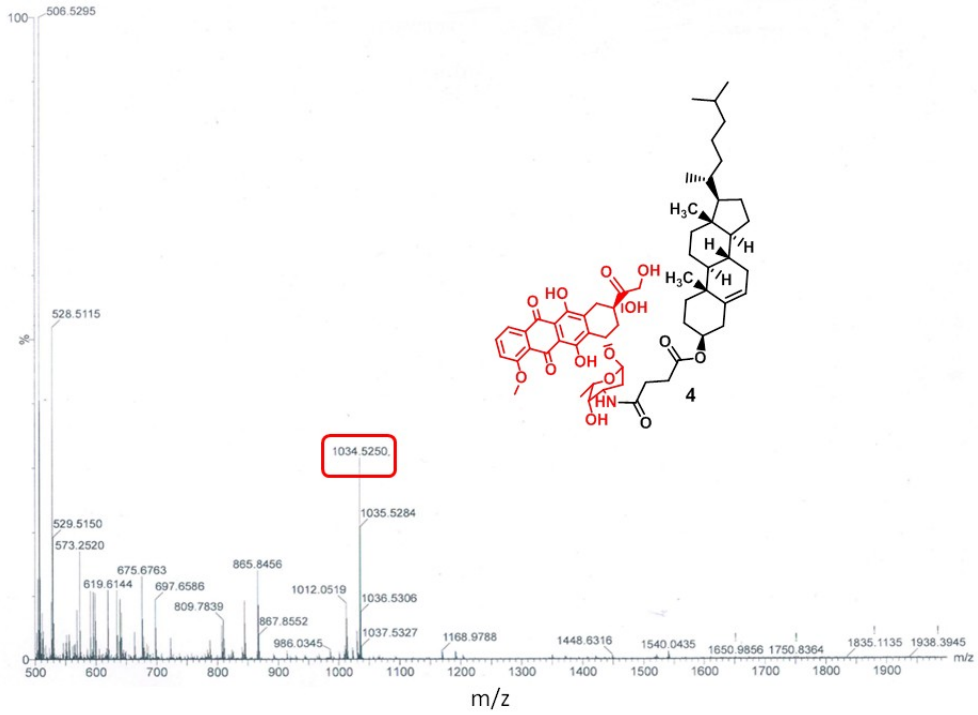

Fig. 28 HR-MS spectra of cholesterol-succinic acid-doxorubicin conjugate (**4**)

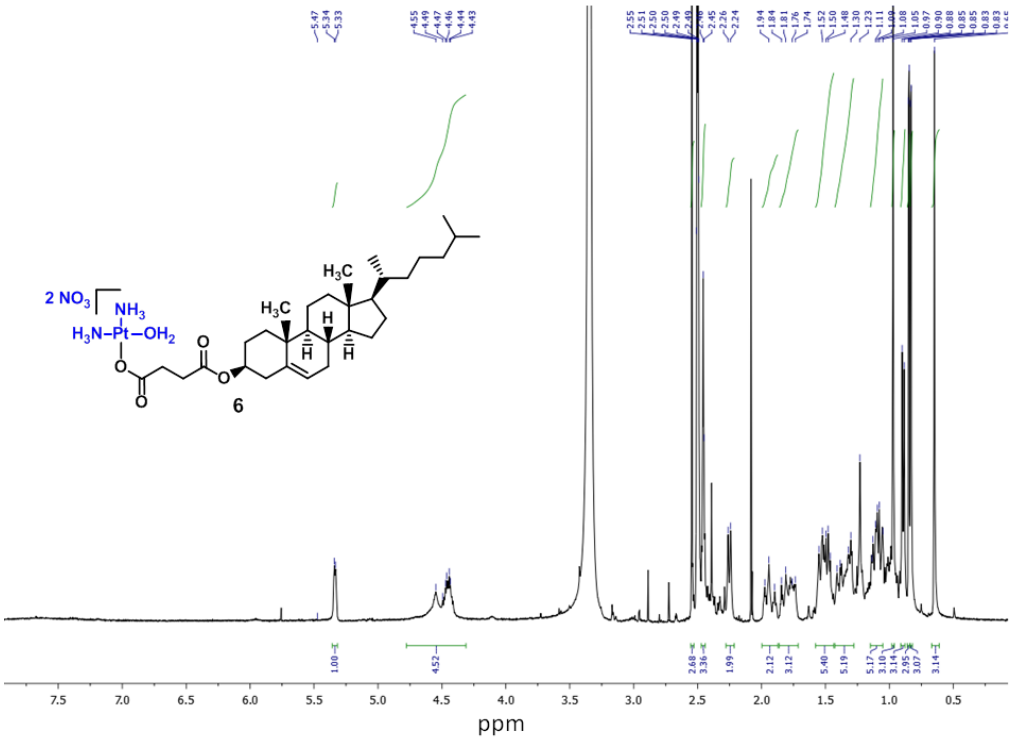

Fig. 29 ^{1}H-NMR spectra of cholesterol-succinic acid-cisplatin conjugate (**6**).

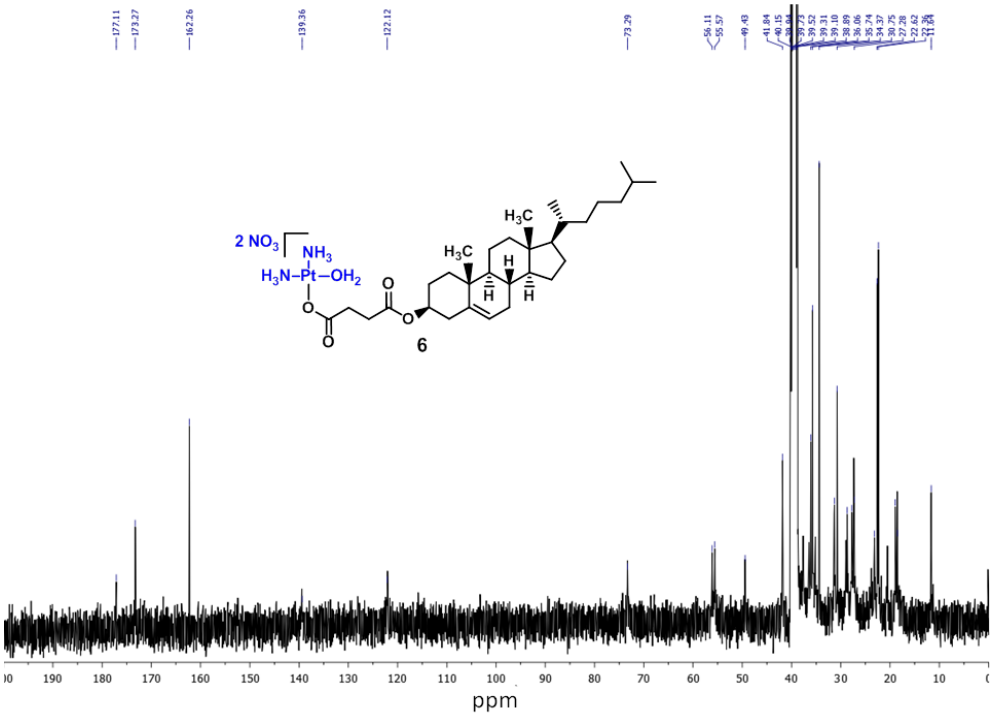

Fig. 30 ^{13}C-NMR spectra of cholesterol-succinic acid-cisplatin conjugate (**6**).

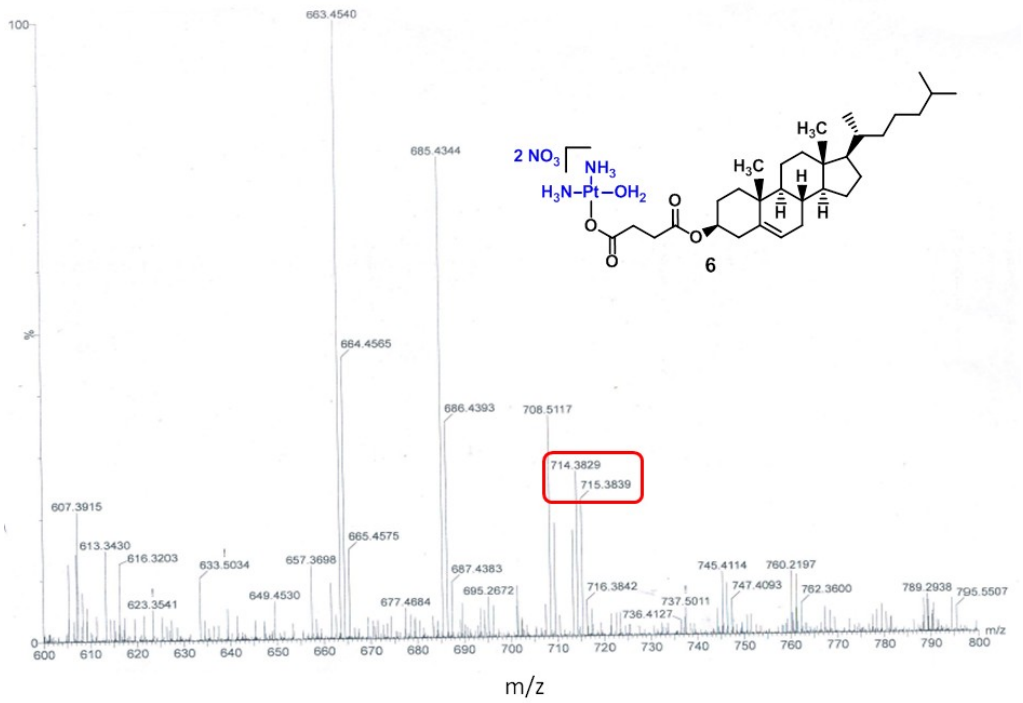

Fig. 31 HR-MS spectra of cholesterol-succinic acid-cisplatin conjugate (**6**).

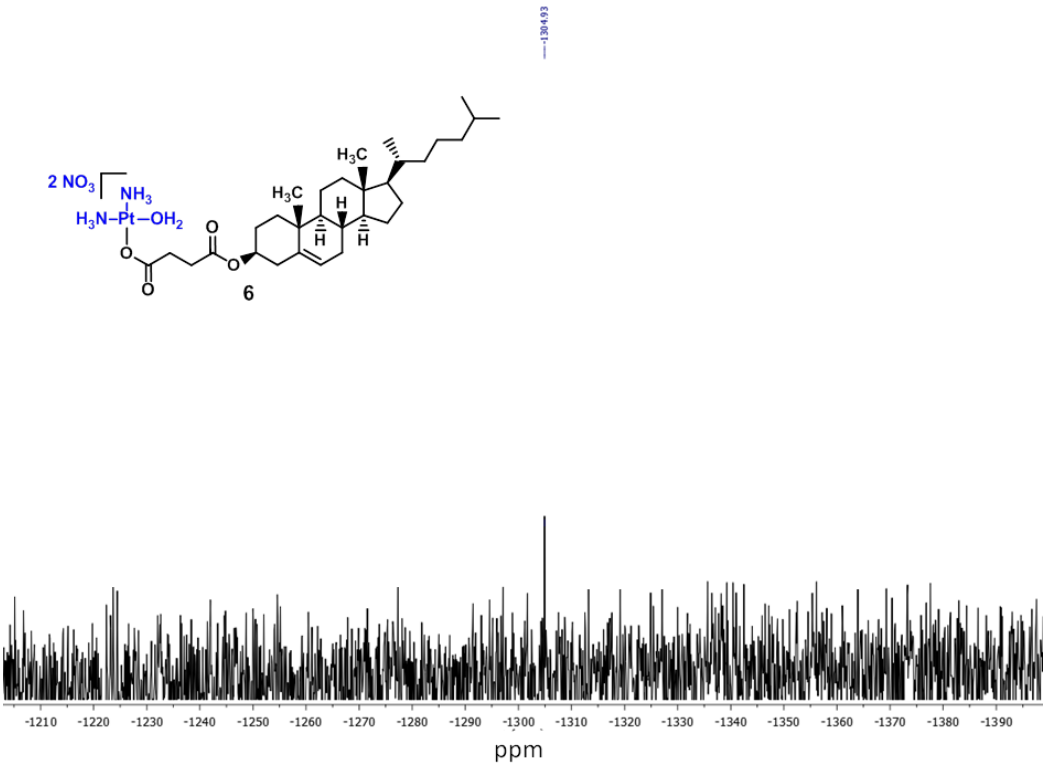

Fig. 32 ^{195}Pt-NMR spectra of cholesterol-succinic acid-cisplatin conjugate (**6**).

3.5 References

1. B. H. Jiang and L. Z. Liu, *Adv. Cancer Res.*, 2009, **102**, 19-65.
2. L. Du, J. Shen, A. Weems and S.-L. Lu, *J. Oncol.*, 2012, **2012**.
3. K. D. Courtney, R. B. Corcoran and J. A. Eng., *J. Clinic. Oncol*, 2010, **28**, 1075-1083.
4. B. T. Hennessy, D. L. Smith, P. T. Ram, Y. Lu and G. B. Mills, *Nat. Rev. Drug Discov.*, 2005, **4**, 988-1004.
5. I. Vivanco and C. L. Sawyers, *Nat. Rev. Cancer*, 2002, **2**, 489-501.
6. N. E. Hynes and G. MacDonald, *Curr. Opin. Cell Biol.*, 2009, **21**, 177-184.
7. M. Cully, H. You, A. J. Levine and T. W. Mak, *Nat. Rev. Cancer*, 2006, **6**, 184.
8. J. A. Engelman, *Nat. Rev. Cancer,* 2009, **9**, 550-62.
9. F. Chang, J. Lee, P. Navolanic, L. Steelman, J. Shelton, W. Blalock, R. Franklin and J. Mc Cubrey, *Leukemia*, 2003, **17**, 590-603.
10. A. Juvekar, H. Hu, S. Yadegarynia, C. A. Lyssiotis, S. Ullas, E. C. Lien, G. Bellinger, J. Son, R. C. Hok and P. Seth, *Proc. Natl. Acad. Sci. U.S.A.*, 2016, **113**, E4338-E4347.
11. D. Opel, M.-A. Westhoff, A. Bender, V. Braun, K.-M. Debatin and S. Fulda, *Cancer Res.*, 2008, **68**, 6271-6280.
12. M.-A. Westhoff, J. Kandenwein, S. Karl, S. Vellanki, V. Braun, A. Eramo, G. Antoniadis, K.-M. Debatin and S. Fulda, *Oncogene*, 2009, **28**, 3586-3596.
13. D. Marklein, U. Graab, I. Naumann, T. Yan, R. Ridzewski, F. Nitzki, A. Rosenberger, K. Dittmann, J. Wienands, L. Wojnowski, S. Fulda and H. Hahn, *PLoS ONE*, 2012, **7**, e52898.
14. A. Pandey, A. Kulkarni, B. Roy, A. Goldman, S. Sarangi, P. Sengupta, C. Phipps, J. Kopparam, M. Oh and S. Basu, *Cancer Res.*, 2014, **74**, 675-685.
15. S. Palvai, J. Nagraj, N. Mapara, R. Chowdhury and S. Basu, *RSC Adv.*, 2014, **4**, 57271-57281.
16. Voet, D.; Voet, J. Biochemistry, 3rd ed; John Wiley & Sons, Inc: New York, 2012; pp 765−796
17. Q.-W. Fan, Z. A. Knight, D. D. Goldenberg, W. Yu, K. E. Mostov, D. Stokoe, K. M. Shokat and W. A. Weiss, *Cancer cell,* 2006**, 9,** 341-349.
18. O. Aronov, A. T. Horowitz, A. Gabizon and D. Gibson, *Bioconju. Chem.,* 2003, **14,** 563-574.

19. S. D. Brown, P. Nativo, J.-A. Smith, D. Stirling, P. R. Edwards, B. Venugopal, D. J. Flint, J. A. Plumb, D. Graham and N. J. Wheate, *J. Am. Chem. Soc.,* 2010, **132,** 4678-4684.
20. B. M. Still, P. A. Kumar, J. R. Aldrich-Wright and W. S. Price, *Chem. Soc. Rev.,* 2007, **36,** 665-686.
21. P. Sengupta, S. Basu, S. Soni, A. Pandey, B. Roy, M. S. Oh, K. T. Chin, A. S. Paraskar, S. Sarangi and Y. Connor, *Proc. Natl. Acad. Sci. U.S.A.,* 2012, **109,** 11294-11299.
22. J. M. Harris and R. B. Chess, *Nat. Rev. Drug Discov.,* 2003, **2,** 214-221.
23. F. I. Raynaud, S. A. Eccles, S. Patel, S. Alix, G. Box, I. Chuckowree, A. Folkes, S. Gowan, A. D. H. Brandon and F. Di Stefano, *Mol. Cancer Ther.,* 2009, **8,** 1725-1738.
24. G. Minotti, P. Menna, E. Salvatorelli, G. Cairo and L. Gianni, *Pharm. Rev.,* 2004, **56,** 185-229.
25. X. Yao, K. Panichpisal, N. Kurtzman and K. Nugent, *Am. j. Med. Sci.,* 2007, **334,** 115-124.
26. J. Gilleron, W. Querbes, A. Zeigerer, A. Borodovsky, G. Marsico, U. Schubert, K. Manygoats, S. Seifert, C. Andree and M. Stöter, *Nat. Biotechnol.,* 2013, **31,** 638-646.
27. Sengupta, S.; Eavarone, D.; Capila, I.; Zhao, G.; Watson, N.; Kiziltepe, T.; Sasisekharan, R. *Nature*, 2005, **436**, 568−572.
28. D. Hanahan and R. A. Weinberg, *Cell,* 2000, **100,** 57-70.
29. G. Sahay, W. Querbes, C. Alabi, A. Eltoukhy, S. Sarkar, C. Zurenko, E. Karagiannis, K. Love, D. Chen and R. Zoncu, *Nat. Biotechnol.,* 2013, **31,** 653-658.
30. T. Franke, *Oncogene,* 2008, **27,** 6473-6488.
31. L. J. Kuo and L.-X. Yang, *In vivo,* 2008, **22,** 305-309.
32. N. J. Curtin, *Nat. Rev. Cancer,* 2012, **12,** 801-817.
33. A. A. Kulkarni, B. Roy, P. S. Rao, G. A. Wyant, A. Mahmoud, M. Ramachandran, P. Sengupta, A. Goldman, V. R. Kotamraju and S. Basu, *Cancer Res.,* 2013, **73,** 6987-6997.

Chapter 4a

Self-Assembled Oleic Acid Nanoparticle Mediated Inhibition of Mitogen Activated Protein Kinase Signaling in Combination with DNA Damage in Cancer Cells

4a.1 Introduction

Traditional cancer chemotherapy uses highly cytotoxic drugs which kill cancer cells as well as healthy cells leading to severe side effects.[1, 2] In last two decades, understanding in cancer biology revealed that mitogen activated protein kinase (MAPK) signaling encompassing RAS-RAF-MEK-ERK cascade plays significant role in different cellular functions including growth, proliferation, differentiation, survival, death, transformation and is hyper-activated in majority of tumors.[3,4] Consequently, MAPK signalling has emerged as one of the most intensively pursued targets[5] leading to the development of several small molecule inhibitors as cancer therapeutics.[6-8] Despite showing revolutionizing potential in cancer treatment, MAPK inhibitors demonstrate severe toxic side effects including immune-toxicity, embryonic developmental lethality and cardiotoxicity.[9, 10] Moreover, MAPK targeted cancer therapeutics often fail when treated as single agent due to emergence of drug resistance through intrinsic or dynamic kinome reprogramming mechanism.[11-14] Furthermore, it was found that DNA damaging cytotoxic anticancer drugs induce resistance by rewiring MAPK signalling cascade,[15, 16] which prompted the necessity to combine MAPK inhibitor with DNA damaging drugs for augmented therapeutic efficacy.[17-19] Nevertheless, administration of multiple drug combination boosts the toxic side effects of the individual drugs due to their diverse bio-distribution and lack of accumulation in the diseased tissues in right dose as discussed in chapter 1. In order to overcome these challenges, several self-assembled nanocarriers have been explored successfully for co-delivery of small molecule drugs, siRNA/gene/miRNA and therapeutic proteins in the cancer tissues to reduce toxic off-target side effects.[20-24] However, for rapid and effective translation into clinics the nanocarriers should be developed from non-toxic, biodegradable, well characterized and easily functionalized materials having extended circulation half-life and long shelf life.[1,25] Although, until now most of the focus in cancer nanomedicine has been dedicated to deliver cytotoxic drugs, not much effort has been devoted to target mitogen-activated protein kinases (MAPK) signalling by delivering MAPK inhibitors selectively into tumor to reduce their off-target side effects.[26] Only recently, Basu et al. developed MAPK inhibitor loaded polymeric nanoparticle, which demonstrated tumor reduction in a synergistic manner in combination with cisplatin as chemotherapeutic agent.[27]

Inspired by the augmented efficacy of MAPK inhibitors in combination with cytotoxic drugs and the need for developing novel clinically translatable nanovectors, we have engineered self-assembled 120 nm particles from biodegradable, non-toxic oleic acid (OA) which can

contain AZD6244 (MEK inhibitor) and cisplatin (DNA damaging anti-cancer drug). To the best of our knowledge, this is the first example of self-assembled blended oleic acid nanoparticle for dual drug delivery in cancer. These self-assembled oleic acid nanoparticles (OA-NPs) would home into the tumor tissues by EPR effect and internalize into the cancer cells by endocytosis to target MAPK signalling and damage DNA simultaneously (Fig. 1b). Excellent stability was shown by these OA-NPs in storage condition (4 °C) for 2 months as well as in blood circulation mimic for 60 days with increased dual drug release in a slow and sustained manner at pH = 5.5 compared to physiological pH = 7.4 for 96 h. These OA-NPs indeed was found to be internalized into the lysosomes through macropinocytosis mediated endocytosis mechanism and showed much improved cytotoxic effects in HeLa cervical cancer cells compared to free drug cocktail through apoptosis by inhibiting MAPK signalling and damaging DNA simultaneously. Moreover, these dual drug loaded OA-NPs demonstrated enhanced efficacy in triple-negative-breast cancer cell (MDA-MB-231), cisplatin sensitive (Hep3B) and cisplatin resistant hepatocellular carcinoma cells (Hep3B-R).

4a.2 Results and Discussion

4a.2.1 Synthesis of oleic acid-drug conjugates: We have chosen oleic acid as naturally occurring biodegradable, non-toxic vector. Oleic acid is classified as monounsaturated C18-ω-9-fatty acid found as esters in triglycerides and glycerophospholipids.[28] Moreover, oleic acid has been used as capping agents for metallic nanoparticle as well as ionic complex-nano-emulsion for drug delivery.[29, 30] However, the potential of oleic acid as nontoxic, biodegradable dual drug delivery vehicle has not been explored much. Furthermore, we envisioned that the hydrophobic mono-unsaturated tail of oleic acid would trigger the self-assembly by forming the lipophilic core of the nanoparticle. We have chosen AZD6244 as a potent, specific allosteric MEK inhibitor, which is currently in phase II clinical trial.[31, 32] Moreover, AZD6244 showed improved efficacy in combination with clinically approved DNA damaging drugs including cisplatin in different types of cancer.[33, 34] We conjugated oleic acid (**1**) with AZD6244 through ester linkage by using EDC and DMAP as coupling reagents to obtain oleic acid-AZD6244 conjugate (**2**) in 77% yield (Fig. 1a). Cisplatin (CDDP) was reacted with silver nitrate to generate cis-$[(NH_3)_2Pt(II)(H_2O)_2](NO_3)_2$ complex (**3**)[35] which was further reacted with oleic acid in 1:1 molar ratio to obtain oleic acid-cisplatin conjugate (**4**) through Pt-O-CO- bond in 74% yield.[36] The chemical structures of **2** and **4** were characterized by ^{1}H, ^{13}C NMR spectroscopy and HR-MS. Moreover, the presence of

fluorine in conjugate **2** and platinum in conjugate **4** were characterized by peaks at -129.0 ppm and -3140.6 ppm in ^{19}F and ^{195}Pt NMR respectively.

4a.2.2 Engineering self-assembled oleic acid nanoparticles (OA-NPs):

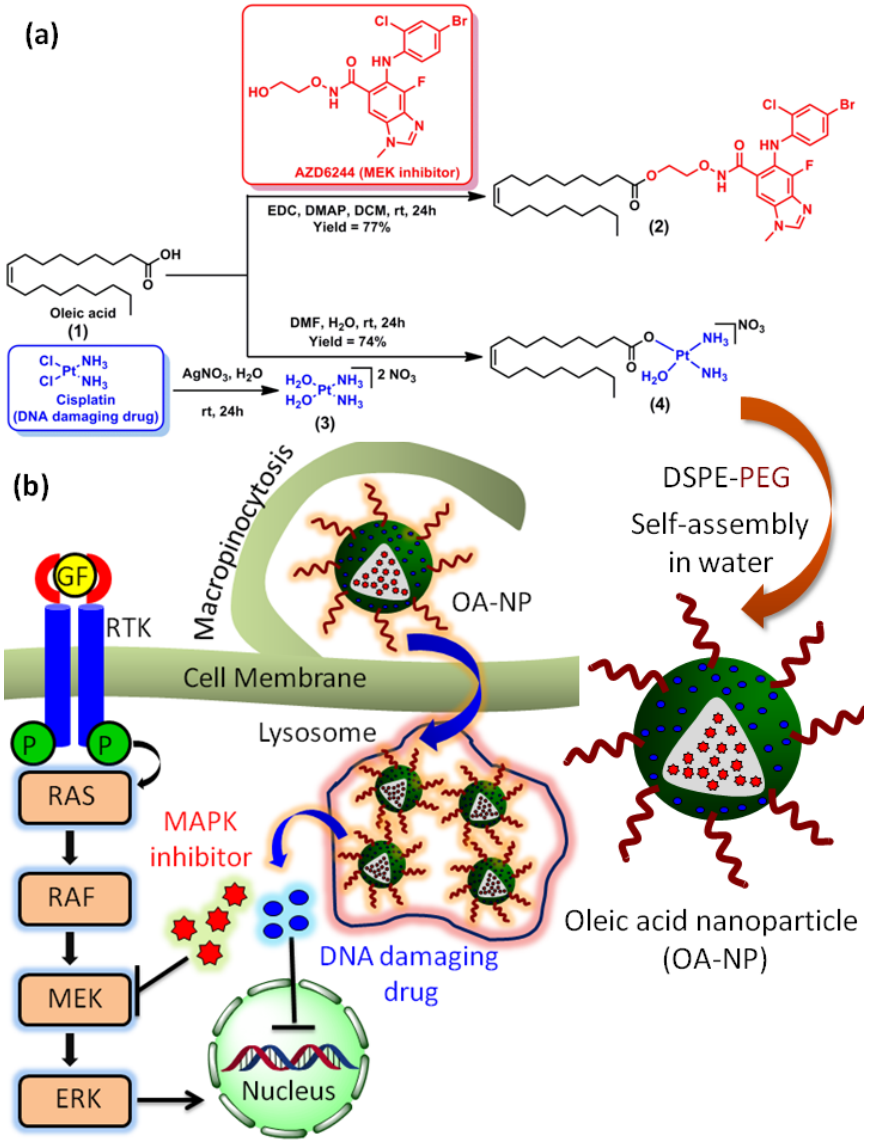

Fig. 1 Engineering of self-assembled oleic acid nanoparticles (OA-NPs). (a) Chemical synthesis of oleic acid-AZD6244 conjugate (**2**), oleic acid-cisplatin conjugate (**4**) starting from oleic acid (**1**) and self-assembly of OA-NPs by blending **2**, **4** and DSPE-PEG. (b) Schematic representation of OA-NPs internalization into cancer cells to inhibit MAPK signaling and damaging DNA simultaneously by macropinocytosis.

To develop self-assembled oleic acid nanoparticles (OA-NPs), we blended oleic acid-AZD6244 conjugate (**2**) and oleic acid-cisplatin conjugate (**4**) with DSPE-PEG in different

weight ratio in order to optimize size and drug loading (Table 1). We used DSPE-PEG to wrap the surface of the OA-NPs with polyethylene glycol to protect them from the reticulo-endothelial system (RES) and increase the stability into the blood circulation.[37] The blended mixture of conjugate **2**, **4** and DSPE-PEG were dissolved in methanol/acetone mixture (1:1) and added slowly into water to self-assemble into OA-NPs followed by ultra-centrifugation at 60000g (Fig. 1a). We evaluated the hydrodynamic diameter and polydispersity index (PDI) of different OA-NPs by dynamic light scattering (DLS) experiment. From table 1 it was clear that the smallest OA-NPs were obtained having weight ratio of oleic acid-AZD6244: oleic acid-cisplatin: DSPE-PEG = 1:1:0.2 with mean hydrodynamic diameter = 119.9 ± 3 nm and PDI = 0.11 ± 0.06 (Fig. 2a). We also evaluated the loading of AZD6244 and cisplatin in different OA-NPs by UV-Vis spectroscopy using concentration versus absorbance graph at characteristic λ_{max} = 273 nm (Fig. 2a) and 706 nm (Fig. 3, Chapter 2) for AZD6244and cisplatin respectively. Fig. 2b clearly showed that the highest mean loading of AZD6244 and cisplatin was found to be 654 µg/mL and 88 µg/mL respectively in OA-NPs having weight ratio of oleic acid-AZD6244: oleic acid-cisplatin: DSPE-PEG = 1:1:0.2. From DLS and loading optimization study it was evident that OA-NPs with smallest size and highest drug loading was obtained from the blending of conjugate **2**, **4** and DSPE-PEG in weight ratio of 1:1:0.2. Hence we used this formulation in OA-NPs for further studies. We evaluated the size, shape and morphology of these self-assembled OA-NPs by AFM (Fig. 3b) and FESEM (Fig. 3c).

Oleic acid-AZD6244 conjugate (2) (mg)	Oleic acid-cisplatin conjugate (4) (mg)	DSPE-PEG (mg)	Size	PDI
1	1	0.2	119.9 ± 3	0.11 ± 0.06
1	0.5	0.2	129.2 ± 1	0.09 ± 0.04
0.5	1	0.2	130.2 ± 3	0.21 ± 0.03

Table 1. Optimization of self-assembled OA-NP synthesis.

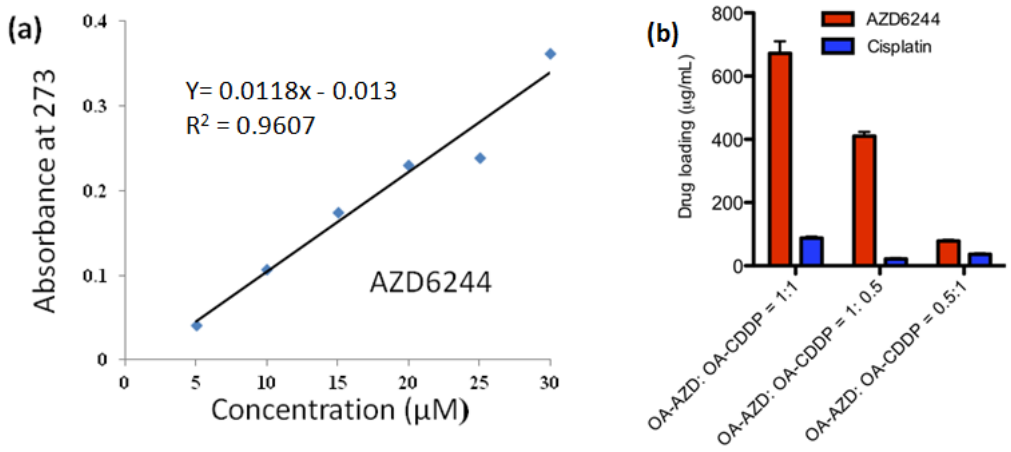

Fig. 2 (a) Absorbance versus concentration calibration graph of AZD6244 at λ_{max} = 273 nm by UV-Vis spectroscopy. (b) Loading of AZD6244 and cisplatin in different OA-NP formulation determined from graph (a).

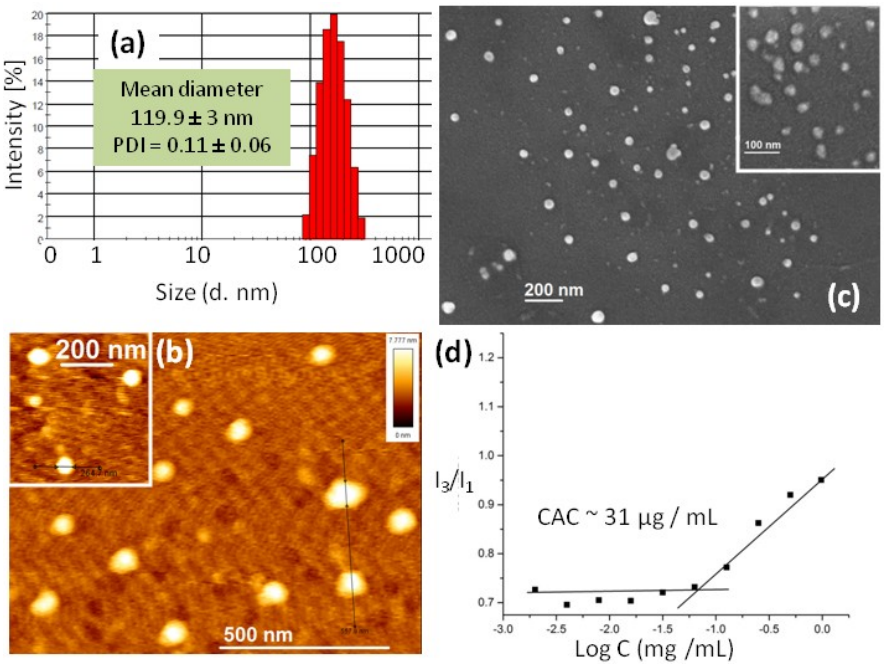

Fig. 3 Characterization of OA-NPs by (a) DLS, (b) AFM and (c) FESEM. (d) Determination of critical aggregation concentration (CAC) of OA-NPs by pyrene encapsulation method.

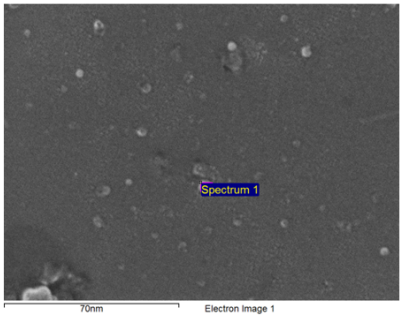

Element	Weight %	Atomic %
C	51.61	81.92
N	1.84	2.50
O	7.08	8.43
Br	23.34	5.57
Pt	16.13	1.58
Total	100	

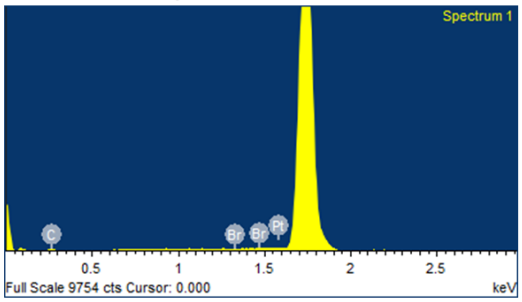

Fig. 4 Determination of Pt metal content and Br content in OA-NPs by energy dispersive X-ray.

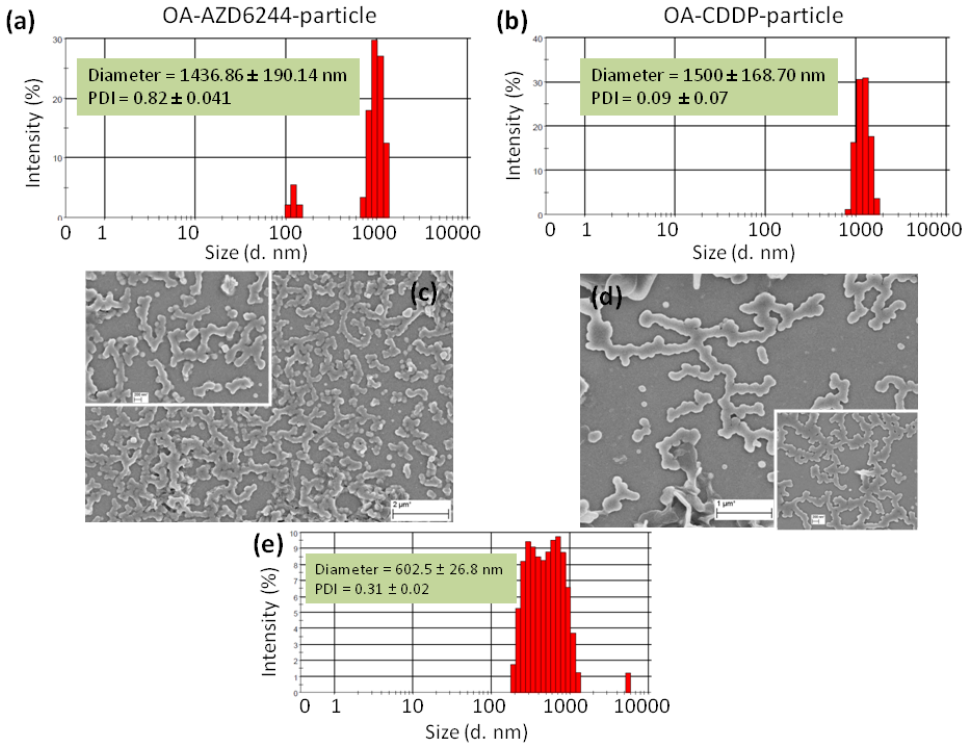

Fig. 5 (a-b) DLS of particles from OA-AZD6244 and OA-CDDP conjugate respectively. (c-d) FESEM images of particles from OA-AZD6244 and OA-CDDP conjugates respectively. (e) DLS of particles formed from oleic acid particle encapsulated AZD6244 and CDDP.

DLS, AFM and FESEM data showed that the OA-NPs are mono-dispersed and spherical in shape with 120 nm size, compatible to be congregated into the tumor tissue by EPR effect. Moreover, we validated the presence of Br and Pt metal by energy-dispersive X-ray spectroscopy (EDX) measurements (Fig. 4) which clearly demonstrated the presence of both the drug molecules in the same particle. Interestingly, only oleic acid-AZD6244 conjugate (**2**) and oleic acid-cisplatin conjugate (**4**) separately did not self-assemble into spherical nanoparticles (Fig. 5a-d). Moreover, oleic acid provided larger self-assembled particles while encapsulating free AZD6244 and cisplatin in combination having 602.5 ± 26.8 nm size and PDI = 0.31 ± 0.02 (Fig. 5e). We anticipate that the oleic acid tails in conjugate **2** and **4** interact with each other leading to co-self-assembly into nanoparticle which is not possible for conjugate **2** and **4** separately. However, the exact mechanism of co-self-assembly is not clearly understood.

To investigate the co-self-assembly of conjugate **2** and **4** in water, we evaluated the critical aggregation concentration (CAC) by using pyrene as fluorescent probe. The fluorescence emission spectra of pyrene contains I_1 and I_3 as first and third bands and I_3/I_1 emission intensity ratio is the indicator of the polarity change in the pyrene surrounding.[38] At low concentration of conjugate **2** and **4** blended mixture at 1:1 weight ratios, the I_3/I_1 value remained almost unchanged (Fig. 3d), indicating pyrene in water medium. With increase in concentration of conjugate **2** and **4** mixture (weight ratio = 1:1), the I_3/I_1 value increased sharply and reached characteristic value of pyrene in hydrophobic environment. From Fig. 3d, the critical aggregation concentration (CAC) was calculated to be 31μg/mL where I_3/I_1 ratios started to increase dramatically.

4a.2.3 Stability of OA-NPs: To be successful in clinics, one of the important criteria for drug containing nano-vehicles is prolonged stability in storage condition as well as in circulating blood stream to allow enough time for accumulating in tumor tissue by EPR effect. To assess the stability in storage condition, we incubated the OA-NPs in water at 4 °C and evaluated the hydrodynamic diameter and PDI values by DLS. The hydrodynamic diameter of OA-NPs changed from 119.3 ± 2.1 nm to 142.0 ± 4 nm with marginal change in PDI value from 0.117 ± 0.004 to 0.387 ± 0.019 over 60 days (Fig. 6a, b). To evaluate the amount of aggregation or sedimentation of OA-NPs over prolonged storage at 4 °C, we measured the scattering intensity change of the particles by DLS. The OA-NPs showed the change of mean scattering intensity of the nanoparticles from 95.6 % to 93.2 % over 60 days (Fig. 7). On the other hand,

the mean scattering intensity of the aggregated particles showed negligible increase from 4.4 % to 6.8 % over 60 days (Fig. 7) which clearly indicated the minimum aggregation or sedimentation of OA-NPs in the storage condition. To mimic the blood circulation milieu we incubated OA-NPs in DMEM cell culture media with 10 % fetal bovine serum (FBS) at

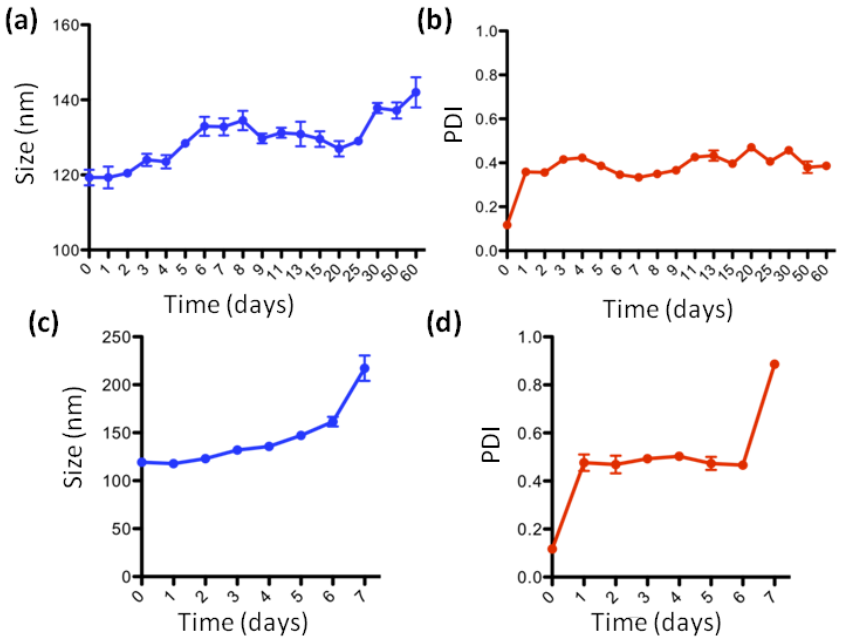

Fig. 6 Stability of OA-NPs determined by DLS (a-b) at 4°C in water for 60 days and (c-d) at 37 °C in DMEM media with 10 % FBS for 7 days.

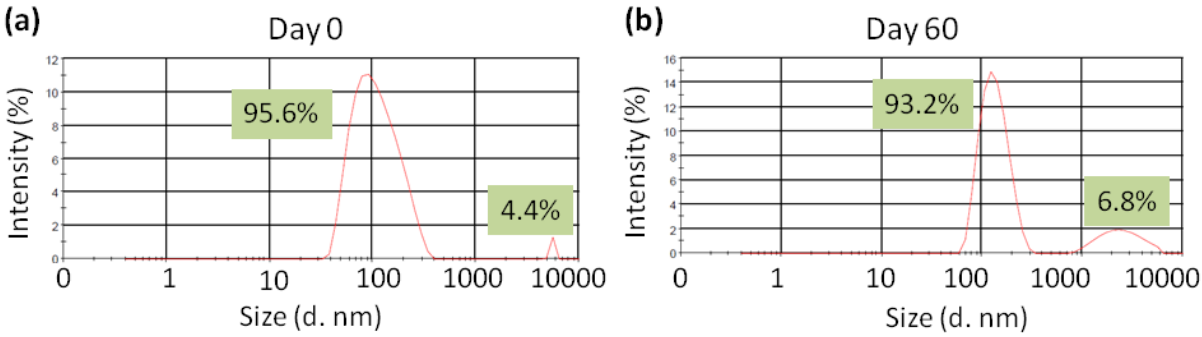

Fig. 7 DLS of OA-NPs at storage condition (4 °C) with scattering intensities of peaks at day 0 and day 60.

37 °C. The hydrodynamic diameter increased from 119.3 ± 2.1 nm to 217.3 ± 13.2 nm with dramatic increase in PDI values from 0.117± 0.004 to 0.887 ± 0.009 over 7 days (Fig. 6c, d). From the stability experiment, it was evident that the OA-NPs are extremely stable at storage

condition for over 2 months. Moreover, the OA-NPs are also highly stable in blood circulation for 6 days, which is adequate to home into tumor tissues by EPR effect.

4a.2.4 Dual drug release: Besides being highly stable, clinically successful nanocarrier should release its payloads in a slow and sustained manner over a long period of time. To evaluate the release profile of dual drugs we used dialysis method.[39] We incubated the OA-NPs in pH = 5.5 solution to mimic the lysosomes in the cancer cells[40] at 37 °C and quantified the amount of drugs released in predetermined time points from absorbance versus concentration calibration graph obtained from UV-Vis spectroscopy (Fig. 2a for AZD6244 and Fig. 3 for cisplatin in chapter 2). These OA-NPs released 90.3 ± 3.3 % of AZD6244 and 85.3 ± 3.0 % of cisplatin after 96 h (Fig. 8a) at pH = 5.5. As control experiment, we incubated the OA-NPs in PBS buffer having pH = 7.4, which mimics the physiological condition and quantified the amount of dual drug released at different time points.

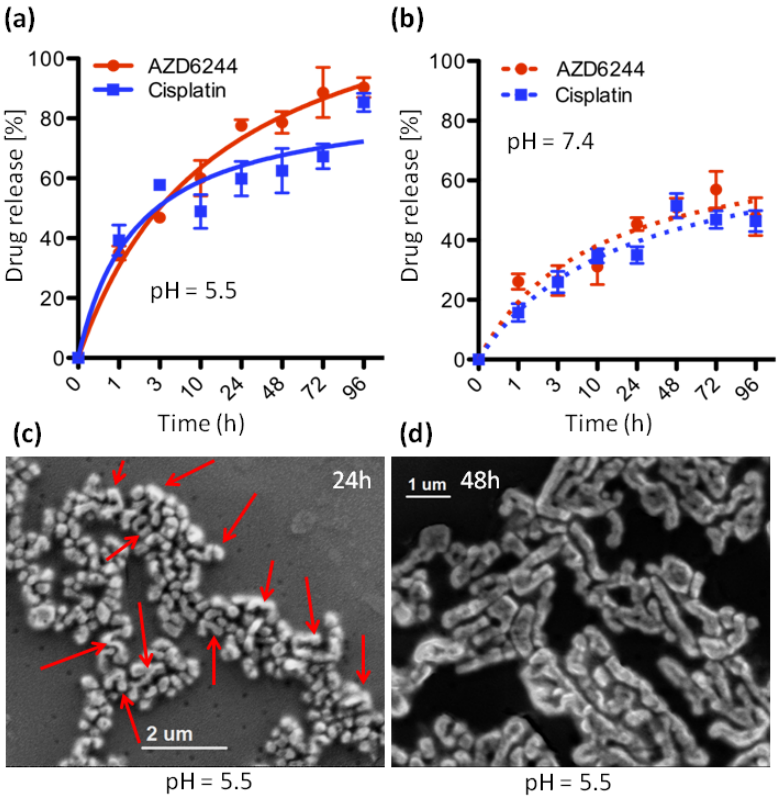

Fig. 8 Release of AZD6244 and cisplatin from OA-NPs (a) at pH = 5.5 as lysosomal compartment mimic and (b) at pH = 7.4 for 96 h at 37 °C (c-d) FESEM images of OA-NPs incubated at pH = 5.5 at 24 h and 48 h to visualize the damage of the morphology after dual drug release.

At pH = 7.4, OA-NPs demonstrated only 47.9 ± 6.3 % of AZD6244 and 46.3 ± 3.4 % of cisplatin release after 96 h (Fig. 8b). To identify the structure of the active drugs after release, we performed the UV-Vis spectroscopy of the released fraction from OA-NPs at pH = 5.5. The characteristic λ_{max} = 706 nm and 273 nm peaks at 24 h and 48 h time points clearly indicated the presence of free cisplatin and AZD6244 released from OA-NPs at pH = 5.5 (Fig. 9).

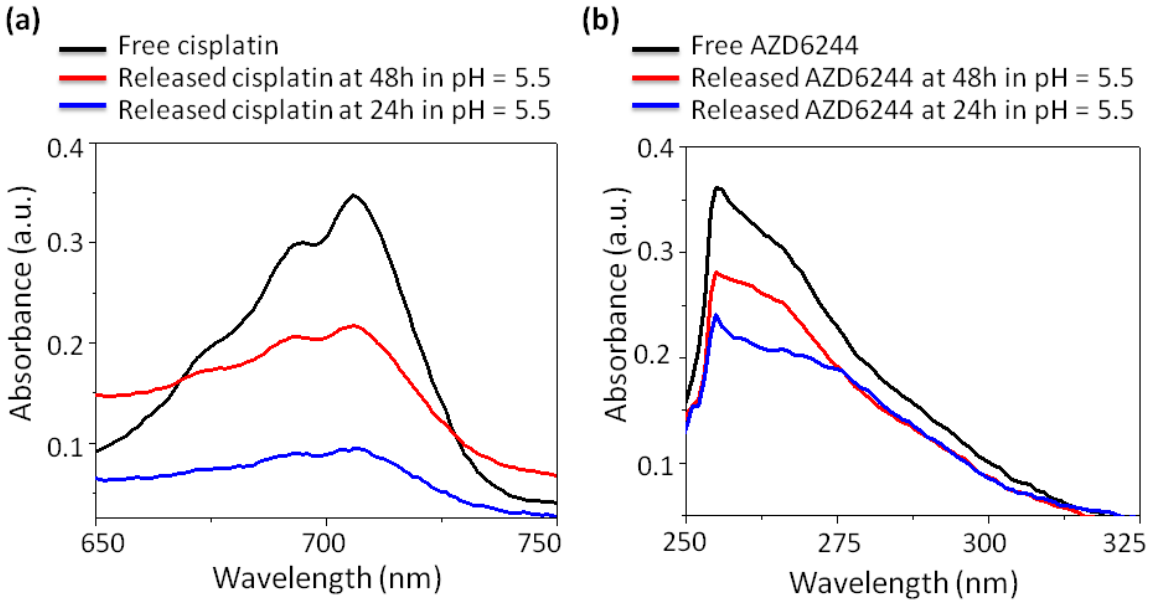

Fig. 9 UV-Vis spectra of (a) cisplatin and (b) AZD6244 after release from OA-NPs after 24 h and 48 h in pH = 5.5.

From this drug release experiment, it was clear that OA-NPs released the dual drugs in much higher quantity at pH = 5.5 compared to pH = 7.4 in a slow and sustained manner over 4 days. Previously, we have demonstrated that ester bonds between drug-lipid conjugates are more labile in acidic pH compared to physiological pH.[41, 42] Similarly, we anticipate that the ester linkage in oleic acid-AZD6244 conjugate (**2**) and Pt-O-CO- linkage in oleic acid-cisplatin conjugate (**4**) are more labile in acidic environment compared to neutral pH. We reasoned that although most of the free drugs were released from the OA-NPs in pH = 5.5 at 37 °C the drug release would be negligible at storage temperature (4 °C) for 60 days.

To understand the improved release profile of dual drugs by breaking the OA-NPs at pH = 5.5 compared to pH = 7.4, we visualized the shape of the OA-NPs in different pH by

FESEM. At pH = 5.5 after 24h the spherical shape of the OA-NPs were mostly shattered (Fig. 8c), whereas after 48h incubation, the OA-NPs lost their spherical shape completely (Fig. 8d). On contrary, at pH = 7.4, OA-NPs maintained their spherical shape intact after 24 h and 48 h incubation (Fig. 10). These FESEM images clearly indicated that the enhanced dual drug release was also triggered by the destruction of spherical shape of OA-NPs at acidic pH compared to neutral pH.

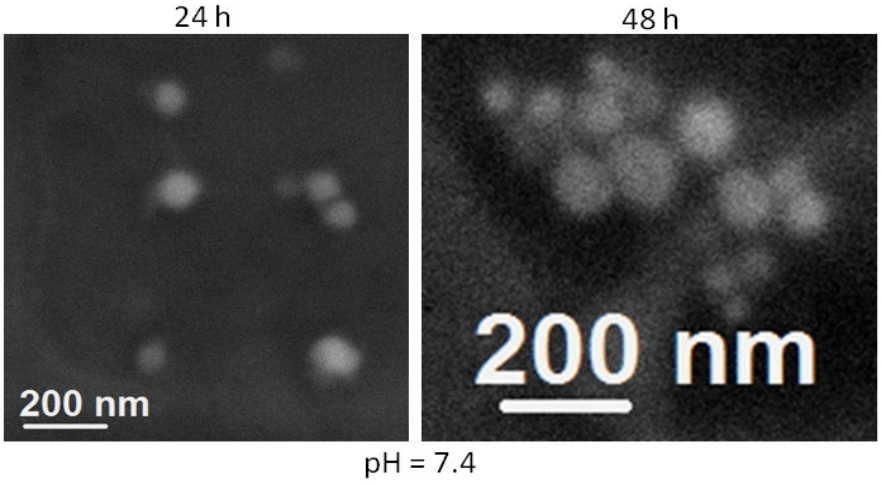

Fig. 10 FESEM images showing the size and shape of OA-NPs after 24 h and 48 h incubation in pH = 7.4

4a.2.5 *In vitro* cytotoxicity assay: To evaluate the potential of AZD6244 and cisplatin containing OA-NPs in cancer therapeutic, we evaluated the *in vitro* cytotoxicity assay in different cancer cell lines. We treated HeLa cervical cancer cells with OA-NPs in a dose dependent manner for 48 h and quantified the percentage of viable cells by using MTT assay. As control, we treated the cells with AZD6244 and cisplatin cocktail in the same concentration present in OA-NP for 48 h and evaluated the cell viability by MTT assay. OA-NPs showed remarkably less IC_{50} = 1.65 μM (cell viability = 33.7 % at 25 μM) compared to IC_{50} = 6.6 μM (cell viability = 6.2 % at 25 μM) for free drug combination in HeLa cells (Fig. 11a). Currently, in clinics, triple negative breast cancer (TNBC) is one of the most challenging cancers to cure due to its resistant nature for most of the chemotherapeutic drugs.[43] Recently, it was shown that MAPK inhibitor can sensitize a subset of TNBC towards DNA damaging drugs.[15] Hence, we treated MDA-MB-231 triple negative breast cancer cells with OA-NPs and quantified the cell viability by MTT assay at 48 h post incubation.

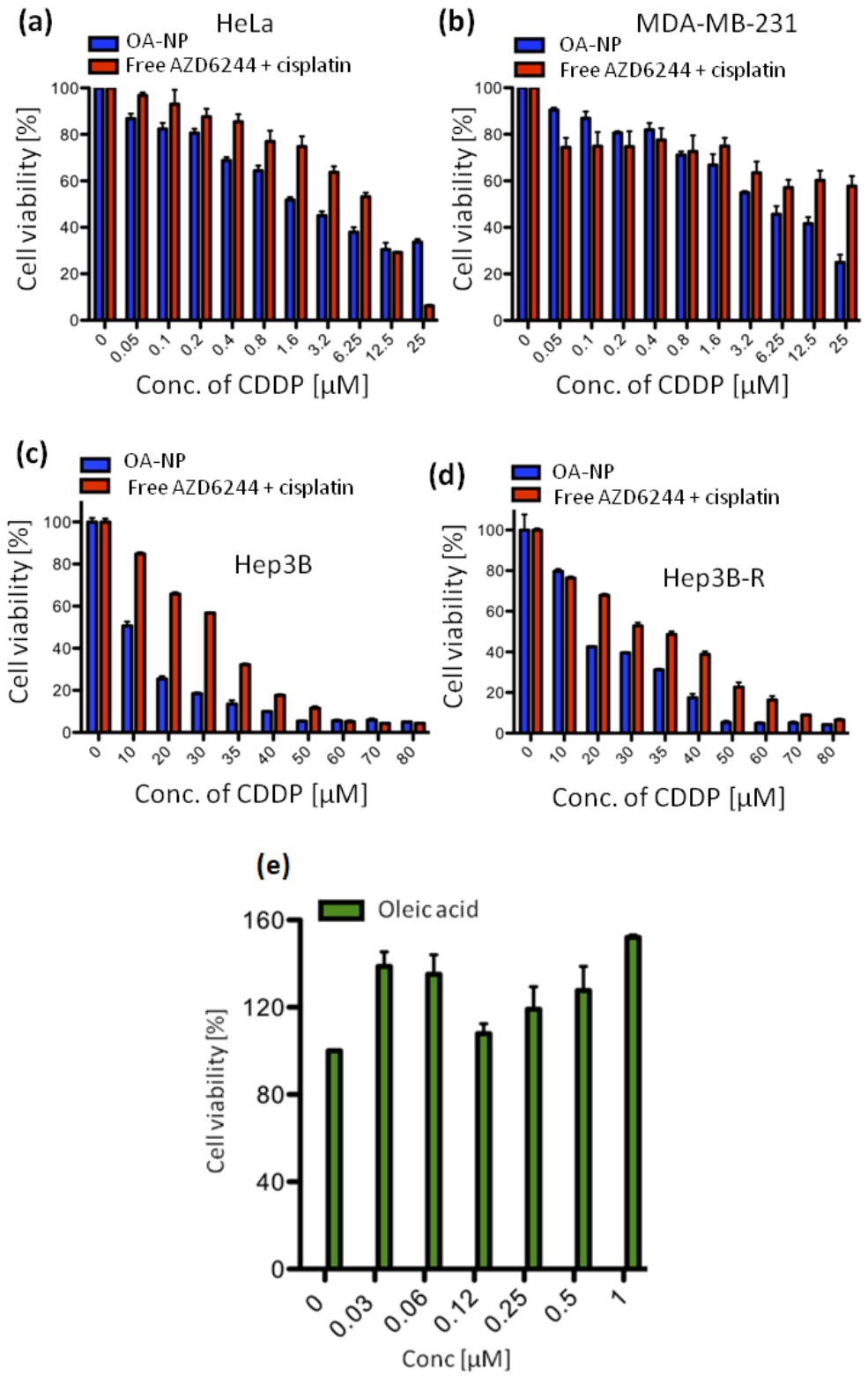

Fig. 11 *In vitro* cell viability assay of OA-NPs determined by MTT assay in (a-b) HeLa and MDA-MB-231 respectively at 48 h post incubation (c-d) Hep3B and Hep3B-R cells respectively at 24 h post incubation compared to free drugs.

Interestingly, OA-NPs showed much lower IC_{50} = 3.5 μM (cell viability = 33.7 % at 25 μM) compared to IC_{50} = 7.1 μM (cell viability = 57.6 % at 25 μM) (Fig. 11b). We also evaluated the cytotoxicity of OA-NPs in cisplatin sensitive hepatocellular carcinoma cells Hep3B. OA-NPs illustrated much less IC_{50} = 10.1 μM (cell viability = 5 % at 80 μM) compared to IC_{50} = 34.1 μM (cell viability = 4.3 % at 80 μM) at 24 h (Fig. 11c). Interestingly, also in the cisplatin-resistant Hep3B-R cells OA-NPs demonstrated much reduced IC_{50} = 17.0 μM (cell viability = 4.2 % at 80 μM) compared to IC_{50} = 31.7 μM (cell viability = 6.5 % at 80 μM) for free drug combination at 24 h (Fig. 11d). These MTT assays showed that OA-NPs induced much superior cytotoxic effects compared to free drug cocktails in cervical cancer, triple negative breast cancer, cisplatin sensitive and resistant hepatocellular carcinoma. Furthermore, to show the biocompatibility and non-toxic nature of oleic acid, we also evaluated the cytotoxicity of oleic acid in HeLa cells. Free oleic acid showed no toxicity in HeLa cells even at 1 μM concentration after 48 h (Fig. 11e) indicated the biocompatibility of oleic acid in developing nano-vehicle.

4a.2.6 Induction of apoptosis: Most of the DNA damaging drugs show their anticancer effects by activating apoptosis. Hence, we have used fluorescence activated cell sorting method (FACS) to quantify the effect of OA-NPs in induction of apoptosis compared to non-treated cells. HeLa cells were treated with OA-NPs for 24 h at 1.65 μM concentration and then labeled with Annexin V-FITC and counterstained the cells with propidium iodide (PI). Indeed, 72.82 % and 3.01 % cells were found in early apoptotic and late apoptotic phase respectively after treating the cells with OA-NPs whereas only 0.03 % and 0.19 % cells were found in early and late apoptotic phase respectively in non-treated control (Fig. 12a). Furthermore, we visualized the apoptosis induction by OA-NPs through confocal laser scanning microscopy (CLSM) experiment. We treated the HeLa cells with OA-NPs for 24 h in 1.65 μM concentration and stained the early and late apoptotic cells by Annexin V-FITC and PI respectively. From the CLSM images in Fig. 12b it was clear that OA-NPs induced much enhanced apoptosis in HeLa cells compared to the non-treated control cells which hardly showed any apoptosis. We also quantified the FITC and PI fluorescent intensity in control and OA-NPs treated cells from CLSM. The OA-NPs treated cells showed 1213.3 folds and 1909.1 folds increase in FITC and PI fluorescence intensity respectively compared to non-treated control cells (Fig. 12c), which indicated the increased number of apoptotic cells in OA-NP treatment. From these FACS analysis and CLSM images it was evident that OA-NPs showed their cytotoxicity through initiation of apoptosis.

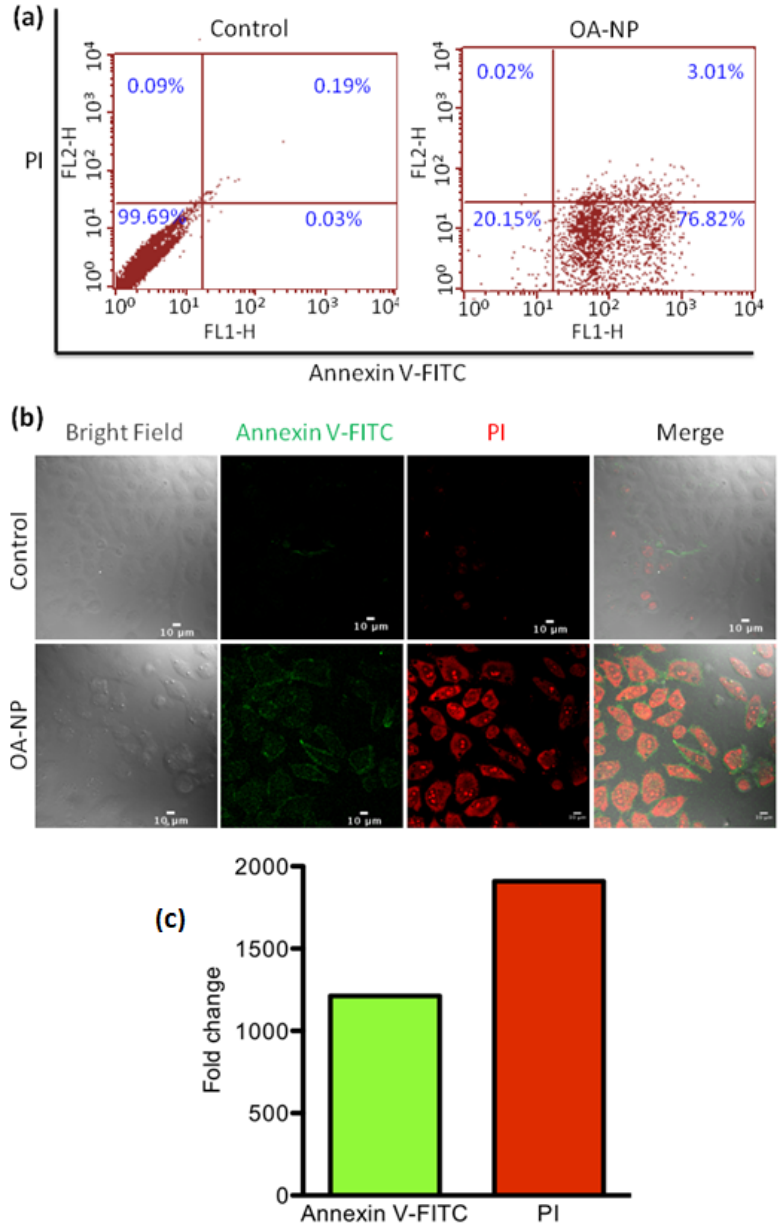

Fig. 12 Determination of apoptosis induction by OA-NPs in HeLa cells by (a) FACS analysis and (b) CLSM images compared to non-treated cells after 24 h post incubation. Early apoptotic and late apoptotic/necrotic cells were stained by Annexin V-FITC (green) and PI (red) dyes respectively. In FACS analysis, healthy cells, early apoptotic cells, late apoptotic cells and necrotics cells were represented in lower left, lower right, upper right and upper left quandrants respectively. Scale bar in CLSM images = 10 µm.

4a.2.7 Cellular internalization: We hypothesized that the OA-NPs having sub 200 nm size would home into the tumor tissue by EPR effect and then internalize into the early endosome

followed by acidic lysosomes through endocytosis leading to the release of MAPK inhibitor and DNA damaging agents to show their effects inside the cancer cells (Fig. 1b). We rationalized that the OA-NPs would release much less active drugs from early endosome having much higher pH (pH ~ 6.8) compared to lysosomes with much less pH (pH ~ 5.5).[40] To test this hypothesis, we visualized the internalization of OA-NPs into HeLa cells in a time dependent manner by confocal laser scanning microscopy (CLSM). We have encapsulated a red fluorescent dye rhodamine into OA-NPs to develop OA-Rho-NP. Characterization of OA-Rho-NPs by DLS and FESEM revealed having hydrodynamic diameter = 156.1 ± 6 nm with spherical shape (Fig. 13 a, b). HeLa cells were then treated with OA-Rho-NPs for 1 h, 3 h and 6 h time points.

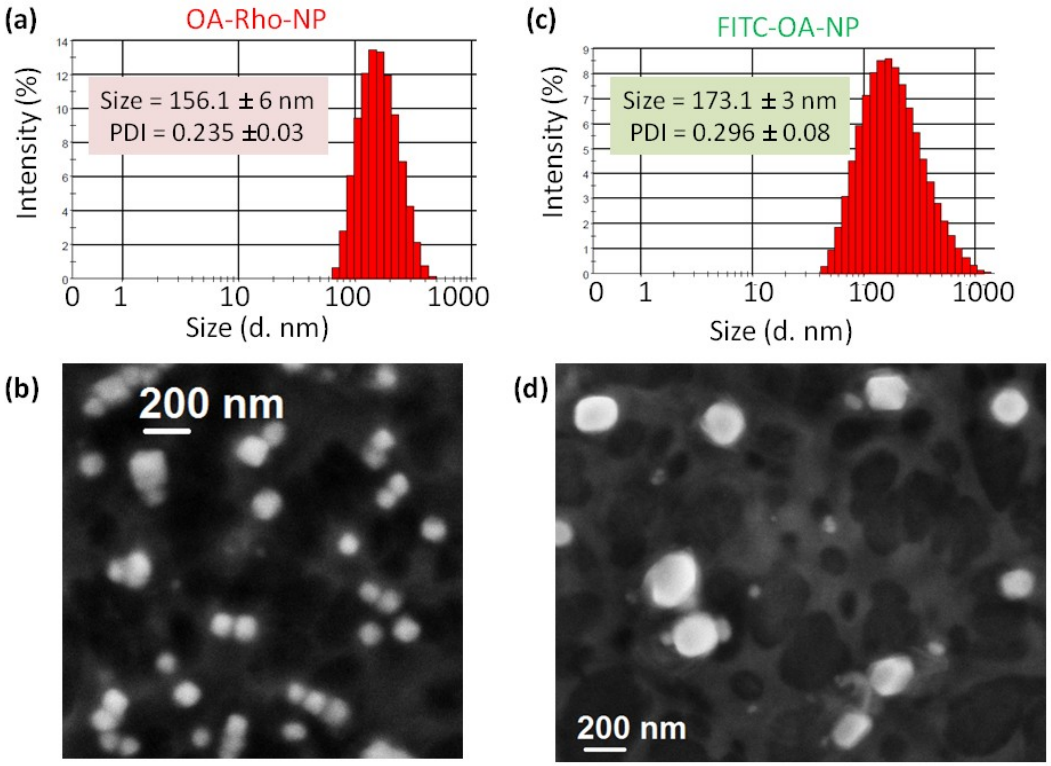

Fig. 13 (a-b) DLS and FESEM of OA-Rho-NPs. (c-d) DLS and FESEM images of FITC-OA-NPs.

We stained the acidic lysosomal compartments with green fluorescent probe LysoTracker DND-26 and counterstained nucleus with blue fluorescent dye DAPI followed by imaging through CLSM. From Fig. 14, it was clear that OA-Rho-NPs internalized into the acidic lysosomal compartments in a time dependent manner over 6 h which led to the co-localization of red and green fluorescence emerging yellow color. The amount of co-

localization of red and green fluorescence was further quantified by Pearsons'correlation coefficient and Manders coefficients. OA-Rho-NPs were internalized with 39.12 %, 42.57 % and 62.39 % volume co-localization at 1 h, 3 h and 6 h time points respectively (Table 2).

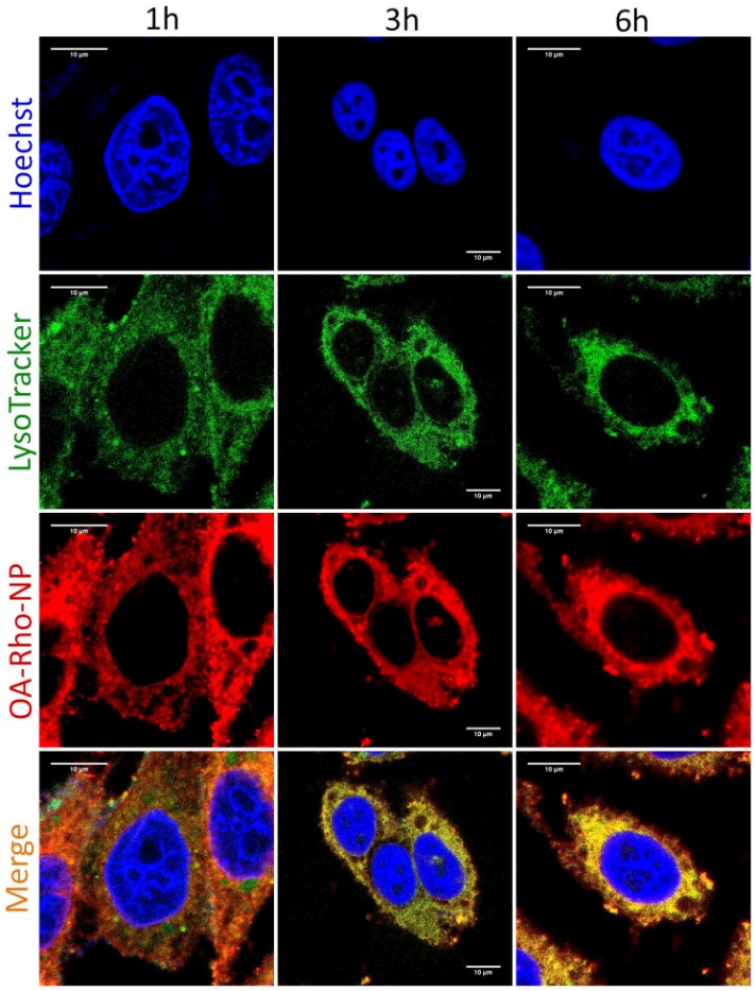

Fig. 14 Cellular internalization of OA-Rho-NPs into HeLa cells in a time dependent manner at 1 h, 3 h and 6 h. Nuclei and lysosomal compartments were stained with DAPI (blue) and LysoTracker DND-26 (green) respectively. Merged images show the co-localization of OA-Rho-NPs into lysosomal compartments to generate yellow color. Scale bar = 10 μm.

.

To understand the mechanism of the endocytosis, we further pre-treated HeLa cells with genistein (caveolae-mediated endocytosis inhibitor), chlorpromazine (clathrin-mediated

endocytosis inhibitor) and amiloride (macropinocytosis inhibitor)[44, 45] for 30 min followed by exposure of fluorescence isothiocyanate labeled FITC-OA-NPs. We have chemically conjugated FITC with ethylenediamine modified oleic acid (**5**) to obtain FITC-oleic acid conjugate (**6**) (Fig. 15) and characterized them by ^{1}H, ^{13}C NMR spectroscopy and MALDI-TOF.

Treatment Time		1 h	3 h	6 h
Image Channels		C2 (green) C3 (red)	C2 (green) C3 (red)	C2 (green) C3 (red)
Pearsons' Correlation Coefficient	r	0.793	0.698	0.675
Manders Coefficients	M1 (fraction of C2 overlapping C3)	0.6050	0.6408	0.8490
	M2 (fraction of C3 overlapping C2)	0.7705	0.7496	0.8472
Percent volume colocalized		39.12	42.57	62.39

Table 2. Quantification of colocalization of OA-Rho-NPs into lysosomal compartments in 1 h, 3 h and 6 h time points determined by CLSM

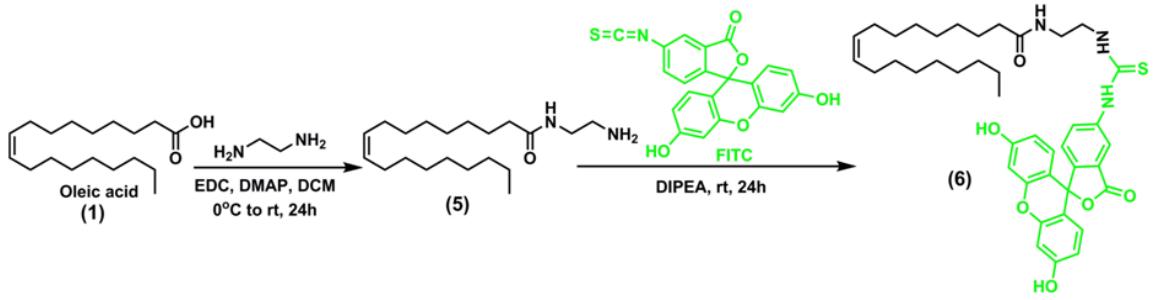

Fig. 15 Synthetic scheme of oleic acid-FITC conjugate.

We have engineered FITC-OA-NPs by blending conjugate **2**, **4**, **6** and DSPE-PEG in 1:1:0.4:0.2 weight ratios. FITC-OA-NPs were characterized by DLS and FESEM showing 173.1 ± 3 nm in diameter with spherical in shape (Fig. 13c, d). We incubated endocytosis inhibitor treated HeLa cells with FITC-OA-NPs for 1 h followed by staining lysosomes by LysoTracker DND-99 (red) dye and nucleus with DAPI (blue). The cells were then imaged by CLSM. Fig. 16 confirmed that amiloride treated cells have highly reduced internalization

of FITC-OA-NPs, in contract to genistein and chlorpromazine treated cells compared to the non-inhibitor treated control cells. Further colocalization quantification from the CLSM showed that amiloride treated cells exhibited only 17.9 % volume colocalization compared to 79.7 %, 73.9 % and 84.4 % volume colocalization for genistein, chlorpromazine treated cells and non-inhibitor treated control cells respectively (Table 3).

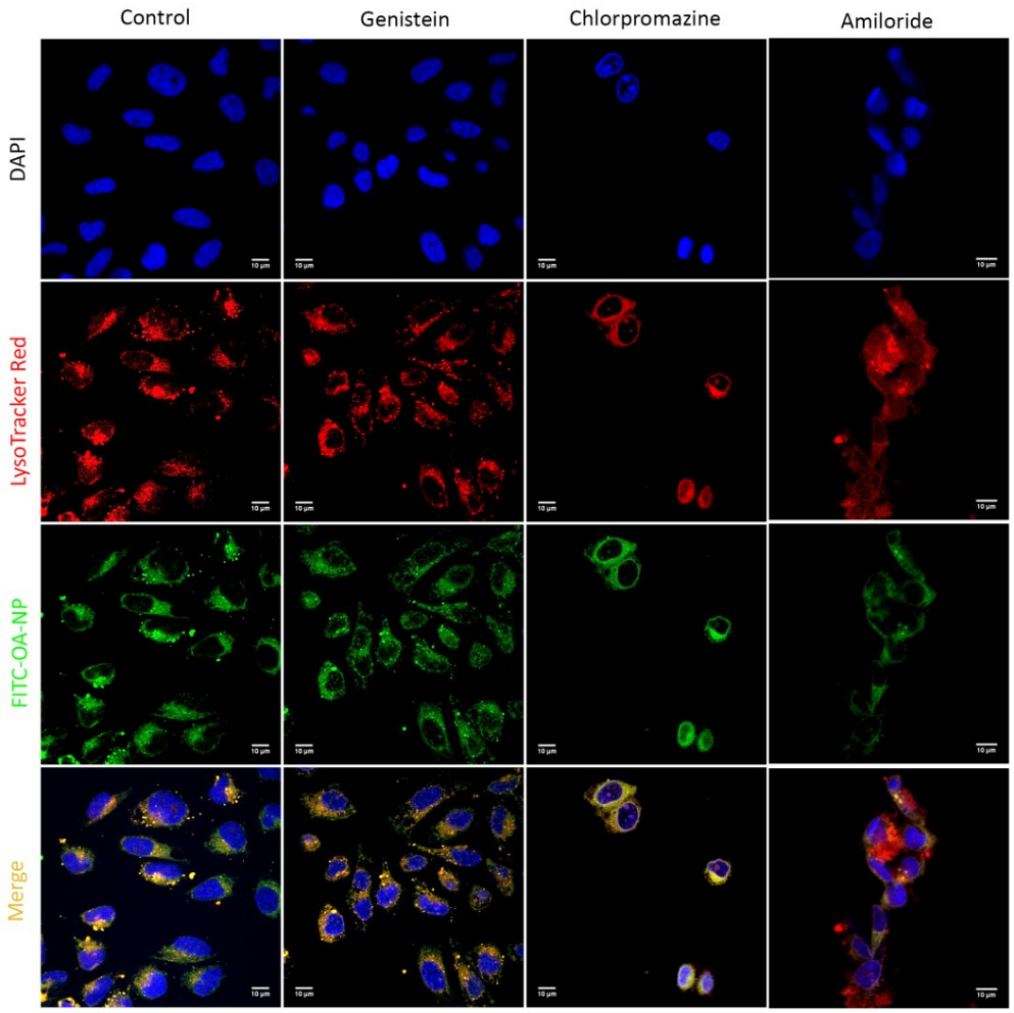

Fig. 16 Cellular internalization of FITC-OA-NPs after 1 h into pre-treated HeLa cells with different endocytosis inhibitors for 30 min. Nuclei and lysosomes were stained with DAPI (blue) and LysoTracker DND-99 (red) respectively. Merged images show the co-localization of FITC-OA-NPs into lysosomes to generate yellow color. Scale bar = 10 µm.

To evaluate the energy dependence of the cellular internalization, we treated HeLa cells with FITC-OA-NPs at 37 °C and 4 °C. The CLSM images in Fig. 17 and colocalization quantification in Table 3 clearly demonstrated the reduction of cellular internalization of

Treatment		Control	Genistein	Chlorpromazine	Amiloride	4°C
Image Channels		C2 (green) C3 (red)	C2 (green) C3 (red)	C2 (green) C3 (red)	C2 (green) C3 (red)	C2 (green) C3 (red)
Pearsons' Correlation Coefficient	r	0.954	0.9747	0.969	0.97	0.952
Manders Coefficients	M1 (fraction of C2 overlapping C3)	0.9534	0.9959	0.9827	0.8454	0.8232
	M2 (fraction of C3 overlapping C2)	0.9838	0.9598	0.9467	0.437	0.9078
Percent volume colocalized		84.36	79.74	73.95	17.90	50.19

Table 3. Quantification of co-localization of FITC-OA-NPs into lysosomes after treatment with endocytosis inhibitors and at 4°C temperature determined by CLSM.

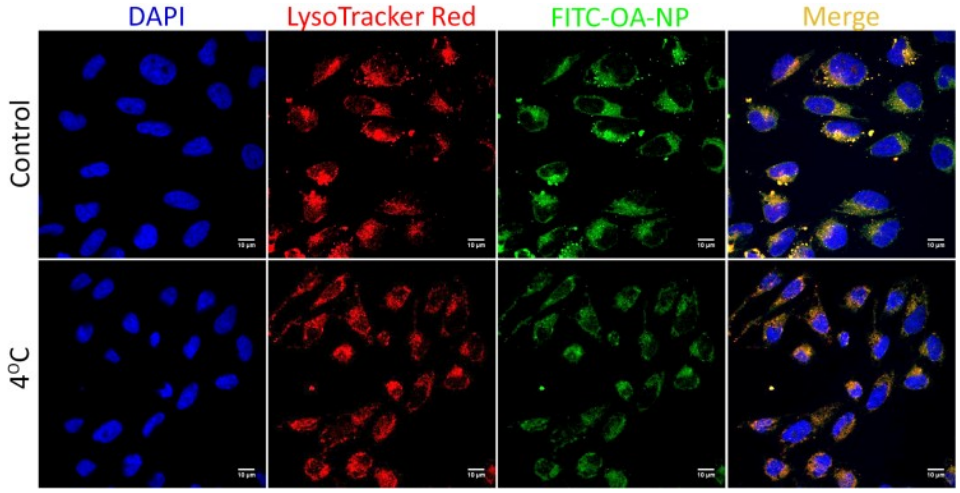

Fig. 17 Cellular internalization of FITC-OA-NPs into HeLa cells at 37°C and 4°C temperatures. Nuclei and lysosomes were stained with DAPI (blue) and LysoTracker DND-99 (red) respectively. Merged images show the co-localization of FITC-OA-NPs into lysosomes to generate yellow color. Scale bar = 10 µm.

FITC-OA-NPs at 4 °C (50.2 % volume colocalization) compared to the cellular internalization at 37 °C (84.4 % volume colocalization). From these CLSM images and

quantification, it was apparent that the OA-NPs endocytosed into the acidic lysosomes in a time and temperature dependent manner through macropinocytosis.

4a.2.8 Mechanism of action: After temporal internalization into the acidic lysosomal compartments, the OA-NPs would release MEK inhibitor AZD6244 and DNA damaging agent cisplatin (Fig. 1b). Consequently, the downstream phosphorylation of ERK should be inhibited by AZD6244. Furthermore, as after effect of DNA damage in nucleus, the cancer cells trigger DNA damage repair mechanism through upregulation of poly (ADP-ribose) polymerase (PARP) family of proteins.[46]

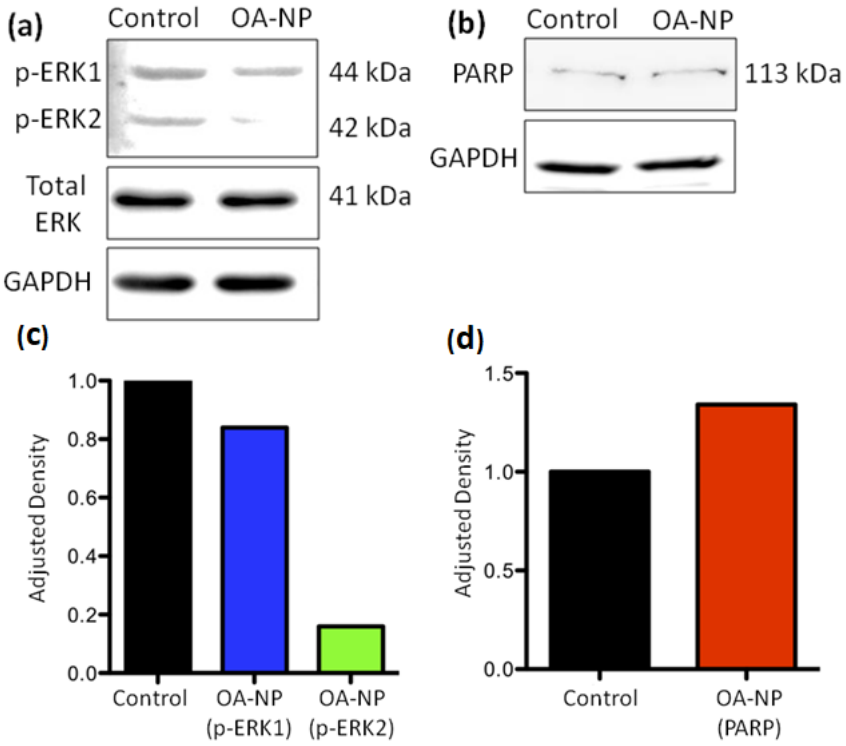

Fig. 18 Mechanism of action of OA-NPs in HeLa cells determined by Western Blot analysis of (a) p-ERK1, p-ERK2 and total ERK as MAPK markers and (b) PARP as DNA damage repair marker after 24 h post incubation.

As a result, PARP has emerged as one of the markers for DNA damage.[47] Hence, to understand the mechanism of action, we treated the HeLa cells with OA-NPs at 1.65 µM concentration for 24 h and evaluated the expression of phospho-ERK and PARP by western blot analysis. The western blot images (Fig. 18a, b) showed that the expression of phospho-ERK1 and phospho-ERK2 was reduced and expression of PARP was increased compared to

the non-treated control cells. From the western blot analysis we quantified the expression of proteins which clearly demonstrated that p-ERK1 and p-ERK2 expression was reduced 1.3 folds and 6.3 folds respectively by the treatment of OA-NPs (Fig. 18 c, d). On the other hand, PARP expression was 1.3 folds increased as effect of OA-NPs treatment compared to no-treatment control cells. This western blot analysis clearly demonstrated that OA-NPs inhibited MAPK pathway by shutting down the phosphorylation of ERK as well as damaged DNA to trigger PARP as DNA damage repair machinery.

4a.3 Conclusions

In conclusion, for the first time, we have successfully developed self-assembled nanoparticles from nontoxic, biodegradable oleic acid, which can simultaneously contain MAPK inhibitor (AZD6244) and DNA damaging drug (cisplatin) in the same particle. These self-assembled oleic acid nanoparticles (OA-NPs) showed extremely high stability at 4 °C for 2 months and at 37 °C in blood circulation mimic for 6 days. Much increased amount of dual drugs were released from these OA-NPs in a slow and sustained manner over 4 days at pH = 5.5 compared to physiological pH. These OA-NPs were endocytosed into the acidic lysosomal compartments in a time and temperature dependent manner through macropinocytosis into HeLa cells and showed their cytotoxicity in cervical cancer, triple negative breast cancer, cisplatin-sensitive and cisplatin resistant hepatocellular cancer cells. Moreover, OA-NPs inhibited MAPK signaling and damaged DNA to induce apoptosis in cervical cancer cells.

4a.4 Experimental Section

4a.4.1 Materials: All the reagents and solvents related to synthesis and characterization of drug conjugates and nanoparticles were purchased from Sigma-Aldrich. AZD6244 was purchased from Selleck Chemicals. DSPE-PEG was bought from Avanti Polar Lipids Inc. DMEM high glucose medium, LysoTracker^{TM} Green DND-26, LysoTracker® Red DND-99 and SlowFade® gold antifade reagents were purchased from Life Technlogies. HeLa, MDA-MB-231 and Hep3B cells were obtained from National Centre for Cell Science (NCCS), Pune. Anti-PARP-1 (p116/p25) rabbit monoclonal antibody, Anti-phospho-Erk1/2 (Thr202/Tyr204, Thr185/Tyr187) recombinant clone AW39R rabbit monoclonal antibody, Anti-MAP kinase 2/Erk2 clone 1B3B9 antibody, anti-GAPDH antibody and Immobilon

western chemiluminescent HRP substrate were obtained from Merck Millipore. FITC Annexin V Apoptosis Detection Kit with PI was obtained from BioLegend.

4a.4.2 Synthesis of oleic acid-AZD6244 conjugate (2): 10 µL of oleic acid (9 mg, 0.031 mmol) was dissolved in dry DCM (3 mL) in a round bottom flask followed by addition of DMAP (3.8 mg, 0.031 mmol), EDC (17.8 mg, 0.093 mmol) and stirred for 10 min. To this solution AZD6244 (14.2 mg, 0.031 mmol) was added and stirred for 24 h at room temperature. Reaction was quenched with 0.1 N HCl solution and diluted with 5 mL DCM. The organic layer was washed with water (2 X 10 mL). The collected organic solution was dried over anhydrous Na_2SO_4, filtered and was removed under reduced pressure. The crude product was purified by silica gel flash chromatography with 1.5 % methanol in DCM to afford the desired product as colorless solid (17.8 mg): Yield 77.4%.

^{1}H NMR: (400 MHz, Chloroform-d): δ = 9.09 (s, 1H), 8.28 (s, 1H), 7.98 (s, 1H), 7.96 (s, 1H), 7.49 (d, J = 2.2 Hz, 1H), 7.16 (dd, J = 8.8, 2.2 Hz, 1H), 6.51 (dd, J = 8.7, 6.6 Hz, 1H), 5.40 – 5.25 (m, J = 5.6 Hz, 2H), 4.58 (dd, J = 5.3, 3.3 Hz, 2H), 4.23 (s, 1H), 3.91 (s, 3H), 2.12 (s, 1H), 2.03 – 1.93 (m, 4H), 1.63 (d, J = 6.7 Hz, 4H), 1.38 – 1.17 (m, J = 13.4 Hz, 23H), 0.87 (t, J = 6.8 Hz, 3H) (Fig. 19).

^{13}C NMR: (101 MHz, Chloroform-d): δ = 172.04, 167.50, 147.68, 139.92, 132.00, 130.55, 130.51, 130.13, 125.25, 125.15, 122.76, 118.01, 116.59, 116.53, 111.72, 109.78, 77.16, 74.18, 62.62, 33.85, 32.36, 32.13, 30.22, 30.16, 29.98, 29.78, 29.68, 29.57, 27.69, 27.62, 25.76, 23.15, 14.59, (Fig. 20).

^{19}F NMR: δ = -129.07, (Fig. 25).

HR-MS: $[M + H]^+$ calculated for $C_{35}H_{47}BrClFN_4O_4$ = 721.2578; found = 721.2524, (Fig. 21).

4a.4.3 Synthesis of oleic acid-cisplatin conjugate (4): 5.5 µL oleic acid (5 mg, 0.017 mmol) was dissolved in 1 mL dimethylformamide (DMF) and aquated cisplatin (3) (932 µL, 4.66 mg, 0.017 mmol) was added into it. The reaction mixture was stirred for 24 h. After 24 h solvent was evaporated by rotary evaporator and the crude product was used for nanoparticle synthesis without further purification. Yield: 6.7 mg (74.3%).

^{1}H NMR: (400 MHz, DMSO-d_6): δ = 5.37–5.26 (m, 2H), 4.65 (s, 2H), 2.16 (t, J = 7.4 Hz, 2H), 1.97 (dd, J = 11.7, 6.1 Hz, 4H), 1.53 – 1.41 (m, 2H), 1.34 – 1.17 (m, 21H), 0.85 (t, J = 6.8 Hz, 3H), (Fig. 22). **^{13}C NMR:** (101 MHz, DMSO-d_6): δ = 174.41, 129.57, 129.54, 33.73, 31.22, 29.04, 28.77, 28.62, 28.52, 28.44, 26.52, 24.49, 22.02, 13.85, (Fig. 23).

^{195}Pt NMR: δ = -3140. 65, (Fig. 26).

HRMS: $[M + H]^+$ calculated for $C_{18}H_{39}N_2O_2Pt$ = 510.27; found = 510.26, (Fig. 24).

4a.4.4 Synthesis of oleic acid-ethylenediamine conjugate (5): Oleic acid (55 µL, 0.177 mmol) was dissolved in dry DCM (3 mL) in a round bottom flask followed by addition of HBTU (114 mg, 0.301 mmol), DIPEA (20 µL, 0.117 mmol) and stirred for 10 min under argon atmosphere. This mixture was added drop wise to the solution of DCM containing ethylene diamine (118 µL, 1.77 mmol) and stirred for 24 h at 0 °C to room temperature. Reaction was quenched with 0.1N HCL solution and diluted with 20 mL DCM. The crude product was purified by silica gel flash chromatography with 4 % methanol in DCM to afford the desired product as colorless solid (41.8 mg): Yield 73%.

^{1}H NMR: (400 MHz, MeOH-d_4): δ = 5.37 – 5.28 (m, 2H), 3.37 (t, J = 6.1 Hz, 2H), 2.94 (t, J = 6.1 Hz, 1H), 2.25 – 2.14 (m, 2H), 2.02 (s, 4H), 1.61 (s, 2H), 1.30 (d, J = 17.2 Hz, 22H), 0.88 (t, J = 6.6 Hz, 3H), (Fig. 27). **^{13}C NMR:** (101 MHz, MeOH-d_4): δ = 176.00, 129.56, 129.39, 39.96, 38.31, 35.72, 31.66, 29.46, 29.22, 29.04, 29.00, 28.97, 28.86, 26.81, 25.42, 22.35, 13.20, (Fig. 28).

MALDI-TOF: $[M + Na]^+$ calculated for $C_{20}H_{40}N_2ONa$ = 347.54; found = 347.30, (Fig. 29).

4a.4.5 Synthesis of oleic acid-FITC conjugate (6): Oleic acid-ethylenediamine conjugate (5) (3 mg, 0.0092 mmol) and fluorescein isothiocyanate (FITC) (7 mg, 0.018 mmol) were dissolved in dry DCM in a round bottom flask followed by addition of DIPEA (1.5 µL, 0.00982 mmol) and stirred for 24 h at room temperature. Reaction was quenched with 0.1 N HCL solution and diluted with 15 mL DCM. The collected organic solution was dried over anhydrous Na_2SO_4, filtered and was removed under reduced pressure. The crude product was purified by silica gel flash chromatography with 7 % methanol in DCM to afford the desired product (4 mg): Yield 60%.

^{1}H NMR: (600 MHz, MeOH-d_4):δ = 7.84 (s, 1H), 7.65 (s, 1H), 7.22 – 7.17 (m, 3H), 6.59 (d, J = 11.2 Hz, 4H), 5.31 (t, 2H), 3.79 (s, 2H), 3.46 (t, J = 5.9 Hz, 2H), 2.20 (t, J = 7.5 Hz, 2H),

1.99 (s, 4H), 1.89 (s, 2H), 1.60 (dt, J = 13.9, 7.1 Hz, 2H), 1.28 (m, 22H), 0.89 (t, J = 7.0 Hz, 3H), (Fig. 30). **^{13}C NMR:** (151 MHz, MeOH-d_4): δ = 191.80, 181.26, 177.71, 175.39, 168.44, 158.33, 132.37, 131.70, 131.64, 131.23, 129.42, 128.61, 128.53, 113.08, 102.77, 78.10, 77.84, 77.66, 43.95, 38.64, 35.80, 31.66, 29.43, 29.41, 29.20, 29.04, 28.97, 28.92, 28.81, 26.71, 25.59, 22.33, 13.06, (Fig. 31).

MALDI-TOF: $[M + H]^+$ calculated for $C_{41}H_{52}N_3O_6S$ = 714.35; found = 714.37, (Fig. 32).

4a.4.6 Synthesis of self-assembled oleic acid nanoparticles (OA-NPs): 1 mg each of oleic acid-AZD6244 conjugate (2) and oleic acid-cisplatin conjugate (4) were dissolved in 0.5 mL of methanol/acetone (1:1) along with 0.2 mg of DSPE-PEG. For OA-FITC-NP synthesis, 0.2 mg of oleic acid-FITC conjugate 6 was mixed with conjugate 2 (1 mg), conjugate 4 (1 mg) and DSPE-EPG (0.2 mg). This solution was added dropwise to 2 mL of distilled water under continuous stirring. The nanoparticle solution was stirred for 4 h for the complete evaporation of organic solvents. The OA-NPs or FITC-OA-NPs were isolated by ultracentrifugation at a speed of 60,000g for 30 min at room temperature. After removing the supernatant the OA-NPs (or FITC-OA-NPs) were re-suspended in 1 mL of distilled water and stored at 4 °C for further usage.

4a.4.7 Determination of critical aggregation concentration (CAC): To determine the CAC value of OA-NPs, pyrene was used as the fluorescence probe. 48.4 µL of pyrene solution (2.5×10^{-5} mol L^{-1}) in acetone was added into 10 different vials followed by adding 1:1 mixture of conjugates 2 and 4 with 10 different concentrations. After evaporation of the solvent 2 mL of de-ionized water was added while the concentration of pyrene in each vial was kept at 6×10^{-7} mol L^{-1}. These solutions were further sonicated for 10 min. The fluorescence emission spectra of all samples were recorded on a LS-50B luminescence spectrometer (Perkin Elmer Co.) at 337 nm excitation wavelength and 4 nm slit width. The I_3/I_1 values of all solution were recorded and plotted against concentration.

4a.4.8 Determination of size, shape and morphology: The size, shape and morphology of the OA-NPs were determined by DLS, FESEM and AFM. DLS was measured using Zetasizer Nano2590 (Malvern, UK). The sample preparation for DLS, FESEM and AFM was done following the procedure described in section 2.4.4, 2.4.5, and 2.4.6 in chapter 2.

4a.4.9 Stability: The stability of the OA-NPs was checked at 37 °C in DMEM media and at 4 °C in water by DLS method using Zetasizer Nano2590 (Malvern, UK) by following the procedure described in section 3.4.8 in chapter 3.

4a.4.10 Quantification of drug loading: A calibration curve was plotted in the concentration range of 2.5 to 15 µM (for cisplatin), and 5 µM to 30 µM for AZD6244, by diluting the 1 mM standard stock solution of drugs in DMSO. The absorbance was measured at 706 nm for cisplatin and 273 nm for AZD6244 against the corresponding solvent blank. The linearity was plotted for absorbance (A) against concentration (C). To find out the drug loading in OA-NPs, they were dissolved in spectroscopic grade DMSO in 2.5 %, 5 % and 7.5 % dilutions. Absorbance was measured at characteristic wavelength against the corresponding solvent blank in 200 µL quartz cuvette and from the calibration curve drug loading was measured. Quantification of cisplatin was done using colorimetric method described in section 2.4.3 in chapter 2. For drug loading in OA-NPs, prepared OA-NPs (5 µL, 10 µL, and 15 µL) were dissolved in 200 µL o-phenylenediamine (1.2 mg /mL of spectroscopic grade DMF). Then it was heated at 100 °C for 4 h until greenish yellow color appears. Absorbance was measured at characteristic wavelength against the corresponding solvent blank in 200 µL quartz cuvette and from the calibration curve drug loading was measured in triplicate.

4a.4.11 Determination of drug release: 250 µL drug loaded OA-NPs were suspended in 250 µL of each two different pH solutions (pH = 5.5 and pH = 7.4) and sealed in a dialysis membrane (MWCO = 1000 Dalton). These dialysis bags were incubated in their respective 10 mL of pH solutions separately at room temperature with gentle shaking. 400 µL portion of the aliquot was collected from the incubation medium at predetermined time intervals and the released dual drugs were quantified by UV-Vis spectrophotometer by using concentration versus absorbance calibration graph.

4a.4.12 Cell viability: Cell viability assay of OA-NPs using MTT reagents in HeLa, Hep3B, Hep3B-R and MDA-MB-231 cells was performed by following the methods described in section 3.4.11 in chapter 3.

4a.4.13 Cellular internalization: Confocal laser scanning microscopy (CLSM) to evaluate the cellular internalization of rhodamine encapsulated OA-Rho-NPs in a time dependent manner was performed using the methods described in section 3.4.13 in chapter 3.

4a.4.14 Cellular internalization mechanism: 5 x 10^4 HeLa cells were seeded on 20 mm coverslips in a 6 well plate, containing DMEM GlutaMAX™ (Gibco®, Thermo Fisher Scientific) supplemented with 10 % FBS (HiMedia) and incubated overnight in a 5 % CO_2 at 37 °C. Cells were then treated with various endocytosis inhibitors (Amiloride 100 µM, Genistein 37 µM and Chlorpromazine 30 µM) for 30 min at 37 °C. Control cells were incubated at 37°C without any treatment of inhibitor. To inhibit energy dependent movement across the cell membrane, one group of cells were incubated at 4 °C for 30 min. After the inhibitor treatment, cells were washed thrice with PBS and then treated with FITC-OA-NPs (at a concentration corresponding to 2 µg mL^{-1} of the FITC) for 1 h at 37 °C. Cells were washed thrice with PBS, fixed and stained for LysoTracker Red (1 µM) and DAPI. Cover slips were then mounted on glass slide and were imaged.

4a.4.15 Apoptosis detection: 5 x 10^4 HeLa cells were seeded on a cover slip in a 6 well plate and incubated overnight in a 5 % CO_2 incubator at 37 °C for attachment. Cells were then treated with OA-NPs at a concentration corresponding to the IC_{50} concentration for 24 h. Cells were washed thrice with PBS followed by addition of 500 µL Annexin V binding buffer. Then, 5 µL FITC Annexin V and 10 µL propidium iodide (PI) solution (FITC Annexin V Apoptosis Detection Kit with PI from BioLegend) was added and incubated at 25 °C in dark for 15 min. Again, cells were washed three times with PBS and fixed with paraformaldehyde for 10 min at 4 °C. Then, cells were washed thrice with PBS and mounted on a glass slide using 5 µL SlowFade® gold antifade reagents. The slides were subjected to fluorescence imaging using CLSM. FITC and PI intensities were calculated using ImageJ software and compared with the untreated control.

4a.4.16: Detection of apoptosis by fluorescence activated cell sorting (FACS): Detection and quantification of apoptosis by FACS was performed by the method described in section 3.4.12 in chapter 3.

4.4.17 Western blot analysis: After 24 hours treatment with OA-NPs at IC_{50} concentration, HeLa cells were lysed and suspended in sample buffer. Proteins were visualized in SDS-polyacrylamide gel electrophoresis (SDS-PAGE) using primary antibody solution (PARP, pERK and ERK2 in 1:1000 dilution and GAPDH in 1:5000 dilution) and then incubated in HRP conjugated secondary antibody solution (1:10000 dilution) using the protocol described in section 3.4.14 in chapter 3.

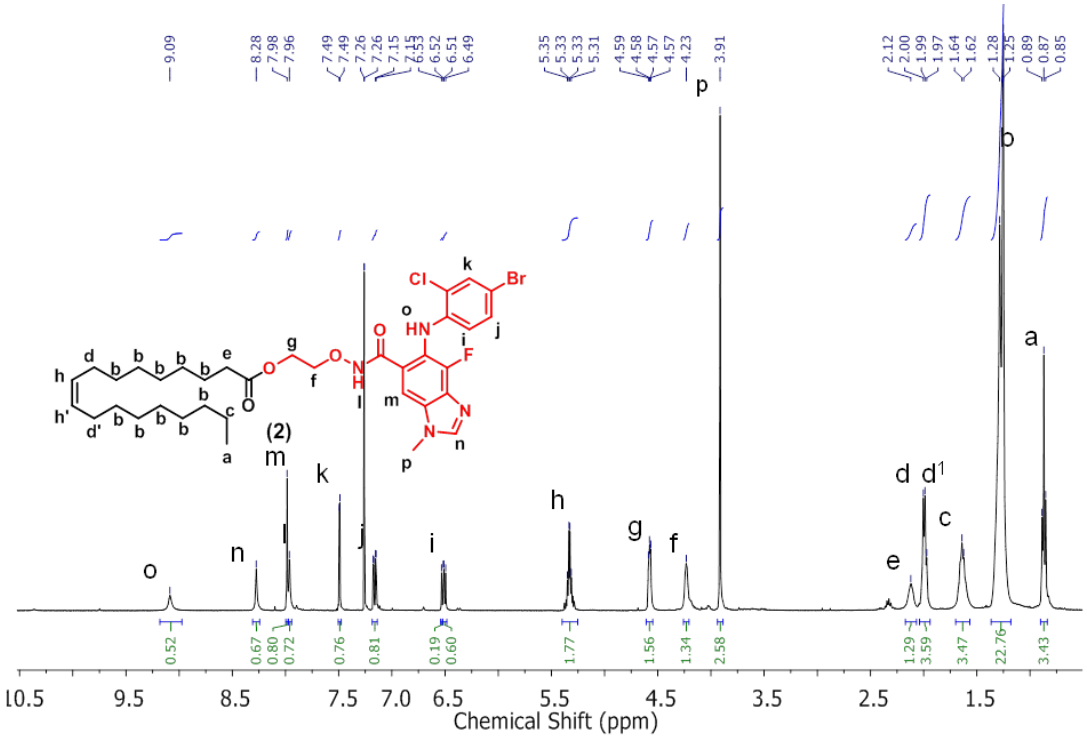

Fig. 19 ^{1}H NMR spectra of oleic acid-AZD6244 conjugate (**2**).

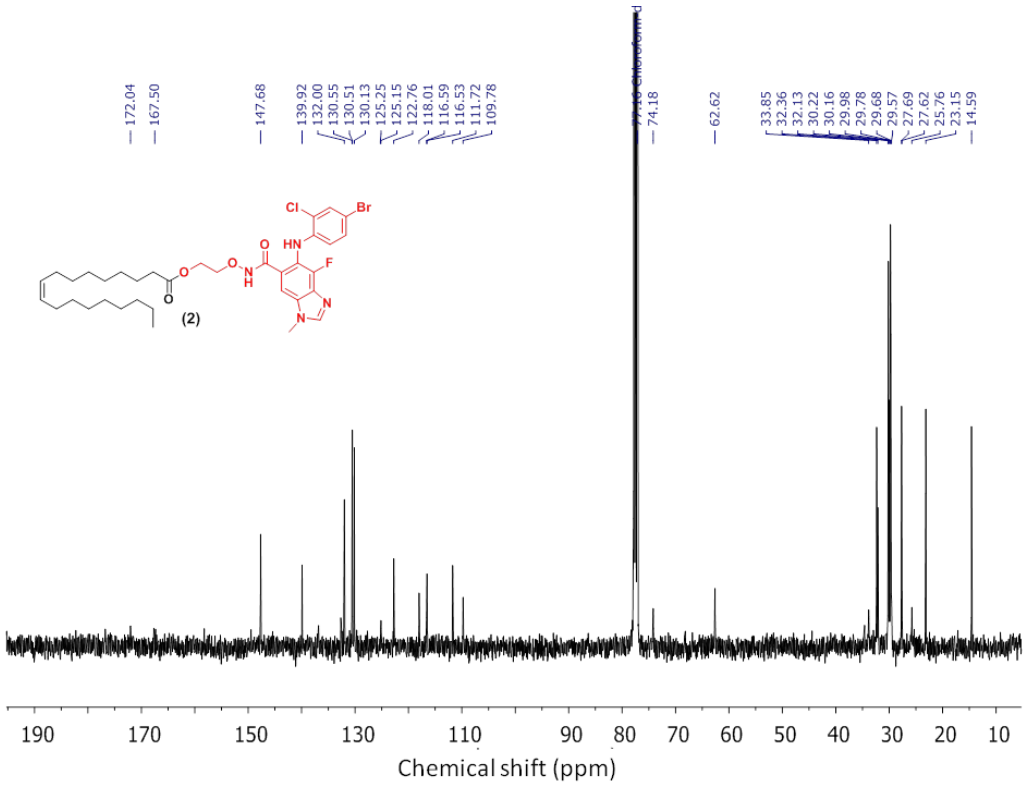

Fig. 20 ^{13}C NMR spectra of oleic acid-AZD6244 conjugate (**2**).

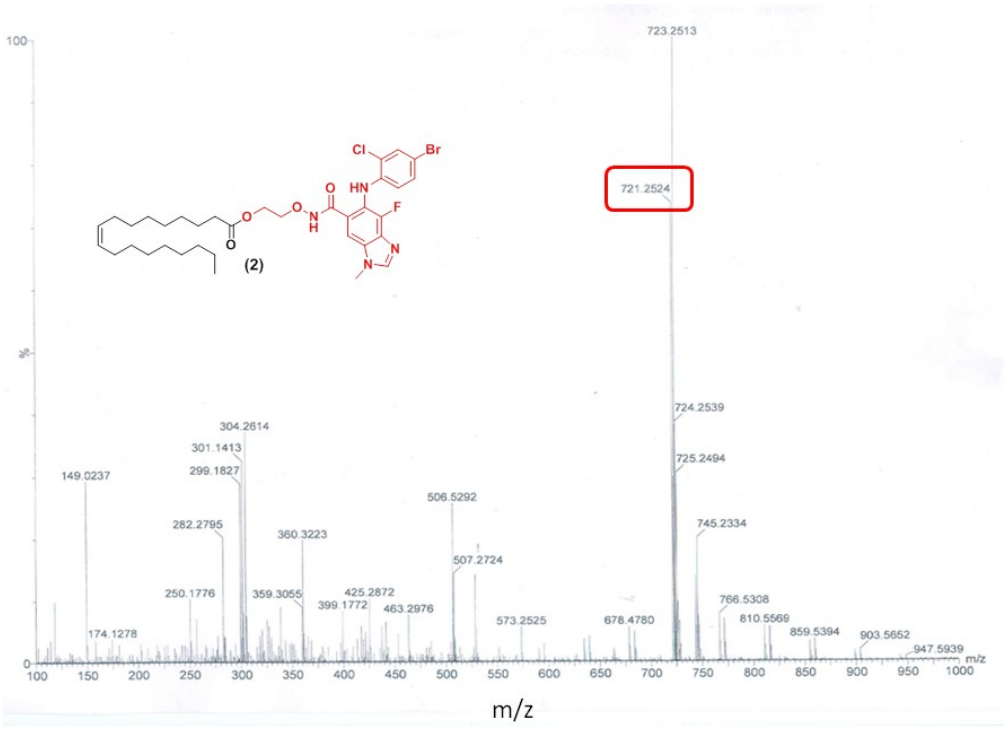

Fig. 21 HR-MS spectra of oleic acid-AZD6244 conjugate (**2**).

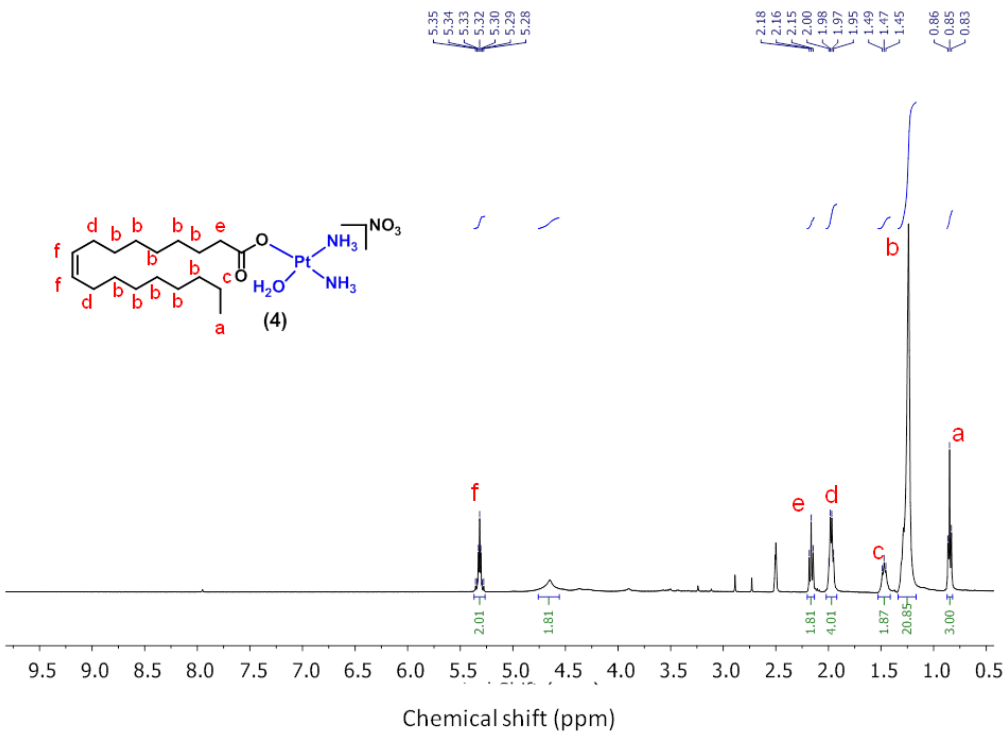

Fig. 22 ^{1}H NMR spectra of oleic acid-cisplatin conjugate (**4**).

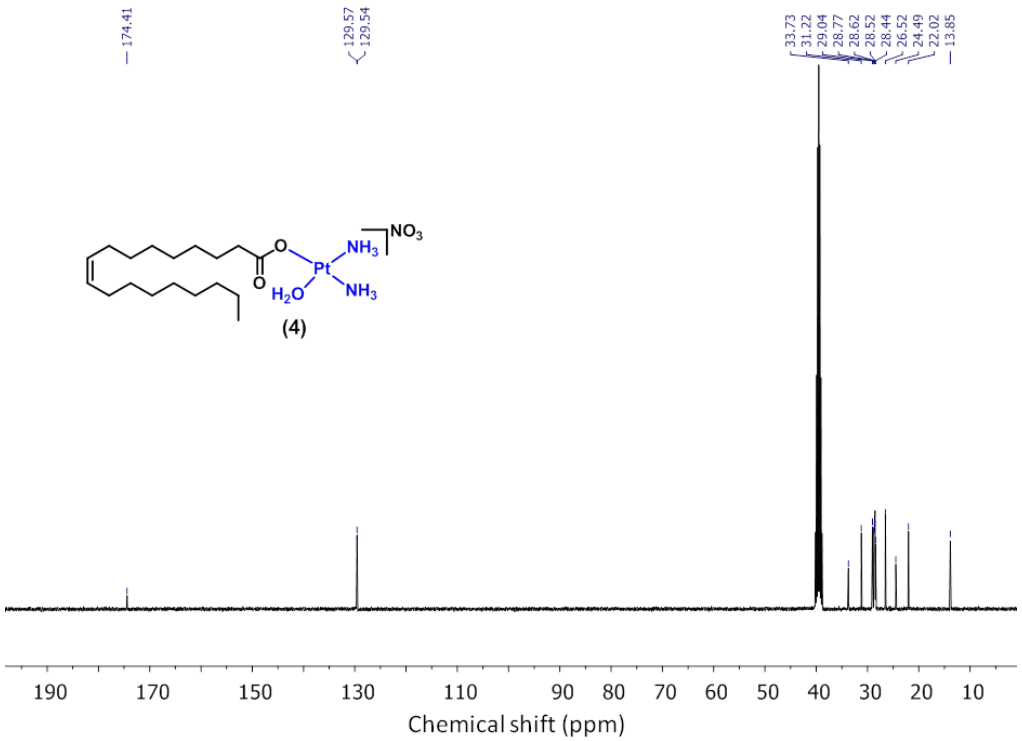

Fig. 23 ^{13}C NMR spectra of oleic acid-cisplatin conjugate (**4**).

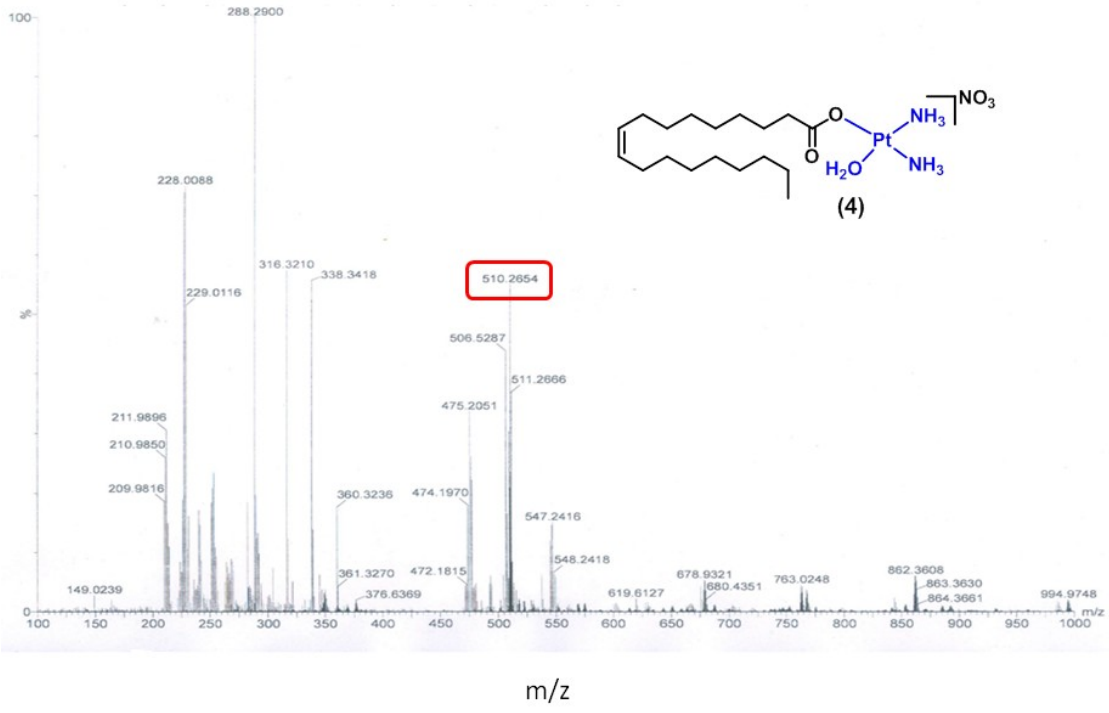

Fig. 24 HR-MS spectra of oleic acid-cisplatin conjugate (**4**).

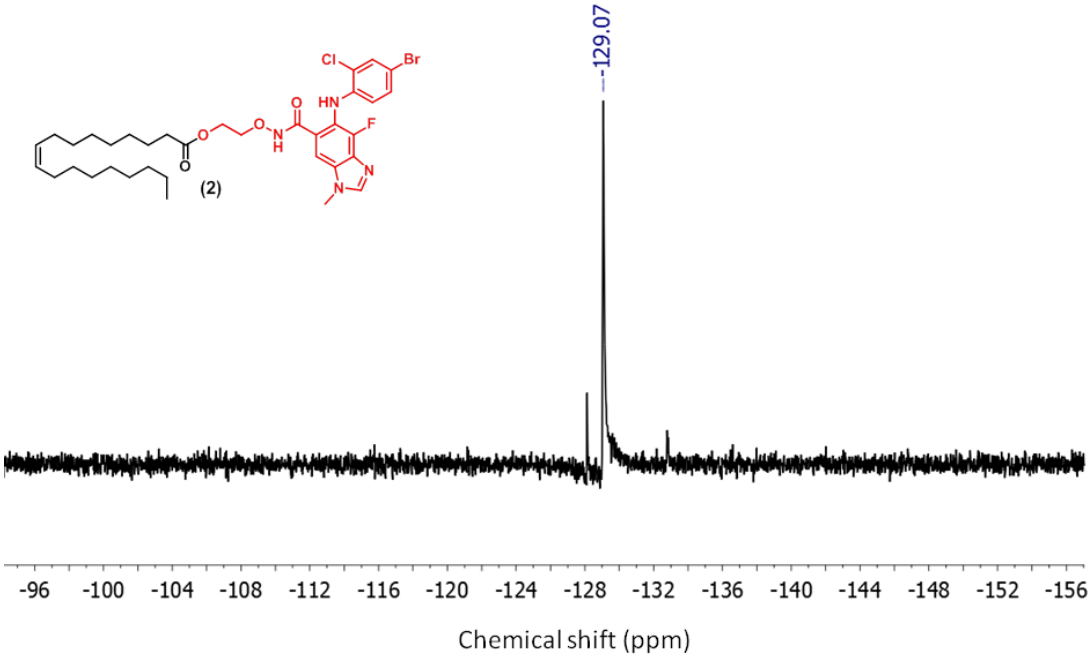

Fig. 25 ^{19}F NMR spectra of oleic acid-AZD6244 conjugate (**2**).

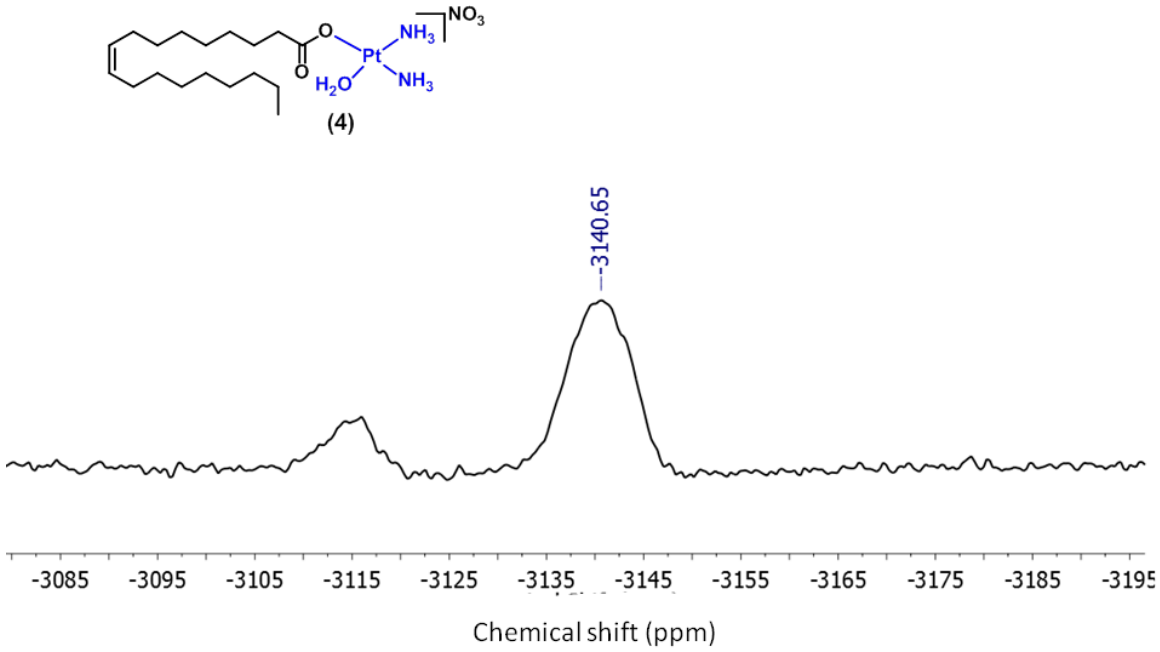

Fig. 26 ^{195}Pt NMR spectra of oleic acid-cisplatin conjugate (**4**).

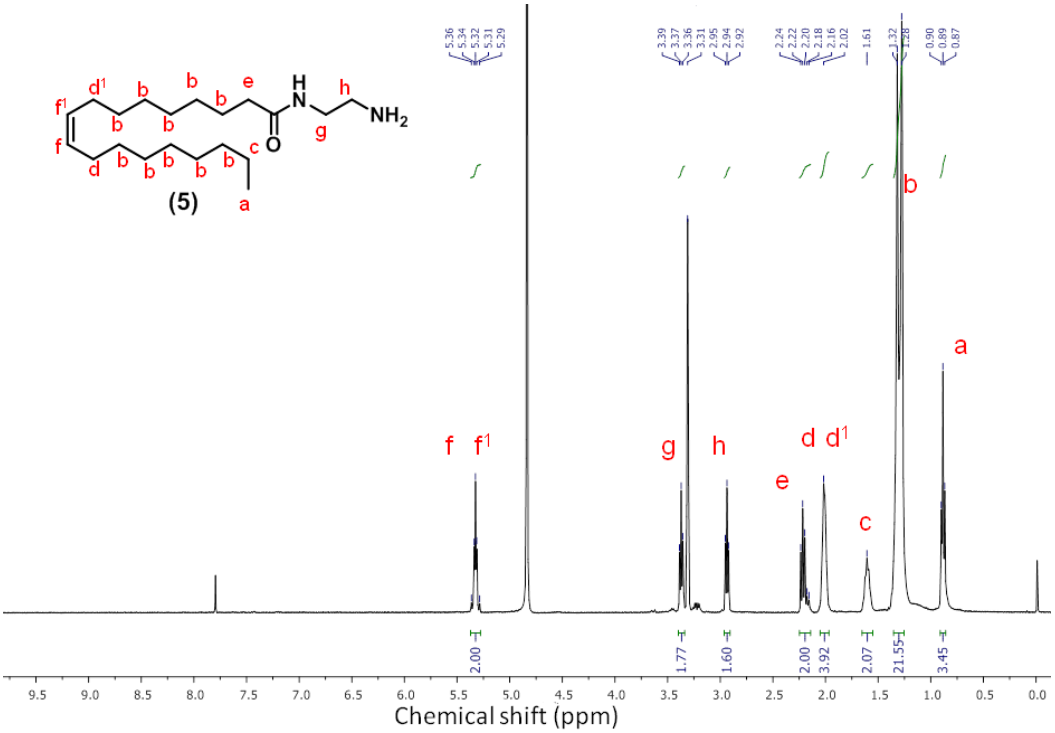

Fig. 27 ^{1}H NMR spectra of oleic acid-ethylenediamine conjugate (**5**).

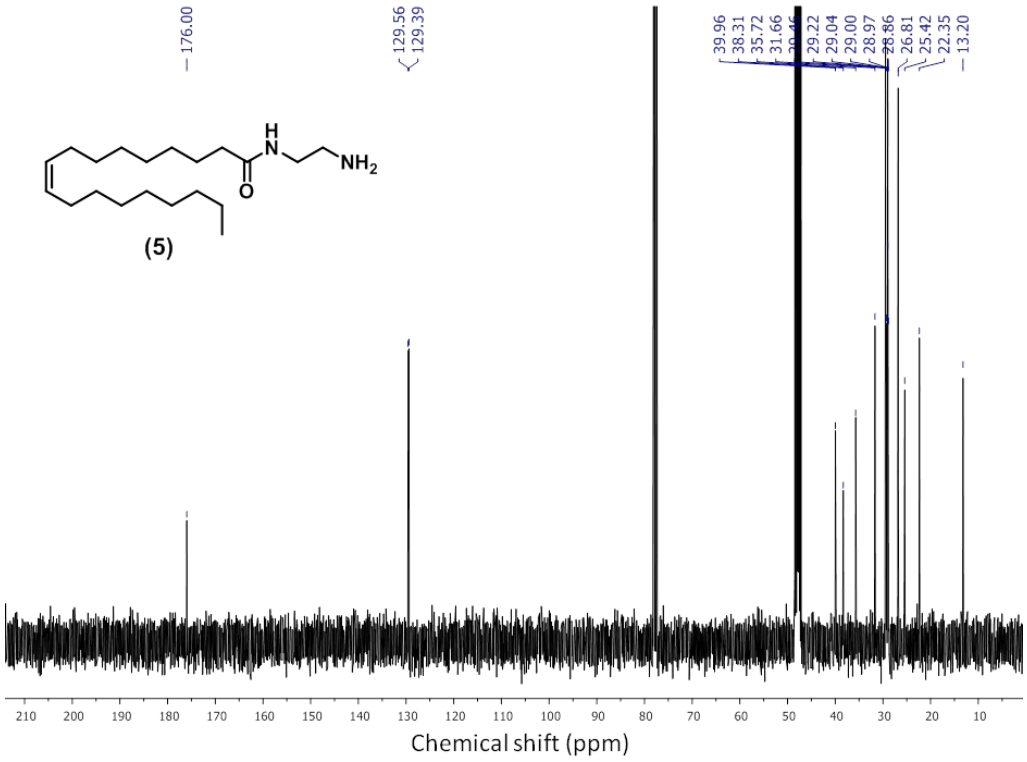

Fig. 28 ^{13}C NMR spectra of oleic acid-ethylenediamine conjugate (**5**).

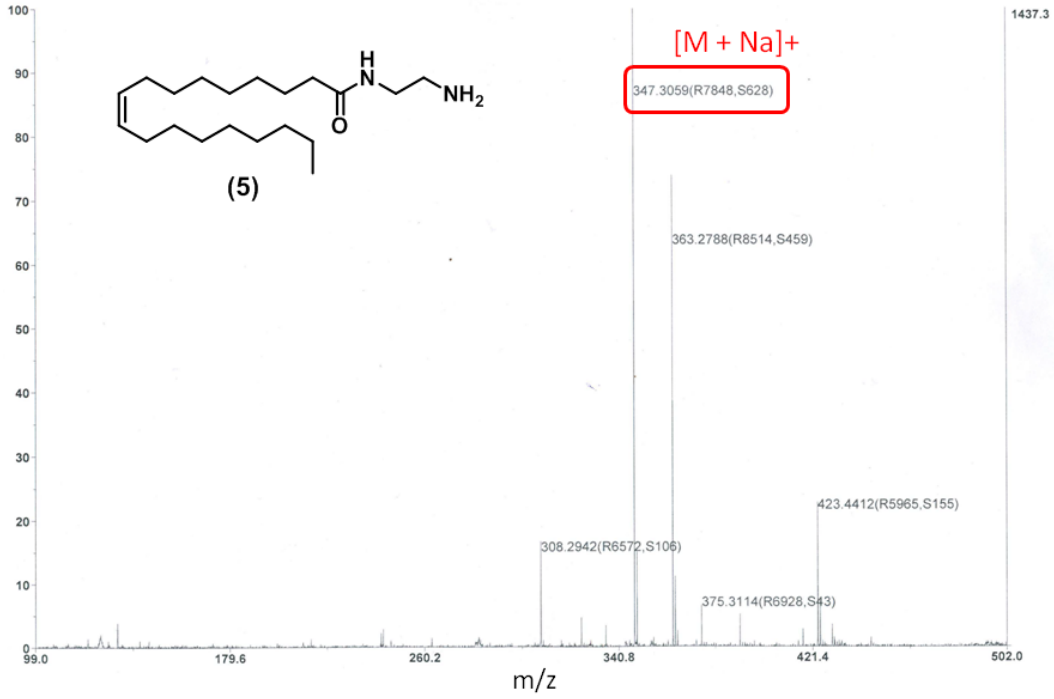

Fig. 29 MALDI-TOF of oleic acid-ethylenediamine conjugate (**5**).

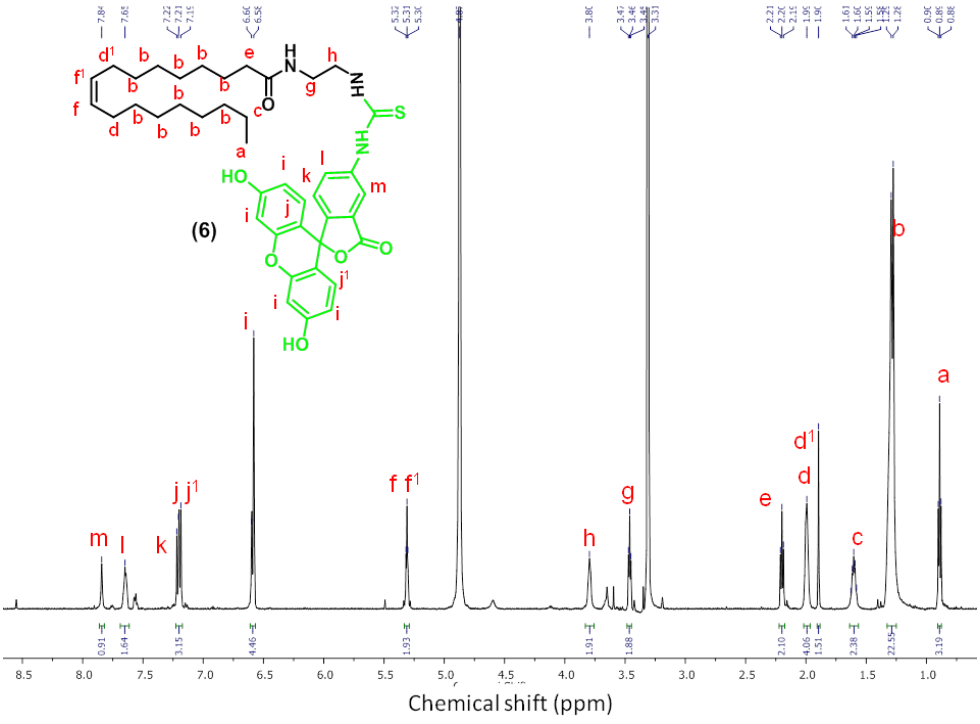

Fig. 30 ^{1}H NMR spectra of oleic acid-FITC conjugate (**6**).

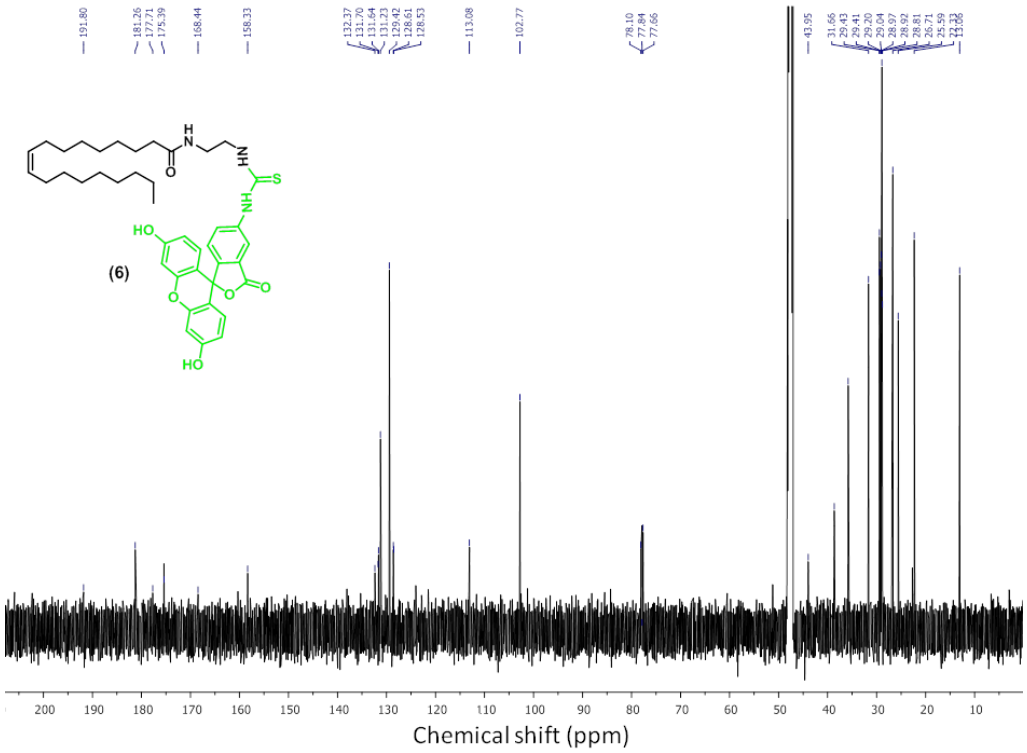

Fig. 31 ^{13}C NMR spectra of oleic acid-FITC conjugate (**6**).

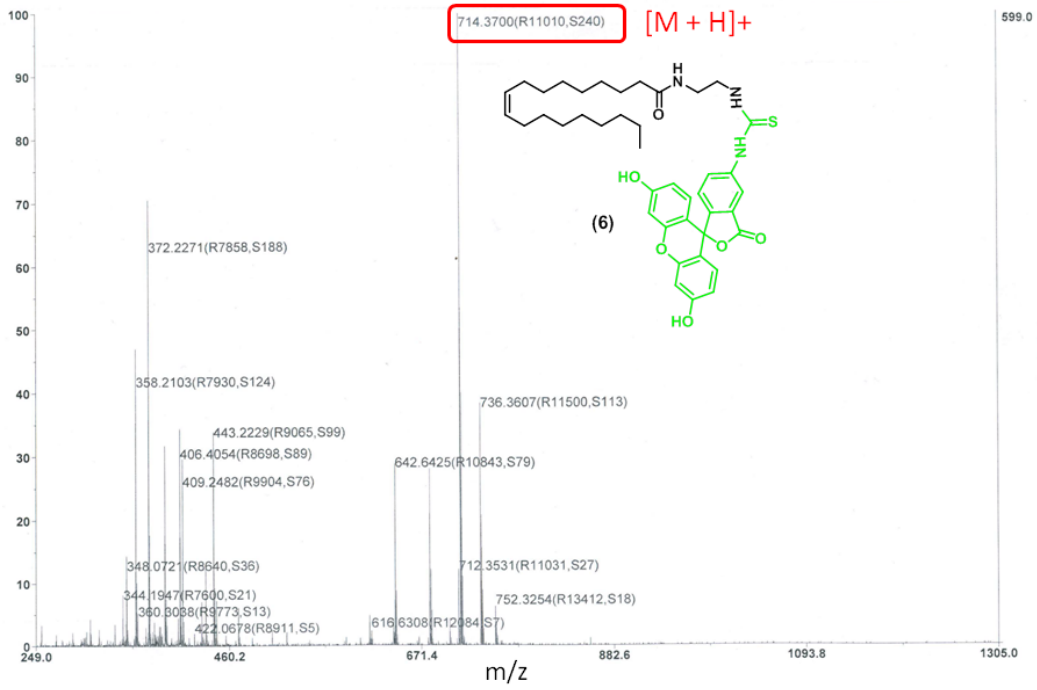

Fig. 32 MALDI-TOF of oleic acid-FITC conjugate (**6**)

4a.5 References

1. D. Peer, J. M. Karp, S. Hong, O. C. Farokhzad, R. Margalit and R. Langer, *Nat. Nanotechnol*, 2007, **2**, 751-760.
2. K. L. Donaldson, G. L. Goolsby and A. F. Wahl, *Int. J. Cancer*, 1994, **57**, 847-855.
3. E. K. Kim and E.-J. Choi, *Biochim. Biophys. Acta, Mol. Basis Dis.* 2010, **1802**, 396-405.
4. J. S. Sebolt-Leopold, R. Herrera, Nat. Rev. *Cancer*, 2004, **4**, 937-947.
5. A. A. Samatar and P. I. Poulikakos, *Nature reviews. Drug Discov.*, 2014, **13**, 928942.
6. U. McDermott and J. Settleman, *Journal of Clinical Oncology*, 2009, **27**, 5650-5659.
7. C. V. Miduturu, X. Deng, N. Kwiatkowski, W. Yang, L. Brault, P. Filippakopoulos, E. Chung, Q. Yang, J. Schwaller and S. Knapp, *Chem. Biol.*, 2011, **18**, 868-879.
8. M. Fabian, W. Biggs, D. Treiber, C. Atteridge, M. Azimioara, M. Benedetti, T. Carter, P. Ciceri, P. Edeen and M. Floyd, *Nat. Biotechnol*, 2005, **23**, 329-336.
9. G. Pagès, S. Guérin, D. Grall, F. Bonino, A. Smith, F. Anjuere, P. Auberger and J. Pouysségur, *Science*, 1999, **286**, 1374-1377.
10. S. Giroux, M. Tremblay, D. Bernard, J. Cardin-Girard, S. Aubry, L. Larouche, S. Rousseau, J. Huot, J. Landry and L. Jeannotte, *Curr. Biol*, 1999, **9**, 369-376.
11. Z. A. Knight, H. Lin and K. M. Shokat, *Nat. Rev. Cancer*, 2010, **10**, 130-137.
12. T. R. Wilson, J. Fridlyand, Y. Yan, E. Penuel, L. Burton, E. Chan, J. Peng, E. Lin, Y. Wang and J. Sosman, *Nature*, 2012, **487**, 505-509.
13. P. Lito, N. Rosen and D. B. Solit, *Nat. Med*, 2013, **19**, 1401-1409.
14. J. S. Duncan, M. C. Whittle, K. Nakamura, A. N. Abell, A. A. Midland, J. S. Zawistowski, N. L. Johnson, D. A. Granger, N. V. Jordan and D. B. Darr, *Cell*, 2012, **149**, 307-321.
15. M. J. Lee, S. Y. Albert, A. K. Gardino, A. M. Heijink, P. K. Sorger, G. MacBeath and M. B. Yaffe, *Cell*, 2012, **149**, 780-794.
16. T. Skorski, *Nat Rev Cancer*, 2002, **2**, 351-360.
17. H. Richly, B. Henning, P. Kupsch, K. Passarge, M. Grubert, R. Hilger, O. Christensen, E. Brendel, B. Schwartz and M. Ludwig, *Ann. Oncol.*, 2006, **17**, 866-873.
18. L. Dal Lago, V. D'Hondt and A. Awada, *Oncologist*, 2008, **13**, 845-858.

19. A. S. Martins, C. Mackintosh, D. H. Martín, M. Campos, T. Hernández, J.-L. Ordóñez and E. de Alava, *Clinic. Cancer Res.*, 2006, **12**, 3532-3540.
20. N. Kolishetti, S. Dhar, P. M. Valencia, L. Q. Lin, R. Karnik, S. J. Lippard, R. Langer and O. C. Farokhzad, *Proc. Natl. Acad. Sci. U.S.A.*, 2010, **107**, 17939-17944.
21. L. Liao, J. Liu, E. C. Dreaden, S. W. Morton, K. E. Shopsowitz, P. T. Hammond and J. A. Johnson, *J. Am. Chem. Soc.*, 2014, **136**, 5896-5899.
22. T. Jiang, R. Mo, A. Bellotti, J. Zhou and Z. Gu, *Adv. Funct. Mater.*, 2014, **24**, 2295-2304.
23. S. Barua and S. Mitragotri, *ACS Nano*, 2013, 7, 9558-9570.
24. T.-M. Sun, J.-Z. Du, Y.-D. Yao, C.-Q. Mao, S. Dou, S.-Y. Huang, P.-Z. Zhang, K. W. Leong, E.-W. Song and J. Wang, *ACS Nano*, 2011, **5**, 1483-1494.
25. D. S. Kohane and R. Langer, *Chem. Sci.*, 2010, **1**, 441-446.
26. S. Monteagudo, F. C. Pérez-Martínez, M. D. Pérez-Carrión, J. Guerra, S. Merino, M. P. Sánchez-Verdú and V. Ceña, *Nanomedicine*, 2012, **7**, 493-506.
27. S. Basu, R. Harfouche, S. Soni, G. Chimote, R. A. Mashelkar and S. Sengupta, *Proc. Natl. Acad. Sci. U.S.A.*, 2009, **106**, 7957-7961.
28. D. Voet, J. Voet in Biochemistry, John Wiley & Sons, Inc, 4th edn, pp. 386-466.
29. M. Bloemen, W. Brullot, T. T. Luong, N. Geukens, A. Gils and T. Verbiest, *J. Nanopart. Res.*, 2012, **14**, 1100-1105.
30. Y. Guo, X. Liu, X. Sun, Q. Zhang, T. Gong and Z. Zhang, *Theranostics*, 2012, **2**, 1104-1114.
31. F. Catalanotti, D. B. Solit, M. P. Pulitzer, M. F. Berger, S. N. Scott, T. Iyriboz, M. E. Lacouture, K. S. Panageas, J. D. Wolchok and R. D. Carvajal, *Clinic. Cancer Res.*, 2013, **19**, 2257-2264.
32. B. R. Davies, A. Logie, J. S. McKay, P. Martin, S. Steele, R. Jenkins, M. Cockerill, S. Cartlidge and P. D. Smith, *Mol. Ther.*, 2007, **6**, 2209-2219.
33. S. V. Holt, A. Logie, R. Odedra, A. Heier, S. Heaton, D. Alferez, B. Davies, R. Wilkinson and P. Smith, *British J. Cancer*, 2012, **106**, 858-866.
34. H. Huynh, P. K. Chow and K.-C. Soo, *Mol. Cancer Ther.*, 2007, **6**, 2468-2476.
35. E. Y. Kim, A. Kim, S. K. Kim and Y. S. Chang, *Cancer Lett.*, 2015, **358**, 85-91.
36. O. Aronov, A. T. Horowitz, A. Gabizon and D. Gibson, *Bioconjug. Chem.*, 2003, **14**, 563-574.
37. J. M. Harris and R. B. Chess, *Nat. Rev. Drug Discov.*, 2003, **2**, 214.

38. G. Kwon, M. Naito, M. Yokoyama, T. Okano, Y. Sakurai and K. Kataoka, *Langmuir*, 1993, **9**, 945-949.
39. P. Sengupta, S. Basu, S. Soni, A. Pandey, B. Roy, M. S. Oh, K. T. Chin, A. S. Paraskar, S. Sarangi and Y. Connor, *Proc. Natl. Acad. Sci. U.S.A.*, 2012, **109**, 11294-11299.
40. J. Gilleron, W. Querbes, A. Zeigerer, A. Borodovsky, G. Marsico, U. Schubert, K. Manygoats, S. Seifert, C. Andree and M. Stöter, *Nat. Biotechnol.*, 2013, **31**, 638-646.
41. A. Mallick, P. More, S. Ghosh, R. Chippalkatti, B. A. Chopade, M. Lahiri and S. Basu, *ACS Appl. Mater. Interfaces*, 2015, **7**, 7584-7598.
42. S. Palvai, J. Nagraj, N. Mapara, R. Chowdhury and S. Basu, *RSC Adv.*, 2014, **4**, 57271-57281.
43. F. Podo, L. Buydens, H. Degani, R. Hilhorst, E. Klipp, I. S. Gribbestad, S. Van Huffel, H. WM van Laarhoven, J. Luts and D. Monleon, *Mol. Oncol.*, 2010, **4**, 209-229.
44. M. Koivusalo, C. Welch, H. Hayashi, C. C. Scott, M. Kim, T. Alexander, N. Touret, K. M. Hahn and S. Grinstein, *J. Cell Biol*, 2010, **188**, 547-63.
45. J. Rejman, A. Bragonzi and M. Conese, *Mol. Ther.*, 2005, **12**, 468-474.
46. A. Ciccia and S. J. Elledge, *Mol. cell*, 2010, **40**, 179-204.
47. N. J. Curtin, *Nat. Rev. Cancer*, 2012, **12**, 801-817.

Chapter 4b

Targeting MAPK Signaling Pathway in Colorectal Cancer Cells by Hyaluronic acid Coated Oleic Acid Nanoparticles

4b.1. Introduction

Colorectal cancer (CRC) remained is the 3rd most major cause of death in the whole world with high mortality and morbidity.[1, 2] Traditional colon cancer treatment using chemotherapeutic drugs (5-fluorouracil, oxaliplatin, irinotecan) leads to unwanted toxic side effects to the patients.[3-5] Hence, targeting specific signaling pathways as oncogenic addiction has emerged as alternative strategy in colon cancer therapy.[6, 7] The growing evidence tells that the early steps of CRC are driven by mutations in *KRAS* and *BRAF* that subsequently lead to constitutive activation of the ERK1/2 signaling cascade. Ras is mutated in about 36% of CRC. In addition to controlling cell proliferation, MAPK pathway is also involved in the processes that are essential for metastasis in several cancers including colorectal cancers. Recently it was found that activation of ERK2 mediates liver metastasis in a xenograft mouse model of CRC.[8] All these evidences clearly indicate the role of MAPK signaling in colon cancer and RAS-RAF-MEK-ERK cascade gained attention as attractive target in colon cancer therapy.[9-12] In chapter 4a we have successfully inhibited MAPK signaling with simultaneous DNA damage in various cancer cell lines including metastatic breast cancer cells and cisplatin resistant Hep3B cell with our dual drug loaded, passively targeted nontoxic oleic acid based nano platform. In this work we mainly focused on inhibiting MAPK signaling specifically in colon cancer cells by using active targeting strategy with the combination regimen of MAPK inhibitors (AZD6244) with DNA damaging agent (cisplatin) for augmented therapeutic outcome.[13-16] To achieve this we have used our previously described oleic acid based nanoplatform.

For active targeting hyaluronic acid gained lots of attention by binding with CD44 receptors over-expressed in cancer cells.[17-19] Despite having immense potential, nanovector mediated active targeting of MAPK signaling in colon cancer remained almost untapped as therapeutic strategy. Motivated by this strategy, in this current work, we have engineered 154 nm sized spherical hyaluronic acid cloaked oleic acid nanoparticle containing simultaneously MAPK inhibitor (AZD6244) and DNA damaging drug (cisplatin) (Scheme 1a). Dual drugs (AZD6244 and cisplatin) were released from these hyaluronic acid coated oleic acid nanoparticles (HA-OA-NPs) slowly over 3 days in acidic milieu. HA-OA-NPs were internalized into colon cancer cells (HCT-116) by CD44 receptor and clathrin mediated endocytosis followed by localization into lysosomes temporally (Scheme 1b). Remarkable

colon cancer cell (HCT-116 and DLD-1) death was induced by HA-OA-NPs in contrast to free drug cocktail as well as non-targeted hyaluronic acid having AZD6244 and cisplatin containing oleic acid nanoparticle through synchronized inhibition of MAPK signaling cascade and damaging sub-cellular DNA.

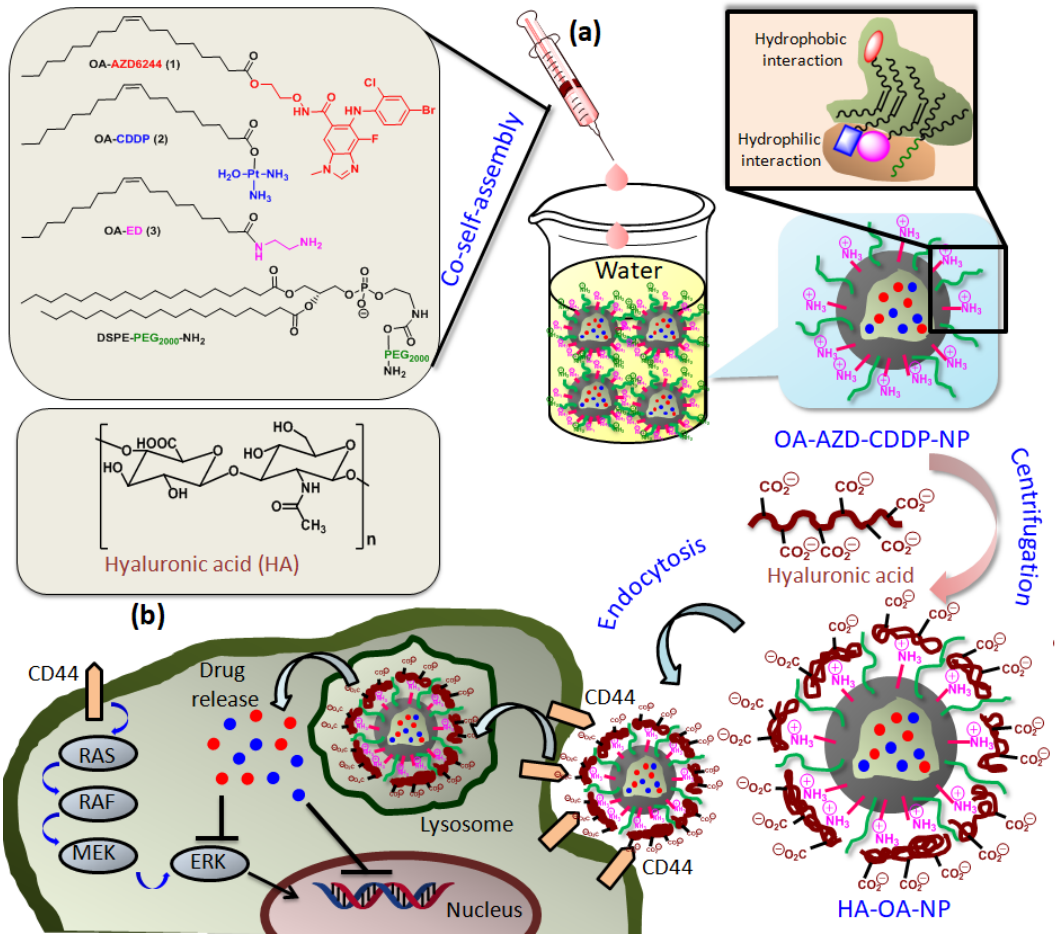

Scheme 1. Schematic representation of (a) engineering hyaluronic acid cloaked oleic acid nanoparticles (HA-OA-NPs) having AZD6244 and cisplatin and (b) cellular internalization of HA-OA-NPs through CD44 receptor mediated endocytosis into lysosomes followed by MAPK signaling inhibition and DNA damage.

4b.2 Results and discussion

4b.2.1 Engineering hyaluronic acid coated oleic acid nanoparticle: We synthesized Oleic acid-AZD6244 (1) conjugate and Oleic acid–CDDP (2) conjugate as described in 4a.4.2 and 4a.4.3 in chapter 4a respectively. To impart positive charge on nanoparticle for further coating with negatively charged HA, we synthesized oleic acid-ethylenediamine (3)

conjugate as described in section 4a.4.4 in chapter 4a. First we engineered the positively charged oleic acid nanoparticle (OA-AZD-CDDP-NPs) containing AZD6244 and cisplatin (CDDP) by co-self-assembly of conjugates 1, 2 and, 3. DSPE-PEG_{2000} was introduced into the co-self-assembly to render the surface of the OA-AZD-CDDP-NPs with stealth polyethylene glycol (PEG) moiety to evade mononuclear phagocytic system (MPS) (Scheme 1a). The size and the surface charge of OA-AZD-CDDP-NPs were determined by DLS. The hydrodynamic diameter and zeta potential were observed to be 128.3 nm and + 46.2 mV respectively (Fig.1a, b).

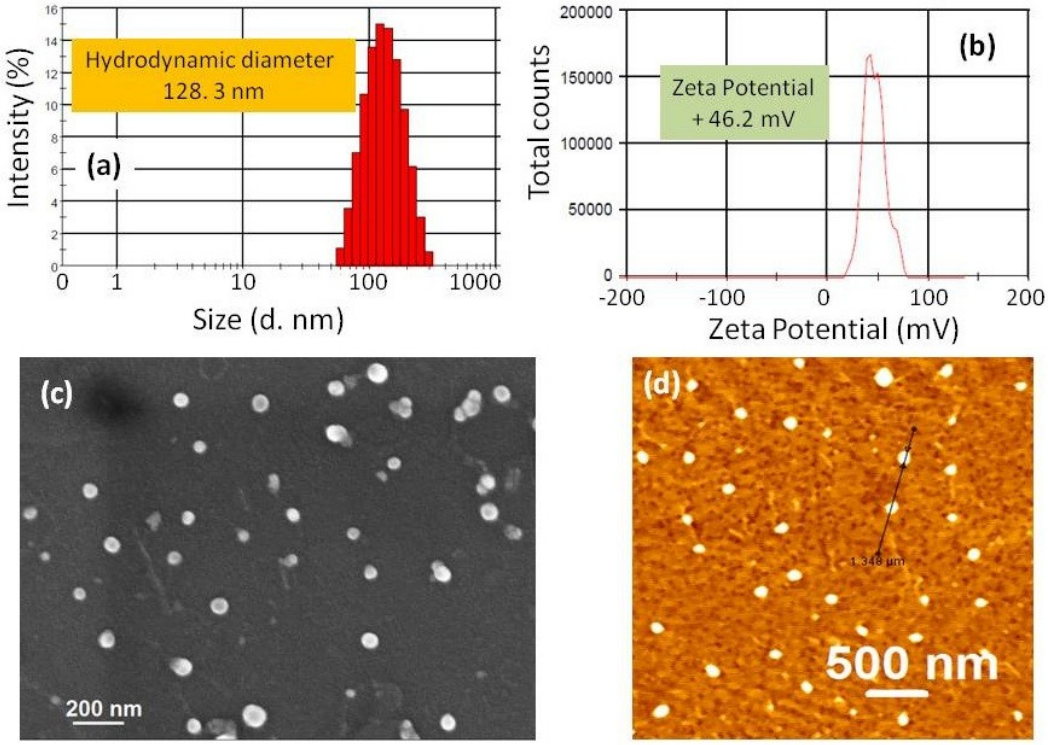

Fig. 1 Characterization of OA-AZD-CDDP-NPs by (a) DLS, (b) seta potential, (c) FE-SEM and (d) AFM.

The positive zeta potential clearly revealed that amine groups from oleic acid-ethylenediamine conjugate (3) were exposed to the surface of the nanoparticles. The spherical shape and morphology of the OA-AZD-CDDP-NPs were further visualized by field-emission scanning electron microscopy (FESEM) and atomic force microscopy (AFM) (Fig.1c, d). We anticipate that hydrophobic-hydrophobic interaction between long unsaturated oleic acid chains and hydrophilic-hydrophilic interaction between cisplatin and primary amine groups (-

NH_2) are responsible for self-assembly process to form OA-AZD-CDDP-NPs (Scheme 1) However, the exact mechanism is still not clear.

4b.2.2 Hyaluronic acid coating: To target over-expressed CD44 receptors in colon cancer cells, hyaluronic acid (HA), a negatively charged polysaccharide composed of repeating disaccharide units of N-acetyl-D- glucosamine (GlcNAc) and D-glucuronic acid (GlcUA) (Scheme 1) was used to cloak the oleic acid nanoparticle.[20-24] Highly positively charged surface of OA-AZD-CDDP-NPs was coated with highly negatively charged CD44 receptor targeting hyaluronic acid (HA) by electrostatic attraction (Scheme 1a). Hyaluronic acid coated OA-AZD-CDDP-NPs were further characterized by DLS.

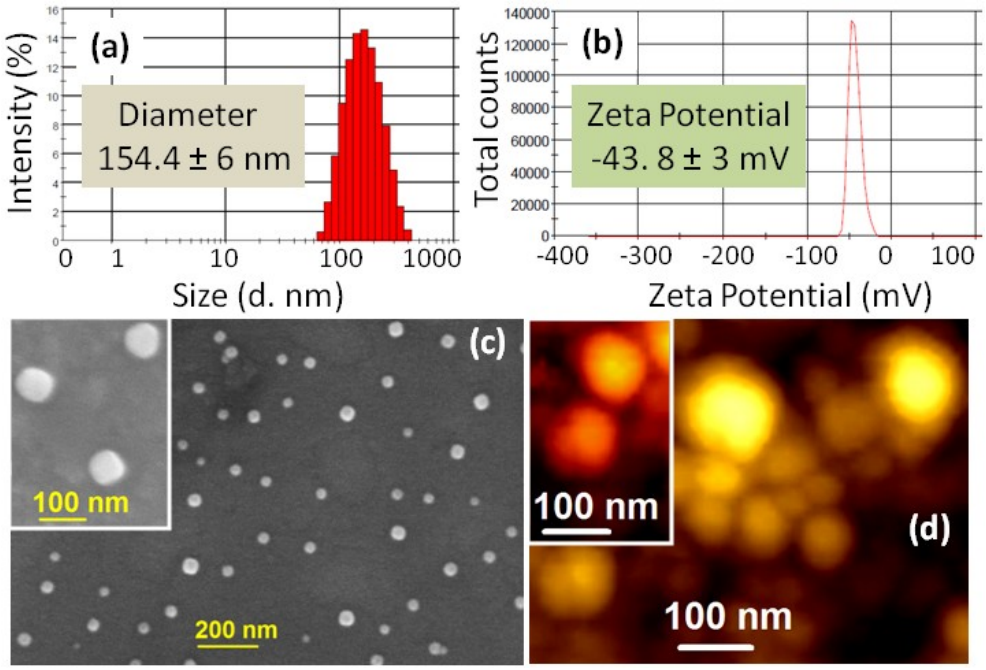

Fig. 2 Characterization of HA-OA-NPs by (a) DLS, (b) zeta potential, (c) FE-SEM (inset: High resolution FESEM images), (d) AFM (inset: high-resolution AFM images).

The increase in hydrodynamic diameter to 154.4 ± 6 nm (n = 3, mean ± SEM) (Fig. 2a) indicated the HA coating to obtain HA-OA-NPs containing AZD6244 and cisplatin. Highly negative zeta potential (ξ = - 43.8 ± 3 mV, n = 3, mean ± SEM, Fig. 2b) also evidently confirmed the successful HA coating over OA-AZD-CDDP-NPs. To engineer HA-OA-NPs with optimum size, zeta potential and loading of MAPK inhibitor and DNA damaging drugs, the nanoparticles were synthesized by varying the ratio of oleic acid-AZD conjugate (1), oleic

acid-CDDP conjugate (2) and oleic acid-ethylenediamine conjugate (3) in co-self-assembly (Table 1). From this optimization study, it was observed that HA-OA-NPs with smallest size (154.25 ± 6 nm), highly negative charge (ξ = - 43.8 ± 3 mV), lowest polydispersity index (PDI = 0.221 ± 0.06) and highest drug loading (AZD6244 = 194.24 ± 8.2 μM and CDDP = 241.56 ± 22.4 μM, n = 3, mean ± SEM) were obtained by blending OA-AZD, OA-CDDP and OA-ED in 1: 0.75: 2 weight ratios. Further chemical and biological evaluation was performed using HA-OA-NPs having these blending ratios. FESEM and AFM images (Fig. 2c, d) also revealed that HA-OA-NPs were spherical in shape with less than 200 nm in size.

OA-AZD (mg)	OA-CDDP (mg)	OA-ED-NH2 (mg)	Hyaluronic acid (HA) (mg)	Size (nm)	PDI	Zeta Potential (mV)	AZD : CDDP (Molar ratio)	Loading of drugs (uM) (AZD : CDDP)
1	1	2	0.2	178.2 ± 8	0.3 ± 0.08	-25.5±5	0.68:1	200.52+ 365.41 (0.54:1)
1	0.75	2	0.2	154.2 ± 6	0.2 ± 0.06	-43.8±3	0.97:1	194.24+ 241.56 (0.8:1)
1	0.5	1.5	0.2	198.2 ± 5	0.5 ± 0.96	-22.5±8	1:0.69	220.24+ 105.01 (1:0.47)
1	0.25	1.5	0.2	228.2 ±15	0.6 ± 0.6	-32.5±3	1:0.34	173.04+ 30.45 (1:0.17)

Table 1. Optimization of size, zeta potential, PDI and dual drug loading in engineering HA-OA-NPs.

Quantification of AZD6244 and cisplatin in HA-OA-NPs was performed by UV-Vis spectroscopy at characteristic λ_{max} = 273 nm (Fig. 2a in chapter 4a) and 706 nm respectively (Fig. 3, chapter 2). Moreover, presence of F in AZD6244 and Pt in cisplatin were detected by energy dispersive-X ray spectroscopy (EDX, Fig. 3).

4b.2.3 Drug release: Blended oleic acid nanoparticle can be taken up by cancer cells through endocytosis and localize into acidic sub-cellular lysosomes.[25] In acidic environment, nanoparticles release the active drugs followed by subsequent targeting of biological molecules. To evaluate the release of AZD6244 and cisplatin from the nanoparticles, HA-OA-NPs were incubated in pH = 5.5 milieu and the release of active drugs were quantified using

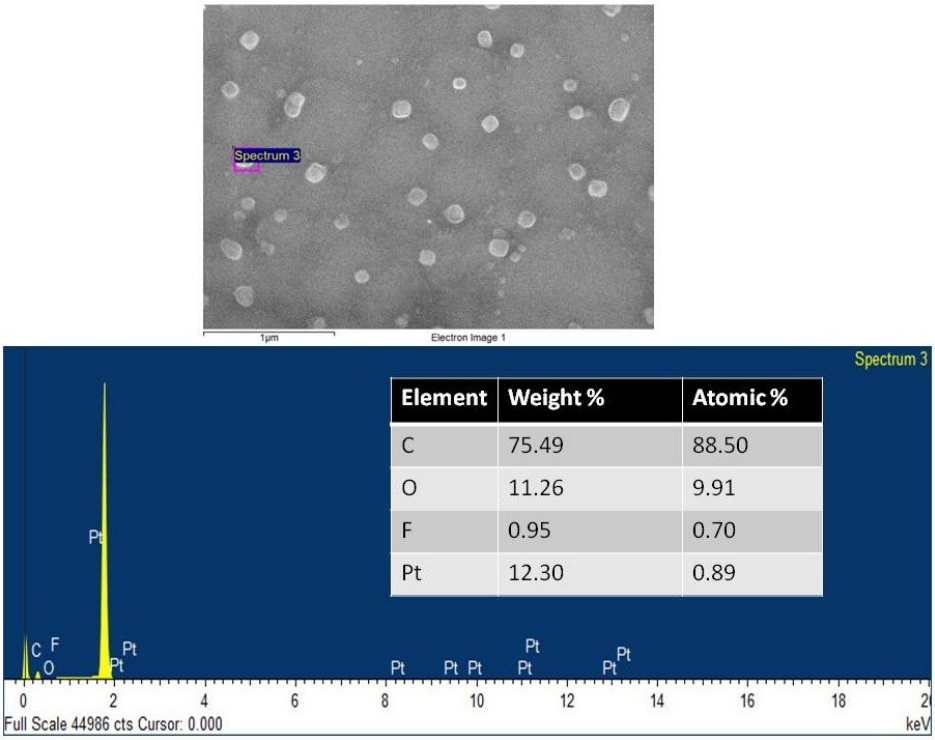

Fig. 3 EDX spectra of HA-OA-NPs to confirm the presence of AZD6244 and cisplatin in the same particle.

UV-Vis spectroscopy in predetermined time points. It was found that at pH = 5.5, HA-OA-NPs released 85.6 ± 3.5 % AZD6244 and 60.6 ± 2.1 % (n = 3, mean ± SEM) cisplatin at 72 h in a sustained manner (Fig. 4a). Ideally, HA-OA-NPs should not release considerable amount of active drugs before localization into acidic lysosomes. Hence, we evaluated the release of active drugs from HA-OA-NPs in physiological pH (pH = 7.4). Interestingly, only 37.6 ± 2.1 % and 31.4 ± 0.2 % (n = 3, mean ± SEM) of AZD6244 and cisplatin were released from HA-OA-NPs even after 72 h respectively (Fig. 4b). In comparison, at pH = 5.5, non-targeted OA-AZD-CDDP-NPs released 88.6 ± 8.4 % and 67.7 ± 4.1 % (n = 3, mean ± SEM) AZD6244 and cisplatin respectively after 72h. On the other hand, at pH = 7.4, 56.9 ± 6.1 % and 46.3 ± 3.4 % (n = 3, mean ± SEM) AZD6244 and cisplatin were released respectively after 72h. This drug release comparison clearly indicated that at acidic environment, both HA-coated and non-HA-coated nanoparticles released the dual drugs in nearly same quantities in a similar time dependent manner. However, at physiological pH, HA-coated nanoparticles released dual drugs in much lower quantities compared to non-HA-coated nanoparticles. Moreover, HA coating protected the drugs to be released prematurely in physiological condition as added

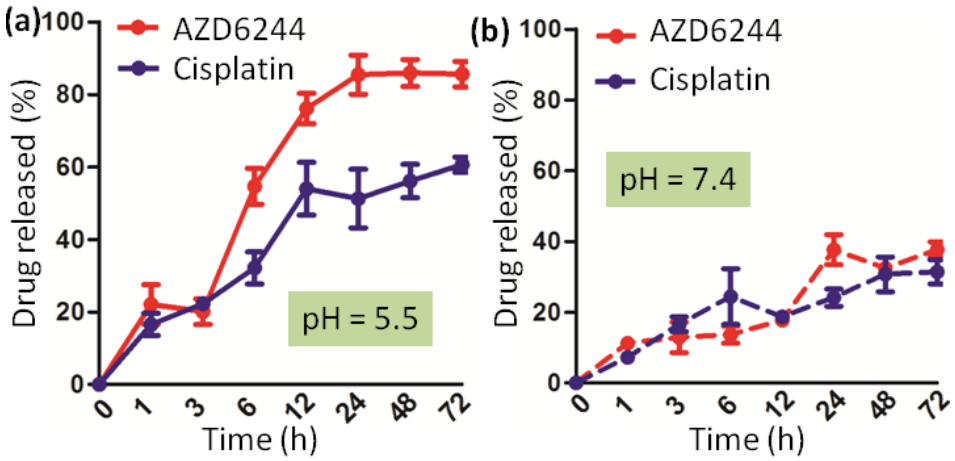

Fig. 4 Release of active AZD6244 and cisplatin from HA-OA-NPs in (a) pH = 5.5 (lysosome mimic) and (b) pH = 7.4 (physiological pH). Data represent mean ± SEM, n = 3.

advantage. As discussed in chapter 4a, both ester linkage and Pt-O coordination bonds in oleic acid-AZD6244 conjugate and oleic acid-CDDP conjugate respectively were highly labile in acidic environment leading to significant release of active drugs within 72 h. Whereas, both ester and Pt-O coordination bonds were enough stable at pH = 7.4 leading to marginal release of active drugs at physiological environment even after prolonged exposure. Hence, these HA-OA-NPs were suitable enough for compartmentalized pH triggered drug release inside the cancer cells.

4b.2.4 Stability: For successful interaction with over-expressed receptors on cancer cells, the nanoparticles should be stable in biological environment. To evaluate the stability in biological milieu, HA-OA-NPs were incubated in cell culture DMEM medium in presence of 10 % fatal bovine serum (FBS) at 37 °C. Hydrodynamic diameter and poly-dispersity index (PDI) were measured by DLS in a time dependent manner as indicators of nanoparticle aggregation. The hydrodynamic diameter was found to be increased from 152.8 ± 1.1 nm to 187.9 ± 2.2 nm (n = 3, mean ± SEM) over 96 h (Fig. 5a). Furthermore, the PDI value was also changed negligibly from 0.133 ± 0.24 to 0.294 ± 0.02 (n = 3, mean ± SEM) over 96 h (Fig. 5b). These marginal changes in hydrodynamic diameter and PDI value clearly demonstrated that HA-OA-NPs were stable even in presence of FBS in biological atmosphere. Moreover, this stability data indicated that, HA-OA-NPs would also be stable at blood circulation mimic for prolonged time to be accumulated in tumor tissues by hyaluronic acid-CD44 receptor mediated active targeting.

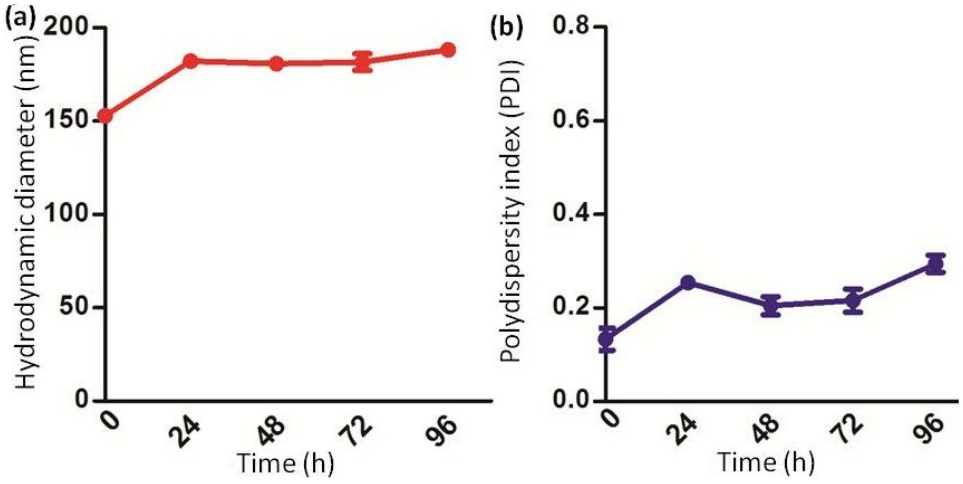

Fig. 5 Stability of HA-OA-NPs in DMEM cell culture media with 10% FBS at 37 °C over 96 h determined by (a) hydrodynamic diameter and (b) polydispersity index (PDI).

4b.2.5 Cellular internalization

4b.2.5.1 Determination of CD44 expression on colon cancer cells:

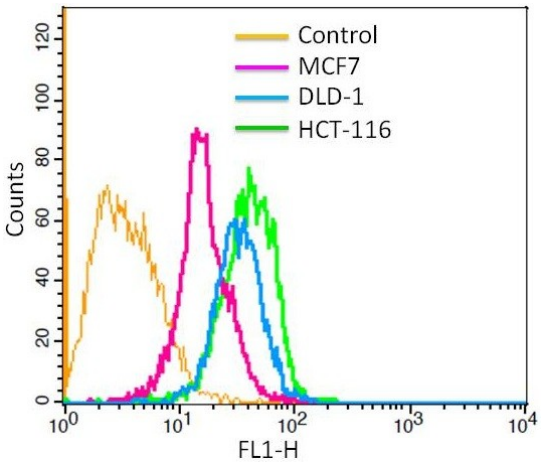

Fig. 6 Flow cytometry analysis of MCF7, DLD-1 and HCT-116 cells to determine the cell surface expression of CD44 receptors by FITC-labelled anti-human CD44 antibody.

Hyaluronic acid coated AZD6244 and cisplatin containing oleic acid nanoparticle (HA-OA-NPs) should interact with CD44 receptors in cancer cells. To evaluate the expression of CD44 receptors, colon cancer cells (HCT-116 and DLD-1) and breast cancer cells (MCF7) were treated with FITC-labeled anti-human CD44 antibody. The amount of CD44 receptors expressed cancer cells were quantified by fluorescence-activated cell sorting (FACS)

analysis. From flow cytometry, it was quantified that MCF7 cells contained least expression of CD44 receptors, whereas DLD-1 and HCT-116 cells contained 1.6 folds and 2 folds (n = 3, mean) expression of CD44 receptor expression compared to MCF7 cells (Fig. 6) Hence, further biological evaluation of HA-OA-NPs was performed in HCT-116 colon cancer cells.

4b.2.5.2 Cellular uptake by confocal microscopy:

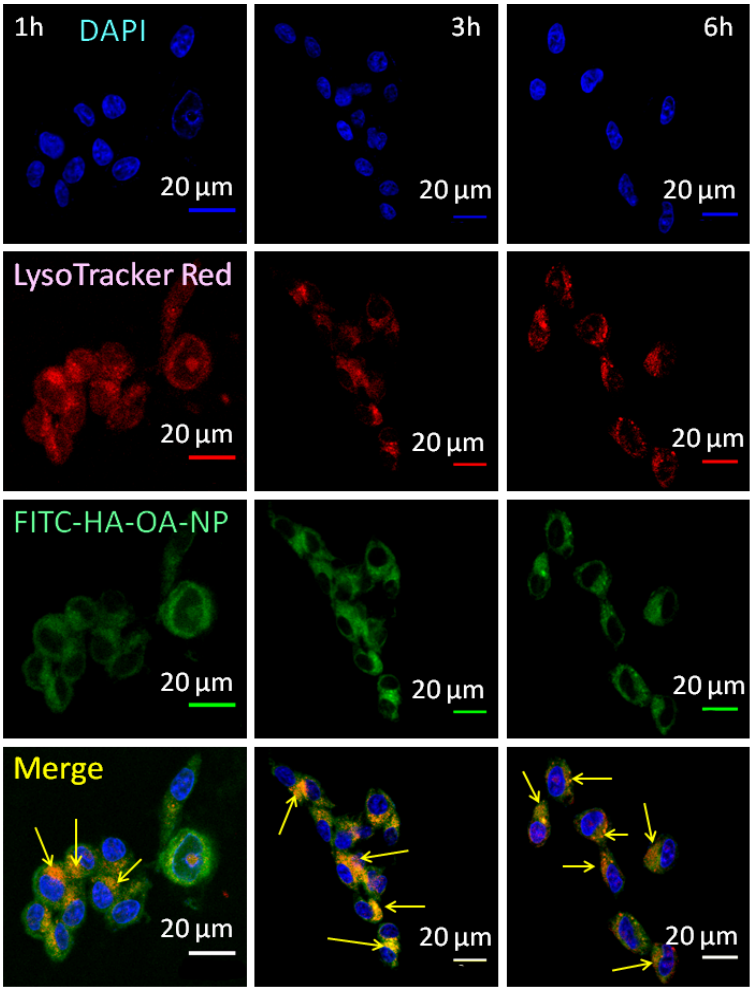

Fig. 7 Confocal laser scanning microscopy (CLSM) images of FITC-HA-OA-NPs internalized into HCT-116 cells at 1 h, 3 h and 6 h time points. Nuclei and lysosomes were stained with DAPI (blue) and LysoTracker Red DND-99 (red) respectively. Scale bar = 20 µm.

We hypothesized that, CD44 receptor binding would lead to the internalization of nanoparticles followed by homing into lysosomes. To validate our hypothesis, we engineered hyaluronic acid cloaked green fluorescently labelled OA-AZD-CDDP-NPs by blending oleic acid-fluorescein isothiocyanate (OA-FITC) conjugate with oleic acid-AZD6244 conjugate (1)

and oleic acid-CDDP conjugate (2).[25] Lysosomes and nuclei in HCT-116 cells were stained by LysoTracker Red DND-99 and DAPI (blue) respectively. HCT-116 cells were treated with FITC-labelled green fluorescent HA-OA-NPs in a time reliant manner (1 h, 3 h and 6 h), followed by visualization through confocal laser scanning microscopy (CLSM). Fluorescence confocal images in Fig. 7 demonstrated that green fluorescent FITC-labelled HA-OA-NPs were slowly co-localized with red fluorescent lysosomes leading to yellow fluorescent merged areas (shown by arrows) temporally from 1 h to 3 h to 6 h.

4b.2.5.3 Hyaluronic acid mediated cellular uptake by CLSM:

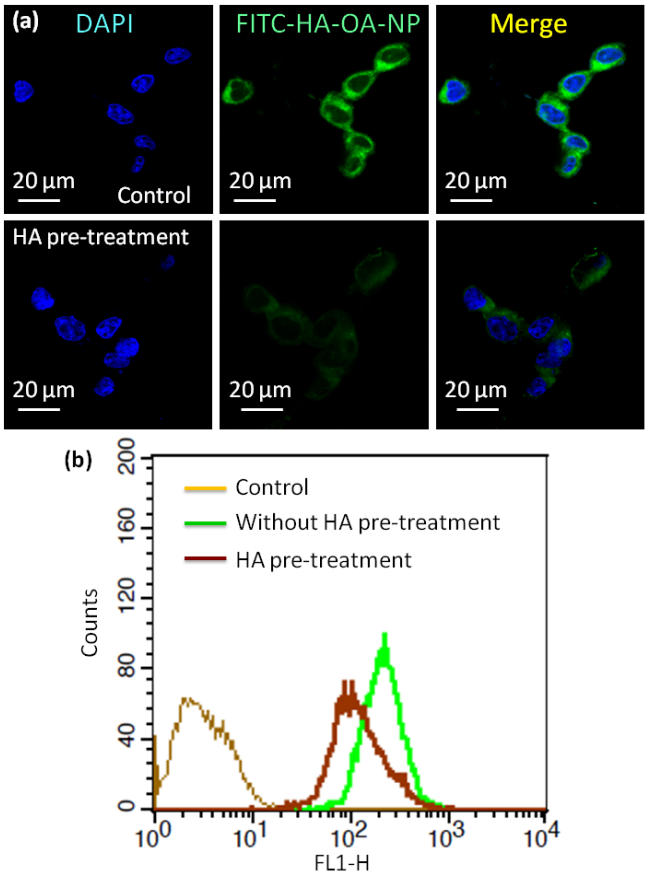

Fig. 8 Cellular internalization of FITC-HA-OA-NPs in HCT-116 cell pre-treated with and without hyaluronic acid determined by (a) confocal laser scanning microscopy (CLSM) and (b) Flow cytometry (FACS). Scale bar = 20 µm.

Moreover, to confirm that, hyaluronic acid cloaking enhanced the cellular internalization of nanoparticles, HCT-116 cells were pre-treated with free hyaluronic acid to saturate all CD44 receptors. We further incubated the cells with FITC-labelled HA-OA-NPs for 2 h and co-

stained the nuclei with DAPI. As control, HCT-116 cells were only treated with green fluorescent HA-OA-NPs without any treatment with hyaluronic acid. We visualized the cellular internalization of FITC-HA-OA-NPs by confocal microscopy. It was evident from Fig. 8a that hyaluronic acid pre-treatment significantly reduced the cellular internalization of green fluorescent HA-OA-NPs compared to no-hyaluronic acid treated control cells

4b.2.5.4 Hyaluronic acid mediated cellular uptake by FACS: We further corroborated the hyaluronic acid assisted cellular internalization of HA-OA-NPs by flow cytometric analysis. HCT-116 cells were pre-treated with hyaluronic acid for 2 h followed by incubation with FITC-HA-OA-NPs for 2 h. Control cells were only treated with FITC-labelled HA-OA-NPs without any hyaluronic acid treatment. The FITC-HA-OA-NP engulfed green fluorescent cells were quantified by FACS analysis. Flow cytometric analysis showed nearly 40 % (n = 3, mean) reduction in HA-OA-NP internalization in hyaluronic acid pre-treated cells compared to no-hyaluronic acid treated control cells (Fig. 8b). These confocal images and FACS analysis clearly confirmed that HA-OA-NPs internalized into colon cancer cells through hyaluronic acid-CD44 interaction followed by homing into lysosomes over 6 h.

4b.2.6 Mechanism of internalization

4b.2.6.1 Cellular uptake pathways by CLSM: After binding with the extracellular CD44 receptors, HA-OA-NPs can be internalized into the cells through diverse pathways.[26] To assess the exact machinery of internalization, HCT-116 cells were pre-treated with chlorpromazine, genistein and amiloride as small molecule inhibitors of clathrin-mediated endocytosis, caveolin-mediated endocytosis and macropinocytosis respectively.[27, 28] Subsequently, cells were treated with FITC-labeled HA-OA-NPs and nuclei were stained with DAPI, followed by confocal laser scanning microscopy. Control cells were only treated with FITC-HA-OA-NPs without any endocytosis inhibitor. Confocal fluorescence microscopy images in Fig. 9 unmistakably showed that chlorpromazine inhibited internalization of FITC-HA-OA-NPs significantly compared to control cells. On the contrary, genistein and amiloride treated cells showed marginal difference in FITC-HA-OA-NP internalization compared to no-inhibitor treated cells.

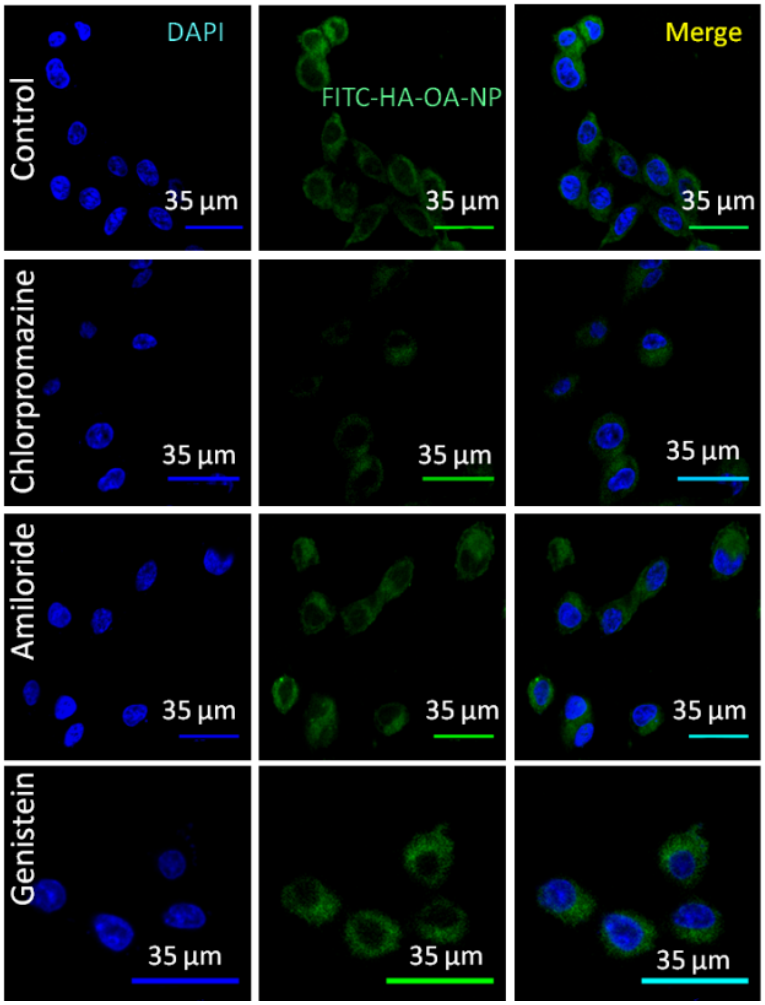

Fig. 9 Confocal laser scanning microscopy (CLSM) images of FITC-HA-OA-NPs internalized into HCT-116 cells after treatment with chlorpromazine, amiloride and genistein for 2 h. Nuclei were stained with DAPI (blue). Scale bar = 35 µm.

4b.2.6.2 Cellular uptake pathways by FACS: To further validate the mechanism of internalization, HCT-116 cells were pre-treated with chlorpromazine, genistein and amiloride, followed by incubation with FITC-HA-OA-NPs. Fluorescently labeled HA-OA-NP engulfed cells were sorted and quantified by FACS analysis. It was observed from the flow cytometric analysis that, chlorpromazine inhibited the cellular uptake of FITC-HA-OA-NPs by 44 % (n = 3, mean) compared to control cells (Fig. 10). On the other hand, genistein and amiloride treatment inhibited the cellular uptake of FITC-HA-OA-NPs by only 7 % and 33 % (n = 3, mean) respectively compared to no-inhibitor treated control cells. To further

investigate the energy dependency of cellular uptake, HCT-116 cells were treated with FITC-HA-OA-NPs at 4 °C and 37 °C followed by quantification by FACS analysis. Flow cytometry data suggested that cellular uptake of FITC-HA-OA-NPs was reduced by 40 % (n = 3, mean) at 4 °C compared to the uptake at 37 °C (Fig. 11). From these fluorescence confocal images and flow cytometry analysis it was confirmed that HA-OA-NPs were internalized by clathrin-mediated endocytosis in temperature dependent manner into HCT-116 cells.

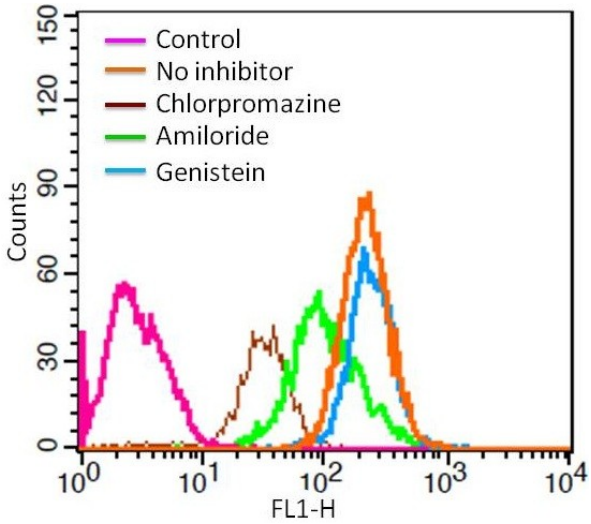

Fig. 10 Flow cytometry analysis of HCT-116 cells pre-treated with chlorpromazine, amiloride and genistein followed by treatment with FITC-HA-OA-NPs.

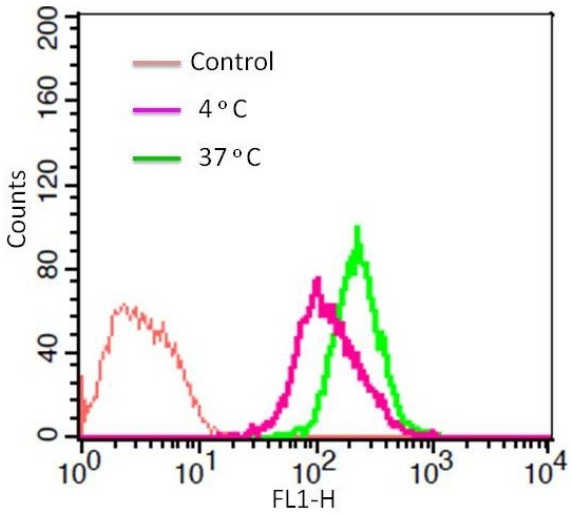

Fig. 11 Flow cytometry analysis of HCT-116 cells after treatment with FITC-HA-OA-NPs at 4 °C and 37 °C.

4b.2.7 Inhibition of MAPK signaling with DNA damage

4b.2.7.1 Inhibition of MAPK signaling: Cellular uptake through CD44 receptor and clathrin-mediated endocytosis localized HA-OA-NPs into acidic lysosomes in time dependent manner. Inside lysosomes, lower pH would trigger the release of active AZD6244 and cisplatin by cleaving acid labile ester and Pt-O coordinate bonds respectively. Consequently, AZD6244 (MEK inhibitor) should inhibit the phosphorylation of extracellular signal-regulated kinase (ERK). To determine the effect of nanoparticles in RAS-RAF-MEK-ERK (MAPK) signaling, HCT-116 cells were treated with HA-OA-NPs for 24 h and estimated the expression of phosphorylated ERK by Western blot analysis. Fig. 12a demonstrated that the expression of phosphor-ERK1 and phosphor-ERK2 was reduced significantly compared to no-nanoparticle treated control cells. Further quantification from Western blot revealed that HA-OA-NP mediated MAPK inhibition led to the reduction of expression of phosphor-ERK1 and phosphor-ERK2 by 2.9 folds and 1.7 folds (n = 3, mean) respectively (Fig. 12c, d).

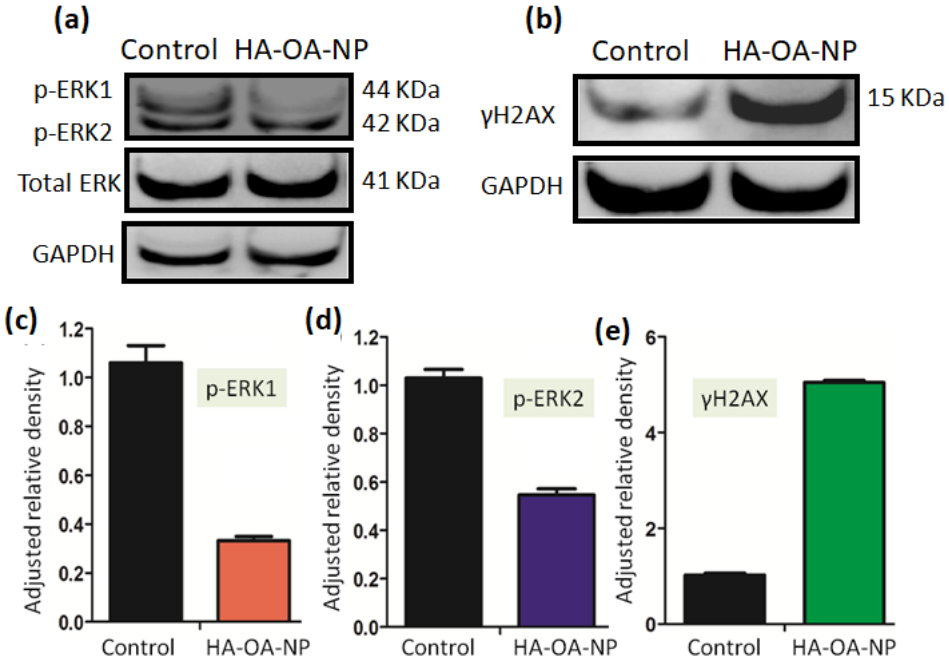

Fig. 12 (a-b) Western blot analysis of p-ERK1/2, total ERK and γH2AX as markers for MAPK inhibition and DNA damage in HCT-116 cells respectively.Quantification of expression of (c) p-ERK1, (d) p-ERK2 and (e) γH2AX from western blot analysis in HCT-116 cells after treatment with HA-OA-NPs for 24 h.

4b.2.7.2 DNA damage: Moreover, HA-OA-NPs would also release free cisplatin at lower pH inside lysososmes, which will lead to sub-cellular DNA damage. To determine the effect of nanoparticles on DNA damage, HCT-116 cells were treated with HA-OA-NPs for 24 h and evaluated the expression of γH2AX (marker for sub-cellular DNA damage)[29] by Western blot. The gel electrophoresis image Figure 12b undoubtedly showed that expression of γH2AX was increased significantly in HA-OA-NP treated cells compared to control cells. Further quantification from gel electrophoresis showed that HA-OA-NPs increased the expression of γH2AX by 5 folds (n = 3, mean) compared to control (Fig. 12e) These western blot analyses demonstrated that HA-OA-NPs inhibited MAPK signaling simultaneously with DNA damage in HCT-116 colon cancer cells.

4b.2.8 Apoptosis and cell death: Simultaneous inhibition of MAPK signaling and DNA damage pushes the cancer cells to programmed cell death (apoptosis).[21] To estimate the effect of nanoparticles in inducing apoptosis, HCT-116 cells were treated with HA-OA-NPs for 24 h followed by staining the apoptotic and necrotic cells by FITC-Annexin V and propidium iodide (PI) respectively.

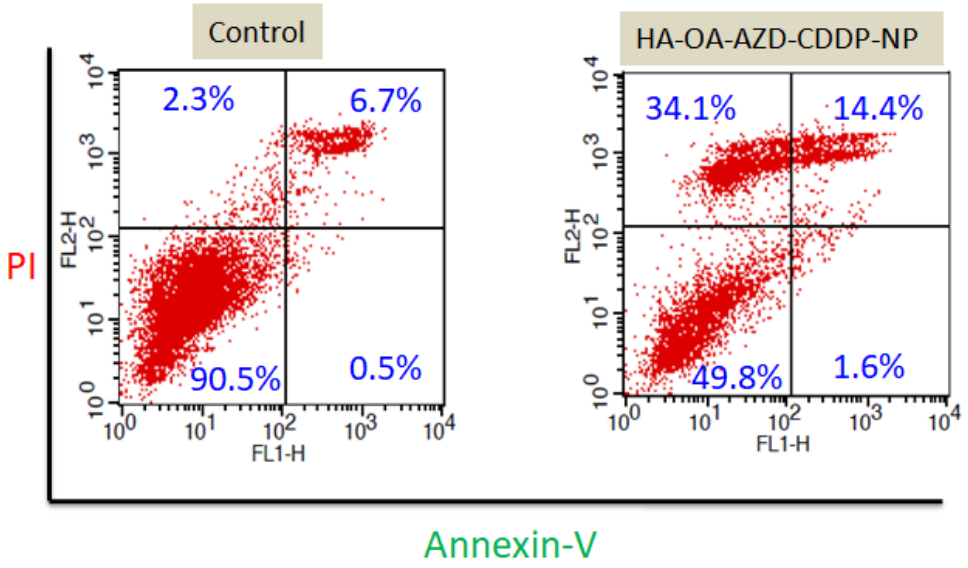

Fig. 13 Flow cytometry analysis to evaluate the effect of HA-OA-NPs in inducing apoptosis and necrosis in HCT-116 cells at 24 h.

The cells in different stages of apoptosis and necrosis were quantified by FACS analysis. From the flow cytometry data, it was observed that HA-OA-NPs induced late apoptosis and necrosis in 14.4 % and 34.1 % cells respectively (Fig. 13), whereas only 6.7 % and 2.3 % (n = 3, mean) cells were in late apoptotic and necrotic stages respectively in non-nanoparticle treated control cells.

4b.2.9 Cell viability: DNA damage and MAPK inhibition induced apoptosis trigger cancer cell death. Finally, colon cancer cell death was evaluated by cell viability assay. HCT-116 cells were treated with HA-OA-NPs and cell death was determined by MTT assay at 24 h post-incubation. As control, cells were treated with free AZD6244 and cisplatin cocktail in the same concentration and ratio present in HA-OA-NPs. In HCT-116, HA-OA-NPs demonstrated highly reduced IC_{50} = 2.7 ± 0.2 μM compared to IC_{50} = 40.7 ± 0.8 μM and 6.6 ± 0.3 μM (n = 3, mean ± SEM) for free drug cocktail and non-targeted OA-AZD-CDDP-NPs respectively (Fig. 14a,c) Moreover, HA-OA-NPs induced only 1.4 ± 0.4 % cell viability compared to 81.5 ± 1.6 % and 15.3 ± 0.6 % (n = 3, mean ± SEM) induced by free drug combination and OA-AZD-CDDP-NPs at 25 μM cisplatin concentration in the drug cocktail.

We also evaluated the effect of HA-OA-NPs in DLD-1 colon cancer cells after 24 h incubation. In DLD-1 cells, HA-OA-NPs again showed much less IC_{50} = 2.7 ± 0.1 μM compared to IC_{50} = 38.5 ± 0.3 μM and 7.6 ± 0.5 μM (n = 3, mean ± SEM) for free AZD6244 and cisplatin combination and OA-AZD-CDDP-NPs respectively (Fig. 14b, d). Again, HA-OA-NPs triggered only 15.7 ± 0.6 % cell viability in contrast to 77.1 ± 0.6% and 32.1 ± 2.6 % (n = 3, mean ± SEM) by free drug combination and OA-AZD-CDDP-NPs respectively at 25 μM cisplatin concentration the drug cocktail. Finally, we evaluated the efficacy of HA-OA-NPs in MCF7 breast cancer cells. In MCF7 cells, at 24 h, HA-OA-NPs demonstrated IC_{50} = 5.8 ± 0.1 μM (cell viability = 14. 8 ± 1.7 % at 25 μM cisplatin concentration) compared to IC_{50} = 37.1 ± 1.0 μM (cell viability = 74.3 ± 2.1 % at 25 μM cisplatin concentration) and 7.0 ± 1.1 μM (cell viability = 26.3 ± 1.3 % at 25 μM cisplatin concentration) for free drug combination and OA-AZD-CDDP-NPs respectively (Fig. 14e, f) The remarkably lower IC_{50} values induced by nanoparticles compared to free drug cocktail was attributed to CD44 mediated improved internalization of HA-OA-NPs inside the cancer cells. In contrast, AZD6244 (hydrophobic) and cisplatin (hydrophilic) have huge difference in their aqueous solubility leading to erratic cellular uptake, hence exposure in sub-cellular milieu in sub-optimal concentration to inhibit the respective.

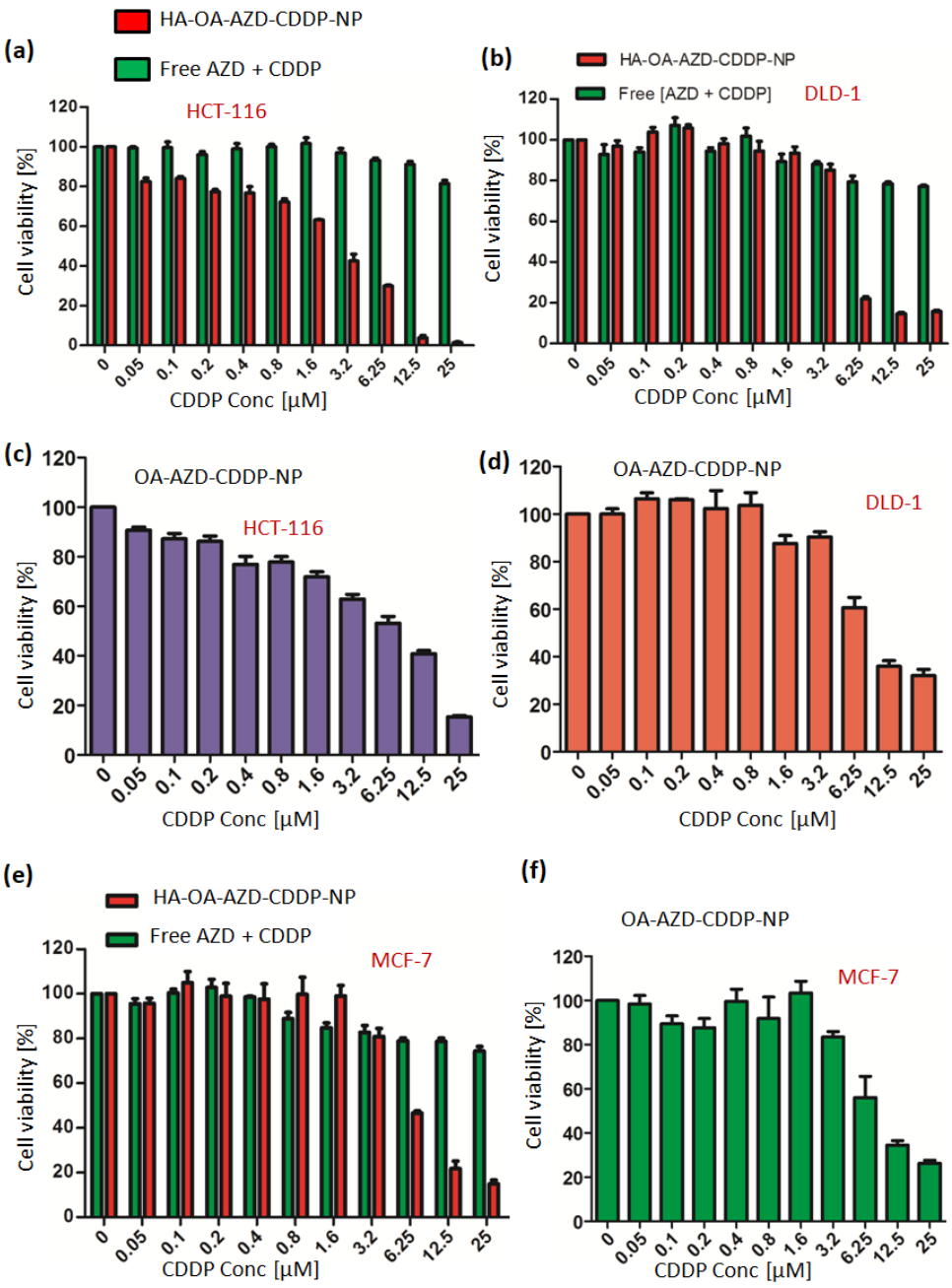

Fug. 14 Concentration dependent cell viability assay of HA-OA-NPs in HCT-116 (a) and DLD-1 (b) cells at 24h post-incubation compared to free drug cocktail, OA-AZD-CDDP-NPs in HCT-116 (c) and DLD-1 (d) colon cancer cells at 24 h post-incubation,(e) HA-OA-AZD-CDDP-NPs and (f) OA-AZD-CDDP-NPs in MCF7 breast cancer cells at 24h post incubation determined by MTT assay. Data represent mean ± SEM, n = 3. Statistical analysis was performed by two-way ANOVA, $p < 0.0001$.

targets. Moreover, while inside the cells HA-OA-NPs keep on releasing dual drugs in a slow and sustained manner over long time (Fig. 4a). From these apoptosis and cell viability assays, it was evident that HA-OA-NPs induced late apoptosis and necrosis lead to much improved efficacy in cancer cells compared to free drug combination. Moreover, it was interesting to note that HA-OA-NPs showed much lower IC_{50} values in higher CD44 expressing HCT-116 and DLD-1 cells compared to lower CD44 expressing MCF7 cells, which validated our initial hypothesis of targeting colon cancer cells by cloaking the nanoparticle with hyaluronic acid for improved efficacy. However, *in vivo* experiments in colon cancer xenograft model need to be done to evaluate the full anticancer efficacy as well as reduced cardio- and immune-toxicity of HA-OA-NPs before proceeding towards clinical translation.

4b.3 Conclusions

In conclusion, in this study, we have engineered hyaluronic acid cloaked oleicacid nanoparticle encompassing AZD6244 (MAPK inhibitor) and cisplatin (DNA damaging drug). The HA-OA-NPs were taken up by colon cancer cells (HCT-116) through CD44 receptor mediated and clathrin-dependent endocytosis to localize into sub-cellular lysosomes. Simultaneous MAPK signaling inhibition and DNA damage was induced by HA-OA-NPs triggered late apoptosis and necrosis in HCT-116 cells. Finally, HA-OA-NPs showed remarkable efficacy in colon cancer cells (HCT-116 and DLD-1) as well as breast cancer cells (MCF7) compared to free drug cocktail.

4b.4 Experimental section

4b.4.1 Materials: AZD6244 was purchased from Selleck Chemicals. Cisplatin, oleic acid, MTT reagent and DAPI were obtained from Sigma Aldrich. Hyaluronic acid (150 kDa) was obtained from Lifecore USA. DMEM (high glucose) medium, LysoTracker™ Red DND-99, and *SlowFade*® diamond antifade reagents were purchased from Life Technologies. HCT116, DLD1 and MCF7 cells were obtained from National Centre for Cell Science (NCCS), Pune. Anti-ERK 1/2 phospho monoclonal antibody, anti-GAPDH antibody, HRP goat anti-mouse IgG antibody and FITC-anti-CD44-human antibody, γH2AX and apoptosis detection kit were purchased from BioLegend.

4b.4.2 Synthesis of oleic acid-drug conjugates: Chemical synthesis and spectroscopic characterization of oleic acid-AZD6244 (1), oleic acid-cisplatin (2), oleic acid-ethylenediamine (3) and oleic acid-FITC conjugates were performed as explained in section 4.4.2, 4.4.3, 4.4.4 and 4.4.5 in chapter 4a respectively.

4b.4.3 Synthesis of hyaluronic acid cloaked oleic acid nanoparticles (HA-OA-NPs): Oleic acid-AZD6244 (1), oleic acid-cisplatin (2), oleic acid-ethylenediamine (3) and DSPE-PEG were taken in 0.5 mg, 0.5 mg, 1 mg and 0.2 mg respectively and dissolved in 0.5 mL of acetone/methanol (1:1). For synthesis of HA-OA-FITC-NPs, 0.2 mg oleic acid-FITC conjugate was mixed with conjugate 1, 2 and 3. The acetone/methanol solution containing conjugates was slowly added to 2 mL of double distilled water with continuous stirring. The solution was stirred for 4 h to evaporate the organic solvent to afford OA-NPs. To this OA-NP solution, 0.5 mL of (0.5 mg/mL) hyaluronic acid (HA) solution was added drop wise under stirring. After 10 minutes, hyaluronic acid coated OA-NPs (HA-OA-NPs) were centrifuged at 70,000 X g. The HA-OA-NPs pellets were washed with water to remove excess hyaluronic acid. HA-OA-NPs were re-suspended in water and stored at 4 °C for further use.

4b.4.4 Size, surface charge, shape and morphology determination of HA-OA-NPs: Hydrodynamic diameter and surface charge of HA-OA-NPs were determined by DLS. Size, shape and morphology of HA-OA-NPs were visualized by AFM and FESEM. Sample preparation and instrumentation were performed followed by the methods described in section 2.2.4, 2.2.5 and 2.2.6 in chapter 2. Hydrodynamic diameter and surface charge from DLS were determined in triplicate.

4b.4.5 Quantification of dual drug loading in HA-OA-NPs: AZD6244 and cisplatin loading in HA-OA-NPs were determined by UV-Vis spectroscopy at λ_{max} = 273 nm and 706 nm respectively from absorbance versus calibration curve (Fig. 2a in chapter 4a for AZD and Fig 3 in chapter 2 for cisplatin) as explained in section 4a.4.10 in chapter 4a. Drug loading was quantified in triplicate.

4b.4.6 Determination of dual drug release from HA-OA-NPs: Release of AZD6244 and cisplatin from HA-OA-NPs was determined by dialysis method as explained in section

4a.4.11 in chapter 4a. The amount of AZD6244 and cisplatin released in predetermined time points were quantified by UV-Vis spectroscopy at λ_{max} = 273 nm and 706 nm respectively.[25] Released AZD6244 and cisplatin in each time point in each pH buffer were quantified in triplicate.

4b.4.7 Stability of HA-OA-NPs: HA-OA-NPs were incubated into DMEM media containing 10 % FBS at 37 °C and stability was determined by checking the hydrodynamic diameter and polydispersity index (PDI) through DLS. Stability determination by DLS in each time points was performed in triplicate.

4b.4.8 Determination of CD44 expression on cancer cells by flow cytometry: 5 X 10^4 cells (HCT116, DLD1 and MCF7) were seeded onto a culture plate at 37 °C and 5 % CO_2 environment for 24 h. Culture medium was removed and cells were washed with PBS. Cells were then trypsinized and centrifuged at 1000 rpm for 5 min followed by washing with 3 mL of cold PBS to remove dead cells. 10^5 cells/ mL were then freshly suspended in cold PBS in flow cytometry tubes. To this cell suspension, 5 µL of FITC anti-human CD44 antibody was added and incubated at 4 °C for 30 min. No antibody was added to the control cells. The cells were washed once with PBS and then resuspended in PBS. FACS measurement was performed under FITC channel by using BD FACS Calibur. Flow cytometric analysis was performed in triplicate to determine the CD44 expression in different cancer cells.

4b.4.9 Cellular internalization study by confocal microscopy: 50,000 HCT116 cells were seeded on cover slips in a 6-well plate. After 24 h, cells were treated with HA-OA-FITC-NPs at a FITC concentration of 2 µg/ mL at 37 °C for 1 h, 3 h and 6 h. After each time points, the cells were washed with PBS and fixed with paraformaldehyde solution (4 %) for 15 min at 4 °C. Lysosomes and nucleus were stained by LysoTracker Red DND-99 and DAPI for 45 min and 3 min respectively. Cells were washed with PBS and mounted on a glass slide using 5 µL SlowFade diamond antifade reagent. The cells were visualized by confocal microscopy (Zeiss LSM 710).

10^5 HCT116 cells were pretreated with different endocytosis inhibitors followed by treatment with HA-OA-FITC-NPs. For hyaluronic acid competitive inhibition study cells were

incubated in 5 mg/mL hyaluronic acid in serum free media for 2h before adding the HA-FITC-CNPs. The cellular internalization was further visualized by confocal microscopy.[25]

4b.4.10 Cellular internalization study by flow cytometry: 10^5 HCT116 cells were treated with various endocytosis inhibitors (amiloride, genistein and chlorpromazine at concentration of 100 µM, 30 µM, and 37 µM respectively for 30 min at 37 °C. Control cells were incubated at 37 °C without any treatment of inhibitor. For hyaluronic acid competitive inhibition study cells were incubated in 5 mg/mL hyaluronic acid in serum free media for 2 h before adding the HA-FITC-CNPs. After washing with PBS incubation, HA-OA-FITC-NPs (FITC concentration = 2 µg/ mL) was added to the cells and incubated for 2 h. Cells were trypsinized, followed by centrifugation at 1000 rpm at 4 °C for 5 min to remove dead cells. Finally, the fluorescently labeled cells were counted by flow cytometry. Temperature dependent cellular internalization study by flow cytometry was performed by the method described in the section 4a.4.14 in chapter 4a.[25] FACS analysis to determine cellular internalization was carried out in triplicate.

4b.4.11 Western blot analysis: HCT116 cells were treated with HA-OA-NPs for 24 h followed by cell lysis and suspension in sample buffer. Proteins were visualized in SDS-polyacrylamide gel electrophoresis (SDS-PAGE) using primary antibody solution (pERK1/2 and ERK2 in 1:1000 dilution, γH2AX in 1:2000 and GAPDH in 1:5000 dilution) and then incubated in HRP conjugated secondary antibody solution (1:10000 dilution). Protein quantification from western blot was performed in triplicate.

4b.4.12 Detection of apoptosis by flow cytometry: Detection and quantification of apoptosis by flow cytometry was performed in triplicate by the method described in section 4a.4.15 in chapter 4a.[25]

4b.4.13 *In vitro* cytotoxicity assay: 5000 cells (HCT116, DLD1 and MCF7) were exposed with serial concentrations of HA-OA-NPs. Free drugs were dissolved in DMSO to make a stock solution equal concentration present in NPs. After 24 h incubation, 20 µL of MTT (5 mg/mL) was added to each well. After 4 h, 100 µL of solubilization buffer (10% SDS in 0.01 M HCl) was added to each well to make the MTT crystals soluble. After overnight

incubation, absorbance was measured with spectrophotometer at 550 nm and the percent cell viability was calculated considering the untreated cells as 100 % viability. All the experiments were performed in triplicate for each group. The statistical analysis was performed by two-way ANOVA.

4b.5 References

1. Colorectal Cancer Facts and Figures 2011–2013, American Cancer Society, https://www.cancer.org/research/cancer-factsstatistics/colorectal-cancer-facts-figures.html.
2. Colorectal Cancer: Estimated Incidence, Mortality and Prevalence Worldwide in 2012, World Health Organization, http://globocan.iarc.fr/old/FactSheets/cancers/colorectalnew.asp
3. L. Rubbia-Brandt, V. Audard, P. Sartoretti, A. Roth, C. Brezault, M. Le Charpentier, B. Dousset, P. Morel, O. Soubrane and S. Chaussade, *Ann. Oncol.,* 2004, **15**, 460-466.
4. T. André, C. Boni, L. Mounedji-Boudiaf, M. Navarro, J. Tabernero, T. Hickish, C. Topham, M. Zaninelli, P. Clingan and J. Bridgewater, *N. Engl. J. Med.,* 2004, **350**, 2343-2351.
5. H. Klotz, W. Weder and F. Largiader, *Surg. Oncol.,* 1994, **3**, 11-16.
6. I. B. Weinstein and A. Joe, *Cancer Res.,* 2008, **68**, 3077-3080.
7. J. Luo, N. L. Solimini and S. J. Elledge, *Cell*, 2009, **136**, 823-837.
8. J. Urosevic, A. R. Nebreda and R. R. Gomis, *Cell Cycle,* 2014, **13**, 2641-2642.
9. P. J. Roberts and C. J. Der, *Oncogene, 2007*, **26**, 3291-3310.
10. K. Zenonos and K. Kyprianou, *World J. Gastrointest. Oncol.,* 2013, **5**, 97-101**.**
11. J. Y. Fang and B. C. Richardson, *Lancet Oncol.,* 2005, **6**, 322-327.
12. L. Santarpia, S. M. Lippman and A. K. El-Naggar, *Expert Opin. Ther Targets,* 2012, **16**, 103-119.
13. S. Y. Yang, A. Miah, K. M. Sales, B. Fuller, A. M. Seifalian and M. Winslet, *Int. J. Oncol.,* 2011, **38**, 1695-1702.
14. H. Richly, B. Henning, P. Kupsch, K. Passarge, M. Grubert, R. Hilger, O. Christensen, E. Brendel, B. Schwartz and M. Ludwig, *Ann. Oncol.,* 2006, **17**, 866-873.

15. L. Dal Lago, V. D'Hondt and A. Awada, *Oncologist,* 2008, **13**, 845-858.
16. E. Martinelli, F. Morgillo, T. Troiani and F. Ciardiello, *Cancer Treat. Rev,* 2017, **53**, 61-69.
17. Y. Lee, H. Lee, Y. B. Kim, J. Kim, T. Hyeon, H. Park, P. B. Messersmith and T. G. Park, *Adv. Mater.,* 2008, **20**, 4154-4157.
18. M. Kamat, K. El-Boubbou, D. C. Zhu, T. Lansdell, X. Lu, W. Li and X. Huang, *Bioconjug. Chem,* 2010, **21**, 2128-2135.
19. K. Y. Choi, E. J. Jeon, H. Y. Yoon, B. S. Lee, J. H. Na, K. H. Min, S. Y. Kim, S.-J. Myung, S. Lee and X. Chen, *Biomaterials,* 2012, **33**, 6186-6193.
20. K. Liu, Z.-q. Wang, S.-j. Wang, P. Liu, Y.-h. Qin, Y. Ma, X.-C. Li and Z.-J. Huo, *Int. J. Nanomed.,* 2015, **10**, 6445-6454.
21. L. Shao, R. Zhang, J. Lu, C. Zhao, X. Deng and Y. Wu, *ACS Applied materials & interfaces,* 2017, **9**, 1226-1236.
22. E. Song, W. Han, C. Li, D. Cheng, L. Li, L. Liu, G. Zhu, Y. Song and W. Tan, *ACS Appl. Mater. Interfaces,* 2014, **6**, 11882-11890.
23. H. S. Jung, W. H. Kong, D. K. Sung, M.-Y. Lee, S. E. Beack, D. H. Keum, K. S. Kim, S. H. Yun and S. K. Hahn, *ACS Nano,* 2014, **8**, 260-268.
24. B. Xiao, M. K. Han, E. Viennois, L. Wang, M. Zhang, X. Si and D. Merlin, *Nanoscale,* 2015, **7**, 17745-17755.
25. S. Palvai, P. More, N. Mapara, J. Nagraj, R. Chowdhury and S. Basu, *ChemNanoMat, 201*6, **2**, 201-211.
26. G. J. Doherty and H. T. McMahon, *Annu. Rev. Biochem.,* 2009, **78**, 857-902.
27. M. Koivusalo, C. Welch, H. Hayashi, C. C. Scott, M. Kim, T. Alexander, N. Touret, K. M. Hahn and S. Grinstein, *J. Cell Biol.,* 2010, **188**, 547-63
28. J. Rejman, A. Bragonzi and M. Conese, *Mol. Ther.,* 2005, **12**, 468-474.
29. L. J. Kuo and L.-X. Yang, *In vivo,* 2008, **22**, 305-309.

Chapter 5

Hyaluronic Acid Coated Chimeric Nanoparticle: Targeting MAPK-PI3K signaling hub in Colon Cancer Cells

5.1 Introduction

The MAPK and PI3K signaling pathways are the major implicated pathways in colorectal cancer (CRC) cells.[1] The PIK3CA gene, encoding the p110*a* catalytic subunit of class I PI3Ks, was found to be mutated in 10–20% of colorectal cancers.[2] Mutations in KRAS, NRAS, or BRAF are very common in CRC, and have been found in 50–60 % of tumors.[3, 4] Constitutive activation of PI3K and MAPK pathway contributes to increased proliferation, resistance to apoptosis and chemo-resistance. However, targeting single pathway fails to attain durable therapeutic responsesdue to tumor heterogeneity, emergence of drug resistance (intrinsic and extrinsic) and complex inter/intra-cascade crosstalk.[5-10] PI3K and MAPK signaling hub form an interconnected network that plays a central role in tumorigenesis.[11, 12] Inhibition of single pathway by small molecules invariably leads to the rewiring in another signaling. With inhibition of the PI3K-AKT-mTOR pathway, the RAS-RAF-MEK-ERK signaling acts as a compensatory mechanism, and vice versa.[9, 13] These considerable cross-talk between the two pathways is one of the major reasons for the failure of only one signaling inhibition and necessitated inhibition of both PI3K and MAPK signaling simultaneously to achieve durable responses in CRC treatment.[3] Further, several studies proved that combination regimen of PI3K/MAPK kinase inhibitors with cytotoxic drugs exhibited efficient cell killing of several cancer cells including colorectal cancer cells.[14-17] However, selective inhibition of these signaling pathways in cancer cells by using small molecule kinase inhibitors remained a major challenge. In chapter 4b, we have successfully inhibited MAPK signaling pathway with simultaneous DNA damage by using dual drug loaded nontoxix oleic acid nanoparticles.[18] Recently, Hammond et al. engineered layer-by-layer polymeric nanoparticles containing PI3K and MAPK signaling inhibitors for horizontal blockade of both the signalings simultaneously.[19] Despite having tremendous advancement in nanotechnology based cancer therapy, unfortunately, ratiometric targeted delivery of PI3K, MAPK inhibitors with cytotoxic drugs to colon cancer cells specifically was almost unexplored.[19] Hence, there is an urgency to develop an efficient therapeutic strategy that can target multiple survival signaling pathways selectively in colon cancer cells to enhance the therapeutic outcome. Recently, our group developed cholesterol based nanotechnology platform to achieve ratiometric loading and controlled delivery of triple drugs to different cancer cells.

Inspired by this lacuna, in this chapter, we have engineered hyaluronic acid coated chimeric nanoparticle (HA-ChNP) comprises AZD6244 (MAPK inhibitor), PI103 (PI3K inhibitor) and cisplatin (DNA damaging FDA approved drug) in a ratio-metric manner. These HA-ChNPs were hypothesized to be internalized more efficiently through CD44 receptor-mediated endocytosis into colon cancer cells to target MAPK-PI3K signaling hub along with sub-cellular DNA damage for improved efficacy (Scheme 1c). These HA-ChNPs were found to be internalized into the colon cancer cells (HCT-116) through a combination of CD44 receptor and clathrin-mediated endocytosis mechanism followed by localization into acidic lysosomal compartments in a time-dependent manner over 6h. Simultaneous inhibition of MAPK and PI3K signaling was achieved along with DNA damage by these HA-ChNPs in HCT-116 cells leading to cell cycle arrest in G0/G1 phase, followed by induction of apoptosis (early and late stage). Finally, these HA-ChNPs demonstrated remarkably improved cell killing ability compared to the free drug combinations in HCT-116 colon cells, without showing toxicity to the healthy fibroblast cells.

5.2 Results and discussion

5.2.1 Engineering hyaluronic acid coated chimeric nanoparticle (HA-ChNPs).

5.2.1.1 Choosing drug combinations and vector: PI103, AZD6244 and cisplatin were chosen for simultaneous inhibition of PI3K and MAPK signaling and to induce DNA damage respectively in colon cancer cells. Nontoxic and biodegradable lipid molecule, cholesterol was selected as a vector for loading ofPI103, AZD6244 and cisplatin into the nanoparticles. Moreover, recently we have shown cholesterol as an efficient vector for loading of triple drugs (PI103, doxorubicin, and cisplatin) in a ratiometric manner. A highly negatively charged hyaluronic acid (HA), was used to decorate the ChNPs surface to target over-expressed CD44 receptors in colon cancer cells.[20, 21]

5.2.1.2 Synthesizing hyaluronic acid coated chimeric nanoparticles (HA-ChNPs): AZD6244 was coupled with conjugate 1 in the presence of EDC and DMAP though an ester linkage to achieve compound 2 with the yield of 78 % (scheme 1a). Cholesterol drug conjugates (3 and 4) were synthesized as explained in chapter 3.[22] Chimeric nanoparticles were synthesized as described in our previous study. In this case, to impart the positive charge on the nanoparticles surface, we incorporated cholesterol ethylene diamine conjugate (5) during the synthesis of ChNPs. Briefly, Conjugate 2, 3, 4, and 5 were mixed with PC and

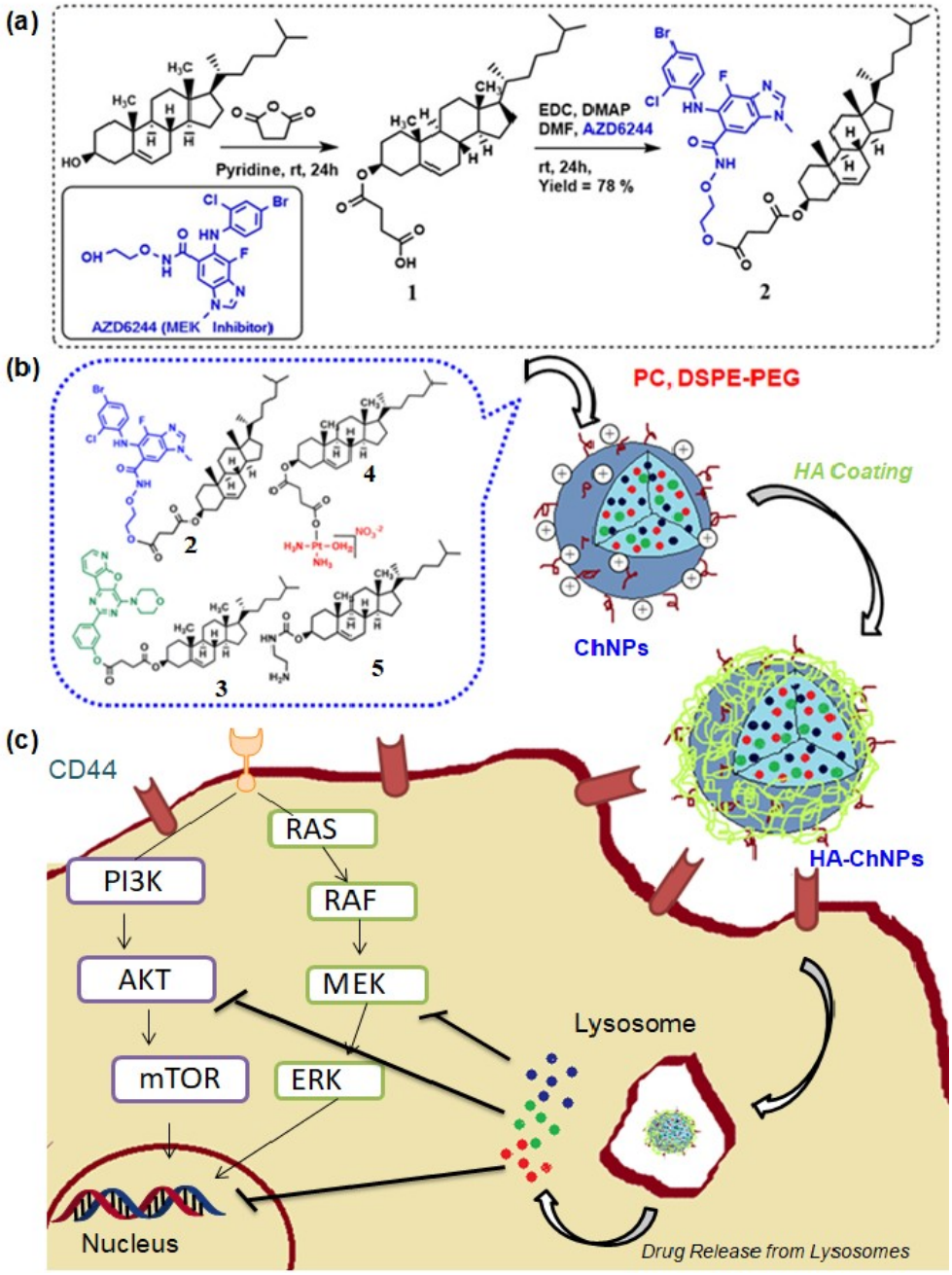

Scheme 1. Schematic representation of (a) Synthesis of Cholesterol-AZD6244 Conjugate (b) engineering hyaluronic acid cloaked chimeric nanoparticles (HA-ChNPs) having PI103, AZD6244 and cisplatin (C) cellular internalization of HA-ChNPs through CD44 receptor mediated endocytosis into lysosomes followed by PI3K and MAPK signaling inhibition and DNA damage.

DSPE-PEG_{2000} to obtain positively charged ChNPs (scheme 1b). DSPE-PEG_{2000} was used to provide stealth properties to the nanoparticles which ensure the nanoparticles to escape from

the opsonisation by macrophages (scheme 1b). The hydrodynamic diameter and zeta potential of the ChNPs were found to be 143.4 nm (polydispersity index = 0.078) and + 36. 4 mV respectively (Fig. 1a and 1b) from DLS studies. In the next step, highly positively charged

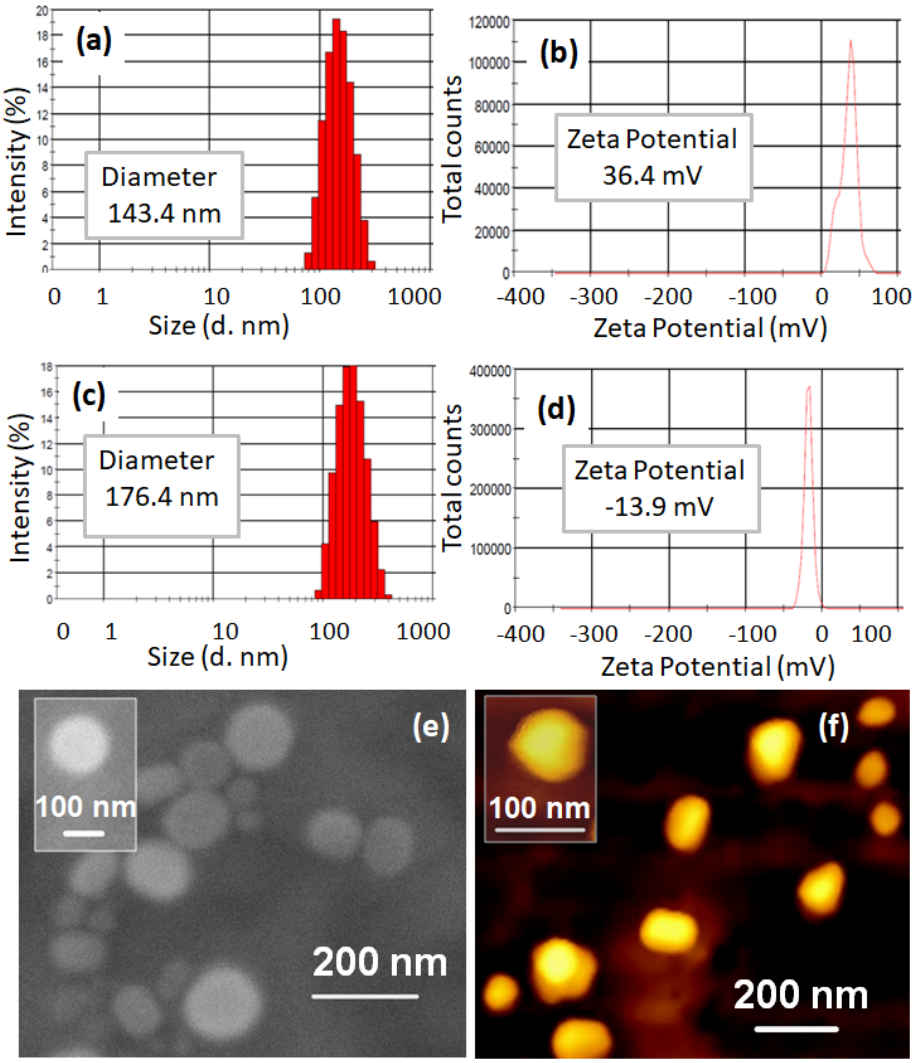

Fig. 1 Characterization of ChNPs by (a) DLS, (b) zeta potential, HA-ChNPs by (c) DLS, (d) zeta potential, (e) FE-SEM (inset: High resolution FESEM images), (f) AFM (inset: high-resolution AFM images).

ChNPs surface was coated with negatively charged hyaluronic acid by electrostatic attractions.[23-25] After coating, the ChNPs surface charge was turned to negative (ξ = -13.4 ± 0.61 mV, Fig. 1d), because of negatively charged carboxylic acid groups in the structure of

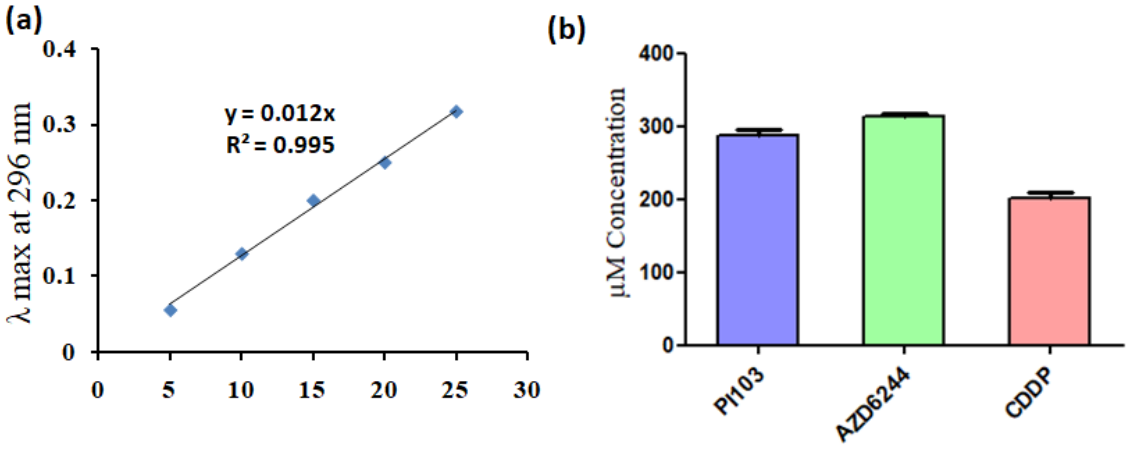

Fig. 2 (a) Calibration graph for PI103 by UV-Vis spectroscopy (b) Loading of AZD6244, PI103, and cisplatin in HA-ChNPs determined by the calibration graph.

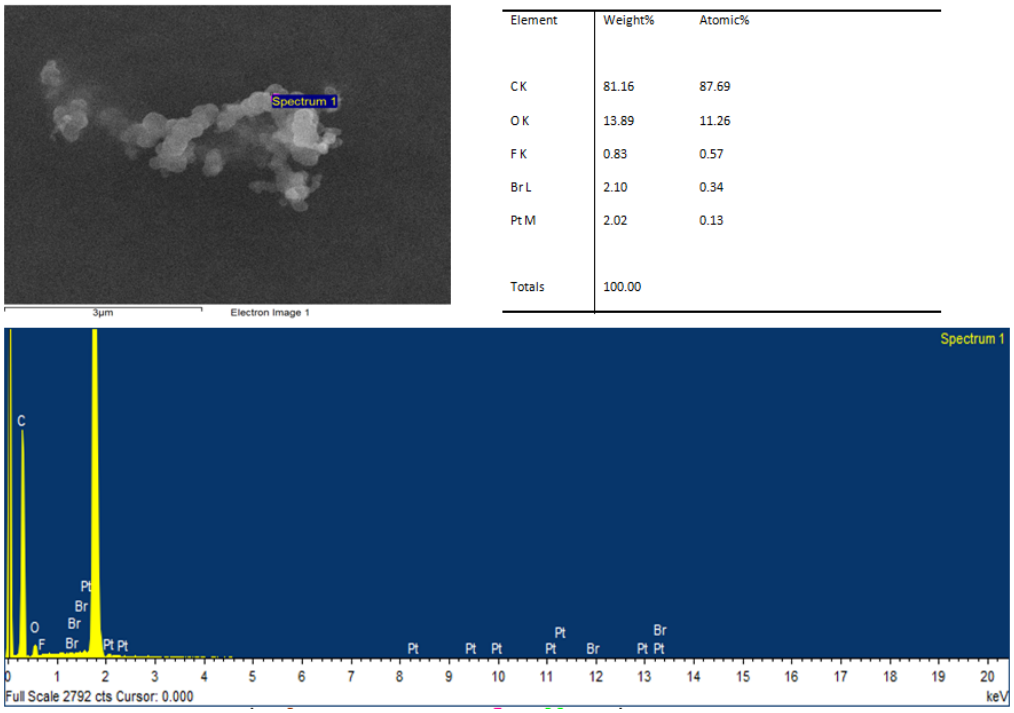

Fig. 3 EDX spectra of HA-ChNPs to confirm the presence of AZD6244 and cisplatin in the same particle.

HA molecules. This change in surface charge of ChNPs proved that HA molecules bound to the surface of nanoparticles by electrostatic interaction. The hydrodynamic diameter of ChNPs was increased to 176.5 nm (PDI = 0.139) (Fig. 1c) which clearly indicated the successful coating of HA onto ChNPs surface to obtain HA-ChNPs which contains PI103, AZD6244, and CDDP. The loading of PI103, AZD6244, and CDDP in HA-ChNPs were found to be 286.66 ± 7.4 μM, 313.38 ± 4.56 μM, and 201.97 ± 6.92 μM respectively (Fig. 2b). FESEM and AFM were used to investigate the morphological characteristics of HA-ChNPs. As represented in Fig. 1e and Fig. 1f, HA-ChNPs were spherical in shape with <200 nm diameter which is suitable for efficient *in vivo* tumor accumulation and disposition of nanoparticles *via* EPR effect. Further, presence of F in AZD6244 and Pt in cisplatin in the particles were detected by energy dispersive-X ray spectroscopy (EDX, Fig. 3).

5.2.2 Cellular uptake of HA-ChNPs: To see the interaction of HA-ChNPs with CD44 overexpressed colon cancer cells, we have chosen CD44 rich HCT116 cells and studied their intracellular fate by using confocal microscopy techniques. We engineered hyaluronic acid coated green fluorescent labeled HA-ChNPs. We have chemically conjugated FITC with cholesterol ethylenediamine conjugate (**5**) to obtain FITC-cholesterol conjugate (**6**) (Fig. 4) and characterized them by ^{1}H, ^{13}C NMR spectroscopy and MALDI-TOF (Fig. 19, 20 and 21 respectively). We further blended cholesterol fluorescein isothiocyanate conjugate with drug conjugate 2, 3, 4, and 5 with PC, DSPE-PEG_{2000} to obtain HA-FITC-ChNPs. The size and zeta potential of FITC-ChNP and HA-FITC-ChNP were determined by DLS study. The mean diameter and zeta potential of FITC-ChNP were found to be 142.4 nm and + 34.6 mV. Whereas, the mean diameter and surface charge of HA-FITC-ChNP were determined to be 162.5 nm and -19.8 mV (Fig. 5). The size and surface charge of HA-FITC-ChNP and HA-ChNP were found to be similar, which assured us to use HA-FITC-ChNP for the cellular internalization study.

HCT-116 cells were treated with FITC-labelled green fluorescent HA-ChNPs at a FITC concentration 2 μg/mL in a time-dependent manner (1 h, 3 h and 6 h), followed by staining lysosomes and nuclei by LysoTracker Red DND-99 and DAPI (blue) respectively. As shown in Fig. 6, CLSM images demonstrated that green fluorescent FITC-labelled HA-ChNPs were slowly colocalized with lysosomes stained with red-fluorescent which yielded yellow

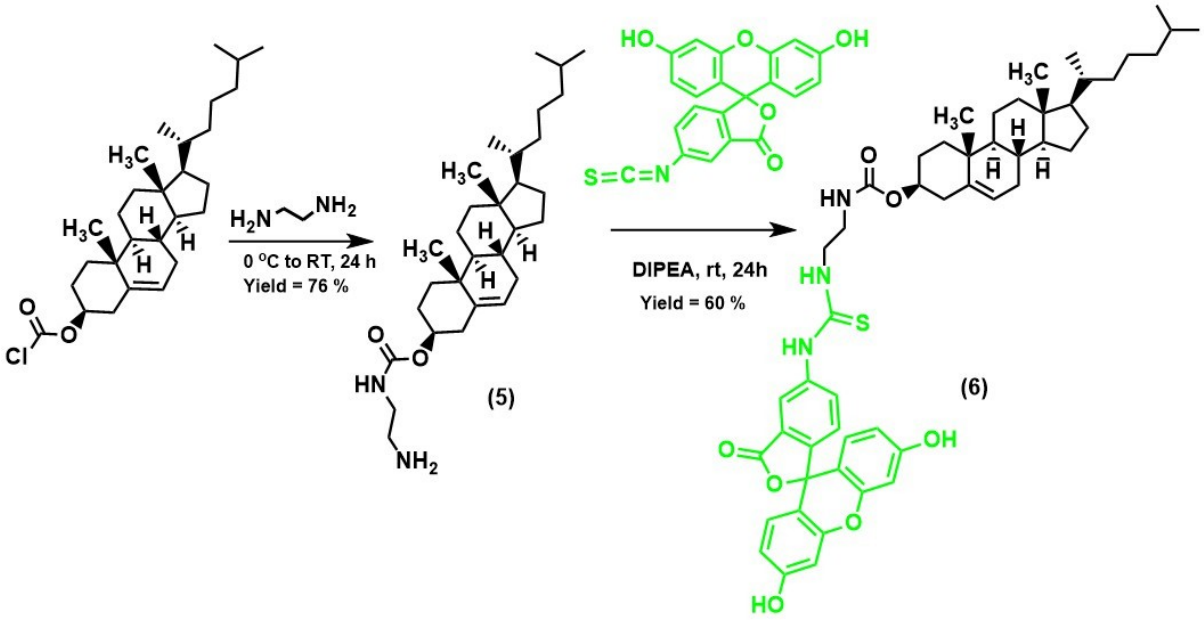

Fig. 4 Synthetic scheme of cholesterol-FITC conjugate (6).

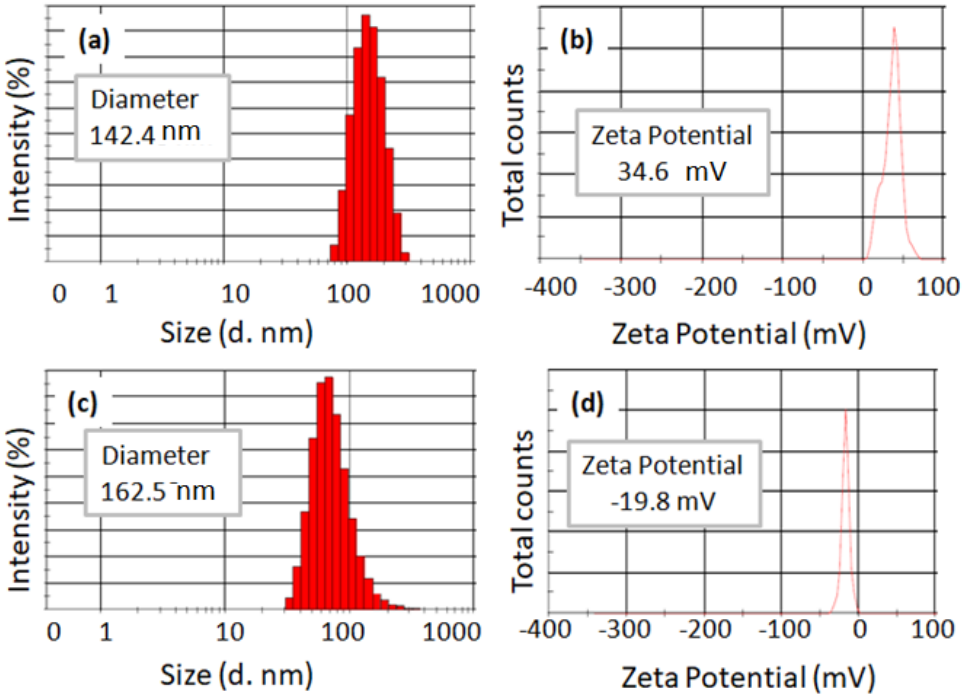

Fig. 5 Characterization of FITC-ChNPs by (a) DLS, (b) zeta potential, and HA-FITC-ChNPs by (c) DLS, (d) zeta potential.

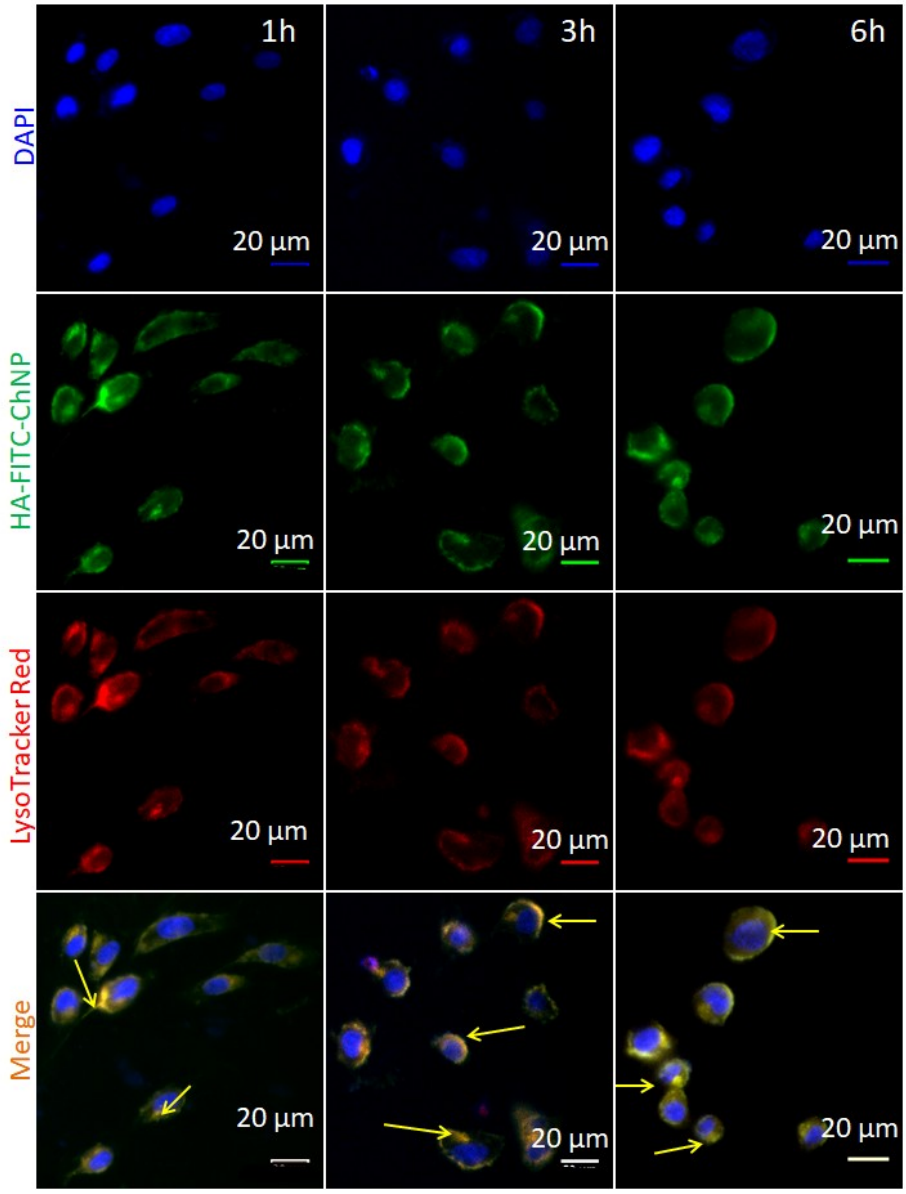

Fig. 6 Confocal laser scanning microscopy (CLSM) images of HA-FITC-ChNPs internalized into HCT-116 cells at 1h, 3h and 6h time points. Nuclei and lysosomes were stained with DAPI (blue) and LysoTracker Red DND-99 (red) respectively. Scale bar = 20 µm.

fluorescent merged areas (shown by arrows) temporally from 1 h to 3 h to 6 h. From the colocalization study by CLSM it is clear that HA-FITC-ChNPs were internalized into the HCT116 cells through endocytosis followed by accumulating into lysosomal compartments in a temporal manner. After localization into acidic lysosomes, the HA-ChNPs should release its drug payload through cleavage of acid labile ester and Pt-O coordinate bonds.[18, 22] To evaluate the drug release in acidic environment, we incubated HA-ChNPs in pH = 5.5 solution (lysosome mimic) and released drugs were quantified in pre-determined time points through concentration versus absorbance calibration graph in UV-Vis spectroscopy (Fig. 2a for PI103

and Fig. 2a in chapter 4a for AZD). At pH = 5.5, it was found that nearly 81.3 ± 3.8 % of Akt-mTOR inhibitor PI103 was released after 72 h (Fig. 7). However, slightly less amount (69.9 ± 8.6 %) of MEK inhibitor AZD6244 was released after 72 h. On the other hand, only 58.5 ± 4.9 % of DNA damaging drug cisplatin was found to be released after 72 h.

We attributed the different amount of inhibitors and cytotoxic drug released in acidic environment towards the relatively labile nature of the chemical bonds through which they are linked with the cholesterol moiety. Phenolic ester linkage is much more labile in acidic medium leading to more amount of free PI103 release from the HA-ChNPs. On the other hand, aliphatic ester linkage in cholesterol-AZD6244 conjugate made it little less labile in acidic medium compare to phenolic ester lead less release of AZD6244 even at 72 h compared to PI103. Finally, Pt-O coordinate bond is much less labile compared to phenolic and aliphatic ester linkages in acidic milieu. Hence, cisplatin release was much less compared to PI103 and AZD6244 after the same time interval (72 h). However, both the signaling inhibitors and the cytotoxic drug showed controlled and continuous release over 3 days.

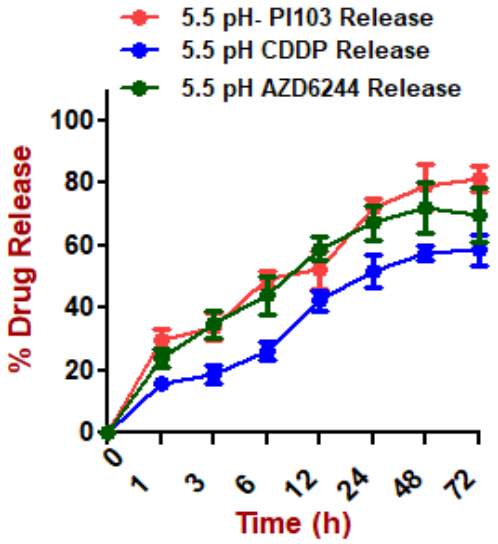

Fig. 7 Release of active PI103, AZD6244 and cisplatin from HA-ChNPs in pH = 5.5 (lysosome mimic). Data represent mean ± SEM, n = 3.

5.2.3 Mechanism of cellular internalization: Nanoparticles can home into the lysosomal compartments through endocytosis under different mechanisms (clathrin-mediated endocytosis, caveolin-mediated endocytosis and macropinocytosis).[26] The exact mechanism

of endocytosis of HA-ChNP was evaluated. HCT-116 cells were pre-treated with specific endocytosis inhibitors (chlorpromazine, genistein, and amiloride) followed by green fluorescent FITC labeled HA-FITC-ChNPs. As a control, HCT-116 cells were treated with only HA-FITC-ChNPs without any pre-treatment with endocytosis inhibitors. Cellular internalization of HA-FITC-ChNPs was visualized by CLSM.

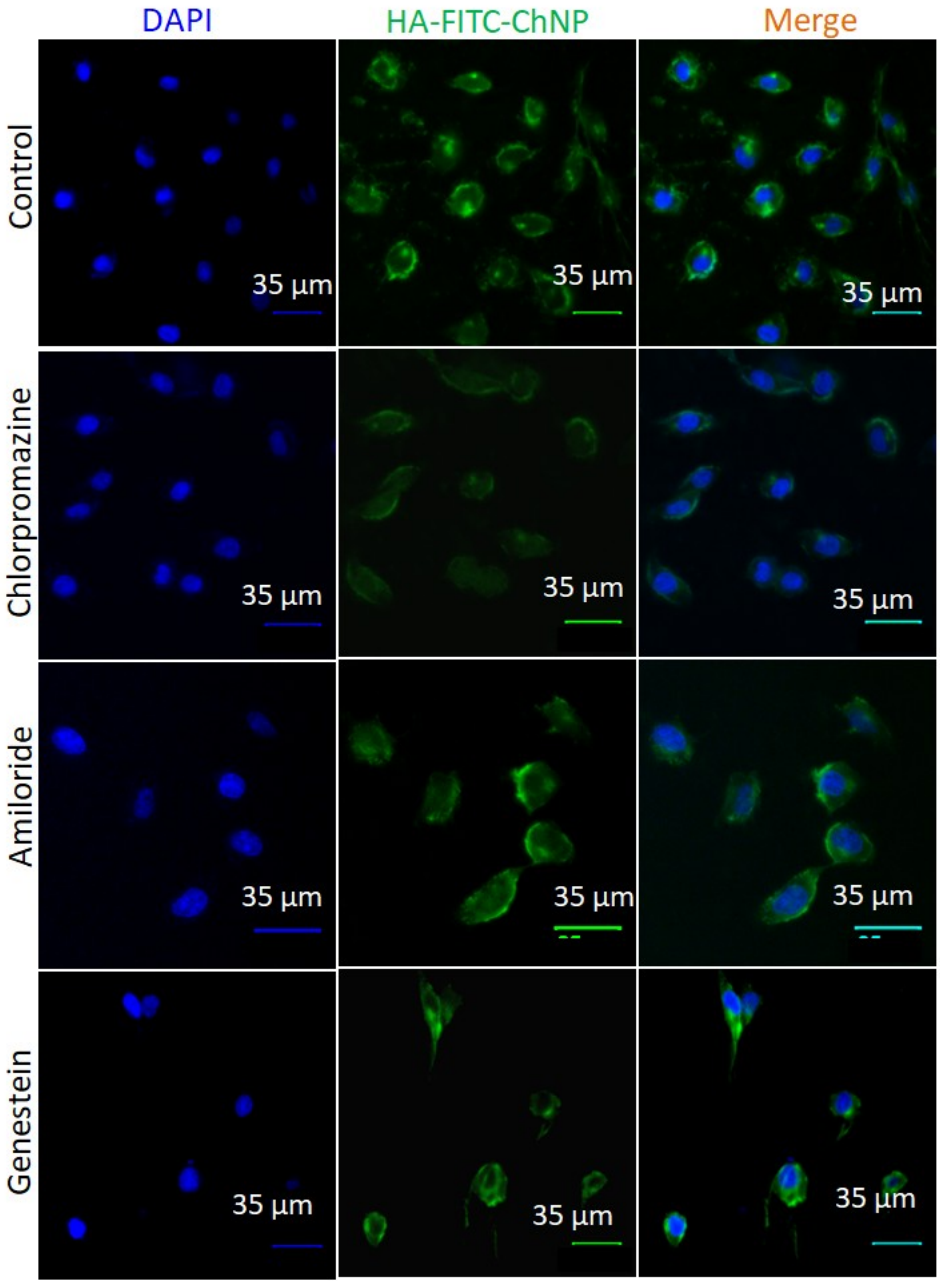

Fig. 8 CLSM images of FITC-HA-ChNPs internalized into HCT-116 cells after treatment with chlorpromazine, amiloride and genistein for 2 h. Nuclei were stained with DAPI (blue). Scale bar = 35 µm.

Confocal microscopy images in Fig. 8 evidently showed that genistein and amiloride treated cells engulfed HA-FITC-ChNPs similarly like control cells. However, chlorpromazine pre-treated cells showed remarkable reduction in HA-FITC-ChNP internalization. The mechanism of endocytosis was further evaluated by flow cytometric analysis. HCT-116 cells were pre-treated with endocytosis inhibitors (chlorpromazine, genistein and amiloride) followed by treatment with HA-FITC-ChNPs. The FITC labelled cells were quantified by fluorescence activated cell sorting (FACS) assay. The FACS data clearly demonstrated that genistein treated cells internalized HA-FITC-ChNPs as good as control cells (treated with HA-FITC-ChNPs only without any inhibitor pre-treatment). However, interestingly chlorpromazine and amiloride treated cells reduced HA-FITC-ChNPs uptake remarkably up to 94.5 % and 47.2 % respectively (Fig. 9).

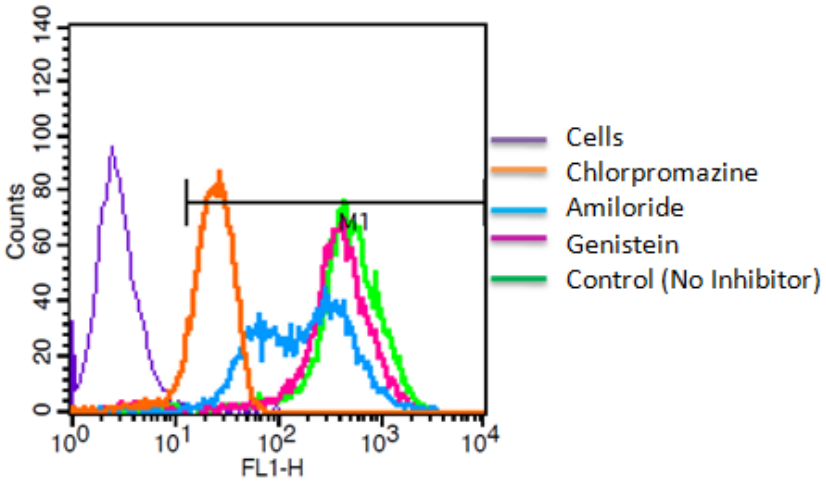

Fig. 9 Flow cytometry analysis of HCT-116 cells pre-treated with chlorpromazine, amiloride and genistein followed by treatment with FITC-HA-ChNPs.

From these microscopy and cell sorting analysis, it was confirmed that HCT-116 cells taken up HA-FITC-ChNPs by a combination of clathrin-mediated endocytosis and macropinocytosis mechanism and home them into lysosomes.

We hypothesized that hyaluronic acid coating over the chimeric nanoparticle containing MAPK-PI3K signaling inhibitors will help them to internalize by the interaction with CD44 receptor over-expressed on colon cancer cells. In our previous study we screened a panel of

colon cancer cells and observed that HCT-116 cells highly over-expressed CD44 receptors.[18] To evaluate our hypothesis, we pre-treated HCT-116 cells with hyaluronic acid to saturate the CD44 receptors followed by incubation with HA-FITC-ChNPs. The control cells were treated with only HA-FITC-ChNPs without pre-treatment with HA. The internalization of green fluorescent HA-FITC-ChNPs was observed by high-resolution CLSM.

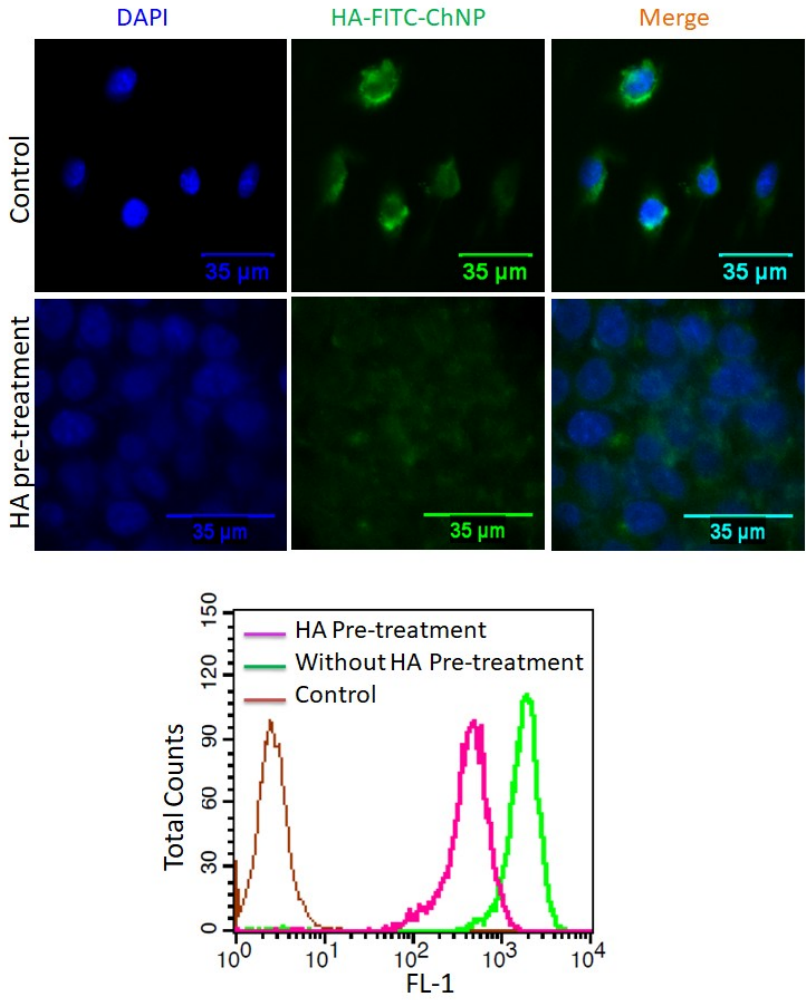

Fig. 10 Cellular internalization of HA-FITC-ChNPs in HCT-116 cell pre-treated with and without hyaluronic acid determined by (a) confocal laser scanning microscopy (CLSM) and (b) Flow cytometry (FACS). Scale bar = 20 µm.

From Fig. 10a, it was clearly observed that HA pre-treated cells internalized highly reduced amount of HA-FITC-ChNPs giving considerably less green fluorescence signal in confocal microscopy. Whereas, without any HA pre-treatment, HCT-116 cells engulfed a large amount of HA-FITC-ChNPs giving rise to high fluorescence intensity in microscopy. Furthermore,

the confocal imaging data was validated with FACS analysis. After pre-treatment with HA followed by HA-FITC-ChNP incubation, the fluorescently labeled HCT-116 cells were quantified by flow cytometry. It was observed from the FACS analysis that HA pre-treated cells were labeled with HA-FITC-ChNPs remarkably less. On the other hand, non-HA pre-treated cells were highly labeled with green fluorescence from HA-FITC-ChNP internalization (Fig. 10b). From these fluorescence microscopy and cell sorting analysis, it was established that HA-FITC-ChNPs were internalized into lysosomes of HCT-116 cells through HA-CD44 interaction mediated endocytosis.

5.2.4 Inhibition of PI3K and MAPK signaling: It was hypothesized that after internalization into acidic lysosomes, HA-ChNPs will release AZD6244 and PI103 for simultaneous inhibition of MAPK-PI3K signalinghub. To validate our hypothesis, we treated HCT-116 cells with HA-ChNPs for 24 h and the expression of MAPK and PI3K signaling proteins were evaluated by western blot analysis. Phosphorylation of extracellular signal regulated kinase (ERK) in MAPK signaling cascade would expect to be inhibited by AZD6244 through perturbation of MEK. From western blot images in Fig. 11a, it was observed that expression of p-ERK was highly reduced after treatment with HA-ChNPs whereas keeping the amount of total ERK unperturbed. Quantification from the protein expression analysis also validated that HA-ChNPs reduced the expression of p-ERK in 2.5 folds compared to non-nanoparticle treated control cells (Fig. 11b). On the other hand, PI103 was expected to inhibit PI3K signaling by inhibiting phosphorylation of Akt. To evaluate the effect of nanoparticle on PI3K signaling, we treated HCT-116 cells with HA-ChNPs for 24 h and the expression of p-Akt was determined by western blot analysis. The gel-electrophoresis in Fig. 11a, clearly demonstrated that HA-ChNP reduced the expression of p-Akt keeping the total amount of Akt protein same. Further quantification from western blot showed that HA-ChNPs reduced the expression of p-Akt nearly 1.5 folds compared to control cells (Fig. 11b). Finally, we evaluated the effect of cisplatin-mediated DNA damage in HCT-116 cells. Poly (ADP-ribose) polymerase (PARP) family proteins are upregulated as a consequence of DNA damage in cancer cells, making them the markers for DNA damage.[27, 28] HCT-116 cells were treated with HA-ChNPs for 24 h and the expression of PARP was visualized through western blot

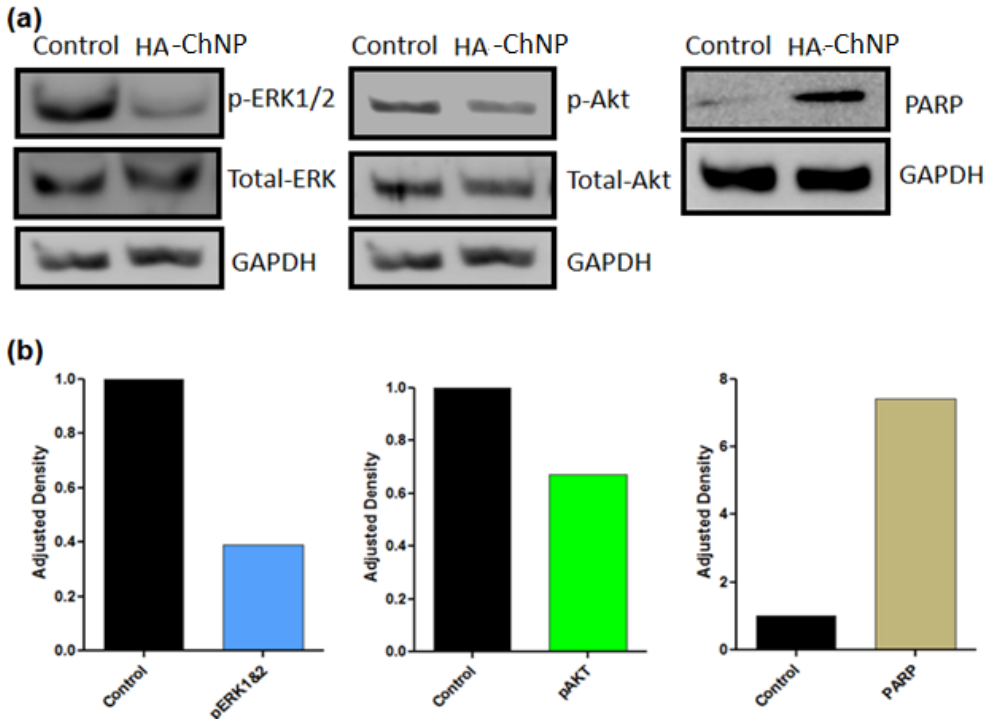

Fig. 11 (a) Western blot analysis of p-ERK1/2, total ERK, pAKT, Total AKT and PARP as markers for MAPK inhibition, PI3K inhibition and DNA damage in HCT-116 cells respectively. Quantification of expression of (b) p-ERK1/2, pAKT and PARP from western blot analysis in HCT-116 cells after treatment with HA-ChNPs for 24 h.

analysis. The gel electrophoresis showed that HA-ChNPs increased the expression of PARP through DNA damage (Fig. 11a). Further quantification from western blot revealed that HA-ChNPs increased the expression of PARP by 7.4 folds compared to the non-nanoparticle treated cells (Fig. 11b). These gel electrophoresis studies evidently confirmed that HA-ChNPs inhibited MAPK-PI3K signaling hub simultaneously with DNA damage in colon cancer cells.

5.2.5 Cell cycle arrest and apoptosis: Inhibition of MAPK-PI3K signaling hub along with DNA damage leads to cell cycle arrest.[29, 30] We assessed the potential of HA-ChNPs to arrest the colon cancer cells into their cell cycle. HCT-116 cells were treated with HA-ChNPs for 24 h followed by staining the cellular DNA with propidium iodide (PI) and quantified the cells in different stages of cell cycle through FACS analysis. The flow cytometry analysis in Fig. 12a revealed that HA-ChNP treated cells were in G0/G1, S and G2/M phase in 87.86 %, 6.39 % and 4.9 % respectively. Whereas, control cells were found to be in G0/G1, S and

G2/M phase in 24.26 %, 11.65 % and 65.45 % respectively. From this FACSanalysis it was confirmed that HA-ChNPs stalled the cell cycle in G0/G1 phase in HCT-116 cells.

Cell cycle arrest into G0/G1 phase would lead the cancer cells into programmed cell death or apoptosis.[26] We further evaluated the induction of apoptosis by HA-ChNPs through flow cytometry analysis. HCT-116 cells were treated with HA-ChNPs for 24 h and the phosphatidylserine flipped at the outer surface of the apoptotic cells were stained with green fluorescent FITC labeled Annexin V. The DNA of the late apoptotic and necrotic cells was counter stained with red fluorescent propidium iodide (PI). The cells in different apoptotic and necrotic stages were quantified with cell sorting analysis.

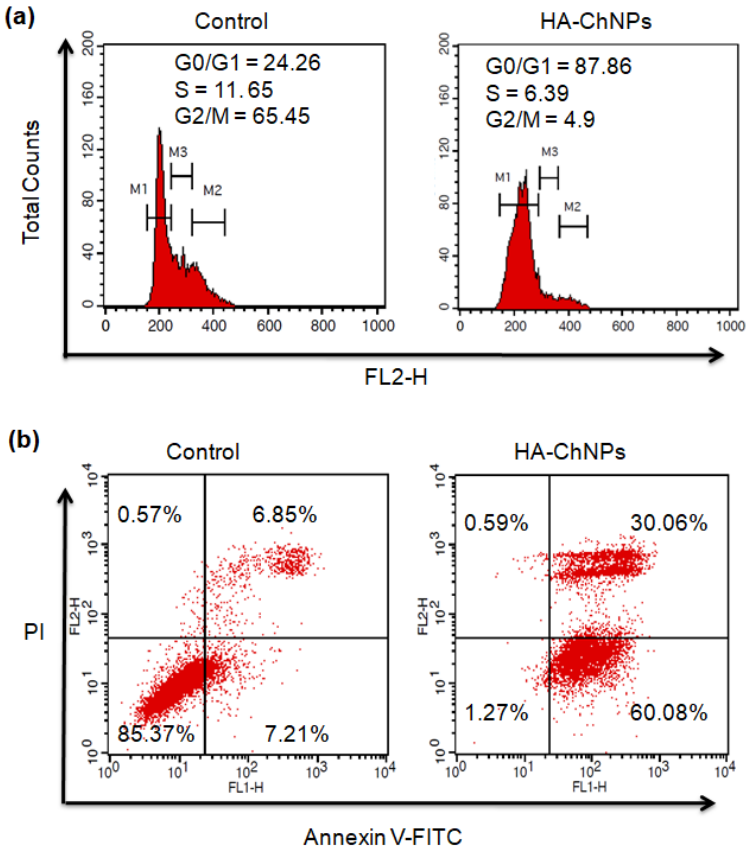

Fig. 12 Flow cytometry analysis to evaluate the effect of HA-ChNPs in inducing apoptosis (a) and cell cycle arrest (b) in HCT-116 cells at 24 h.

The FACS analysis in Fig. 12b demonstrated that HA-ChNPs induced a remarkably higher number of cells into early (60.08 %) and late (30.06 %) apoptosis. On the other hand, non-nanoparticle treated control cells showed only 7.21 % and 6.85 % cells in early and late apoptotic stages respectively. This FACS data clearly confirmed that HA-ChNP mediated

inhibition of MAPK-PI3K signaling hub in combination with DNA damage followed by cell cycle arrest in G0/G1 phase triggered the colon cancer cells into apoptosis.

5.2.6 Cell viability assay: One of the hallmarks of cancer is to resist programmed cell death or apoptosis.[31] Hence, induction of apoptosis to the cancer cells would lead to cell death. We evaluated the potential of HA-ChNPs to trigger cell death in colon cancer cells. HCT-116 cells were treated with HA-ChNPs in a dose-dependent manner over 24 h and the amount of viable cells was determined by MTT assay. As a control we treated HCT-116 cells with the cocktail of free inhibitors (AZD6244 and PI103) and cisplatin in the same ratio present in HA-ChNPs (AZD6144: PI103: CDDP = 1.5: 1.4:1).

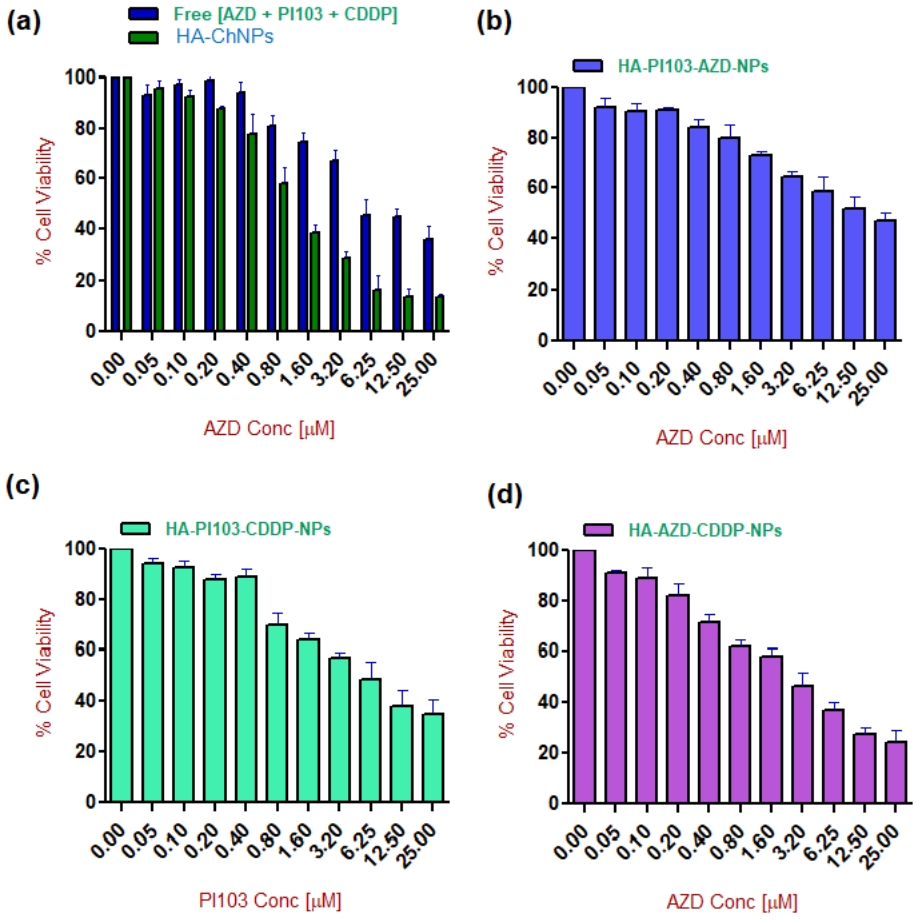

Fig. 13 Concentration dependent cell viability assay of HA-ChNPs in HCT-116 (a) at 24 h post-incubation compared to free drug cocktail, HA-PI103-AZD-NPs (b), HA-PI103-CDDP-NPs, and HA-AZD-CDDP-NPs (d) at 24 h post-incubation in HCT-116 cells determined by MTT assay. Data represent mean ± SEM, n = 3.

It was found that HA-ChNPs killed HCT-116 cells with extremely reduced IC_{50} = 0.91 ± 0.09 µM with only 13.7 ± 1.2 % viable cells at 25 µM concentration of AZD6244 (Fig. 13a). Whereas, combination of free AZD6244, PI103 and cisplatin cocktail showed much higher IC_{50} = 5.7 ± 0.8 µM with high cell viability (35. 7 ± 5.8 %) at 25 µM concentration of AZD6244. To assess those HA-ChNPs were more effective compared to their dual drug-loaded counterparts; we synthesized HA-AZD-PI103-NPs, HA-PI103-CDDP-NPs and HA-AZD-CDDP-NP by using the same method and having same drug loading. We further treated HCT-116 cells with HA-coateddualdrug-loaded nanoparticles in a dose-dependent manner for 24 h, and cell viability was quantified by MTT assay. Interestingly, it was observed that HA-AZD-PI103-NPs, HA-PI103-CDDP-NPs and HA-AZD-CDDP-NPs, showed much higher IC_{50} = 13.0 ± 1.13 µM, 6.05 ± 0.86 µM and 2.96 ± 0.33 µM, respectively compared to HA-ChNPs (Fig. 13 b-d). Moreover, HA-AZD-CDDP-NPs, HA-AZD-PI013-NPs and HA-PI103-CDDP-NPs demonstrated much less efficacy in killing HCT-116 cells in the highest concentration (25 µM) indicated by high cell viability = 24.6 ± 4.4 %, 47.2 ± 3.1 % and 34.9 ± 5.7 %.

One of the major challenges of targeting MAPK-PI3K signaling hubs in cancer cells specifically is not to induce any off-target toxicity to the healthy cells. To address this issue, we further evaluated the effect of HA-ChNPs on L929 fibroblast cells. L929 cells were incubated with HA-ChNPs in a dose-dependent manner for 24 h, and the cellular viability was measured by MTT assay. Interestingly, it was found that HA-ChNPs showed almost no toxicity to the fibroblast cells even at highest concentration (cell viability = 107.1 ± 4.5 % at 25 µM concentration of AZD6244) (Fig.14).

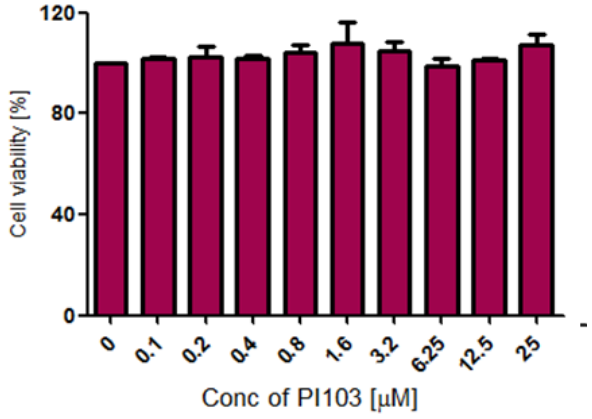

Fig. 14 Concentration dependent cell viability assay of HA-ChNPs in L929 at 24 h post-incubation.

From these cell viability assays, it was confirmed that HA-ChNPs showed remarkable efficacy in HCT-116 colon cancer cells compare to free drug cocktail as well as HA-coated dual drug-loaded nanoparticles. Moreover, HA-ChNPs showed negligible toxicity towards healthy fibroblast cells to show their benign nature towards non-cancerous cells.

5.3 Conclusion

In this chapter, hyaluronic acid coated chimeric nanoparticles comprising PI103 (P13K inhibitor) AZD6244 (MAPK inhibitor) and cisplatin (DNA damaging agent) were engineered having spherical morphology with the size less than 200nm. Colon cancer cells (HCT-116) engulfed these HA-ChNPs through CD44 receptor-mediated and clathrin-dependent endocytosis to localize into sub-cellular lysosomes. HA-ChNPs simultaneously inhibited PI3K and MAPK signaling pathways in HCT-116 cells along with DNA damage. Inhibition of MAPK-PI3K signaling hub with DNA damage triggered apoptosis and arrested cells in G0/G1 phase. Finally, HA-ChNPs showed remarkable colon cancer cell death than the free drug cocktail keeping healthy fibroblast cells unharmed.

5.4 Materials and Methods

5.4.1 Material: All the chemicals, reagents, and solvents required for synthesis of cholesterol-drug conjugates and HA-ChNPs, cisplatin, 3-(4, 5-dimethylthiazol-2-yl)-2,5-diphenyltetrazolium bromide (MTT), DAPI and propidium iodide for cell cycle analysis were purchased from Sigma-Aldrich. PI103 and AZD6244 were purchased from Selleck Chemicals. DSPE-PEG2000 and mini extruder were procured from Avanti Polar Lipids Inc. Cell culture media, LysoTracker DND-26, and SlowFade antifade reagents were bought from Life Technologies. HCT116 cells were obtained from National Centre for Cell Science (NCCS), Pune. Anti phospho-Akt(Thr308) rabbit monoclonal antibody, Anti-ERK 1/2 phospho monoclonal antibody, anti-AKT antibody, anti ERK1/2 antibody, anti-GAPDH antibody, HRP goat anti-mouse IgG antibody and apoptosis detection kit were purchased from Bio Legend.

5.4.2 Synthesis of Cholesterol-drug-Conjugates

5.4.2.1 Synthesis of Cholesterol-AZD6244 Conjugate (2): Cholesterol-succinic acid conjugate (1) was synthesized from cholesterol by using the procedure previously described

in ref 22. A mixture of compound 1 (5 mg, 0.01 mmol), EDCI (5.68 mg, 0.015mmol), and DMAP (2.5 µL, 0.015 mmol) in dry DMF (2 mL) was reacted for 10 min. AZD6244 (6.9 mg, 0.012 mmol) was added and reacted for 24 h. To quench the reaction, 0.1 N HCl solution was added. The organic layer was washed with water (10 mL × 2). Then the collected organic solvent was dried and product was purified by silica gel column with dichloromethane/methanol as the eluent to afford a pure cholesterol-AZD6244 conjugate (4). Yield = 70%.

^{1}H NMR (400 MHz, $CDCl_3$): δ = 8.91 (s, 1H), 8.23 (s, 1H), 8.00 (s, 1H), 8.05 (s, 1H), 7.49 (d, J = 2.2 Hz, 1H), 7.16-7.18 (dd, J = 8.8, 2.2 Hz, 1H), 6.55 – 6.52 (m, 1H), 5.35 (s, 1H), 4.59 (s, 2H), 4.23 (m, 2H), 3.93 (s, 3H), 2.66 (s, 2H), 2.39 (s, 1H), 2.29 (d, J = 7.6 Hz, 2H), 2.01– 1.8 (m, 4H), 1.57 – 1.41 (m, 14H), 1.25 (m, 3H), 1.11 (m, 7H), 0.99 (s, 4H), 0.85 – 0.92 (m, 10H), 0.67 (s, 3H) (Fig. 15).

^{13}C NMR (101 MHz, $CDCl_3$): δ = 172.34, 147.37, 139.70, 139.62, 131.69, 130.23, 124.96, 122.97, 122.46, 117.99, 116.26, 116.22, 111.29, 109.52, 77.16, 74.88, 73.98, 62.37, 59.67, 56.83, 56.27, 50.15, 42.46, 39.86, 39.66, 38.30, 38.20, 37.07, 36.72, 36.33, 35.94, 32.04, 31.98, 31.78, 31.39, 29.85, 29.64, 29.61, 28.37, 28.17, 27.87, 24.42, 23.97, 22.97, 22.71, 21.16, 19.43, 18.86, 11.57 (Fig. 16).

^{19}F NMR (376 MHz, CDCl3): δ = -129.16 (Fig. 17). **MALDI-TOF (m/z):** Calculated mass = 924.3604 for $C_{48}H_{63}BrClFN_4O_6$, observed = 925.4789 for $C_{48}H_{64}BrClFN_4O_6$ $[M+H]^+$ (Fig. 18).

5.4.2.2 Synthesis of Cholesterol-PI103-Conjugate (3) and cholesterol-cisplatin conjugate (4): Compound 3 and 4 were synthesized by following the procedure described section 3.4.2, 3.4.4 and 3.4.5 in chapter 3.

5.4.2.3 Synthesis of Cholesterol-Ethylenediamine Conjugate (5): Conjugate 6 was synthesized as explained in the ref 32. Briefly, 140 µL (2.2 mmol, 10 Equiv) Ethylenediamine was added into RB flask containing 3 mL of anhydrous DCM followed by cooling down to 0–5 °C with ice. 100 mg of cholesterol chloroformate (0.22 mmol, 1.0 Equiv) was taken in anhydrous DCM, and this solution was slowly added dropwise to above mixture under continuous stirring. After 24 h stirring, the reaction was worked up using water

(30 mL × 3) and DCM (30 mL), and the collected organic layer was dried over anhydrous sodium sulfate and evaporated with the help of a rotary evaporator. Light yellow colored oily product (compound 5) was purified by silica gel column with dichloromethane/methanol as the eluent to afford a pure cholesterol-$EtNH_2$ conjugate (5). Yield = 76%.

5.4.2.4 Synthesis of Cholesterol-FITC Conjugate (6): 10 mg (0.0211 mmol, 1.0 Equiv) of conjugate 5 was added in to 3 mL of anhydrous DMF. To this solution 12.3 mg (0.031 mmol, 1.5 Equvi) of FITC was added followed by adding 3.6 µL (2.2 mmol, 10 Equiv) of DIPEA under rigorous stirring. After 24 h of continuous stirring, the reaction was worked up using water (30 mL × 3) and DCM (30 mL), and the collected organic layer was dried over anhydrous sodium sulfate and evaporated with the help of a rotary evaporator. The resulted light green colored product was purified by silica gel column with dichloromethane/methanol as the eluent to afford a pure cholesterol-FITC conjugate (6). Yield = 60.23%.

^{1}H NMR (400 MHz, MeOD): δ = 7.80 (s, 1H), 7.58 (d, J = 7.7 Hz, 1H), 7.16 – 7.23 (m, J = 16.4, 8.8 Hz, 3H), 6.57 (s, 1H), 6.55 (s, 3H), 5.22 (s, 1H), 3.81 – 3.68 (m, 2H), 3.46 – 3.35 (m, J = 6.5 Hz, 2H), 2.23 (s, 1H), 2.02 (s, 1H), 1.96 – 1.77 (m, 4H), 1.78 – 1.64 (m, 2H), 1.63 – 1.47 (m, J = 6.9 Hz, 3H), 1.47 – 1.33 (m, 8H), 1.33 – 1.24 (m, 3H), 1.22 – 1.08 (m, 5H), 0.99 – 0.84 (m, 14H), 0.68 (s, 3H) (Fig. 19).

^{13}C NMR (101 MHz, MeOD): δ = 182.81, 180.80, 173.47, 160.16, 160.11, 141.44, 132.93, 132.80, 126.46, 126.36, 123.67, 123.52, 123.49, 114.46, 114.37, 104.60, 104.51, 100.95, 75.74, 58.59, 58.19, 57.83, 51.71, 49.00, 47.21, 45.12, 43.69, 41.31, 40.90, 39.95, 38.31, 37.76, 37.60, 37.37, 35.52, 33.99, 33.31, 33.02, 29.53, 29.35, 25.49, 25.24, 24.36, 23.40, 23.15, 22.30, 19.93, 19.48, 12.50 (Fig. 20).

MALDI-TOF (m/z): Calculated mass = 861.4387 for $C_{51}H_{63}N_3O_7S$, observed = 862.73 for $C_{51}H_{64}N_3O_7S$ $[M+H]^+$ (Fig. 21).

5.4.3 Synthesis of Hyaluronic acid coated Chimeric Nanoparticles (HA-ChNPs): Firstly, 6.0 mg of PC, 3 mg of conjugate 5, 1 mg of each drug conjugate compound 2, 3, and 4; and 0.6 mg of DSPE-PEG2000 were dissolved in DCM. ChNPs were synthesized by the method described in the section 5.4.3 in chapter 4a.[22]. Further, Hyaluronic acid coating of ChNPs was carried out as mentioned in chapter 4b. Briefly, to the above resulted ChNPs solution, 0.5 mL

of (0.5 mg/mL) hyaluronic acid (HA) solution was added dropwise under rigorous stirring. After 10 minutes, hyaluronic acid coated ChNPs (HA-ChNPs) were centrifuged at 45,000 X g. The HA-ChNPs pellets were washed with water to remove the excess hyaluronic acid. HA-ChNPs were re-suspended in water and stored at 4 °C for further use.

5.4.4 Size, surface charge, shape and morphology determination of HA-ChNPs: Hydrodynamic diameter and surface charge of ChNPs and HA-ChNPs were determined by DLS. Size, shape and morphology of HA-ChNPs were visualized by AFM and FE-SEM. Sample preparation and instrumentation were performed followed by the methods described in section 2.4.4, 2.4.5, and 2.4.6 in chapter 2. Hydrodynamic diameter and surface charge from DLS were determined in triplicate**.**

5.4.5 Quantification of triple drug loading in HA-ChNPs: PI103, AZD6244 and cisplatin loading in HA-ChNPs were determined by UV-Vis spectroscopy at λ max = 296 nm, 267 nm, and 706 nm respectively from absorbance versus calibration curve. Drug loading was quantified in triplicate.

5.4.6 Determination of triple drug release from HA-ChNPs: The release of triple drugs (PI103, AZD6244, and cisplatin) from HA-ChNPs was determined by dialysis method as described in section 2.4.8 in chapter 2. The amount of PI103, AZD6244, and cisplatin released at predetermined time points were quantified by UV-Vis spectroscopy at λmax = 296, 267 nm and 706 nm respectively. Released PI103, AZD6244, and cisplatin in each time point were quantified in triplicate.

5.4.7 Cellular internalization study by confocal microscopy: 50,000 HCT116 cells were seeded on coverslips in a 6-well plate. After 24 h, cells were treated with HA-FITC-ChNPs at a FITC concentration of 2 µg/ mL at 37 °C for 1 h, 3 h, and 6 h. After each time points, the cells were washed with PBS and fixed with paraformaldehyde solution (4 %) for 15 min at 4 °C. Lysosomes and nucleus were stained by LysoTracker Red DND-99 and DAPI for 45 min and 5 min respectively. Cells were washed with PBS and mounted on a glass slide using 5 µL SlowFade diamond antifade reagent. The cells were visualized by confocal microscopy (Zeis LSM 710). HCT116 cells were pretreated with different endocytosis inhibitors followed by treatment with HA-FITC-ChNPs. For hyaluronic acid competitive inhibition study cells were incubated in 5 mg/mL hyaluronic acid in serum free media for 2h before adding the HA-FITC-ChNPs. The cellular internalization was further visualized by confocal microscopy.

5.4.8 Cellular internalization study by flow cytometry: HCT116 cells were treated with various endocytosis inhibitors (amiloride, genistein, and chlorpromazine at a concentration of 100 µM, 30 µM, and 37 µM respectively for 30 min at 37 °C. Control cells were incubated at 37 °C without any treatment of inhibitor. After washing with PBS incubation, HA-FITC-ChNPs (FITC concentration = 2 µg/mL) was added to the cells and incubated for2 h. For hyaluronic acid competitive inhibition study cells were incubated in 5 mg/mL hyaluronic acid in serum free media for 2h before adding the HA-FITC-ChNPs. Cells were trypsinized, followed by centrifugation at 1000 rpm at 4 °C for 5 min to remove dead cells. Finally, the fluorescently labelled cells were counted by using BD FACS Calibur.

5.4.9 Western blot analysis: 2 X 10^5 HCT116 cells were treated with HA-ChNPs for 24 h followed by cell lysis and suspension in sample buffer. Proteins were visualized by SDS-polyacrylamide gel electrophoresis (SDS-PAGE) using primary antibody solution (pAKT, AKT, pERK1/2, and ERK1/2 in 1:2000 dilution, and GAPDH in 1:5000 dilution) and then incubated in HRP conjugated secondary antibody solution (1:10000 dilution).

5.4.10 Detection of apoptosis by flow cytometry: Detection and quantification of apoptosis by flow cytometry was performed by the method described in section 4.4.15 in chapter 4a.

5.4.11 Cell Cycle Analysis: 2 × 10^6 cells were seeded and allowed to attach in a 6 well plate in a 5% CO2 incubator at 37 °C. Cells were treated with HA-ChNPs at a concentration corresponding to the IC_{50} value of respective drugs for 24 h. After the treatment, the cells trypsinized and washed with 1 mL of PBS (pH = 7.4) and then centrifuged at 1000 rpm for 5 min. Cells were fixed in 70% ice-chilled ethyl alcohol for 30 min at −20 °C. Fixed cells were centrifuged at 1000 rpm for 5 min, and fixing solution was replaced and washed with 1 mL ice-chilled PBS twice. Finally, cells were resuspended in 0.5 mL of the staining solution (50 µL of 1 mg mL−1 propidium iodide, 50 µL of 1 mg mL^{-1} RNase and 400 µL PBS) and FACS measurement was performed by using BD FACS Calibur.

5.4.12 *In vitro* cytotoxicity assay: 5 × 10^3 cells (HCT116) were seeded into 96-well and exposed with serial concentrations of HA-ChNPs. Free drugs stock solution with equal concentration present in NPs was prepared in DMSO. After 24 h incubation with HA-ChNPs, 20 µL of MTT (5 mg/mL) was added to each well and left it for 4 h. After 4 h, 100 µL of solubilization buffer (10% SDS in 0.01 M HCl) was added to each well and allowed overnight incubation to make the MTT crystals soluble. After overnight incubation, absorbance was measured with spectrophotometer at 540 nm, and the percent cell viability

was calculated considering the untreated cells as 100% viability. All the experiments were performed in triplicate.

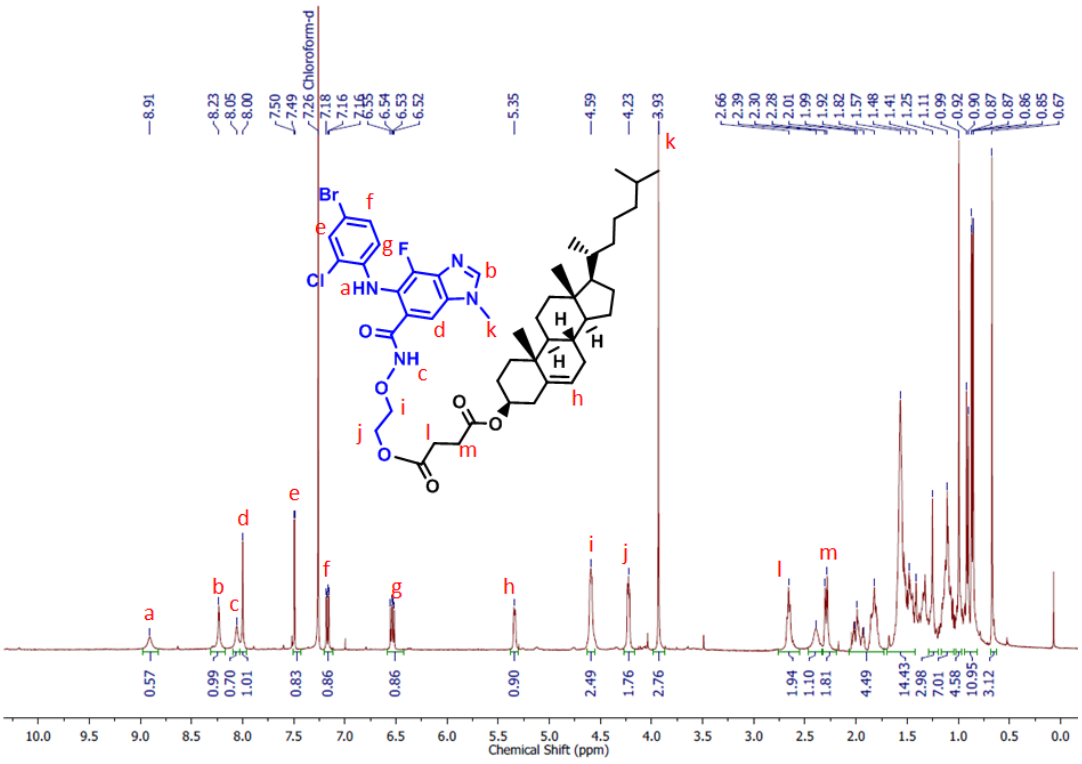

Fig. 15 ^{1}H NMR spectra of cholesterol-AZD6244 conjugate.

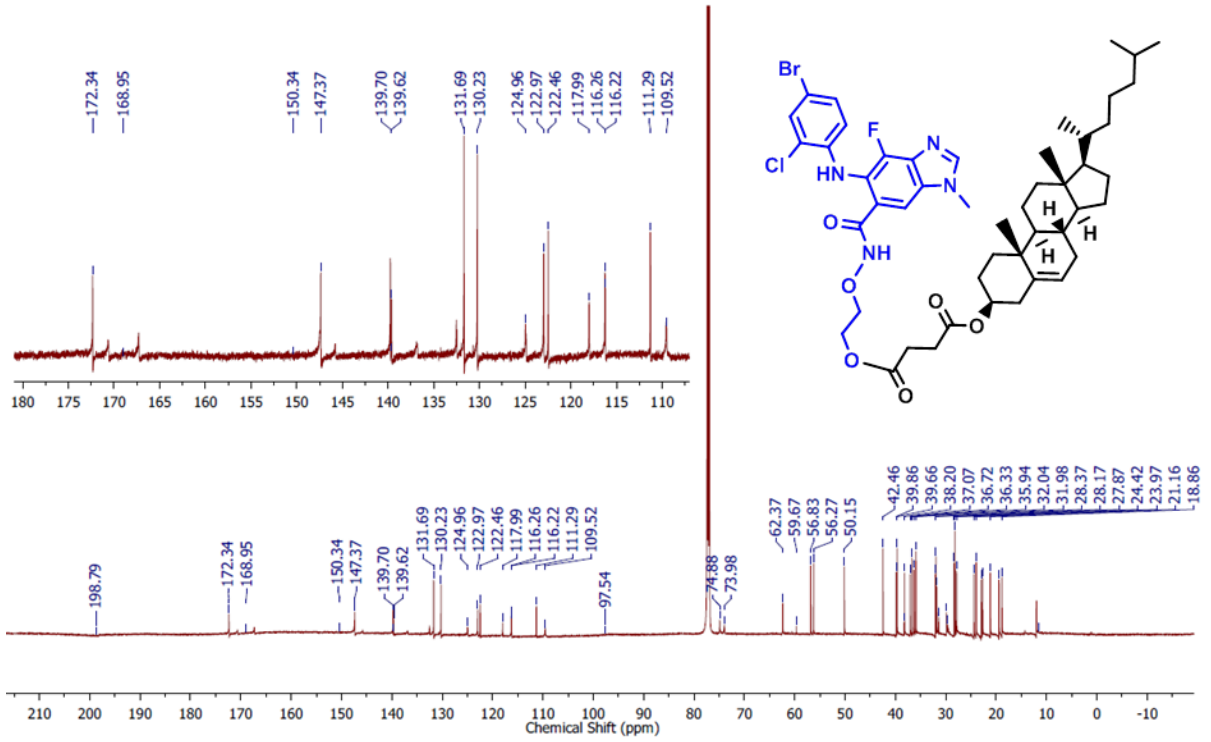

Fig. 16 ^{13}C NMR spectra of cholesterol-AZD6244 conjugate.

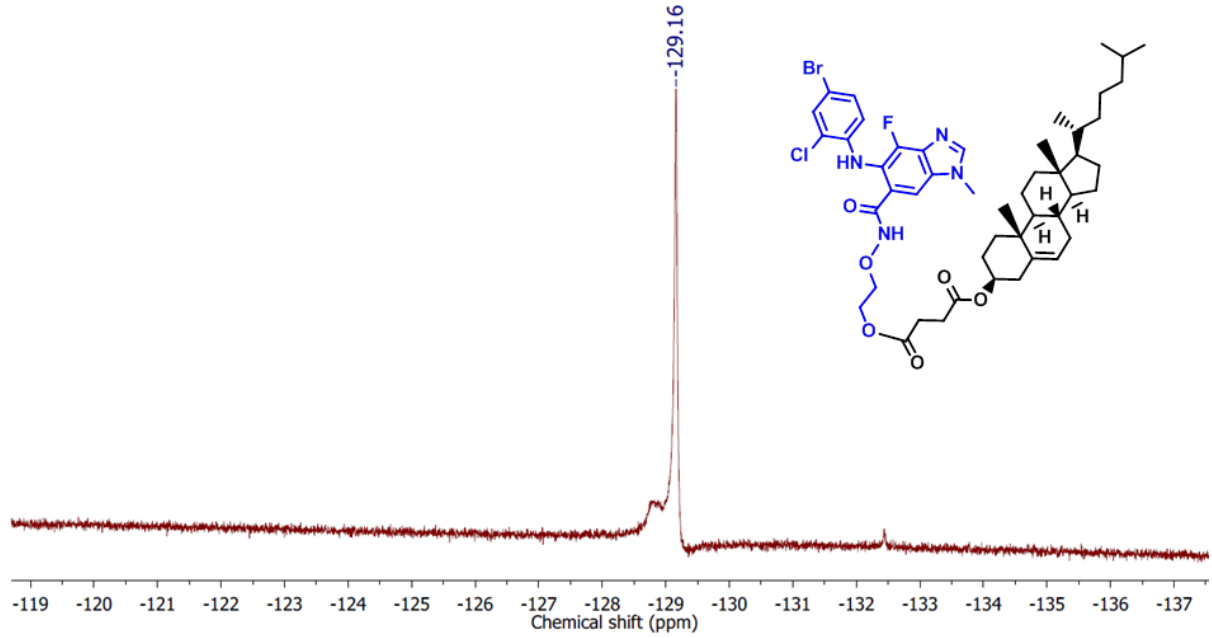

Fig. 17 ^{19}F NMR spectra of cholesterol-AZD6244 conjugate.

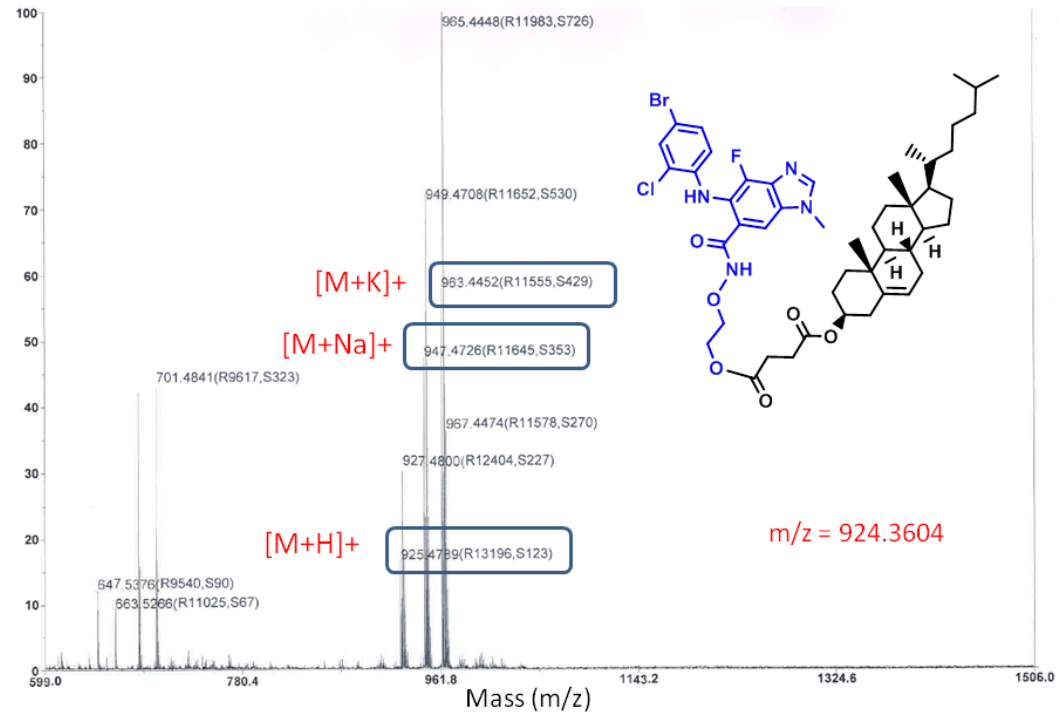

Fig. 18 MALDI-TOF spectra of cholesterol-AZD6244 conjugate.

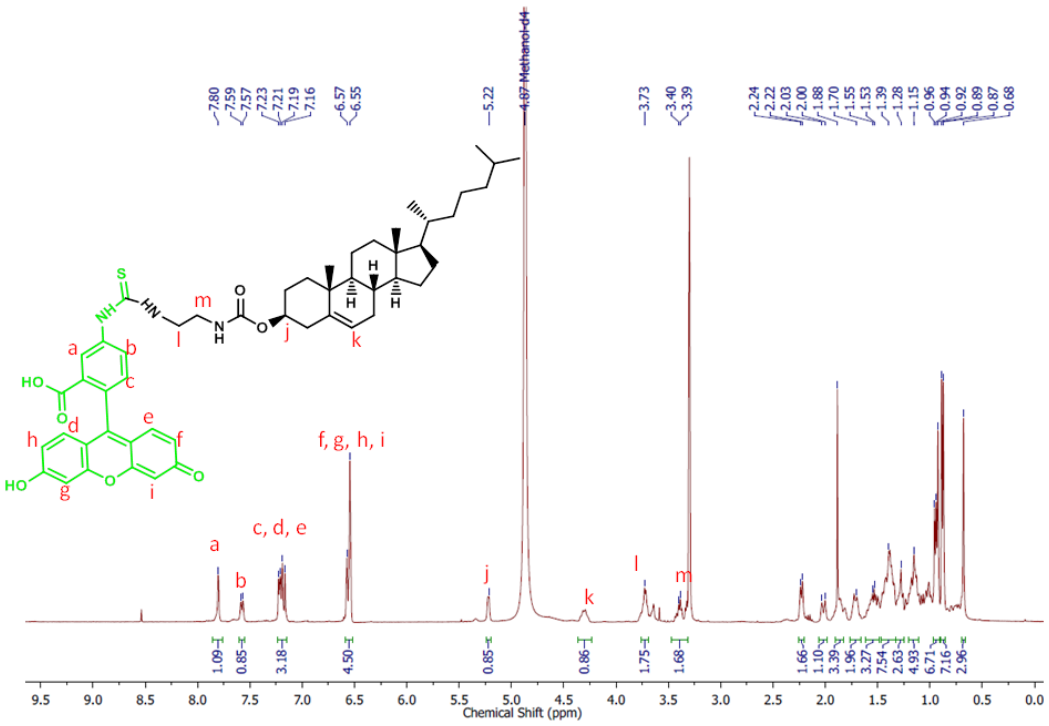

Fig. 19 ^{1}H NMR spectra of FITC-cholesterol conjugate.

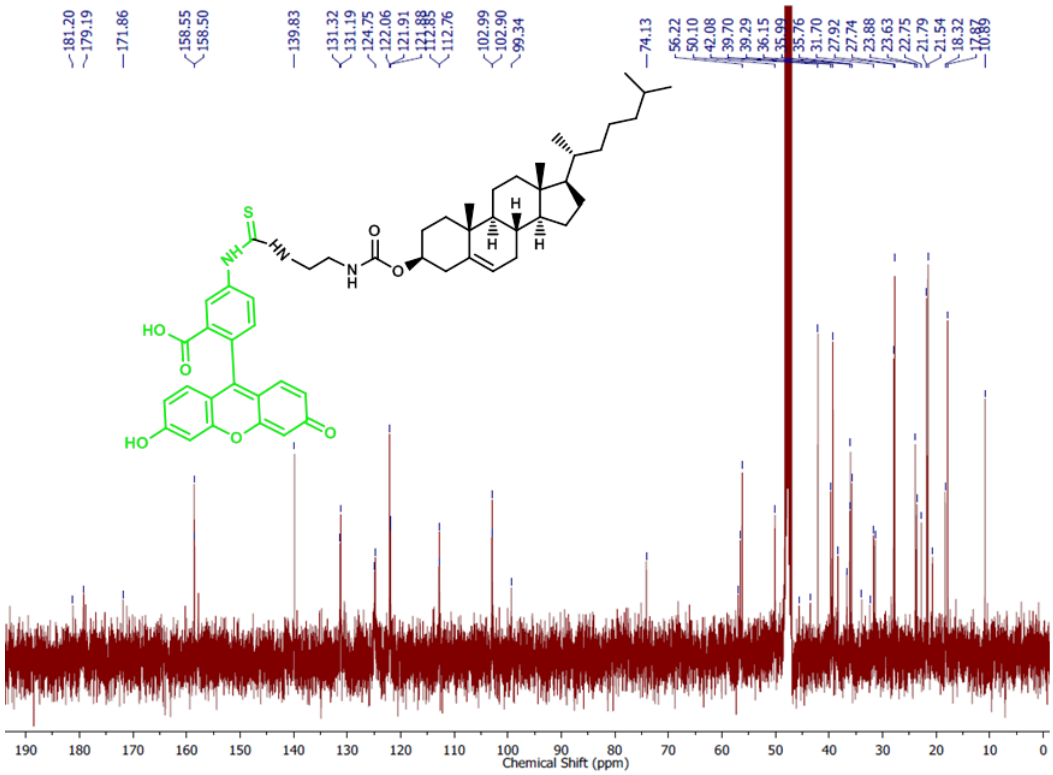

Fig. 20 ^{13}C NMR spectra of FITC-cholesterol conjugate.

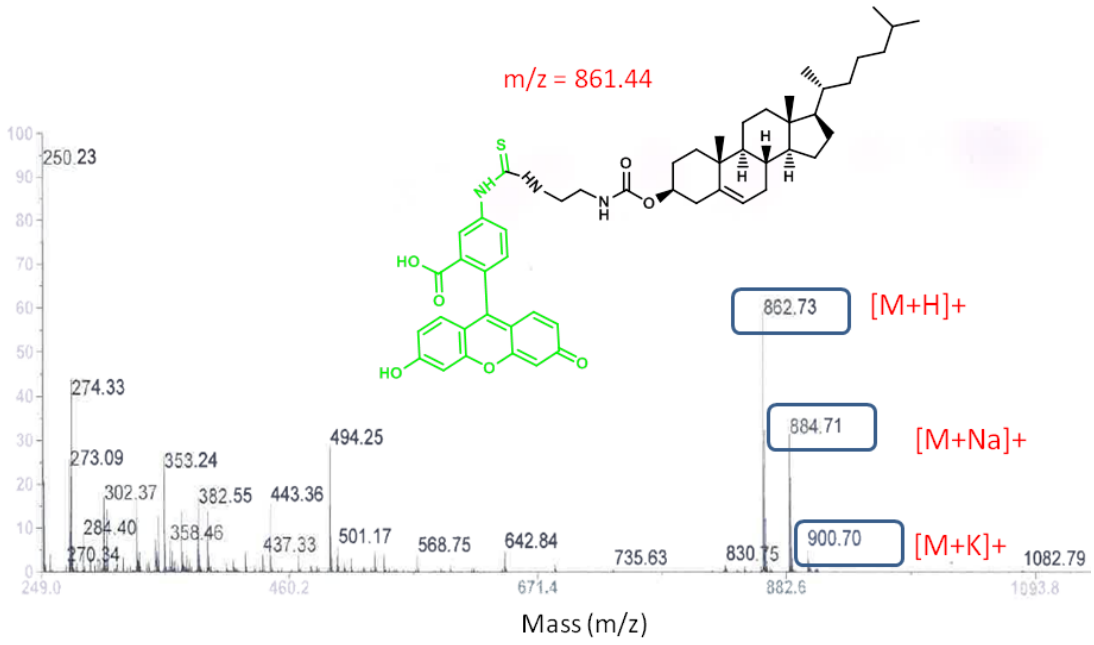

Fig. 21 MALDI-TOF spectra of FITC-cholesterol conjugate.

5.5 References

1. N. The Cancer Genome Atlas, *Nature*, 2012, **487**, 330-337.
2. Y. Samuels, Z. Wang, A. Bardelli, N. Silliman, J. Ptak, S. Szabo, H. Yan, A. Gazdar, S. M. Powell and G. J. Riggins, *Science*, 2004, **304**, 554-554.
3. *Nature*, 2012, **487**, 330-337.
4. M. O. Nandan and V. W. Yang, *Curr. Colorectal Cancer Rep.*, 2011, **7**, 113-120.
5. C. Holohan, S. Van Schaeybroeck, D. B. Longley and P. G. Johnston, *Nat. Rev. Cancer*, 2013, **13**, 714-726.
6. T. R. Wilson, J. Fridlyand, Y. Yan, E. Penuel, L. Burton, E. Chan, J. Peng, E. Lin, Y. Wang, J. Sosman, A. Ribas, J. Li, J. Moffat, D. P. Sutherlin, H. Koeppen, M. Merchant, R. Neve and J. Settleman, *Nature*, 2012, **487**, 505-509.
7. P. L. Bedard, A. R. Hansen, M. J. Ratain and L. L. Siu, *Nature*, 2013, **501**, 355-364.
8. A. B. Turke, Y. Song, C. Costa, R. Cook, C. L. Arteaga, J. M. Asara and J. A. Engelman, *Cancer Res.*, 2012, **72**, 3228-3237.
9. K. E. O'Reilly, F. Rojo, Q.-B. She, D. Solit, G. B. Mills, D. Smith, H. Lane, F. Hofmann, D. J. Hicklin and D. L. Ludwig, *Cancer Res.*, 2006, **66**, 1500-1508.
10. C. D. Britten, *Cancer Chemother. Pharmacol.*, 2013, **71**, 1395-1409.
11. R. J. Shaw and L. C. Cantley, *Nature*, 2006, **441**, 424-430.
12. H. Davies, G. R. Bignell, C. Cox, P. Stephens, S. Edkins, S. Clegg, J. Teague, H. Woffendin, M. J. Garnett, W. Bottomley, N. Davis, E. Dicks, R. Ewing, Y. Floyd, K. Gray, S. Hall, R. Hawes, J. Hughes, V. Kosmidou, A. Menzies, C. Mould, A. Parker, C. Stevens, S. Watt, S. Hooper, R. Wilson, H. Jayatilake, B. A. Gusterson, C. Cooper, J. Shipley, D. Hargrave, K. Pritchard-Jones, N. Maitland, G. Chenevix-Trench, G. J. Riggins, D. D. Bigner, G. Palmieri, A. Cossu, A. Flanagan, A. Nicholson, J. W. C. Ho, S. Y. Leung, S. T. Yuen, B. L. Weber, H. F. Seigler, T. L. Darrow, H. Paterson, R. Marais, C. J. Marshall, R. Wooster, M. R. Stratton and P. A. Futreal, *Nature*, 2002, **417**, 949-954.
13. K. Zitzmann, J. von Rüden, S. Brand, B. Göke, J. Lichtl, G. Spöttl and C. J. Auernhammer, *Cancer Lett.*, 2010, **295**, 100-109.
14. D. Marklein, U. Graab, I. Naumann, T. Yan, R. Ridzewski, F. Nitzki, A. Rosenberger, K. Dittmann, J. Wienands, L. Wojnowski, S. Fulda and H. Hahn, *PLoS ONE*, 2012, **7**, e52898.

15. D. Opel, M.-A. Westhoff, A. Bender, V. Braun, K.-M. Debatin and S. Fulda, *Cancer Res.*, 2008, **68**, 6271-6280.
16. S. Y. Yang, A. Miah, K. M. Sales, B. Fuller, A. M. Seifalian and M. Winslet, *Int. J. Oncol.*, 2011, **38**, 1695-1702.
17. H. Richly, B. Henning, P. Kupsch, K. Passarge, M. Grubert, R. Hilger, O. Christensen, E. Brendel, B. Schwartz and M. Ludwig, *Ann. Oncol.*, 2006, **17**, 866-873.
18. S. Palvai, M. M. Kuman and S. Basu, *J. Mater. Chem. B*, 2017, **5**, 3658-3666.
19. E. C. Dreaden, Y. W. Kong, S. W. Morton, S. Correa, K. Y. Choi, K. E. Shopsowitz, K. Renggli, R. Drapkin, M. B. Yaffe and P. T. Hammond, *Clinic. Cancer Res.*, 2015, **21**, 4410-4419.
20. L. Shao, R. Zhang, J. Lu, C. Zhao, X. Deng and Y. Wu, *ACS Appl. Mater. Interfaces*, 2017, **9**, 1226-1236.
21. H. S. Jung, W. H. Kong, D. K. Sung, M.-Y. Lee, S. E. Beack, D. H. Keum, K. S. Kim, S. H. Yun and S. K. Hahn, *ACS Nano*, 2014, **8**, 260-268.
22. S. Palvai, P. More, N. Mapara and S. Basu, *ACS Appl. Mater. Interfaces*, 2015, **7**, 18327-18335.
23. X.-y. Yang, Y.-x. Li, M. Li, L. Zhang, L.-x. Feng and N. Zhang, *Cancer Lett.*, 2013, **334**, 338-345.
24. H. Shen, S. Shi, Z. Zhang, T. Gong and X. Sun, *Theranostics*, 2015, **5**, 755-771.
25. T. H. Tran, J. Y. Choi, T. Ramasamy, D. H. Truong, C. N. Nguyen, H.-G. Choi, C. S. Yong and J. O. Kim, *Carbohydrate Polymers*, 2014, **114**, 407-415.
26. S. Mayor and R. E. Pagano, *Nat. Rev. Mol. Cell Biol.*, 2007, **8**, 603-612.
27. A. Ciccia and S. J. Elledge, *Mol. Cell*, 2010, **40**, 179-204.
28. N. J. Curtin, *Nat. Rev. Cancer*, 2012, **12**, 801-817.
29. S. Meloche and J. Pouyssegur, *Oncogene*, 0000, **26**, 3227-3239.
30. S. K. Roy, R. K. Srivastava and S. Shankar, *J. Mol. Signal.*, 2010, **5**, 10.
31. D. L. Stoler, *Cell*, 2000, **100**, 57-70.
32. P. Sengupta, S. Basu, S. Soni, A. Pandey, B. Roy, M. S. Oh, K. T. Chin, A. S. Paraskar, S. Sarangi and Y. Connor, *Proc. Natl. Acad. Sci. U.S.A.*, 2012, **109**, 11294-11299.

SYNOPSIS

The thesis titled “Inhibition of PI3K/MAPK Signaling with Simultaneous DNA Damage in Cancer Cells by Lipidic Nanoparticles” deals with targeting multiple upregulated signaling pathways in cancer cells by nanotechnology-based platforms. In this thesis we have mainly focused on inhibiting PI3K and MAPK signaling with simultaneous downstream DNA damage in cancer cells for augmented effect. We adopted nanotechnology platforms to address the challenges associated with signaling inhibition with simultaneous DNA damage. In the current thesis, we have also focused on exploring several lipid molecules as a vehicle to carry multiple signaling inhibitors and drugs to the tumor tissue. It is obvious that the success of potential nanocarrier also depends on the actual composition of nanomaterial. Biodegradable and nontoxic vectors which are used in the nanoparticle synthesis would minimise the carrier related toxicity in *in vitro* and *in vivo* application. Interestingly, not much was explored on nanoparticle mediated PI3K/MAPK inhibition with simultaneous DNA damage in cancer cells and very few reports are there in the current literature. To this end, we have explored nontoxic, biodegradable lipidic molecules such as cholesterol, vitamin D3, and oleic acid as vectors to synthesize nanoparticles comprising signaling inhibitors and DNA-damaging agents together. These nanoparticles were demonstrated to inhibit PI3K, MAPK and both PI3K, MAPK signaling with simultaneous DNA damage in several cancer cells like breast cancer, cervical cancer and colon cancer cells. Further, we also surface decorated the engineered nanoparticles with hyaluronic acid to target CD44 receptors over-expressed on colorectal cancer cells more specifically in which PI3K and MAPK signaling pathways are highly deregulated.

In chapter 2, to validate the importance of PI3K signaling inhibition with simultaneous DNA damage in cancer cells, we engineered vitamin D3 nanoparticles (NPs) loaded with PI3K inhibitor in combination with DNA damaging agent (cisplatin/doxorubicin/proflavine) and characterized by light scattering and electron microscopy techniques. A slow and sustained release of drugs from NPs was observed over a period of time rather burst release at tumor physiological pH = 5.4. These nanoparticles showed improved efficacy in human hepatocellular carcinoma cells (Hep3B), as well as cisplatin resistant-Hep3B (Hep3B-R) compared to free drug treatment. The combination of PI103-DOX, and PI103-CDDP in nanoparticle formulation exhibited a strong synergistic effect in killing both HEP-3B and

Hep3B-R cells as compared to their respective mono drug-loaded nanoparticles. These nanoparticles also induced apoptosis through a DNA damaging mechanism.

In chapter 3, Drug molecules (PI103, cisplatin, and doxorubicin) were chemically conjugated to biocompatible cholesterol and engineered into chimeric nanoparticles (ChNPs) to achieve enhanced therapeutic efficacy. A ratiometric drug loading of all three drug conjugates in ChNPs was obtained. ChNPs internalized into the cancer cells (MCF7, MDA-MB-237, and HeLa) by endocytosis and inhibited PI3K pathway by downregulating pAKT with damaging DNA in HeLa cells leading to induction of apoptosis. Interestingly, ChNPs induced improved cytotoxicity in all these cancer cells compared to free drug combination and this effect was even more severe in triple negative drug resistance breast cancer cells.

In chapter 4a, we engineered novel biocompatible oleic acid nanoparticles comprising MEK inhibitor (AZD6244) and DNA damaging agent (cisplatin) to target MAPK signaling in cancer cells. Drug molecules were chemically conjugated to oleic acid and were co-self-assembled into 120 nm sized particles. NPs showed the controlled release of drugs at tumor pH mimic (pH = 5.5). These NPs internalized into HeLa cells by macropinocytosis pathway and inhibited MAPK signaling along with DNA damage in cervical cancer cells. Moreover, NPs showed enhanced cytotoxicity in several cancer cells including drug resistant ones.

Further, in chapter 4b, to inhibit MAPK signaling specifically in colorectal cancer cells, NPs were decorated with hyaluronic acid (HA) to enhance the cellular uptake in CD44 receptor over-expressed colon cancer cells (HCT-116) and to escalate cytotoxicity. Interestingly, HA coated NPs were internalized into HCT116 cells via CD44 receptor-mediated and clathrin-mediated endocytosis and inhibited MAPK signaling by exhibiting enhanced cytotoxicity over free drug cocktail treatment.

Crosstalk between PI3K and MAPK pathway often would lead to failure of monotherapy where a single pathway is targeted. To address this, in chapter 5, we have engineered hyaluronic acid coated chimeric nanoparticles (HA-ChNPs) which contain PI3K and MAPK signaling inhibitors (PI103 and AZD6244) and a DNA damaging agent (cisplatin). All three drugs were chemically conjugated to cholesterol and co-self-assembled into chimeric nanoparticles which were further coated with hyaluronic acid. These HA-ChNPs internalized into cells by receptor-mediated endocytosis and caused cell death at much lower IC_{50} values compared to free drug mixture. HA-CNPs induced apoptosis and demonstrated cell cycle

arrest at G1 phase by successfully inhibiting both PI3K and MAPK pathway in colon cancer cells.

Future Prospective

In this current thesis, I have engineered multidrug loaded nontoxic lipidic nanoparticles to target PI3K/MAPK signaling with simultaneous DNA damage in cancer cells. These nanoparticles exhibited enhanced therapeutic activity in several cancer cells including drug resistant ones by successfully inhibiting PI3K and MAPK signaling also by inducing simultaneous DNA damage *in vitro*. We further would like to study *in vivo* efficacy of the engineered nanoparticle in inhibiting PI3K/MAPK signaling.

Furthermore, considering the complex nature of cancer, I would like to merge chemotherapy with several other promising technologies like photothermal/photodynamic therapies and immunotherapy to get augmented therapeutic outcomes by nanotechnology-based platforms in my future research activities. In this thesis, signaling inhibitors and DNA damaging agents were conjugated to biocompatible lipids such as cholesterol, vitamin D3 and oleic acid, which were co-self-assembled into nanoparticles carrying multiple drugs to cancer cells. This approach could be a promising platform to load and deliver several other therapeutic agents such as small molecule inhibitors, chemotherapeutic, siRNA (or genes) and photosensitizing agents in combination to target cancer cells more efficiently.